Title

The roles of the Coq10 chaperone protein, cardiolipin, and endoplasmic reticulum-mitochondria contact sites in coenzyme Q biosynthesis and function

Author

Tsui, Hui Su

Publication Date

2019

Peer reviewed|Thesis/dissertation

UNIVERSITY OF CALIFORNIA

Los Angeles

The roles of the Coq10 chaperone protein, cardiolipin, and endoplasmic reticulum-mitochondria contact sites in coenzyme Q biosynthesis and function

A dissertation submitted in partial satisfaction of the

requirements for the degree Doctor of Philosophy

in Biochemistry and Molecular Biology

by

Hui Su Tsui

2019

ABSTRACT OF THE DISSERTATION

The roles of the Coq10 chaperone protein, cardiolipin, and endoplasmic reticulum-mitochondria contact sites in coenzyme Q biosynthesis and function

by

Hui Su Tsui

Doctor of Philosophy in Biochemistry and Molecular Biology

University of California, Los Angeles, 2019

Professor Catherine F. Clarke, Chair

Coenzyme Q (CoQ) is an essential lipid molecule for cellular bioenergetics, cellular antioxidant defense, and is a co-factor for enzymes participating in fatty acid β-oxidation and pyrimidine biosynthesis. The biosynthetic machinery of CoQ consists of a cohort of Coq polypeptides that are organized in a multi-subunit complex known as the CoQ synthome, residing on the mitochondrial inner membrane. Although CoQ is almost exclusively produced inside the mitochondria, it exists in most cellular membranes. The hydrophobicity of CoQ, especially CoQ isoforms with long polyisoprenyl tail prevents CoQ from being distributed to cellular membranes via diffusion. Thus, protein complexes localized at the membrane contact sites between two organelles, and lipid-binding chaperones play important roles redistributing CoQ and escorting CoQ from place where it is being synthesized to places where it functions. My research uses *Saccharomyces cerevisiae* (hereafter termed “yeast”) as the model organism because many of the enzymes involved in the yeast CoQ biosynthesis are conserved in

humans. Additionally, the ability of yeast cells to survive by fermentation allows genetic manipulation of genes that are essential for respiratory growth.

Chapter 1 provides an overview of the biosynthesis of CoQ in both yeast and human cells, and highlights the functional conservation of many of the enzymes involved in the CoQ production. Chapter 2 focuses on the biochemical characterization of two human steroidogenic acute regulatory protein (StAR)-related lipid transfer (START) domain proteins, COQ10A and COQ10B. These two human COQ10 paralogs are co-orthologous to yeast Coq10, which is essential for CoQ function and is required for efficient de novo CoQ biosynthesis. Expression of either one of the two human COQ10 paralogs restores CoQ function in yeast *coq10* deletion mutant, but neither is able to restore de novo CoQ production. This result implies divergent functions of yeast Coq10 and its human COQ10 co-orthologs for CoQ production, and the existence of a second protein that needs to function concurrently with Coq10 for efficient CoQ biosynthesis in yeast. Chapter 3 explores CoQ biosynthesis in yeast mutants lacking the endoplasmic reticulum (ER)-mitochondria encounter structure (ERMES) complex at the ER and mitochondria membrane contact sites. In collaboration with Dr. Maya Schuldiner's lab, we found that the de novo production and distribution of CoQ in the ERMES deletion mutants are distorted due to the destabilization of the CoQ synthome in the absence of ERMES complex. Fluorescent microcopy data suggests close proximity of the CoQ synthome and the ERMES complex, implying a spatially coordinated regulation of CoQ biosynthesis and distribution by two closely apposed organelles. Chapter 4 examines the antioxidant property of CoQ. In collaboration with Dr. Anne Murphy's lab and Dr. Mikhail Shchepinov from Retrotope, Inc., We showed that the yeast CoQ-less mutants are exquisitely sensitive to polyunsaturated fatty acid (PUFA)-induced lipid peroxidation, and these CoQ-less mutants can be protected from oxidative damage by substituting the exogenously supplied PUFA with isotope-reinforced PUFA with its bis-allylic hydrogen replaced with deuterium atom. Chapter 5 studies CoQ biosynthesis and CoQ synthome assembly in yeast mutants that have defects in cardiolipin biosynthesis and

remodeling. Cardiolipin (CL) is a unique phospholipid that is found exclusively within the mitochondrial membranes. In yeast, unmodified CL functions almost identically to remodeled CL, and the CL remodeling process is thought to remove and repair damaged CL. The yeast mutants with defects in CL biosynthesis and remodeling synthesize CoQ less efficiently, despite that the CoQ synthome assembly is only marginally affected. Last but not least, Chapter 6 describes efforts made towards characterizing the biological function of Coq10 with preliminary data collected with help from Kate Liu, Dr. Dyna Shirasaki, Dr. Frederik Lermyte, Dr. Brendan Amer, and Alice Hsu. Collectively, my work explores the biosynthesis and molecular functions of CoQ, and provides new insight into the regulation of CoQ production.

The dissertation of Hui Su Tsui is approved.

Joseph Ambrose Loo

Alexander M. van der Bliek

Catherine F. Clarke, Committee Chair

University of California, Los Angeles

2019

This work is dedicated to my grandparents, my parents, and Harvey, with my gratitude for their support, encouragement, understanding and laughter that get me through good and bad times.

TABLE OF CONTENTS

LIST OF TABLES AND FIGURES

ACKNOWLEDGEMENTS

First and foremost, I would like to express my sincere gratitude to my advisor, Dr. Catherine Clarke, for her guidance, encouragement, mentorship, and support that have made me who I am today.

November 2011, I was in my last quarter of senior year, desperately looking for a lab to join so that I can apply for the Departmental Scholar program in the Chemistry and Biochemistry Department. As a graduating senior with no previous lab experience, it was not easy to land on an undergraduate researcher position. My luck turned around on the day that I met Cathy. I introduced myself to her and she immediately agreed to take me in as an undergraduate researcher! At our second meeting, Cathy and I were already talking about the project!! Under her guidance and mentorship, I got accepted as a Departmental Scholar, and graduated with Bachelor and Master degrees in 2013. After graduation, I was at a crossroads in life, not knowing what I wanted to do. It was Cathy, who encouraged me to pursue my interest in research and supported my application for graduate school. If it were not for Cathy, who has opened the door for me to research, my path in life would have been very different. To me, Cathy has been a great mentor with her passion and knowledge in science. However, I appreciate her more for being a great listener and supporter, when I was struggling with failed experiments, stressful graduate school, and things happened in my life. Thank you for always being there for me. I have been very fortunate, and I am forever grateful to you, Cathy!

I am also extremely grateful to my thesis committee, Dr. Joseph Loo, Dr. Robert Clubb, Dr. Steven Bensinger, and Dr. Alexander van der Bliek. Joe and Rachel have been so kind and patient, lending me knowledge for my research project, and offering me opportunities to work and connect with people in industry. Aside from Cathy, Joe has been my go-to person for career advice or just a chat. Rob has been super understanding and supportive of my research project and career choice. Thank you for telling me that I am not alone in face of tough decisions for my

career choices. I am also fortunate to have Steve and Alex on my committee. They have provided valuable ideas to guide my research and made this thesis possible.

Beside myself, this thesis contains data and ideas that were contributed by a lot of other talented individuals. Chapter 1 is a reprint of a review article in *Essays in Biochemistry* (2018) 62.3: 361-376. I would like to thank all the co-authors in the Clarke lab who have contributed to this publication, and Portland Press for permission to use this copyrighted material. For the Coq10 project descried in Chapter 2, I would like to thank Dr. Brendan Amer, from whom I have learned so much about protein purification. I would also like to thank Dr. Crysten Blaby-Haas for her wonderful analysis on the Coq10 orthologs; Dr. Marcus Gallagher-Jones for his work on generating the models of human COQ10A and COQ10B; Jason Gosschalk's work on CC1736 ligand docking; Michelle Bradley's work on obtaining the Coq11 antibody. This work is now accepted for publication in the Journal of Lipid Research. Chapter 3 is a reprint of a recent publication in *Contact* (2019) 2: 1-14, and I would like to thank SAGE Publishing for permission to use this copyrighted material. I am truly grateful to the collaboration with Michal Eisenberg-Bord, Dr. Maya Schuldiner, Diana Antunes, Dr. Doron Rapaport, Dr. Lucía Fernández-del-Río, and other co-authors. Long time ago, Dr. Theresa Nguyen has studied the cellular localization of the GFP-tagged Coq polypeptide, and has shown punctate fluorescent signals of several Coq polypeptides. However, the functional significant of this special organization of Coq polypeptides was unclear until Michal's fluorescent microscopy work, which has provided the first piece of evidence indicating the co-localization of these Coq polypeptide with the ERMES complex subunits at the ER mitochondria membrane contact sites. This finding provides the groundwork for future investigation of spatially coordinated CoQ production and trafficking. Chapter 4 is a reprint of a published work in *Free Radical Biology and Medicine* (2015) 82: 63-72. I would like to thank Elsevier and the primary author Dr. Alexander Andreyev for permission to use this copyrighted material. I would also like to thank Dr. Mikhail S. Shchepinov from Retrotope Inc., who has brought together some extraordinarily talented scientists and initiated collaborations to

elucidate the protective effect of isotope-reinforced PUFAs. The idea of investigating the CoQ biosynthesis and the assembly of CoQ synthome in yeast cells with defective CL biosynthesis and remodeling described in Chapter 5 was originated from my discussion with Dr. Steven Claypool at the SFRBM conference in West Palms, FL. He has provided us the yeast strains, human cell lines necessary for this work. He has also provided valuable feedbacks and comments on the write up of this project. Chapter 5 was recently submitted to the Journal of Lipid Research. Chapter 6 contains additional work that I have done with the help from Kate Liu, Dr. Dyna Shirasaki, and Dr. Frederik Lermyte for proteomic analysis of the Coq10-interacting protein partner; Dr. Brendan Amer and Dr. Chingnam (Keith) Cheung for Coq10 purification with affinity column chromatography; my former undergraduate student Alice Hsu for carrying out the rescue experiment with exogenous CoQ. This thesis also cannot come true without the help from Dr. Xin Cong, Dr. Melissa Sondej, Dr. Yu Chen, Dr. William Silkworth, and Dr. Martin Philips at the UCLA Molecular Instrumentation Center and the UCLA-DOE & Biochemistry Shared Instrumentation Core Facility. All work is supported by the National Science Foundation Grant MCB-1330803 to Dr. Catherine F. Clarke and by the National Institutes of Health Grant T32 GM 008496 to Hui Su Tsui.

I would like to express my deepest appreciation to all of my colleagues for their mentorship and friendship. Former Clarke lab members, Dr. Letian Xie, Dr. Cuiwen He, Dr. Theresa Nguyen, and Dr. Chris Allan who have taught me all the lab skills that I have learned and mastered today. I would like to thank Chris, for offering me tremendous help when I first took over the Coq10 project. I would like to thank all current Clarke lab members, Dr. Lucía Fernández-del-Río, Dr. Agape Awad, Michelle Bradley, and Anish Nag for making our lab a pleasant place to work. I am truly grateful to Kelly Quinn, who spent the night with me in lab for those long experiments; Charles Wang and Dr. Cuiwen He, with whom I shared moments of deep anxiety and are my go-to persons for emotional ventilation; Dr. Sean Shen, who introduced me to my internship at the UCLA Technology Development Group; Dr. Xiaoyu Xia,

who has helped me looking for jobs; Dr. Hui Ding, Dr. Zhengao Feng, and Maria Gutierrez, who always share their fruits with me at lunches; Dr. Janette Kropat, who always rushes to help when I need help with a broken instrument; and everyone from the Torres lab, who are great lunch buddies. I would like to express my deepest appreciation to all the undergraduate students, Nguyen Pham, Hope Ibarra, Alice Hsu, Minhhan Pham, and Yvonne Nong, whom I have mentored during graduate school. I cherish the time we spent together, and the friendship we have developed over time. I have realized that the presence of all my colleagues, and the corridor chats with them were incredibly important for me in a process that is often felt as solitaire.

Finally, I want to thank my mom and dad, my grandparents, and my husband Harvey. I want to thank my parents for raising me in such a loving family, and Harvey for providing me a second home. You have given me all the freedom and support that I needed to pursue my dreams. You are my motivation and strength to get things done.

VITA

2010	Associate of Science College of the Canyons Santa Clarita, CA
2009-2010	National Science Foundation Transitions Scholarship for Mathematics, Engineering, Science Achievement College of the Canyons Santa Clarita, CA
2012	Chemistry and Biochemistry Alumni Undergraduate Summer Research Fellowship University of California, Los Angeles Los Angeles, CA
2013	B.S. & M.S. Biochemistry *cum laude* University of California, Los Angeles Los Angeles, CA
2013	Dolores Cannon Southam Award for Excellence in Research University of California, Los Angeles Los Angeles, CA
2013	Division of Physical Sciences Alumni Association Fellowship University of California, Los Angeles Los Angeles, CA
2013-2019	Research Assistant Department of Chemistry and Biochemistry University of California, Los Angeles Los Angeles, CA
2014-2019	Teaching Assistant Department of Chemistry and Biochemistry University of California, Los Angeles Los Angeles, CA
2015	Excellence in Second Year Academics and Research Award Department of Chemistry and Biochemistry University of California, Los Angeles Los Angeles, CA
2015-2019	Technology Fellow UCLA Technology Development Group Los Angeles, CA
2016-2018	The Cellular and Molecular Biology Fellow University of California, Los Angeles Los Angeles, CA

2019 Daniel E. Atkinson & Charles A. West Award
University of California, Los Angeles
Los Angeles, CA

2019 Biochemistry Dissertation Award
University of California, Los Angeles
Los Angeles, CA

PUBLICATIONS

Tsui, H.S., Pham, N.V.B., Amer, B.R., Bradley, M.C., Gosschalk, J.E., Gallagher-Jones, M., Ibarra, H., Clubb, R.T., Blaby-Haas, C., Clarke, C.F. (2019) Human COQ10A and COQ10B are distinct lipid-binding START domain proteins required for coenzyme Q function. *Journal of Lipid Research*. **In Press.**

Tsui, H.S., Pham, N.V.B., Fernández-del-Río, L., Acoba, M.G., Claypool, S.M., Clarke, C.F. Disturbed cardiolipin metabolism impairs coenzyme Q biosynthesis. **Submitted.**

Tsui, H.S., and Clarke, C.F. (2019) Ubiquinone biosynthetic complexes in prokaryotes and eukaryotes. *Cell chemical biology* 26 (4): 465-467.

Eisenberg-Bord, M., **Tsui, H.S.**, Antunes, D., Fernández-del-Río, L., Bradley, M.C., Dunn, C.D., Nguyen, T.P.T., Rapaport, D., Clarke, C.F., Schuldiner, M. (2019) The endoplasmic reticulum-mitochondria encounter structure complex coordinates coenzyme Q biosynthesis. *Contact*, 2: 1-14.

Awad, A. M., Bradley, M. C., Fernández-del-Río, L., Nag, A., **Tsui, H.S.**, Clarke, C. F. (2018) Coenzyme Q_{10} deficiencies: pathways in yeast and humans. *Essays in Biochemistry*, 62.3: 361-376.

Andreyev, A.Y., **Tsui, H.S.**, Milne, G.L., Shmanai, V.V., Bekish, A.V., Fomich, M.A., Pham, M.N., Nong, Y., Murphy, A.N., Clarke, C.F., Shchepinov, M.S. (2015) Isotope-reinforced polyunsaturated fatty acids protect mitochondria from oxidative stress. *Free Radical Biology and Medicine*, 82: 63-72.

Shchepinov, M. S., Roginsky, V. A., Brenna, J. T., Molinari, R. J., To, R., **Tsui, H.,** Clarke, C. F., and Manning-Bog, A. B. (2014) Deuterium protection of polyunsaturated fatty acids against lipid peroxidation: A novel approach to mitigating mitochondrial neurological diseases. *Omega 3 Fatty Acids in Brain and Neurologic Health*, 367-377. (BOOK CHAPTER)

Hill, S., Lamberson, C.R., Xu, L., To, R., **Tsui, H.S.**, Shmanai, V.V., Bekish, A.V., Awad, A.M., Marbois, B.N., Cantor, C.R., Porter, N.A., Clarke, C.F., Shchepinov, M.S. (2012) Small amounts of isotope-reinforced polyunsaturated fatty acids suppress lipid autoxidation. *Free Radical Biology and Medicine*, 53 (4): 893-906.

CHAPTER 1

Coenzyme Q_{10} deficiencies: pathways in yeast and humans

Essays in Biochemistry (2018) **62** 361–376
https://doi.org/10.1042/EBC20170106

PORTLAND PRESS

Review Article

Coenzyme Q_{10} deficiencies: pathways in yeast and humans

Agape M. Awad, Michelle C. Bradley, Lucía Fernández-del-Río, Anish Nag, Hui S. Tsui and Catherine F. Clarke

Department of Chemistry and Biochemistry, Molecular Biology Institute, UCLA, Los Angeles, CA 90095, U.S.A.

Correspondence: Catherine F. Clarke (cathy@chem.ucla.edu)

Coenzyme Q (ubiquinone or CoQ) is an essential lipid that plays a role in mitochondrial respiratory electron transport and serves as an important antioxidant. In human and yeast cells, CoQ synthesis derives from aromatic ring precursors and the isoprene biosynthetic pathway. *Saccharomyces cerevisiae coq* mutants provide a powerful model for our understanding of CoQ biosynthesis. This review focusses on the biosynthesis of CoQ in yeast and the relevance of this model to CoQ biosynthesis in human cells. The *COQ1–COQ11* yeast genes are required for efficient biosynthesis of yeast CoQ. Expression of human homologs of yeast *COQ1–COQ10* genes restore CoQ biosynthesis in the corresponding yeast *coq* mutants, indicating profound functional conservation. Thus, yeast provides a simple yet effective model to investigate and define the function and possible pathology of human *COQ* (yeast or human gene involved in CoQ biosynthesis) gene polymorphisms and mutations. Biosynthesis of CoQ in yeast and human cells depends on high molecular mass multisubunit complexes consisting of several of the *COQ* gene products, as well as CoQ itself and CoQ intermediates. The CoQ synthome in yeast or Complex Q in human cells, is essential for *de novo* biosynthesis of CoQ. Although some human CoQ deficiencies respond to dietary supplementation with CoQ, in general the uptake and assimilation of this very hydrophobic lipid is inefficient. Simple natural products may serve as alternate ring precursors in CoQ biosynthesis in both yeast and human cells, and these compounds may act to enhance biosynthesis of CoQ or may bypass certain deficient steps in the CoQ biosynthetic pathway.

Introduction

Coenzyme Q (ubiquinone or CoQ) is a vital lipid component in mitochondrial energy metabolism. It is a two-part molecule containing a long polyisoprenyl tail of *n* isoprene units positioning the molecule in the mid-plane of membrane bilayer, and a fully substituted benzoquinone ring that undergoes reversible reduction and oxidation. The redox chemistry of CoQ and $CoQH_2$ (ubiquinol, a hydroquinone) allows it to play its best-known role in mitochondrial respiration, accepting electrons and protons from Complex I or Complex II and donating them to Complex III, thereby establishing a proton gradient across the mitochondrial inner membrane. CoQ also serves as an essential electron and proton acceptor in other aspects of metabolism including fatty acid β-oxidation, uridine biosynthesis, and oxidation of sulphide, proline, glycerol-3-phosphate, choline, dimethylglycine, and sarcosine [1,2]. $CoQH_2$ also serves a crucial antioxidant function, protecting membranes as a chain terminator of lipid peroxidation reactions, and in the maintenance of reduced forms of vitamin E [1,3]. CoQ/$CoQH_2$ is a component of lipoproteins and is present in all cellular membranes including the plasma membrane where it functions in cellular redox regulation as part of the plasma membrane oxidoreductase system [1].

The focus of this review is on the biosynthesis of CoQ_6 in the yeast *Saccharomyces cerevisiae* and the relevance of this model to the biosynthesis of CoQ_{10} in human cells. Readers are directed to other

Received: 26 February 2018
Revised: 08 April 2018
Accepted: 14 May 2018

Version of Record published: 06 July 2018

Essays in Biochemistry (2018) **62** 361–376
https://doi.org/10.1042/EBC20170106

recent reviews that discuss the biosynthesis of CoQ in prokaryotes such as *Escherichia coli* [4], and in eukaryotes including *Schizosaccharomyces pombe*, plants, *Caenorhabditis elegans*, *Mus musculus*, and humans [5-7]. For an in-depth discussion of the effects of CoQ_{10} deficiencies and the clinical syndromes associated with these deficiencies, readers are directed to the article by Brea-Calvo and colleagues [8] in this issue of *Essays in Biochemistry*.

Overview of CoQ biosynthesis

S. cerevisiae is an extraordinarily useful model for understanding the biosynthesis of CoQ. Early yeast classic and molecular genetics combined with subcellular fractionation, biochemical assays, and lipid chemistry have helped to identify many of the steps required for CoQ biosynthesis. In particular, the collection of respiratory deficient *coq* mutants identified by Tzagoloff [9,10] set the stage for isolation and characterization of the yeast *COQ* genes. A particular advantage is that the CoQ-less *coq* mutants are viable when cultured on growth medium containing a fermentable carbon source, but are incapable of growth on medium containing a non-fermentable carbon source. In most cases, expression of the human COQ (human polypeptide involved in CoQ_{10} biosynthesis) homolog restores function in the corresponding yeast *coq* mutant. This rescue of yeast *coq* mutants by human *COQ* genes is a powerful and simple functional assay still being used to ascertain the effects of human mutations or polymorphisms on human *COQ* gene function. Thus, what we have learned about the biosynthesis of CoQ_6 in the yeast model is highly relevant to the biosynthesis of CoQ_{10} in humans (Figure 1).

The yeast model also provided early evidence that the eukaryotic CoQ biosynthetic pathway was localized to mitochondria. The Coq (denotes *S. cerevisiae* polypeptide involved in CoQ_6 biosynthesis) polypeptides are nuclear encoded, and amino-terminal mitochondrial targetting sequences are needed to direct their transport to the mitochondrial matrix (Coq1, Coq3–Coq11) or to the inner mitochondrial membrane (Coq2). Assembly of Coq3–Coq9 plus Coq11 polypeptides into a high molecular mass complex termed the CoQ synthome in yeast (Figure 2) and Complex Q in human cells is another conserved feature of CoQ biosynthesis [7,11]. These complexes are essential for the biosynthesis of CoQ in yeast and human cells, and may serve to enhance catalytic efficiency and to minimize the escape of intermediates that may be toxic due to their redox or electrophilic properties. The CoQ-intermediates are quite hydrophobic and at least some of them appear to be essential partners in the assembly of the membrane-bound CoQ synthome [12] and Complex Q [7,13].

Ring precursors utilized in biosynthesis of CoQ

Origin of 4-hydroxybenzoic acid

In yeast and human cells, the primary precursor molecule that leads to the biosynthesis of CoQ is 4-hydroxybenzoic acid (4HB). Yeast cells generate 4HB via the shikimate pathway, but also utilize tyrosine as a ring precursor [14]. Unlike yeast, human cells contain phenylalanine hydroxylase, and so either phenylalanine or tyrosine may be utilized as precursors for the biosynthesis of 4HB. Many steps involved in the generation of 4HB from tyrosine are yet to be characterized [15,16]. However, two recent studies have shed light on the first and the last steps involved in yeast 4HB biosynthesis [17,18]. The first step involves the deamination of tyrosine to 4-hydroxyphenylpyruvate (4-HPP), catalyzed by either of the aminotransferases Aro8 or Aro9 [17]. Payet et al. [17] also identified 4-hydroxybenzaldehyde (4HBz) as the final intermediate leading to the biosynthesis of 4HB. The oxidation of 4HBz to 4HB is catalyzed by the aldehyde dehydrogenase Hfd1. Hfd1 is a mitochondrial outer membrane protein [19] indicating that 4HB is synthesized in the cytosol, and must be imported into the mitochondrial matrix, where it is incorporated into CoQ. Hence, there should be a mitochondrial transporter for 4HB that remains to be identified [7], and is responsible for use of exogenously added 4HB. Inactivation of *HFD1* results in CoQ_6 deficiency that may be complemented by the addition of exogenous 4HB. Expression of the human homolog ALDH3A1 restored CoQ_6 biosynthesis in the *hfd1* yeast mutant, and was shown to oxidize 4HBz to 4HB [17]. In an independent study Stefely et al. [18] confirmed these findings; MS was used to characterize the proteomes, lipidomes, and metabolomes of a large selection of yeast strains, each lacking a distinct gene related to mitochondrial biology. This multi-omic approach revealed that yeast Hfd1 and human ALDH3A1 serve as the aldehyde dehydrogenases responsible for the oxidation of 4HBz to 4HB. It will be important to determine whether human *ALDH3A1* is required for CoQ_{10} biosynthesis in human cells; if so, it may be a potential target gene that should be considered when screening for CoQ_{10} deficiencies in patients.

Other aromatic ring precursors of CoQ

In addition to 4HB, yeast utilize *para*-aminobenzoic acid (pABA) as a ring precursor of CoQ_6 [20,21]. Yeast Coq6 and Coq9 polypeptides are required for this metabolism. Yeast Coq6 is required for the oxidative deamination of

Essays in Biochemistry (2018) **62** 361–376
https://doi.org/10.1042/EBC20170106

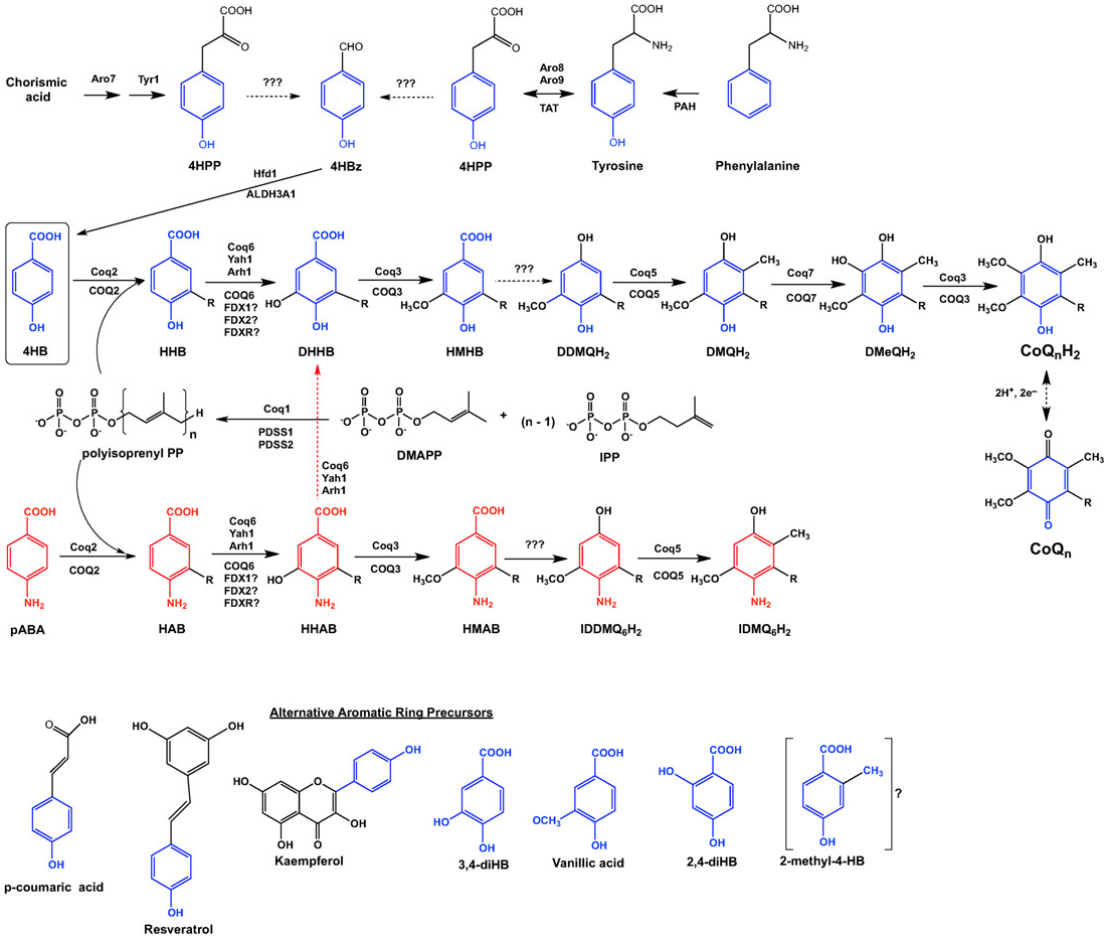

Figure 1. CoQ biosynthetic pathways in the yeast *S. cerevisiae* and in humans

The CoQ biosynthetic pathway has been shown to involve at least 14 nuclear-encoded proteins that are necessary for mitochondrial CoQ biosynthesis in *S. cerevisiae*. Black dotted arrows denote more than one step. Solid arrows denote a single step attributed to the corresponding yeast polypeptide named above each arrow. The corresponding human homologs are named below each arrow. The main ring precursor used by both yeast and humans is 4-hydroxybenzoic acid (4HB). Yeasts synthesize 4HB *de novo* from chorismate or may obtain it from the metabolism of tyrosine. Humans rely on tyrosine to produce 4HB (or on phenylalanine and phenylalanine hydroxylase to produce tyrosine). Yeast and human cells produce isopentenyl pyrophosphate (IPP) and dimethylally pyrophosphate (DMAPP) as precursors to form hexaprenyl diphosphate (n=6) via Coq1 in yeast or decaprenyl diphosphate (n=10) via PDSS1/PDSS2 in humans. Yeast Coq2 and human COQ2 attach the polyisoprenyl tail to 4HB. Subsequent to this step, the next three intermediates are identified as yeast hexaprenyl-intermediates: HHB, 3-hexaprenyl-4HB; DHHB, 3-hexaprenyl-4,5-dihydroxybenzoic acid; HMHB, 3-hexaprenyl-4-hydroxy-5-methoxybenzoic acid. The next three intermediates are hydroquinones: $DDMQH_2$, 2-hexaprenyl-6-methoxy-1,4-benzenediol; $DMQH_2$, 2-hexaprenyl-3-methyl-6-methoxy-1,4-benzenediol; $DMeQH_2$, 2-hexaprenyl- 3-methyl-6-methoxy-1,4,5-benzenetriol; to ultimately produce the final reduced product (CoQ_nH_2). Red text identifies *para*-aminobenzoic acid (pABA) as an alternate ring precursor utilized by yeast (but not by humans). The next three intermediates are identified as yeast hexaprenyl-intermediates: HAB, 4-amino-3-hexaprenylbenzoic acid; HHAB, 4-amino-3-hexaprenyl-5-hydroxybenzoic acid; HMAB, 4-amino-3-hexaprenyl-5-methoxybenzoic acid. The next two intermediates are: $IDDMQH_2$, 4-amino-3-hexaprenyl-5-methoxyphenol; $IDMQH_2$, 4-amino-3-hexaprenyl-2-methyl-5-methoxyphenol. The step denoted by the red dotted arrow depends on yeast Coq6 and converts HHAB into DHHB. Interconversion of (CoQ_nH_2) and (CoQ_n) is shown via a reversible two-electron reduction and oxidation. Steps indicated by '???' are catalyzed by as yet unknown enzymes. Alternative compounds that may serve as ring precursors in CoQ biosynthesis are shown at the bottom of the

Essays in Biochemistry (2018) **62** 361–376
https://doi.org/10.1042/EBC20170106

panel: *p*-coumaric acid, resveratrol, and kaempferol. Analogs of 4HB that can function to bypass certain deficiencies in the CoQ biosynthetic pathway include: 3,4-dihydroxybenzoic acid (3,4-diHB), vanillic acid and 2,4-dihydroxybenzoic acid (2,4-diHB). It is not yet known whether 2-methyl-4HB (2-methyl-4HB) may also serve a bypass function.

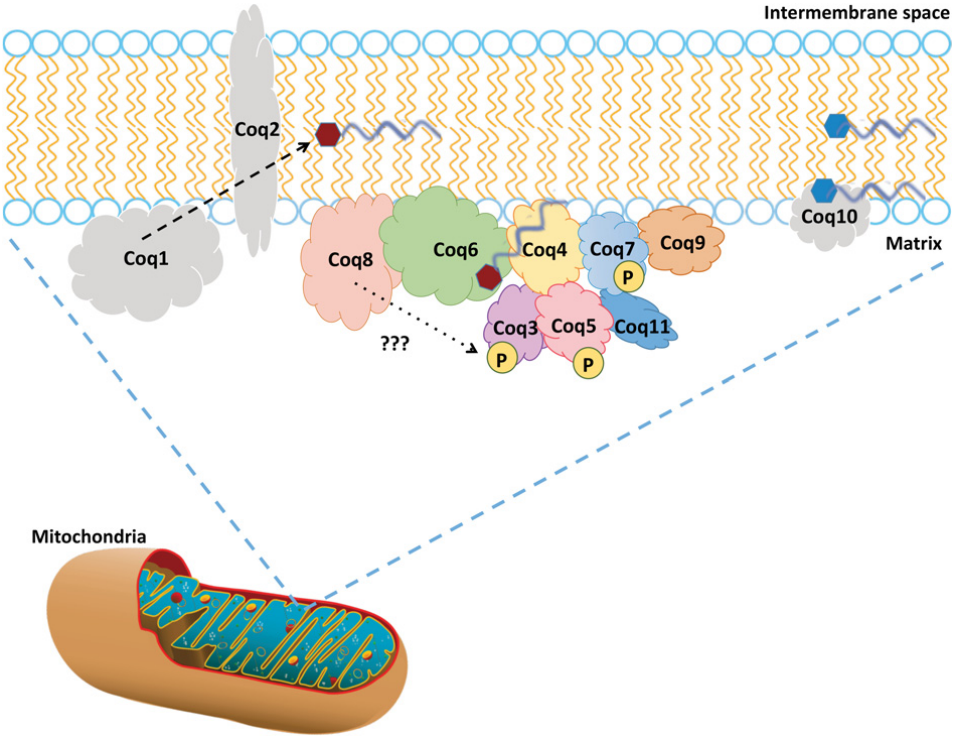

Figure 2. A model of the CoQ Synthome in the yeast *S. cerevisiae*

Studies in *S. cerevisiae* have provided evidence for a high-molecular mass multisubunit protein and lipid complex, the CoQ synthome (see text for references). The Coq3–Coq9 and Coq11 polypeptides, designated in color, co-purify, and are members of this complex that is peripherally associated with the matrix-side of the inner mitochondrial membrane. Coq1, Coq2, and Coq10 are individual polypeptides that do not associate with the complex (indicated in gray). Coq1 and Coq2 synthesize the early intermediates HHB and HAB (denoted by red hexagon with a gray hexaprenyl tail). Coq10 binds CoQ (and also late-stage CoQ-intermediates denoted as blue hexagons with a gray tail), and functions as a chaperone for this hydrophobic lipid that normally resides at the mid-plane of the membrane bilayer. The Coq3, Coq5, and Coq7 polypeptides are phosphorylated in a Coq8-dependent manner (shown by '???'). The function of Coq8 is still under investigation; although part of a family of atypical kinases, Coq8 has been shown to autophosphorylate, but not yet shown to phosphorylate any other proteins, *in vitro* or *in vivo*. It is speculated to have ATPase function and potentially has the ability to phosphorylate lipids or other small molecules. Hence the phosphorylation of Coq3, Coq5, and Coq7 may be from Coq8 or be produced via another kinase that is recruited to the CoQ synthome to act upon those particular polypeptides. In yeast, it has been shown that the phosphatase that dephosphorylates Coq7 is $Ptc7_S$, the product of the spliced form of *PTC7* (not shown).

the ring nitrogen substituent [22]. Coq9 is also required for Coq6 activity, including the Coq6-mediated deamination function [23,24]. Analogs of 4HB, including 2,4-dihydroxybenzoic acid (2,4-diHB), 3,4-dihydroxybenzoic acid (3,4-diHB) and vanillic acid may be incorporated into CoQ_6 [16] (Figure 1). These analogs may allow for the bypass of CoQ_6 biosynthetic defects in certain yeast *coq6* and *coq7* mutants [16,24,25], as discussed in 'Yeast and human

genes essential for CoQ biosynthesis'. Additional aromatic ring precursors incorporated into CoQ_6 in yeast include *p*-coumarate and the polyphenols resveratrol and kaempferol [26,27] (Figure 1), although the use of kaempferol by yeast is very marginal.

In contrast, pABA is not utilized for CoQ synthesis by human or mouse cells [26], and instead it acts to inhibit the incorporation of 4HB into CoQ [16,28,29]. In mammalian cells, *p*-coumarate, vanillic acid, 3,4-diHB, resveratrol, and kaempferol also serve as CoQ ring precursors, with the difference that in this case kaempferol is a very efficient precursor that is even able to up-regulate CoQ_9 and CoQ_{10} levels in human and mouse kidney cells [27]. While the mechanism underlying the use of polyphenols is still unknown, it is clear that a highly specific process occurs because other polyphenols with similar structures, such as piceatannol or apigenin, are not used for CoQ synthesis in mammalian cells [27].

A hypothesis for the use of *p*-coumarate, resveratrol, and kaempferol as ring precursors of CoQ is that they are metabolized to produce 4HB. The set of reactions that allow this conversion is not yet identified but, independent of the metabolic route involved, an increase in alternative CoQ ring precursors in cells will only turn into higher CoQ levels if cells have a low availability of endogenous 4HB, which is the primary precursor of CoQ. The fact that the availability of 4HB is a rate-limiting step in the CoQ biosynthetic pathway has been previously described in yeast and in mammalian kidney cells [21,27]. Supplementing mammalian kidney cells with exogenous 4HB resulted in an increase in CoQ levels four- to six-fold higher as compared with the non-supplemented control [27]. This observation led the authors to propose the possibility that increasing the availability of CoQ precursors in cells could move the metabolic flux in favor of the biosynthesis of CoQ, helping to ameliorate the phenotype associated with certain Q deficiencies.

Yeast and human genes essential for CoQ biosynthesis

Yeast *COQ1*; human *PDSS1* and *PDSS2*

In yeast and human cells, the synthesis of the polyisoprenyl diphosphate tail derives from a non-sterol branch of the mevalonate pathway [7]. Yeast Coq1 is responsible for the synthesis of the hexaprenyl diphosphate tail moiety from the precursors dimethylallyl diphosphate and isopentenyl diphosphate [30]. The Coq1 polypeptide is peripherally associated with the matrix side of the inner mitochondrial membrane [31]. The analogous polyprenyl diphosphate synthases in other species determine the tail length (*n*) of the CoQ_n (ubiquinone-n or coenzyme Q_n (refers to a specific isoform, where n is number of isoprenyl units in the tail of CoQ_n, e.g. CoQ_{10} in humans, CoQ_6 in *S. cerevisiae*)) produced [32], and when expressed in yeast direct the synthesis of corresponding isoforms of CoQ_n [33]. The yeast Coq1 polypeptide is not associated with the CoQ synthome, but its lipid product is essential for the formation and/or stabilization of this complex [31,34].

PDSS1 and PDSS2 form a heterotetramer responsible for the synthesis of the decaprenyl-diphosphate tail precursor used to synthesize CoQ_{10} in human cells [35]. Patients with partial deficiencies in PDSS1 [36] and PDSS2 [37] show severe disruptions in multiple organ systems. As reviewed in this volume [8], the complexity of phenotypes is a hallmark of mitochondrial deficiency diseases.

Yeast *COQ2*; human *COQ2*

The yeast Coq2 polypeptide is required for the attachment of the polyisoprenyl 'tail' to 4HB [38]. In yeast, Coq2 generates 3-hexaprenyl-4-hydroxy benzoic acid (HHB; Figure 1), the first polyisoprenylated ring CoQ-intermediate in the biosynthetic pathway. This early hydrophobic CoQ-intermediate was found to accumulate in many of the yeast *coq* null mutants, including the *coq3-coq9* null mutants [39,40]. Coq2 is imported into mitochondria via the Tim23 pathway [41], and is an integral membrane protein of the inner mitochondrial membrane [34]. It was originally hypothesized that Coq2 might serve to anchor the CoQ-synthome to the inner mitochondrial membrane [11], however there is no evidence that Coq2 is associated with the other Coq polypeptides that assemble into the CoQ-synthome [12]. Instead it appears that polyisoprenylated CoQ-intermediates produced by Coq1 and Coq2 are important for the stabilization of the CoQ synthome [34] (Figure 2).

Forsgren et al. [42] isolated human *COQ2* cDNA and showed its expression in a yeast *coq2* null mutant restored CoQ_6 biosynthesis. Recently, Desbats et al. [43] have defined the 5′ transcription start sites of the human *COQ2* transcript, indicating that of four potential upstream ATG translation initiation codons, the first two are rarely (if ever) used and that it is the fourth ATG that is in fact predominant. All isoforms of COQ2 were shown to co-localize to mitochondria. This finding argues against the previous hypothesis that the shorter COQ2 isoforms may represent non-mitochondrial polypeptides that may mediate cytoplasmic prenylation of 4HB [42]. The predominant use of the fourth ATG results in a shorter COQ2 polypeptide and the authors suggest new numbering that should be used to

Essays in Biochemistry (2018) **62** 361–376
https://doi.org/10.1042/EBC20170106

designate mutations of human COQ2 [43]. Desbats et al. [43] found a good correlation between disease severity in patients and the effect of *COQ2* mutations on the decreased production of CoQ_6 in a yeast complementation assay. Patients who harbored two alleles that markedly impair CoQ biosynthesis manifested multisystem severe clinical symptoms at birth or infancy, while patients who had a least one allele with residual CoQ biosynthesis manifested isolated steroid resistant nephrotic syndrome (SRNS) or adult onset encephalopathy [43].

Based on two structures determined for prokaryotic homologs of COQ2 (UbiA family aromatic prenyltransferases), human COQ2 is proposed to contain nine transmembrane helices [43]. The C-terminus of human COQ2 resides in the intermembrane space in mitochondria of HEK293 cells [43]. A recent structural model is compatible with this suggestion and predicts that the active site of human COQ2 faces the matrix [44]. Two of the disease-related mutations (given in the old nomenclature) are posited to interfere with the binding of the polyisoprenyl diphosphate (R197H) or to clash with the Mg^{2+} ions that participate in catalysis (A302V) [44].

A recent study by Herebian et al. [45] demonstrated that supplementation with 4HB fully restores endogenous CoQ_{10} biosynthesis in partially deficient COQ2 human fibroblasts harboring homozygous mutant alleles, including the A302V severe allele. Based on an *in silico* model of human COQ2, the authors identified several binding sites for 4HB and posited a channel for 4HB transport across the inner mitochondrial membrane. The authors proposed that the rescue of CoQ_{10} synthesis in fibroblasts from COQ2-deficient patients by treatment with 4HB may represent amelioration of a 4HB transport deficit and/or an enhancement of activity by increased supply of the ring substrate [45]. It will be important to experimentally determine whether the COQ2 polypeptide also functions as a 4HB transporter. In addition to restoring CoQ_{10} levels, the 4HB treatment also increased the steady state levels of COQ4 and COQ7 proteins involved in CoQ biosynthesis, and enhanced cell viability in response to stress conditions. This finding makes sense in light of the important role that CoQ and CoQ-intermediates play in stabilizing the CoQ-synthome in yeast and Complex Q in human cells [7,12,34]. This rescue of COQ2-deficient cells by 4HB treatment is quite striking and deserves further testing as a potential therapy. Even a small enhancement in the biosynthesis of CoQ is able to restore a wide array of phenotypes associated with CoQ deficiency [46].

Yeast *COQ3*; human *COQ3*

Yeast Coq3 is an *S*-adenosylmethionine (AdoMet)-dependent methyltransferase required for the two *O*-methylation steps of CoQ biosynthesis [47-49]. Coq3 is peripherally associated with the matrix-side of the mitochondrial inner membrane [49]. Recent studies reveal that *E. coli* UbiG, a functional homolog of Coq3, binds to liposomes containing cardiolipin [50]. Structural determination of UbiG identifies it as a seven β-strand AdoMet-dependent methyltransferase that contains an unusual insertion sequence that mediates UbiG binding to membranes, and is required for CoQ biosynthesis [50].

Assays with farnesylated analogs of CoQ-intermediates provided early evidence that a complex of yeast Coq polypeptides is required to observe the Coq3 *O*-methyltransferase activity and hence CoQ biosynthesis [39,51]. Recovery of the yeast Coq3-consecutive non-denaturing affinity purification (CNAP) tagged polypeptide from digitonin-solubilized mitochondrial extracts showed that it co-purified with Coq4, Coq5, Coq6, Coq7, Coq9, and Coq11 polypeptides, in a high molecular mass complex that contained CoQ_6 and several CoQ_6-intermediates [12]. Thus Coq3 is an integral member of the CoQ synthome in yeast. The phosphorylation state of Coq3 may modulate the stability of the Coq3 polypeptide and that of the CoQ synthome [52,53]. Overexpression of Coq8, an atypical putative protein kinase, has been shown to stabilize several Coq polypeptides and the CoQ synthome in certain yeast *coq* null mutants [24,34]. Indeed, overexpression of Coq8 in the yeast *coq3* null mutant increased steady state levels of the Coq4, Coq6, Coq7, and Coq9 polypeptides, and stabilized the CoQ synthome. Treatment of *coq3* null mutants overexpressing Coq8 with vanillic acid (a 4HB analog that should bypass the first hydroxylation and first methylation steps) resulted in the production of the late stage CoQ-intermediate DMQ_6 [24] (Figure 1). This finding indicates the potential difficulties in using analogs of 4HB to bypass deficiencies in Coq3, due to its involvement in two *O*-methylation steps, and to the apparent absence of Coq7 hydroxylase activity. It is tempting to speculate that treatment with 2,3-dimethoxy-4HB might serve to bypass both *O*-methyltransferase deficient steps in the *coq3* null mutant. Such bypass would require that this analog could still be prenylated by Coq2, and subjected to decarboxylation, hydroxylation and *C*-methylation steps.

Expression of human COQ3 in yeast *coq3* null mutants rescued growth on a non-fermentable source and partially restored the biosynthesis of CoQ_6 [54]. Assays with farnesylated analogs of CoQ-intermediates showed that mitochondria prepared from *coq3* null mutant yeast expressing human COQ3 performed both *O*-methylation steps [54]. Many lines of evidence indicate a similar Complex Q containing the COQ3–COQ9 polypeptides is involved in

human CoQ_{10} biosynthesis [7]. So far, no mutations causing primary CoQ_{10} deficiency have been reported for the human *COQ3* gene.

Yeast *COQ4*; human *COQ4*

Yeast Coq4 is required for CoQ_6 biosynthesis in yeast, and is peripherally associated with the inner mitochondrial membrane on the matrix side [55]. It is thought to serve as a scaffold or organizer for the CoQ synthome [34,56], as it is associated with Coq3, Coq6, and Coq9 [12,51,57]. No enzyme activity or exact function has been associated with the Coq4 polypeptide. A known crystal structure of the Coq4 domain, determined as part of the structural genomics effort (PDB: 3KB4, Northeastern structural genomics program) identified long hydrophobic α helices bound to a geranylgeranyl monophosphate lipid. A conserved $HDxxHx_{10-13}E$ motif [56] chelated a magnesium ion (Mg^{2+}) near to the phosphate head group [57]. From this structure, the function of Coq4 is speculated to bind the long polyisoprenyl tail of CoQ-intermediates and/or CoQ and to organize the enzymes that perform the ring modifications [34,57] (Figure 2).

Human COQ4 was shown to be a functional ortholog of yeast Coq4, and is capable of restoring CoQ_6 biosynthesis in the yeast *coq4* null mutant [58]. Distinct *COQ4* RNA transcripts indicated the potential for two different isoforms of the human COQ4 polypeptide; the longest isoform was shown to possess a mitochondrial targetting sequence, was localized to mitochondria in HeLa cells, and restored CoQ_6 biosynthesis in the yeast *coq4* null mutant. The functional significance of the shorter isoform is not known; it lacks the mitochondrial targetting sequence and failed to rescue *coq4* mutant yeast.

Patients who harbor two recessive *COQ4* mutant alleles exhibit a broad spectrum of mitochondrial disorders associated with CoQ_{10} deficiencies [59]. Intriguingly, haploinsufficiency of *COQ4* also causes CoQ_{10} deficiency in both human and yeast diploid cells [60]. Recently a heterozygous missense E161D mutation in *COQ4* was reported in a patient with lethal rhabdomyolysis; introduction of the missense mutation was introduced to iPSCs, and recapitulated the muscle-specific CoQ_{10} deficiency [61].

Yeast *COQ5*; human *COQ5*

The yeast Coq5 polypeptide is an AdoMet-dependent methyltransferase required for the *C*-methylation step of CoQ biosynthesis [62,63]. It is peripherally associated with the matrix-side of the mitochondrial inner membrane [64]. Dai et al. [65] determined the structure of yeast Coq5; it has a typical seven β-strand AdoMet methyltransferase structure, and the protein was crystallized both in the presence and absence of AdoMet. The catalytic mechanism is yet to be determined; based on modeling the authors proposed an active site highly conserved Arg^{201} or Tyr^{78} act to deprotonate a water molecule that then acts as the base to deprotonate the C5-ring H from $DDMQ_6H_2$ [65]. Yeast *coq5* point mutants that harbor mutations in the Class I methyltransferase motifs result in a loss of *C*-methyltransferase function, but retain steady state levels of the Coq5 polypeptide, and of the Coq polypeptide partner proteins of the CoQ synthome. In contrast, these CoQ synthome partner proteins are destabilized in the *coq5* null mutant [64]. Overexpression of Coq8 in the *coq5* null yeast mutant results in the increased steady-state levels of the Coq4, Coq7, Coq9 polypeptides, the stabilization of the CoQ synthome, and the accumulation of $DDMQ_6H_2$, the substrate of Coq5 [24,34] (Figure 1). It is possible that the 4HB analog 2-methyl-4-BH might function to bypass the defect in *coq5* point mutants with stable Coq5 polypeptide, however, this has not yet been tested.

Regulated expression of yeast Coq5 is necessary for the correct assembly of the CoQ synthome. Recently, two mechanisms of COQ5 post-transcriptional regulation have been elucidated. The RNA binding protein Puf3 regulates the translation of appropriate amounts of Coq5 so the CoQ synthome can be assembled [66]. Oct1 is a mitochondrial matrix-localized protease that removes eight residues from the amino-terminal mitochondrial targetting sequence of Coq5 and is essential for formation of the mature amino-terminus of Coq5 and its stability [67]. There is also evidence that yeast Coq5 is phosphorylated in a Coq8-dependent manner [53].

Expression of the human COQ5 polypeptide was found to rescue the CoQ_6 biosynthetic defect of the *coq5* point mutants or in a *coq5* null mutant overexpressing Coq8, but not a *coq5* null mutant [68]. Thus, human COQ5 is an ortholog of yeast Coq5, but can rescue yeast only when the other yeast Coq partner proteins are present and the CoQ synthome is assembled. Primary CoQ_{10} deficiency has been recently diagnosed due to a partial loss of function of COQ5 [69]. The deficiency is shown to be due to a duplication of the *COQ5* gene, and that due to alternative splicing appears to generate an unstable *COQ5* mRNA with a long 3′-UTR. Steady state levels of the COQ5 polypeptide were dramatically decreased in fibroblasts from the affected homozygous patients as compared with controls. The affected patients had variable degrees of cerebellar ataxia, and showed a modest decrease in the levels of CoQ_{10} in peripheral blood leukocytes, and a more dramatic decrease in CoQ_{10} levels in a skeletal muscle biopsy [69]. The reduction in

Essays in Biochemistry (2018) **62** 361–376
https://doi.org/10.1042/EBC20170106

CoQ_{10} levels is consistent with the observation that decreases in COQ5-containing mitochondrial protein complex impairs the production of CoQ_{10} [70].

Yeast *COQ6*; human *COQ6*

The yeast Coq6 polypeptide is characterized as a flavin-dependent monooxygenase [71]. Conserved catalytic regions in Coq6 include the ADP binding fingerprint, the NAD(P)H/FAD binding motif, and the ribityl binding region [71]. Yeast Coq6 co-purifies with a tightly bound FAD, and modeling studies are consistent with its proposed activity as a ring hydroxylase [72]. Yeast Coq6 is responsible for the first hydroxylation step (ring C5) in CoQ biosynthesis [73]. It is also necessary for the deamination of ring C4 in *S. cerevisiae* when pABA is used an aromatic ring precursor [22]. The yeast Coq6 polypeptide is peripherally associated with inner mitochondrial membrane on the matrix side [71], and associates with Coq4, Coq5, Coq7, Coq8, and Coq9 polypeptides of the CoQ synthome [12]. Recent investigations discovered a physical association of Coq6 with Coq8 [12]. Yeast *coq6* point mutants that affect the active site but preserve steady state levels of the Coq6 polypeptide and assembly of the CoQ synthome may be rescued by providing alternate ring precursors such as 3,4-diHB and vanillic acid (Figure 1). These alternate ring precursors, once prenylated by Coq2, allow the defective *coq6* step to be bypassed [73]. Such bypass is also effective in *coq6* null yeast mutants provided yeast *COQ8* is overexpressed [24].

The human homolog COQ6, is able to rescue a yeast *coq6* null mutant [25,74], and interacts with human COQ8B (ADCK4) and COQ7 [75]. Yeast *coq6* null mutants expressing certain hypomorphic mutations of human *COQ6* are rescued by treatment with either 3,4-diHB or vanillic acid [25]. The effectiveness of such bypass therapies as treatments for patients with mutations in *COQ6* remains to be explored. It seems possible that these alternate ring precursors might serve to restore endogenous CoQ_{10} biosynthesis in patients with *COQ6* deficiencies.

Mutations in human *COQ6* have been implicated in an autosomal recessive disease characterized by severe progressive nephrotic syndrome and deafness [74]. It has been suggested that kidney biopsy should be performed on young children present with SRNS and sensorineural hearing loss [76]. The rationale for this suggestion is that the abnormal mitochondria in podocytes may provide an early diagnostic clue of mutations in CoQ biosynthetic genes. Supplementation with high doses of CoQ_{10} can stop the progression of kidney disease, and this therapy should be started immediately at first suspicion of CoQ_{10} deficiency [76,77].

Yeast *YAH1* and *ARH1*; human *FDX1*, *FDX2*, and *FDXR*

Unlike most flavin-dependent monooxygenases that utilize NAD(P)H directly as a source of electrons, the electrons from NAD(P)H are funneled indirectly to yeast Coq6 via the coupled system of ferredoxin (Yah1) an iron–sulphur protein, and ferredoxin reductase (Arh1) [73]. Yeast engineered to be transiently depleted in Yah1 or Arh1 were shown to be defective in the same C5 ring-hydroxylation step, and to accumulate the same polyisoprenylated ring-intermediates as yeast mutants harboring inactive *coq6* alleles [21,73]. *YAH1* and *ARH1* are essential genes in yeast, and in addition to CoQ biosynthesis, are also required for iron–sulphur cluster biosynthesis [78].

There are two human homologs of yeast Yah1 – FDX1 and FDX2. Human FDX2 was shown to complement the iron–sulphur cluster biosynthetic defect of Yah1 depleted yeast [79]. However, neither human FDX1 nor FDX2 were able to complement the CoQ_6 biosynthetic defect of Yah1 depleted yeast [73]. The human homolog of Arh1 is termed as FDXR, which functions as an electron transfer protein in cholesterol biosynthesis and overall steroid metabolism, as well as iron–sulphur cluster biosynthesis [78]. Whether FDX1, FDX2, or FDXR function to assist human COQ6 catalytic activity in the biosynthesis of CoQ_{10} is not yet known.

Yeast *COQ7 (CAT5)* and *PTC7*; human *COQ7* (*CAT5*, *CLK-1*) and *PPTC7*

Yeast Coq7 is a hydroxylase responsible for catalyzing the penultimate step of the CoQ biosynthetic pathway [80-82]. The hydroxylase activity depends on a carboxylate-bridged diiron binding motif, first identified as a highly conserved sequence across a wide array of organisms, and predicted to mediate hydroxylation similar to other members of the carboxylate-bridged diiron protein family, such as methane monoxygenase, ribonucleotide reductase, and phenol-hydroxylase [82]. Modeling predicted Coq7 to be a four-helix bundle protein with an additional helix mediating an interfacial association with the membrane [82]. Experiments with isolated mitochondria and mitoplasts show yeast Coq7 polypeptide is peripherally associated with inner mitochondrial membrane on the matrix side [34].

Expression of human COQ7 rescues the CoQ_6 deficiency of yeast *coq7* null mutants [83], indicating profound conservation of function. Overexpression of a soluble fusion protein containing human COQ7 polypeptide fused to an immunoglobulin-binding domain of protein G was purified (termed as GB1-hCLK-1) and spectroscopic and kinetic methods provided evidence for the presence of the diiron center [84]. Binding of the substrate analogs DMQ_0 or

DMQ_2 to GB1-hCLK1 mediated the reduction in the diiron site by NADH and in the presence of O_2 the hydroxylation step was catalyzed [84].

Yeast *coq7* null mutants accumulate the early CoQ-intermediates HHB and HAB, while *coq7* point mutants [80] and *coq7* null mutants overexpressing Coq8 accumulate DMQ_6 the penultimate intermediate in the pathway [24,85]. Expression of the unrelated *E. coli* UbiF hydroxylase rescued a *coq7* point mutant, but failed to rescue the *coq7* null mutant [86]. These findings indicated Coq7 is an important polypeptide partner of the CoQ synthome; indeed, Coq7 co-purifies with tagged forms of Coq3, Coq6, and Coq9 polypeptides [12].

A mutation in the human *COQ7* gene is associated with a primary ubiquinone deficiency, and results in multiple organ involvement [87]. Interestingly, the deficiencies in CoQ_{10} content and mitochondrial respiratory activities in fibroblasts isolated from this patient were improved following treatment with 2,4-diHB, a 4HB analog that bypasses the COQ7-dependent hydroxylase step [87]. The effectiveness of treatment with 2,4-diHB depends on the type of *COQ7* mutation(s) present in patients [88]. It is likely that the success of these bypass therapies will depend on the stable presence of other COQ polypeptides and their ability to form the CoQ synthome (or complex Q) [16,24]. Regulated expression of COQ7 has been shown to impact the rates of CoQ_{10} biosynthesis, both at the level of NF-κB transcriptional up-regulation of *COQ7* gene expression [89], and at the level of RNA binding proteins that mediate stability of *COQ7* mRNA [90]. The regulated expression of COQ7 and the other component polypeptides of the CoQ synthome seem likely to influence its assembly and function, and so impact biosynthesis of CoQ_{10}.

Yeast Coq7 is modified by phosphorylation [12,53]. Predictive algorithms suggested that the phosphorylation status of Coq7 was regulatory for CoQ_6 biosynthesis, with at least three predicted phosphorylation sites on Ser^{20}, Ser^{28}, and Thr^{32} [91]. When these residues are replaced with alanine, phosphorylation was abolished and CoQ_6 levels were significantly increased in yeast expressing Coq7 with the triple-Alanine substitution. In contrast, yeast expressing the Coq7 with substitution of acidic residues at these residues (Asp^{20}, Glu^{28}, and Asp^{32}) had decreased levels of CoQ_6 and accumulated DMQ_6, indicating that the non-phosphorylatable form of Coq7 is the active form that catalyzes the penultimate pathway step [91]. Other sites of phosphorylation may also influence Coq7 activity; yeast expressing Coq7 harboring the phosphomimetic Ser^{114}Glu substitution also produced lower amounts of CoQ_6 and accumulated DMQ_6 [92].

The phosphatase responsible for Coq7 dephosphorylation is Ptc7, a *bona fide* mitochondrial serine/threonine protein phosphatase belonging to the PPM family of phosphatases [93]. It was recently discovered that two distinct forms of *PTC7* RNA exist, spliced and non-spliced forms, displaying a rare case of alternative splicing in yeast that results in two viable isoforms of a spliced protein [94,95]. The previously reported Ptc7 phosphatase was shown to be the spliced form ($Ptc7_s$) that resides in the mitochondria, while the non-spliced form ($Ptc7_{ns}$) is a nuclear membrane localized protein that contains a transmembrane helix that anchors it to the nuclear membrane [94]. Exclusive expression of $Ptc7_s$ showed significantly higher *de novo* CoQ biosynthesis, as compared with $Ptc7_{ns}$. These findings suggest that the mitochondrial targetting of the Ptc7s results in Coq7 dephosphorylation, and allows Coq7 to catalyze the penultimate step of the CoQ biosynthetic pathway [95]. Ptc7s acts to dephosphorylate other mitochondrial proteins, and deletion of *ptc7* perturbs mitochondrial function [96]. PPTC7 is the human serine/threonine phosphatase homolog of yeast Ptc7, however it is not known whether phosphorylation regulates human COQ7, and if so, whether PPTC7 recognizes it as a substrate.

Yeast *COQ8*; human *COQ8A* (*ADCK3*) and *COQ8B* (*ADCK4*)

The *S. cerevisiae* Coq8 polypeptide is identified as a putative kinase in the biosynthetic pathway of CoQ_6. Coq8 harbors six of twelve motifs present in protein kinases and is required to observe the presence of phosphorylated forms of Coq3, Coq5, and Coq7 polypeptides [53]. Coq8 co-purifies with the CoQ synthome [12]. Further, overexpression of Coq8 in certain of the *coq* null strains restores steady state levels of Coq4, Coq7, and Coq9, and stabilizes the formation of the CoQ synthome [24,34].

Expression of human COQ8A (ADCK3) in yeast *coq8* mutant strains restored CoQ_6 biosynthesis and the phosphorylation state of several of the yeast Coq polypeptides, indicating a profound conservation of function [53]. Rescue of yeast *coq8* mutants by human COQ8A depended on fusion to a yeast mitochondrial targetting sequence [53]. Yeast Coq8 and human COQ8A are homologs of atypical protein kinases. These proteins are able to autophosphorylate and show a surprising affinity and selectivity for ADP, as opposed to ATP [97]. Human COQ8A lacks *in vitro* protein kinase activity and instead shows ATPase activity that is essential for CoQ biosynthesis [98]. The ATPase activity is strongly activated by cardiolipin and small molecule mimics of CoQ intermediates [99]. Thus, the ATPase function of yeast Coq8 and human COQ8A is proposed to function in a chaperone-like activity to facilitate the assembly of the CoQ synthome and *de novo* [65] biosynthesis of CoQ [99].

Essays in Biochemistry (2018) **62** 361–376
https://doi.org/10.1042/EBC20170106

Expression of human COQ8B (ADCK4) also rescues CoQ_6 biosynthesis in yeast *coq8* mutants [100]. Although the amino terminus of COQ8B has a typical mitochondrial matrix targetting sequence, rescue of *coq8* mutant yeast by COQ8B depends on the addition of a yeast mitochondrial targetting sequence [100]. The effect of a *COQ8B* polymorphism present in 50% of the European population (COQ8B-H174R) was tested in the yeast expression model. Yeast *coq8* mutants expressing the human COQ8B-His^{174} polypeptide had decreased steady state levels of the COQ8B polypeptide, decreased growth on medium containing a non-fermentable carbon source, and decreased CII + CIII activity as compared with mutants expressing the COQ8B-Arg^{174} polypeptide [100]. Thus, it is possible that this common COQ8B polymorphism may represent a risk factor for secondary CoQ_{10} deficiencies. Various human diseases are directly associated with mutations in the *COQ8A* and *COQ8B* genes. Most prevalent are recessive ataxia and childhood-onset cerebellar ataxia associated with mutated *COQ8A* [101,102], and a steroid-resistant nephrotic disease related to mutated *COQ8B* [75,100].

Yeast *COQ9*; human *COQ9*

In *S. cerevisiae,* Coq9 is required for CoQ biosynthesis, is a member of the CoQ synthome, and is peripherally associated with the inner mitochondrial membrane, on the matrix side [34,103]. A temperature-sensitive *coq9* mutant (*coq9-ts19*) shifted to the non-permissive temperature results in the disassembling of the CoQ synthome, demonstrating that Coq9 is essential for the formation and stabilization of the high-molecular mass complex [23]. Coq9 is required for the deamination of Carbon 4 on CoQ-intermediates when pABA is utilized as the ring precursor in yeast [23]. The removal of the ring nitrogen substituent depends on the function of Coq6, and yeast with *coq9* mutations accumulate 3-hexaprenyl-4-aminophenol (4-AP), an intermediate that has also been shown to build up in a *coq6* null mutant overexpressing *COQ8* [24]. It is therefore likely that both Coq6 and Coq9 are needed for the 5-hydroxylation and 4-deamination steps of CoQ-intermediates. Additionally, an accumulation of late-stage intermediates suggests Coq7 is not active in the absence of Coq9 [6,24]. In summary, the yeast Coq9 polypeptide is required for both Coq6 and Coq7 hydroxylation steps, via an indirect or supportive role.

Attempts to rescue yeast *coq9* null mutants by expression of human COQ9 have so far failed [104-106]. However, expression of human COQ9 rescued the yeast *coq9-ts19* mutant [106]. Under these conditions, a small amount of the human COQ9 polypeptide enhanced the synthesis of CoQ_6 from 4HB (but not from pABA) and co-purified with the yeast Coq6-CNAP tagged polypeptide, indicating that human COQ9 is able to interact with the yeast CoQ synthome.

The presence of both human COQ9 and human COQ7 are needed for the hydroxylation step catalyzed by COQ7, and the two polypeptides interact [13]. Human cells with deficiencies in COQ9 accumulate DMQ_{10}, the same intermediate that accumulates in COQ7 deficient cells [107]. Both COQ7 and COQ9 deficient cell lines respond to treatment with 2,4-diHB, another example of bypass therapy [108,109]. In fact, human fibroblasts with mutations in COQ9 show decreased steady state levels of the COQ7 polypeptide [109]. Interestingly, treatment with vanillic acid also restored function in the COQ9 deficient cells, but not the COQ7 deficient cells [108]. Perhaps human COQ9 and COQ6 function may also be linked, similar to the situation in yeast. In humans, *COQ9* mutations result in various disease states, including predominant encephalomyopathy and an autosomal-recessive neonatal-onset CoQ deficiency [104,107].

Yeast and human genes required for efficient CoQ biosynthesis

Yeast *COQ10*; human *COQ10A, COQ10B*

Unlike the completely CoQ-less *coq1–coq9* null mutants, the yeast *coq10* null mutant produces near wild-type levels of CoQ at stationary phase, but synthesizes CoQ less efficiently during log phase growth [110,111]. While CoQ is eventually produced at near normal levels, the *coq10* null mutant still has severe defects in respiratory electron transport and is sensitive to treatment with polyunsaturated fatty acids, phenotypes that are hallmarks of the *coq1–coq9* null mutants [110]. Thus, even though CoQ_6 content is similar to that of wild-type yeast, Coq10 is required for efficient function and biosynthesis of CoQ_6. The Coq10 polypeptide contains a steroidogenic acute regulatory (StAR)-related lipid transfer (StART) domain, and binds CoQ and late-stage CoQ-intermediates both *in vitro* and *in vivo*, suggesting Coq10 may function as a lipid chaperone involving delivery of CoQ from site of synthesis to sites of function [110-114].

Humans have two homologs of yeast *COQ10*, namely *COQ10A* and *COQ10B*. Each isoform has several transcript variants as a result of alternative transcription initiation and/or alternative splicing [6]. The function of the COQ10 polypeptide is widely conserved across different organisms; expression of homologs from either *Caulobacter crescentus* or human COQ10A rescue the impaired growth of yeast *coq10Δ* mutant yeast [110]. Currently, there is no

known disease phenotype associated with mutations in human *COQ10A* or *COQ10B*. However, the postulated lipid chaperone function of COQ10A and COQ10B makes these polypeptides intriguing targets for study of the movement of CoQ between mitochondrial membranes and the respiratory complexes.

Yeast *COQ11*; human *NDUFA9*

COQ11 (*YLR290C*) was recently identified to be required for efficient *de novo* CoQ biosynthesis in *S. cerevisiae*. Affinity purification of CNAP-tagged Coq11 showed Coq11-CNAP co-purified with Coq4, Coq5, and Coq7 – members of the high molecular mass CoQ synthome [12]. A separate high throughput study also identified Coq11 as a mitochondrial protein, confirming its localization to the portion of the cell where CoQ is synthesized [115]. Due to its novelty, the functional roles, organization, and stoichiometry of Coq11 within the CoQ-synthome are not yet fully understood. However, numerous features of Coq11 and its homologs solidify its link to CoQ biosynthesis. In five fungal genomes, the existence of Coq11-Coq10 fusion proteins suggests these proteins may have a functional relationship [12]. High throughput studies found *COQ11* to have a genetic correlation with both *COQ2* and *COQ10,* which further supports this hypothesis [115]. Sequence analyses establish Coq11 as a member of the atypical short-chain dehydrogenase/reductase superfamily of oxidoreductases (SDR). SDR superfamily proteins contain a conserved Rossmann fold, a protein structural motif used to bind nucleotide co-factors such as FAD, FMN, and NAD(P) [116]. This bound co-factor is then used to assist the protein in its catalysis of different chemical reactions including isomerization, decarboxylation, epimerization, imine reduction, and carbonyl-alcohol oxidoreduction [116,117]. It is therefore tempting to speculate that Coq11 may use its Rossmann fold to perform enzymatic reactions within the CoQ biosynthetic pathway.

Interestingly, a protein similarity network analysis reveals that the taxonomy of YLR290C-like proteins includes the SDR subfamily protein NDUFA9, an auxiliary subunit of Complex I in humans important for complex stability [12,118-120]. Patients with decreased levels of NDUFA9 are unable to assemble Complex I properly and may develop a degenerative infancy respiratory disorder known as Leigh syndrome, which is often fatal in the first years of life [121,122]. Differences in *NDUFA9* deficiency produce phenotypic variations in patients [46]. It will be challenging to evaluate whether NDUFA9 deficiencies impact CoQ biosynthesis directly, because the deficiencies resulting from Complex I defects (and other mitochondrial defects) may secondarily influence CoQ biosynthesis [123,124]. Further exploration of Coq11 homology with NDUFA9 will help define their functional relationship.

Summary

- The *COQ1–COQ11* genes identified in the *S. cerevisiae* yeast model are required for efficient biosynthesis of CoQ_6.
- Expression of human homologs of yeast *COQ1–COQ10* genes restore CoQ biosynthesis in the corresponding yeast *coq* mutants, indicating profound functional conservation.
- Yeast provides a simple yet powerful model to investigate and define the function and possible pathology of human *COQ* gene polymorphisms and mutations.
- Simple natural products may serve as alternate ring precursors in CoQ biosynthesis, and these compounds may act to enhance biosynthesis of CoQ or may bypass select deficient steps.
- Biosynthesis of CoQ in yeast and human cells depends on high molecular mass multi-subunit complexes consisting of several of the *COQ* gene products, as well as CoQ itself and CoQ-intermediates.
- Thus the CoQ synthome in yeast, or Complex Q in human cells is essential for *de novo* biosynthesis of CoQ.

Acknowledgements

We thank Dr A. Tzagoloff (Columbia University) for the original yeast *coq* mutant strains. We also thank the UCLA Molecular Instrumentation Core for the use of the QTRAP 4000.

Essays in Biochemistry (2018) **62** 361–376
https://doi.org/10.1042/EBC20170106

Competing interests

The authors declare that there are no competing interests associated with this manuscript.

Funding

This work was supported in part by the National Science Foundation [grant number MCB-1330803 (to C.F.C.)]; and the National Institutes of Health [grant number T32 GM 008496 (to M.C.B. and H.T.)].

Author contribution

A.M.A., M.C.B., L.F.-d.-R., A.N., H.T., and C.F.C. contributed to drafting this review, revising it for intellectual content and approved the final version. A.M.A., A.N., L.F.-d.R., and C.F.C. contributed to preparation of the figures.

Abbreviations

AdoMet, *S*-adenosylmethionine; CNAP, consecutive non-denaturing affinity purification; CoQ, ubiquinone or coenzyme Q; $CoQH_2$, ubiquinol or CoQ hydroquinone; CoQ_n, ubiquinone-n or coenzyme Q_n (refers to a specific isoform, where n is number of isoprenyl units in the tail of CoQ_n, e.g. CoQ_{10} in humans, CoQ_6 in *Saccharomyces cerevisiae*); Coq, *Saccharomyces cerevisiae* polypeptide involved in CoQ_6 biosynthesis; COQ, human polypeptide involved in CoQ_{10} biosynthesis; *COQ*, yeast or human gene involved in CoQ biosynthesis; pABA, *para*-aminobenzoic acid; SDR, short-chain dehydrogenase/reductase superfamily of oxidoreductases; SRNS, steroid resistant nephrotic syndrome; 2,4-diHB, 2,4-dihydroxybenzoic acid; 3,4-diHB, 3,4-dihydroxybenzoic acid; 4HB, 4-hydroxybenzoic acid; 4HBz, 4-hydroxybenzaldehyde.

References

1 Turunen, M., Olsson, J. and Dallner, G. (2004) Metabolism and function of coenzyme Q. *Biochim. Biophys. Act.* **1660**, 171–199, https://doi.org/10.1016/j.bbamem.2003.11.012
2 Crane, F.L. (2001) Biochemical functions of coenzyme Q_{10}. *J. Am. Coll. Nutr.* **20**, 591–598, https://doi.org/10.1080/07315724.2001.10719063
3 Bentinger, M., Brismar, K. and Dallner, G. (2007) The antioxidant role of coenzyme Q. *Mitochondrion* **7S**, S41–S50, https://doi.org/10.1016/j.mito.2007.02.006
4 Aussel, L., Pierrel, F., Loiseau, L., Lombard, M., Fontecave, M. and Barras, F. (2014) Biosynthesis and physiology of coenzyme Q in bacteria. *Biochim. Biophys. Acta* **1837**, 1004–1011, https://doi.org/10.1016/j.bbabio.2014.01.015
5 Hayashi, K., Ogiyama, Y., Yokomi, K., Nakagawa, T., Kaino, T. and Kawamukai, M. (2014) Functional conservation of coenzyme Q biosynthetic genes among yeasts, plants, and humans. *PLoS ONE* **9**, 14, https://doi.org/10.1371/journal.pone.0099038
6 Wang, Y. and Hekimi, S. (2013) Molecular genetics of ubiquinone biosynthesis in animals. *Crit. Rev. Biochem. Mol. Biol.* **48**, 69–88, https://doi.org/10.3109/10409238.2012.741564
7 Stefely, J.A. and Pagliarini, D.J. (2017) Biochemistry of mitochondrial coenzyme Q biosynthesis. *Trends Biochem. Sci.* **42**, 824–843, https://doi.org/10.1016/j.tibs.2017.06.008
8 Alcázar-Fabra, M., Trevisson, E. and Brea-Calvo, G. (2018) Clinical syndromes associated with Coenzyme Q_{10} deficiency. *Essays Biochem.* **62**, 377–398, https://doi.org/10.1042/EBC20170107
9 Tzagoloff, A., Akai, A. and Needleman, R.B. (1975) Assembly of the mitochondrial membrane system. Characterization of nuclear mutants of *Saccharomyces cerevisiae* with defects in mitochondrial ATPase and respiratory enzymes. *J. Biol. Chem.* **250**, 8228–8235
10 Tzagoloff, A. and Dieckmann, C.L. (1990) *PET* genes of *Saccharomyces cerevisiae*. *Microbiol. Rev.* **54**, 211–225
11 Tran, U.C. and Clarke, C.F. (2007) Endogenous synthesis of coenzyme Q in eukaryotes. *Mitochondrion* **7S**, S62–S71, https://doi.org/10.1016/j.mito.2007.03.007
12 Allan, C.M., Awad, A.M., Johnson, J.S., Shirasaki, D.I., Wang, C., Blaby-Haas, C.E. et al. (2015) Identification of Coq11, a new coenzyme Q biosynthetic protein in the CoQ-Synthome in *Saccharomyces cerevisiae*. *J. Biol. Chem.* **290**, 7517–7534, https://doi.org/10.1074/jbc.M114.633131
13 Lohman, D.C., Forouhar, F., Beebe, E.T., Stefely, M.S., Minogue, C.E., Ulbrich, A. et al. (2014) Mitochondrial COQ9 is a lipid-binding protein that associates with COQ7 to enable coenzyme Q biosynthesis. *Proc. Natl. Acad. Sci. U.S.A.* **111**, E4697–E4705, https://doi.org/10.1073/pnas.1413128111
14 Clarke, C.F. (2000) New advances in coenzyme Q biosynthesis. *Protoplasma* **213**, 134–147, https://doi.org/10.1007/BF01282151
15 Kawamukai, M. (2016) Biosynthesis of coenzyme Q in eukaryotes. *Biosci. Biotechnol. Biochem.* **80**, 23–33, https://doi.org/10.1080/09168451.2015.1065172
16 Pierrel, F. (2017) Impact of chemical analogs of 4-hydroxybenzoic acid on coenzyme Q biosynthesis: from inhibition to bypass of coenzyme Q deficiency. *Front. Physiol.* **8**, 436, https://doi.org/10.3389/fphys.2017.00436
17 Payet, L.A., Leroux, M., Willison, J.C., Kihara, A., Pelosi, L. and Pierrel, F. (2016) Mechanistic details of early steps in coenzyme Q biosynthesis pathway in yeast. *Cell Chem. Biol.* **23**, 1241–1250, https://doi.org/10.1016/j.chembiol.2016.08.008
18 Stefely, J.A., Kwiecien, N.W., Freiberger, E.C., Richards, A.L., Jochem, A., Rush, M. J.P. et al. (2016) Mitochondrial protein functions elucidated by multi-omic mass spectrometry profiling. *Nat. Biotechnol.* **34**, 1191–1197, https://doi.org/10.1038/nbt.3683
19 Zahedi, R.P., Sickmann, A., Boehm, A.M., Winkler, C., Zufall, N., Schonfisch, B. et al. (2006) Proteomic analysis of the yeast mitochondrial outer membrane reveals accumulation of a subclass of preproteins. *Mol. Biol. Cell* **17**, 1436–1450, https://doi.org/10.1091/mbc.e05-08-0740

20 Marbois, B., Xie, L.X., Choi, S., Hirano, K., Hyman, K. and Clarke, C.F. (2010) para-Aminobenzoic acid is a precursor in coenzyme Q_6 biosynthesis in *Saccharomyces cerevisiae*. *J. Biol. Chem.* **285**, 27827–27838, https://doi.org/10.1074/jbc.M110.151894
21 Pierrel, F., Hamelin, O., Douki, T., Kieffer-Jaquinod, S., Muhlenhoff, U., Ozeir, M. et al. (2010) Involvement of mitochondrial ferredoxin and para-aminobenzoic acid in yeast coenzyme Q biosynthesis. *Chem. Biol.* **17**, 449–459, https://doi.org/10.1016/j.chembiol.2010.03.014
22 Ozeir, M., Pelosi, L., Ismail, A., Mellot-Draznieks, C., Fontecave, M. and Pierrel, F. (2015) Coq6 is responsible for the C4-deamination reaction in coenzyme Q biosynthesis in *Saccharomyces cerevisiae*. *J. Biol. Chem.* **290**, 24140–24151, https://doi.org/10.1074/jbc.M115.675744
23 He, C.H., Black, D.S., Nguyen, T.P., Wang, C., Srinivasan, C. and Clarke, C.F. (2015) Yeast Coq9 controls deamination of coenzyme Q intermediates that derive from para-aminobenzoic acid. *Biochim. Biophys. Acta* **1851**, 1227–1239, https://doi.org/10.1016/j.bbalip.2015.05.003
24 Xie, L.X., Ozeir, M., Tang, J.Y., Chen, J.Y., Jaquinod, S.K., Fontecave, M. et al. (2012) Overexpression of the Coq8 kinase in *Saccharomyces cerevisiae coq* null mutants allows for accumulation of diagnostic intermediates of the coenzyme Q_6 biosynthetic pathway. *J. Biol. Chem.* **287**, 23571–23581, https://doi.org/10.1074/jbc.M112.360354
25 Doimo, M., Trevisson, E., Airik, R., Bergdoll, M., Santos-Ocana, C., Hildebrandt, F. et al. (2014) Effect of vanillic acid on *COQ6* mutants identified in patients with coenzyme Q_{10} deficiency. *Biochim. Biophys. Acta* **1842**, 1–6, https://doi.org/10.1016/j.bbadis.2013.10.007
26 Xie, L.X., Williams, K.J., He, C.H., Weng, E., Khong, S., Rose, T.E. et al. (2015) Resveratrol and para-coumarate serve as ring precursors for coenzyme Q biosynthesis. *J. Lipid Res.* **56**, 909–919, https://doi.org/10.1194/jlr.M057919
27 Fernandez-Del-Rio, L., Nag, A., Gutierrez Casado, E., Ariza, J., Awad, A.M., Joseph, A.I. et al. (2017) Kaempferol increases levels of coenzyme Q in kidney cells and serves as a biosynthetic ring precursor. *Free Radic. Biol. Med.* **110**, 176–187, https://doi.org/10.1016/j.freeradbiomed.2017.06.006
28 Alam, S.S., Nambudiri, A.M. and Rudney, H. (1975) J-Hydroxybenzoate: polyprenyl transferase and the prenylation of 4-aminobenzoate in mammalian tissues. *Arch. Biochem. Biophys.* **171**, 183–190, https://doi.org/10.1016/0003-9861(75)90022-3
29 Gonzalez-Aragon, D., Buron, M.I., Lopez-Lluch, G., Herman, M.D., Gomez-Diaz, C., Navas, P. et al. (2005) Coenzyme Q and the regulation of intracellular steady-state levels of superoxide in HL-60 cells. *Biofactors* **25**, 31–41, https://doi.org/10.1002/biof.5520250105
30 Ashby, M.N. and Edwards, P.A. (1990) Elucidation of the deficiency in two yeast coenzyme Q mutants. Characterization of the structural gene encoding hexaprenyl pyrophosphate synthetase. *J. Biol. Chem.* **265**, 13157–13164
31 Gin, P. and Clarke, C.F. (2005) Genetic evidence for a multi-subunit complex in coenzyme Q biosynthesis in yeast and the role of the Coq1 hexaprenyl diphosphate synthase. *J. Biol. Chem.* **280**, 2676–2681, https://doi.org/10.1074/jbc.M411527200
32 Okada, K., Suzuki, K., Kamiya, Y., Zhu, X., Fujisaki, S., Nishimura, Y. et al. (1996) Polyprenyl diphosphate synthase essentially defines the length of the side chain of ubiquinone. *Biochim. Biophys. Acta* **1302**, 217–223, https://doi.org/10.1016/0005-2760(96)00064-1
33 Okada, K., Kainou, T., Matsuda, H. and Kawamukai, M. (1998) Biological significance of the side chain length of ubiquinone in *Saccharomyces cerevisiae*. *FEBS Lett.* **431**, 241–244, https://doi.org/10.1016/S0014-5793(98)00753-4
34 He, C.H., Xie, L.X., Allan, C.M., Tran, U.C. and Clarke, C.F. (2014) Coenzyme Q supplementation or over-expression of the yeast Coq8 putative kinase stabilizes multi-subunit Coq polypeptide complexes in yeast *coq* null mutants. *Biochim. Biophys. Acta* **1841**, 630–644, https://doi.org/10.1016/j.bbalip.2013.12.017
35 Saiki, R., Nagata, A., Kainou, T., Matsuda, H. and Kawamukai, M. (2005) Characterization of solanesyl and decaprenyl diphosphate synthases in mice and humans. *FEBS J.* **272**, 5606–5622, https://doi.org/10.1111/j.1742-4658.2005.04956.x
36 Mollet, J., Giurgea, I., Schlemmer, D., Dallner, G., Chretien, D., Delahodde, A. et al. (2007) Prenyldiphosphate synthase, subunit 1 (*PDSS1*) and OH-benzoate polyprenyltransferase (*COQ2*) mutations in ubiquinone deficiency and oxidative phosphorylation disorders. *J. Clin. Invest.* **117**, 765–772, https://doi.org/10.1172/JCI29089
37 Lopez, L.C., Schuelke, M., Quinzii, C.M., Kanki, T., Rodenburg, R.J., Naini, A. et al. (2006) Leigh syndrome with nephropathy and CoQ_{10} deficiency due to decaprenyl diphosphate synthase subunit 2 (*PDSS2*) mutations. *Am. J. Hum. Genet.* **79**, 1125–1129, https://doi.org/10.1086/510023
38 Ashby, M.N., Kutsunai, S.Y., Ackerman, S., Tzagoloff, A. and Edwards, P.A. (1992) *COQ2* is a candidate for the structural gene encoding para-hydroxybenzoate:polyprenyltransferase. *J. Biol. Chem.* **267**, 4128–4136
39 Hsu, A.Y., Do, T.Q., Lee, P.T. and Clarke, C.F. (2000) Genetic evidence for a multi-subunit complex in the O-methyltransferase steps of coenzyme Q biosynthesis. *Biochim. Biophys. Acta* **1484**, 287–297, https://doi.org/10.1016/S1388-1981(00)00019-6
40 Johnson, A., Gin, P., Marbois, B.N., Hsieh, E.J., Wu, M., Barros, M.H. et al. (2005) *COQ9*, a new gene required for the biosynthesis of coenzyme Q in *Saccharomyces cerevisiae*. *J. Biol. Chem.* **280**, 31397–31404, https://doi.org/10.1074/jbc.M503277200
41 Leuenberger, D., Bally, N.A., Schatz, G. and Koehler, C.M. (1999) Different import pathways through the mitochondrial intermembrane space for inner membrane proteins. *EMBO J.* **18**, 4816–4822, https://doi.org/10.1093/emboj/18.17.4816
42 Forsgren, M., Attersand, A., Lake, S., Grunler, J., Swiezewska, E., Dallner, G. et al. (2004) Isolation and functional expression of human *COQ2*, a gene encoding a polyprenyl transferase involved in the synthesis of CoQ. *Biochem. J.* **382**, 519–526, https://doi.org/10.1042/BJ20040261
43 Desbats, M.A., Morbidoni, V., Silic-Benussi, M., Doimo, M., Ciminale, V., Cassina, M. et al. (2016) The *COQ2* genotype predicts the severity of coenzyme Q_{10} deficiency. *Hum. Mol. Genet.* **25**, 4256–4265, https://doi.org/10.1093/hmg/ddw257
44 Li, W. (2016) Bringing bioactive compounds into membranes: the UbiA superfamily of intramembrane aromatic prenyltransferases. *Trends Biochem. Sci.* **41**, 356–370, https://doi.org/10.1016/j.tibs.2016.01.007
45 Herebian, D., Seibt, A., Smits, S. H.J., Rodenburg, R.J., Mayatepek, E. and Distelmaier, F. (2017) 4-Hydroxybenzoic acid restores CoQ_{10} biosynthesis in human COQ2 deficiency. *Ann. Clin. Transl. Neurol.* **4**, 902–908, https://doi.org/10.1002/acn3.486
46 Baertling, F., Sanchez-Caballero, L., van den Brand, M. A.M., Fung, C.W., Chan, S.H., Wong, V.C. et al. (2018) *NDUFA9* point mutations cause a variable mitochondrial complex I assembly defect. *Clin. Genet.* **93**, 111–118, https://doi.org/10.1111/cge.13089
47 Clarke, C.F., Williams, W. and Teruya, J.H. (1991) Ubiquinone biosynthesis in *Saccharomyces cerevisiae*. Isolation and sequence of *COQ3*, the 3,4-dihydroxy-5-hexaprenylbenzoate methyltransferase gene. *J. Biol. Chem.* **266**, 16636–16644

48 Hsu, A.Y., Poon, W.W., Shepherd, J.A., Myles, D.C. and Clarke, C.F. (1996) Complementation of *coq3* mutant yeast by mitochondrial targeting of the *Escherichia coli* UbiG polypeptide: evidence that UbiG catalyzes both O-methylation steps in ubiquinone biosynthesis. *Biochemistry* **35**, 9797–9806, https://doi.org/10.1021/bi9602932

49 Poon, W.W., Barkovich, R.J., Hsu, A.Y., Frankel, A., Lee, P.T., Shepherd, J.N. et al. (1999) Yeast and rat Coq3 and *Escherichia coli* UbiG polypeptides catalyze both *O*-methyltransferase steps in coenzyme Q biosynthesis. *J. Biol. Chem.* **274**, 21665–21672, https://doi.org/10.1074/jbc.274.31.21665

50 Zhu, Y., Wu, B., Zhang, X., Fan, X., Niu, L., Li, X. et al. (2015) Structural and biochemical studies reveal UbiG/Coq3 as a class of novel membrane-binding proteins. *Biochem. J.* **470**, 105–114, https://doi.org/10.1042/BJ20150329

51 Marbois, B., Gin, P., Faull, K.F., Poon, W.W., Lee, P.T., Strahan, J. et al. (2005) Coq3 and Coq4 define a polypeptide complex in yeast mitochondria for the biosynthesis of coenzyme Q. *J. Biol. Chem.* **280**, 20231–20238, https://doi.org/10.1074/jbc.M501315200

52 Tauche, A., Krause-Buchholz, U. and Rodel, G. (2008) Ubiquinone biosynthesis in *Saccharomyces cerevisiae*: the molecular organization of *O*-methylase Coq3p depends on Abc1p/Coq8p. *FEMS Yeast Res.* **8**, 1263–1275, https://doi.org/10.1111/j.1567-1364.2008.00436.x

53 Xie, L.X., Hsieh, E.J., Watanabe, S., Allan, C.M., Chen, J.Y., Tran, U.C. et al. (2011) Expression of the human atypical kinase ADCK3 rescues coenzyme Q biosynthesis and phosphorylation of Coq polypeptides in yeast *coq8* mutants. *Biochim. Biophys. Acta* **1811**, 348–360, https://doi.org/10.1016/j.bbalip.2011.01.009

54 Jonassen, T. and Clarke, C.F. (2000) Isolation and functional expression of human *COQ3*, a gene encoding a methyltransferase required for ubiquinone biosynthesis. *J. Biol. Chem.* **275**, 12381–12387, https://doi.org/10.1074/jbc.275.17.12381

55 Belogrudov, G.I., Lee, P.T., Jonassen, T., Hsu, A.Y., Gin, P. and Clarke, C.F. (2001) Yeast *COQ4* encodes a mitochondrial protein required for coenzyme Q synthesis. *Arch. Biochem. Biophys.* **392**, 48–58, https://doi.org/10.1006/abbi.2001.2448

56 Marbois, B., Gin, P., Gulmezian, M. and Clarke, C.F. (2009) The yeast Coq4 polypeptide organizes a mitochondrial protein complex essential for coenzyme Q biosynthesis. *Biochim. Biophys. Acta* **1791**, 69–75, https://doi.org/10.1016/j.bbalip.2008.10.006

57 Rea, S.L., Graham, B.H., Nakamaru-Ogiso, E., Kar, A. and Falk, M.J. (2010) Bacteria, yeast, worms, and flies: exploiting simple model organisms to investigate human mitochondrial diseases. *Dev. Disabil. Res. Rev.* **16**, 200–218, https://doi.org/10.1002/ddrr.114

58 Casarin, A., Jimenez-Ortega, J.C., Trevisson, E., Pertegato, V., Doimo, M., Ferrero-Gomez, M.L. et al. (2008) Functional characterization of human *COQ4*, a gene required for Coenzyme Q_{10} biosynthesis. *Biochem. Biophys. Res. Commun.* **372**, 35–39, https://doi.org/10.1016/j.bbrc.2008.04.172

59 Brea-Calvo, G., Haack, T.B., Karall, D., Ohtake, A., Invernizzi, F., Carrozzo, R. et al. (2015) *COQ4* mutations cause a broad spectrum of mitochondrial disorders associated with CoQ_{10} deficiency. *Am. J. Hum. Genet.* **96**, 309–317, https://doi.org/10.1016/j.ajhg.2014.12.023

60 Salviati, L., Trevisson, E., Rodriguez Hernandez, M.A., Casarin, A., Pertegato, V., Doimo, M. et al. (2012) Haploinsufficiency of *COQ4* causes coenzyme Q_{10} deficiency. *J. Med. Genet.* **49**, 187–191, https://doi.org/10.1136/jmedgenet-2011-100394

61 Romero-Moya, D., Santos-Ocana, C., Castano, J., Garrabou, G., Rodriguez-Gomez, J.A., Ruiz-Bonilla, V. et al. (2017) Genetic rescue of mitochondrial and skeletal muscle impairment in an induced pluripotent stem cells model of coenzyme Q_{10} deficiency. *Stem Cells* **35**, 1687–1703, https://doi.org/10.1002/stem.2634

62 Barkovich, R.J., Shtanko, A., Shepherd, J.A., Lee, P.T., Myles, D.C., Tzagoloff, A. et al. (1997) Characterization of the *COQ5* gene from *Saccharomyces cerevisiae*. Evidence for a C-methyltransferase in ubiquinone biosynthesis. *J. Biol. Chem.* **272**, 9182–9188, https://doi.org/10.1074/jbc.272.14.9182

63 Dibrov, E., Robinson, K.M. and Lemire, B.D. (1997) The *COQ5* gene encodes a yeast mitochondrial protein necessary for ubiquinone biosynthesis and the assembly of the respiratory chain. *J. Biol. Chem.* **272**, 9175–9181, https://doi.org/10.1074/jbc.272.14.9175

64 Baba, S.W., Belogrudov, G.I., Lee, J.C., Lee, P.T., Strahan, J., Shepherd, J.N. et al. (2004) Yeast Coq5 C-methyltransferase is required for stability of other polypeptides involved in coenzyme Q biosynthesis. *J. Biol. Chem.* **279**, 10052–10059, https://doi.org/10.1074/jbc.M313712200

65 Dai, Y.N., Zhou, K., Cao, D.D., Jiang, Y.L., Meng, F., Chi, C.B. et al. (2014) Crystal structures and catalytic mechanism of the C-methyltransferase Coq5 provide insights into a key step of the yeast coenzyme Q synthesis pathway. *Acta Crystallogr. Sec. D Biol. Crystallogr.* **70**, 2085–2092, https://doi.org/10.1107/S1399004714011559

66 Lapointe, C.P., Stefely, J.A., Jochem, A., Hutchins, P.D., Wilson, G.M., Kwiecien, N.W. et al. (2018) Multi-omics reveal specific targets of the RNA-binding protein Puf3p and its orchestration of mitochondrial biogenesis. *Cell Syst.* **6**, 125–135.e126

67 Veling, M.T., Reidenbach, A.G., Freiberger, E.C., Kwiecien, N.W., Hutchins, P.D., Drahnak, M.J. et al. (2017) Multi-omic mitoprotease profiling defines a role for Oct1p in coenzyme Q production. *Mol. Cell* **68**, 970–977.e911, https://doi.org/10.1016/j.molcel.2017.11.023

68 Nguyen, T.P., Casarin, A., Desbats, M.A., Doimo, M., Trevisson, E., Santos-Ocana, C. et al. (2014) Molecular characterization of the human COQ5 C-methyltransferase in Coenzyme Q biosynthesis. *Biochim. Biophys. Acta*, https://doi.org/10.1016/j.bbalip.2014.08.007

69 Malicdan, M. C.V., Vilboux, T., Ben-Zeev, B., Guo, J., Eliyahu, A., Pode-Shakked, B. et al. (2018) A novel inborn error of the coenzyme Q_{10} biosynthesis pathway: cerebellar ataxia and static encephalomyopathy due to COQ5 C-methyltransferase deficiency. *Hum. Mutat.* **39**, 69–79, https://doi.org/10.1002/humu.23345

70 Yen, H.C., Liu, Y.C., Kan, C.C., Wei, H.J., Lee, S.H., Wei, Y.H. et al. (2016) Disruption of the human COQ5-containing protein complex is associated with diminished coenzyme Q_{10} levels under two different conditions of mitochondrial energy deficiency. *Biochim. Biophys. Acta* **1860**, 1864–1876, https://doi.org/10.1016/j.bbagen.2016.05.005

71 Gin, P., Hsu, A.Y., Rothman, S.C., Jonassen, T., Lee, P.T., Tzagoloff, A. et al. (2003) The *Saccharomyces cerevisiae COQ6* gene encodes a mitochondrial flavin-dependent monooxygenase required for coenzyme Q biosynthesis. *J. Biol. Chem.* **278**, 25308–25316, https://doi.org/10.1074/jbc.M303234200

72 Ismail, A., Leroux, V., Smadja, M., Gonzalez, L., Lombard, M., Pierrel, F. et al. (2016) Coenzyme Q biosynthesis: evidence for a substrate access channel in the FAD-dependent monooxygenase Coq6. *PLoS Comput. Biol.* **12**, e1004690, https://doi.org/10.1371/journal.pcbi.1004690

73 Ozeir, M., Muhlenhoff, U., Webert, H., Lill, R., Fontecave, M. and Pierrel, F. (2011) Coenzyme Q biosynthesis: Coq6 is required for the C5-hydroxylation reaction and substrate analogs rescue Coq6 deficiency. *Chem. Biol.* **18**, 1134–1142, https://doi.org/10.1016/j.chembiol.2011.07.008

74 Heeringa, S.F., Chernin, G., Chaki, M., Zhou, W., Sloan, A.J., Ji, Z. et al. (2011) *COQ6* mutations in human patients produce nephrotic syndrome with sensorineural deafness. *J. Clin. Invest.* **121**, 2013–2024, https://doi.org/10.1172/JCI45693
75 Ashraf, S., Gee, H.Y., Woerner, S., Xie, L.X., Vega-Warner, V., Lovric, S. et al. (2013) *ADCK4* mutations promote steroid-resistant nephrotic syndrome through CoQ_{10} biosynthesis disruption. *J. Clin. Invest.* **123**, 5179–5189, https://doi.org/10.1172/JCI69000
76 Park, E., Ahn, Y.H., Kang, H.G., Yoo, K.H., Won, N.H., Lee, K.B. et al. (2017) *COQ6* mutations in children with steroid-resistant focal segmental glomerulosclerosis and sensorineural hearing loss. *Am. J. Kidney Dis.* **70**, 139–144, https://doi.org/10.1053/j.ajkd.2016.10.040
77 Gigante, M., Diella, S., Santangelo, L., Trevisson, E., Acosta, M.J., Amatruda, M. et al. (2017) Further phenotypic heterogeneity of CoQ_{10} deficiency associated with steroid resistant nephrotic syndrome and novel *COQ2* and *COQ6* variants. *Clin. Genet.* **92**, 224–226, https://doi.org/10.1111/cge.12960
78 Sheftel, A., Stehling, O. and Lill, R. (2010) Iron-sulfur proteins in health and disease. *Trends Endocrinol. Metab.* **21**, 302–314, https://doi.org/10.1016/j.tem.2009.12.006
79 Sheftel, A.D., Stehling, O., Pierik, A.J., Elsasser, H.P., Muhlenhoff, U., Webert, H. et al. (2010) Humans possess two mitochondrial ferredoxins, Fdx1 and Fdx2, with distinct roles in steroidogenesis, heme, and Fe/S cluster biosynthesis. *Proc. Natl. Acad. Sci. U.S.A.* **107**, 11775–11780, https://doi.org/10.1073/pnas.1004250107
80 Marbois, B.N. and Clarke, C.F. (1996) The *COQ7* gene encodes a protein in *Saccharomyces cerevisiae* necessary for ubiquinone biosynthesis. *J. Biol. Chem.* **271**, 2995–3004, https://doi.org/10.1074/jbc.271.6.2995
81 Jonassen, T., Proft, M., Randez-Gil, F., Schultz, J.R., Marbois, B.N., Entian, K.D. et al. (1998) Yeast Clk-1 homologue (Coq7/Cat5) is a mitochondrial protein in coenzyme Q synthesis. *J. Biol. Chem.* **273**, 3351–3357, https://doi.org/10.1074/jbc.273.6.3351
82 Stenmark, P., Grunler, J., Mattsson, J., Sindelar, P.J., Nordlund, P. and Berthold, D.A. (2001) A new member of the family of di-iron carboxylate proteins. Coq7 (clk-1), a membrane-bound hydroxylase involved in ubiquinone biosynthesis. *J. Biol. Chem.* **276**, 33297–33300, https://doi.org/10.1074/jbc.C100346200
83 Vajo, Z., King, L.M., Jonassen, T., Wilkin, D.J., Ho, N., Munnich, A. et al. (1999) Conservation of the *Caenorhabditis elegans* timing gene *clk-1* from yeast to human: a gene required for ubiquinone biosynthesis with potential implications for aging. *Mamm. Genome* **10**, 1000–1004, https://doi.org/10.1007/s003359901147
84 Lu, T.T., Lee, S.J., Apfel, U.P. and Lippard, S.J. (2013) Aging-associated enzyme human clock-1: substrate-mediated reduction of the diiron center for 5-demethoxyubiquinone hydroxylation. *Biochemistry* **52**, 2236–2244, https://doi.org/10.1021/bi301674p
85 Padilla, S., Tran, U.C., Jimenez-Hidalgo, M., Lopez-Martin, J.M., Martin-Montalvo, A., Clarke, C.F. et al. (2009) Hydroxylation of demethoxy-Q_6 constitutes a control point in yeast coenzyme Q_6 biosynthesis. *Cell. Mol. Life Sci.* **66**, 173–186, https://doi.org/10.1007/s00018-008-8547-7
86 Tran, U.C., Marbois, B., Gin, P., Gulmezian, M., Jonassen, T. and Clarke, C.F. (2006) Complementation of *Saccharomyces cerevisiae coq7* mutants by mitochondrial targeting of the *Escherichia coli* UbiF polypeptide. Two functions of yeast Coq7 polypeptide in coenzyme Q biosynthesis. *J. Biol. Chem.* **281**, 16401–16409, https://doi.org/10.1074/jbc.M513267200
87 Freyer, C., Stranneheim, H., Naess, K., Mourier, A., Felser, A., Maffezzini, C. et al. (2015) Rescue of primary ubiquinone deficiency due to a novel *COQ7* defect using 2,4-dihydroxybensoic acid. *J. Med. Genet.* **52**, 779–783, https://doi.org/10.1136/jmedgenet-2015-102986
88 Wang, Y., Smith, C., Parboosingh, J.S., Khan, A., Innes, M. and Hekimi, S. (2017) Pathogenicity of two *COQ7* mutations and responses to 2,4-dihydroxybenzoate bypass treatment. *J. Cell. Mol. Med.* **21**, 2329–2343, https://doi.org/10.1111/jcmm.13154
89 Brea-Calvo, G., Siendones, E., Sanchez-Alcazar, J.A., de Cabo, R. and Navas, P. (2009) Cell survival from chemotherapy depends on NF-kappaB transcriptional up-regulation of coenzyme Q biosynthesis. *PLoS ONE* **4**, e5301, https://doi.org/10.1371/journal.pone.0005301
90 Cascajo, M.V., Abdelmohsen, K., Noh, J.H., Fernandez-Ayala, D.J., Willers, I.M., Brea, G. et al. (2016) RNA-binding proteins regulate cell respiration and coenzyme Q biosynthesis by post-transcriptional regulation of COQ7. *RNA Biol.* **13**, 622–634, https://doi.org/10.1080/15476286.2015.1119366
91 Martin-Montalvo, A., Gonzalez-Mariscal, I., Padilla, S., Ballesteros, M., Brautigan, D.L., Navas, P. et al. (2011) Respiratory-induced coenzyme Q biosynthesis is regulated by a phosphorylation cycle of Cat5p/Coq7p. *Biochem. J.* **440**, 107–114, https://doi.org/10.1042/BJ20101422
92 Busso, C., Ferreira-Junior, J.R., Paulela, J.A., Bleicher, L., Demasi, M. and Barros, M.H. (2015) Coq7p relevant residues for protein activity and stability. *Biochimie* **119**, 92–102, https://doi.org/10.1016/j.biochi.2015.10.016
93 Martin-Montalvo, A., Gonzalez-Mariscal, I., Pomares-Viciana, T., Padilla-Lopez, S., Ballesteros, M., Vazquez-Fonseca, L. et al. (2013) The phosphatase Ptc7 induces coenzyme Q Biosynthesis by activating the hydroxylase Coq7 in yeast. *J. Biol. Chem.* **288**, 28126–28137, https://doi.org/10.1074/jbc.M113.474494
94 Juneau, K., Nislow, C. and Davis, R.W. (2009) Alternative splicing of *PTC7* in *Saccharomyces cerevisiae* determines protein localization. *Genetics* **183**, 185–194, https://doi.org/10.1534/genetics.109.105155
95 Awad, A.M., Venkataramanan, S., Nag, A., Galivanche, A.R., Bradley, M.C., Neves, L.T. et al. (2017) Chromatin-remodeling SWI/SNF complex regulates coenzyme Q_6 synthesis and a metabolic shift to respiration in yeast. *J. Biol. Chem.* **292**, 14851–14866, https://doi.org/10.1074/jbc.M117.798397
96 Guo, X., Niemi, N.M., Hutchins, P.D., Condon, S.G., Jochem, A., Ulbrich, A. et al. (2017) Ptc7p dephosphorylates select mitochondrial proteins to enhance metabolic function. *Cell Rep.* **18**, 307–313, https://doi.org/10.1016/j.celrep.2016.12.049
97 Stefely, J.A., Reidenbach, A.G., Ulbrich, A., Oruganty, K., Floyd, B.J., Jochem, A. et al. (2015) Mitochondrial ADCK3 employs an atypical protein kinase-like fold to enable coenzyme Q biosynthesis. *Mol. Cell* **57**, 83–94, https://doi.org/10.1016/j.molcel.2014.11.002
98 Stefely, J.A., Licitra, F., Laredj, L., Reidenbach, A.G., Kemmerer, Z.A., Grangeray, A. et al. (2016) Cerebellar ataxia and coenzyme Q deficiency through loss of unorthodox kinase activity. *Mol. Cell* **63**, 608–620, https://doi.org/10.1016/j.molcel.2016.06.030
99 Reidenbach, A.G., Kemmerer, Z.A., Aydin, D., Jochem, A., McDevitt, M.T., Hutchins, P.D. et al. (2018) Conserved lipid and small-molecule modulation of COQ8 reveals regulation of the ancient kinase-like UbiB family. *Cell Chem. Biol.* **25**, 154–165.e111, https://doi.org/10.1016/j.chembiol.2017.11.001

100 Vazquez Fonseca, L., Doimo, M., Calderan, C., Desbats, M.A., Acosta, M.J., Cerqua, C. et al. (2018) Mutations in *COQ8B* (*ADCK4*) found in patients with steroid-resistant nephrotic syndrome alter COQ8B function. *Hum. Mutat.* **39**, 406–414, https://doi.org/10.1002/humu.23376
101 Lagier-Tourenne, C., Tazir, M., Lopez, L.C., Quinzii, C.M., Assoum, M., Drouot, N. et al. (2008) ADCK3, an ancestral kinase, is mutated in a form of recessive ataxia associated with coenzyme Q_{10} deficiency. *Am. J. Hum. Genet.* **82**, 661–672, https://doi.org/10.1016/j.ajhg.2007.12.024
102 Mollet, J., Delahodde, A., Serre, V., Chretien, D., Schlemmer, D., Lombes, A. et al. (2008) *CABC1* gene mutations cause ubiquinone deficiency with cerebellar ataxia and seizures. *Am. J. Hum. Genet.* **82**, 623–630, https://doi.org/10.1016/j.ajhg.2007.12.022
103 Hsieh, E.J., Gin, P., Gulmezian, M., Tran, U.C., Saiki, R., Marbois, B.N. et al. (2007) *Saccharomyces cerevisiae* Coq9 polypeptide is a subunit of the mitochondrial coenzyme Q biosynthetic complex. *Arch. Biochem. Biophys.* **463**, 19–26, https://doi.org/10.1016/j.abb.2007.02.016
104 Duncan, A.J., Bitner-Glindzicz, M., Meunier, B., Costello, H., Hargreaves, I.P., Lopez, L.C. et al. (2009) A nonsense mutation in *COQ9* causes autosomal-recessive neonatal-onset primary coenzyme Q_{10} deficiency: a potentially treatable form of mitochondrial disease. *Am. J. Hum. Genet.* **84**, 558–566, https://doi.org/10.1016/j.ajhg.2009.03.018
105 Hayashi, K., Ogiyama, Y., Yokomi, K., Nakagawa, T., Kaino, T. and Kawamukai, M. (2014) Functional conservation of coenzyme Q biosynthetic genes among yeasts, plants, and humans. *PLoS ONE* **9**, e99038, https://doi.org/10.1371/journal.pone.0099038
106 He, C.H., Black, D.S., Allan, C.M., Meunier, B., Rahman, S. and Clarke, C.F. (2017) Human COQ9 rescues a *coq9* yeast mutant by enhancing coenzyme Q biosynthesis from 4-hydroxybenzoic acid and stabilizing the CoQ-synthome. *Front. Physiol.* **8**, 463, https://doi.org/10.3389/fphys.2017.00463
107 Danhauser, K., Herebian, D., Haack, T.B., Rodenburg, R.J., Strom, T.M., Meitinger, T. et al. (2016) Fatal neonatal encephalopathy and lactic acidosis caused by a homozygous loss-of-function variant in COQ9. *Eur. J. Hum. Genet.* **24**, 450–454, https://doi.org/10.1038/ejhg.2015.133
108 Herebian, D., Seibt, A., Smits, S. H.J., Bunning, G., Freyer, C., Prokisch, H. et al. (2017) Detection of 6-demethoxyubiquinone in CoQ_{10} deficiency disorders: Insights into enzyme interactions and identification of potential therapeutics. *Mol. Genet. Metab.* **121**, 216–223, https://doi.org/10.1016/j.ymgme.2017.05.012
109 Luna-Sanchez, M., Diaz-Casado, E., Barca, E., Tejada, M.A., Montilla-Garcia, A., Cobos, E.J. et al. (2015) The clinical heterogeneity of coenzyme Q_{10} deficiency results from genotypic differences in the *Coq9* gene. *EMBO Mol. Med.* **7**, 670–687, https://doi.org/10.15252/emmm.201404632
110 Allan, C.M., Hill, S., Morvaridi, S., Saiki, R., Johnson, J.S., Liau, W.S. et al. (2013) A conserved START domain coenzyme Q-binding polypeptide is required for efficient Q biosynthesis, respiratory electron transport, and antioxidant function in *Saccharomyces cerevisiae*. *Biochim. Biophys. Acta* **1831**, 776–791, https://doi.org/10.1016/j.bbalip.2012.12.007
111 Barros, M.H., Johnson, A., Gin, P., Marbois, B.N., Clarke, C.F. and Tzagoloff, A. (2005) The *Saccharomyces cerevisiae COQ10* gene encodes a START domain protein required for function of coenzyme Q in respiration. *J. Biol. Chem.* **280**, 42627–42635, https://doi.org/10.1074/jbc.M510768200
112 Busso, C., Bleicher, L., Ferreira, J.R. and Barros, M.H. (2010) Site-directed mutagenesis and structural modeling of Coq10p indicate the presence of a tunnel for coenzyme Q_6 binding. *FEBS Lett.* **584**, 1609–1614, https://doi.org/10.1016/j.febslet.2010.03.024
113 Cui, T.Z. and Kawamukai, M. (2009) Coq10, a mitochondrial coenzyme Q binding protein, is required for proper respiration in *Schizosaccharomyces pombe*. *FEBS J.* **276**, 748–759, https://doi.org/10.1111/j.1742-4658.2008.06821.x
114 Shen, Y., Goldsmith-Fischman, S., Atreya, H.S., Acton, T., Ma, L., Xiao, R. et al. (2005) NMR structure of the 18 kDa protein CC1736 from *Caulobacter crescentus* identifies a member of the START domain superfamily and suggests residues mediating substrate specificity. *Proteins* **58**, 747–750, https://doi.org/10.1002/prot.20365
115 Perocchi, F., Jensen, L.J., Gagneur, J., Ahting, U., von Mering, C., Bork, P. et al. (2006) Assessing systems properties of yeast mitochondria through an interaction map of the organelle. *PLoS Genet.* **2**, e170, https://doi.org/10.1371/journal.pgen.0020170
116 Marchler-Bauer, A., Zheng, C., Chitsaz, F., Derbyshire, M.K., Geer, L.Y., Geer, R.C. et al. (2013) CDD: conserved domains and protein three-dimensional structure. *Nucleic Acids Res.* **41**, D348–D352, https://doi.org/10.1093/nar/gks1243
117 Rossmann, M.G., Moras, D. and Olsen, K.W. (1974) Chemical and biological evolution of nucleotide-binding protein. *Nature* **250**, 194–199, https://doi.org/10.1038/250194a0
118 Pagliarini, D.J., Calvo, S.E., Chang, B., Sheth, S.A., Vafai, S.B., Ong, S.E. et al. (2008) A mitochondrial protein compendium elucidates complex I disease biology. *Cell* **134**, 112–123, https://doi.org/10.1016/j.cell.2008.06.016
119 Hirst, J. (2011) Why does mitochondrial complex I have so many subunits? *Biochem. J.* **437**, e1–e3, https://doi.org/10.1042/BJ20110918
120 Stroud, D.A., Formosa, L.E., Wijeyeratne, X.W., Nguyen, T.N. and Ryan, M.T. (2013) Gene knockout using transcription activator-like effector nucleases (TALENs) reveals that human NDUFA9 protein is essential for stabilizing the junction between membrane and matrix arms of complex I. *J. Biol. Chem.* **288**, 1685–1690, https://doi.org/10.1074/jbc.C112.436766
121 Leshinsky-Silver, E., Lev, D., Tzofi-Berman, Z., Cohen, S., Saada, A., Yanoov-Sharav, M. et al. (2005) Fulminant neurological deterioration in a neonate with Leigh syndrome due to a maternally transmitted missense mutation in the mitochondrial ND3 gene. *Biochem. Biophys. Res. Commun.* **334**, 582–587, https://doi.org/10.1016/j.bbrc.2005.06.134
122 van den Bosch, B.J., Gerards, M., Sluiter, W., Stegmann, A.P., Jongen, E.L., Hellebrekers, D.M. et al. (2012) Defective NDUFA9 as a novel cause of neonatally fatal complex I disease. *J. Med. Genet.* **49**, 10–15, https://doi.org/10.1136/jmedgenet-2011-100466
123 Kuhl, I., Miranda, M., Atanassov, I., Kuznetsova, I., Hinze, Y., Mourier, A. et al. (2017) Transcriptomic and proteomic landscape of mitochondrial dysfunction reveals secondary coenzyme Q deficiency in mammals. *Elife* **6**, https://doi.org/10.7554/eLife.30952
124 Yubero, D., Montero, R., Martin, M.A., Montoya, J., Ribes, A., Grazina, M. et al. (2016) Secondary coenzyme Q_{10} deficiencies in oxidative phosphorylation (OXPHOS) and non-OXPHOS disorders. *Mitochondrion* **30**, 51–58, https://doi.org/10.1016/j.mito.2016.06.007

CHAPTER 2

Human COQ10A and COQ10B are distinct lipid-binding START domain proteins required for coenzyme Q function

ABSTRACT

Coenzyme Q (ubiquinone or CoQ) serves as an essential redox-active lipid in respiratory electron and proton transport during cellular energy metabolism. CoQ also functions as a membrane-localized antioxidant protecting cells against lipid peroxidation. CoQ deficiency is associated with multiple human diseases; CoQ_{10} supplementation in particular has noted cardioprotective benefits. In *Saccharomyces cerevisiae*, Coq10, a putative START domain protein, is believed to chaperone CoQ to sites where it functions. Yeast *coq10* deletion mutants (*coq10Δ*) synthesize CoQ inefficiently during log phase growth, are respiratory defective and sensitive to oxidative stress. Humans have two orthologs of yeast *COQ10*, *COQ10A* and *COQ10B*. Here, we tested the human co-orthologs for their ability to rescue the yeast mutant. We showed that expression of either human ortholog, COQ10A or COQ10B, rescues yeast *coq10Δ* mutant phenotypes, restoring the function of respiratory-dependent growth on a non-fermentable carbon source and sensitivity to oxidative stress induced by treatment with polyunsaturated fatty acids. These effects indicate a strong functional conservation of Coq10 across different organisms. However, neither COQ10A nor COQ10B restored CoQ biosynthesis when expressed in the yeast *coq10Δ* mutant. The involvement of yeast Coq10 in CoQ biosynthesis may rely on its interactions with another protein, possibly Coq11, which is not found in humans. Co-expression analyses of yeast *COQ10*, and human *COQ10A* and *COQ10B* provide additional insights to functions of these START domain proteins, and their potential roles in other biologic pathways.

INTRODUCTION

Coenzyme Q (CoQ) is a lipid composed of a fully substituted, redox-active benzoquinone ring attached to a long polyisoprenoid chain. The polyisoprenoid chain of CoQ_n, with n ≥ 6 isoprene units, anchors CoQ at the mid-plane of the membrane phospholipid bilayers. The reversible reduction and oxidation of CoQ and $CoQH_2$ enables the transport of electrons and protons necessary for cellular respiration. CoQ also serves as an important electron acceptor for enzymes involved in fatty acid β-oxidation, oxidation of proline, sulfide, and pyrimidine biosynthesis (1-3). The reduced or hydroquinone form of $CoQH_2$ serves as a chain-terminating antioxidant that slows lipid peroxidation (2).

Although CoQ exists in most biological membranes, its synthesis occurs exclusively inside the mitochondria in eukaryotes, or in the cytosol in *Escherichia coli*, catalyzed by a cohort of enzymes, many of which are organized in a complex known as the CoQ synthome (a.k.a., Complex Q) in eukaryotes, or the Ubi metabolon in *E. coli* (4-6). In *Saccharomyces cerevisiae*, currently known members of the CoQ synthome consist of Coq3-Coq9 and Coq11 (4, 5). Together, they modify the quinone head group through a series of methylation (Coq3 and Coq5), deamination (Coq6, Coq9), and hydroxylation (Coq6, Coq7, Coq9) reactions (4, 5). The definitive functions of the remaining members of the CoQ synthome (Coq4, Coq8, and Coq11) are yet to be fully characterized. Attachment of the polyisoprenoid chain to the aromatic ring precursor precedes the ring modification steps. Coq1, a hexaprenyl pyrophosphate synthetase condenses farnesyl pyrophosphate (FPP) with three molecules of isopentenyl pyrophosphate (IPP) to form hexaprenyldiphosphate, which is transferred to the 4-hydroxybenzoic acid (4HB) or *para*-aminobenzoic acid (pABA) ring at the C3 position by Coq2 (4, 5). The number of isoprene units (n) in the polyisoprenoid chain of CoQ_n varies between organisms as determined by the specific polyprenyl diphosphate synthase (7), and consists of six isoprene units in *S. cerevisiae* (CoQ_6), eight isoprene units in *E. coli* (CoQ_8), and predominantly ten isoprene units in

Schizosaccharomyces pombe and humans (CoQ_{10}) (8). Each of the yeast *coq1Δ* - *coq9Δ* mutants shows complete abolishment of CoQ_6 biosynthesis, and fails to respire (5). Their defects in respiration can be readily restored by exogenous supplementation with CoQ_6 (5).

The *coq10Δ* mutant is unusual amongst the yeast *coq* mutants because it produces wild-type content of CoQ_6 at stationary phase, yet its de novo synthesis of CoQ_6 during log phase is inefficient (9, 10). Despite having normal or nearly normal steady state levels of CoQ_6, the *coq10Δ* mutant displays a respiratory deficient phenotype shown by anemic growth on medium containing a non-fermentable carbon source, and decreased NADH and succinate oxidase activities (10). In addition, the *coq10Δ* mutant is sensitive to lipid peroxidation induced by exogenously added polyunsaturated fatty acids (PUFAs) (9). Thus, the CoQ_6 present in *coq10Δ* mutant is not utilized efficiently for either respiration or for its function as an antioxidant.

The NMR structure of CC1736, a Coq10 ortholog in *Caulobacter crescentus*, identified it as a member of the steroidogenic acute regulatory protein (StAR)-related lipid transfer (START) domain superfamily (11). This family includes proteins that bind polycyclic compounds such as cholesterol and polyketides in a signature hydrophobic cavity (11). The START domain typically spans ~210 residues (12), and folds into a helix-grip structure consisting of antiparallel β-sheets flanked by one α-helix on each side (13). START domain containing proteins are primarily involved in non-vesicular transport of lipids between membranes (14). For instance, STARD4 is a START domain protein that binds and transports cholesterol from plasma membrane to mitochondria, endoplasmic reticulum (ER), as well as the endocytic recycling compartment, equilibrating cholesterol content among cellular membranes to fit their biophysical properties and physiological needs (15). Purified CC1736 binds to CoQ_n with variable polyisoprenoid chain lengths and to the farnesylated analog of a late-stage CoQ intermediate, demethoxy-CoQ_3 (DMQ_3) (9). Coq10 polypeptides isolated from *S. cerevisiae* and *S. pombe* co-purify with CoQ_6

and CoQ_{10}, respectively (10, 16). Similarly, CoQ_8 co-purifies with the *S. pombe* Coq10 polypeptide expressed in *E. coli* (16). These observations have led to the current hypothesis that the Coq10 polypeptide is a putative CoQ_n chaperone, necessary for delivering CoQ from its site of synthesis and/or the pool of free CoQ to sites of function.

Complex III inhibitors antimycin A and myxothiazol enhance reactive oxygen species (ROS) formation by blocking oxidation of cytochrome b_H at the N-site, or inhibiting reduction of cytochrome b_L at the P-site, respectively (17-19). Thereby, antimycin A induces ROS through reverse electron flow from cytochrome b_L to CoQ to form the semiquinone radical (20), whereas myxothiazol-dependent ROS production results from incomplete $CoQH_2$ oxidation by slow reduction of the Rieske iron-sulfur protein (18, 19). Mitochondria isolated from yeast *coq10Δ* produce significantly elevated ROS in the presence of antimycin A, but not myxothiazol, suggesting that in the absence of the Coq10 polypeptide, electron transfer from $CoQH_2$ to the Rieske iron-sulfur protein is defective (20). This specific requirement for the presence of the Coq10 START domain polypeptide for functional electron transfer by complex III is further substantiated by the binding of both oxidized and reduced forms of a photo-reactive azido-quinone probe to the Coq10 polypeptide (21).

CoQ deficiencies are associated with human disease and the beneficial effects of CoQ_{10} supplementation in therapeutic regimens are increasingly appreciated (1, 4). Mutations in several genes encoding CoQ biosynthetic enzymes result in primary CoQ deficiency and cause encephalopathy, cerebellar ataxia, cardiomyopathy, nephrotic syndrome, and myopathy (1, 4). CoQ deficiency can also occur secondary to mutations in aprataxin (APTX), electron transfer flavoprotein dehydrogenase (ETFDH), or serine/threonine-protein kinase B-Raf (BRAF) (3). CoQ_{10} supplementation rescues the proteinuria in patients with nephrotic syndrome, provided therapy is initiated early (22). Patients who develop myalgia under statin administration are

often prompted to take CoQ_{10} supplements to mitigate adverse symptoms (23). Long term CoQ_{10} treatment has also been shown to improve symptoms and reduce major adverse cardiovascular events when it is used as adjunctive treatment in patients with chronic heart failure (24, 25).

Yeast is a superb model organism to study CoQ biosynthesis because many of the enzymes involved in CoQ biosynthesis are functionally conserved from yeast to humans (4, 5). In this work, we test the human co-orthologs of yeast Coq10, COQ10A and COQ10B, for their ability to complement the yeast c*oq10Δ* mutant. We show that expression of either human COQ10A or COQ10B rescues yeast *coq10Δ* defective respiration and its sensitivity to oxidative stress, and restores steady-state levels of Coq polypeptides. However, neither COQ10A nor COQ10B expression is able to stabilize the yeast CoQ synthome or rescue the partial defect in de novo CoQ_6 biosynthesis characteristic of the yeast *coq10Δ* mutant.

MATERIALS AND METHODS

Yeast strains and growth media

S. cerevisiae strains used in this study are described in Table 1. Growth media for yeast included YPD (1% Bacto yeast extract, 2% Bacto peptone, 2% dextrose), YPG (1% Bacto yeast extract, 2% Bacto peptone, 3% glycerol), and YPGal (1% Bacto yeast extract, 2% Bacto peptone, 2% galactose, 0.1% dextrose) (26). Synthetic Dextrose/Minimal-Complete (SD-Complete) and Synthetic Dextrose/Minimal minus uracil (SD-Ura) (0.18% Difco yeast nitrogen base without amino acids and ammonium sulfate, 0.5% $(NH_4)_2SO_4$, 0.14% NaH_2PO_4, 2% dextrose, complete amino acid supplement, or amino acid supplement lacking uracil) were prepared as described (27). Solid media contained additional 2% Bacto agar.

Construction of single- and multi-copy yeast expression vectors of human COQ10A and COQ10B

Plasmids used in this study are listed in Table 2. Generation of single-copy (pQM) and multi-copy (pRCM) yeast expression vectors was previously described (9, 28). Both pQM and pRCM contain the yeast *CYC1* promoter and the first 35 residues of the yeast *COQ3* ORF, corresponding to the proposed Coq3 mitochondrial leader sequence to direct import of human proteins into yeast mitochondria. To generate the single- and multi-copy yeast expression vectors of human COQ10A, the human *COQ10A* ORF (mRNA#1, Figure 1A), encoding residues 44-247 was PCR amplified from pHCOQ10/ST1 (10) with primers 5'-ggccATCGATATGAGGTTTCTGACCTCCTGC-3', and 5'-ggccGGTACCTCAAGTCTGGTGCACCTC-3' and cloned into pQM and pRCM vectors using restriction enzymes ClaI and KpnI (New England BioLabs) to generate pQM COQ10A and pRCM COQ10A, respectively. Similarly, full-length human *COQ10B* ORF (mRNA #1, Figure 1A), encoding residues 1-238 was PCR amplified from COQ10B cDNA clone (GeneCopoeia) with primers 5'- ggccATCGATATGGCAGCTCGGACTGGTCAT-3' and 5'-

ggccGGTACCTTATGTGTGATGGACTTCATGAAGCATTAACTCC-3' to generate pQM COQ10B and pRCM COQ10B.

Complementation of yeast *coq10Δ* by human COQ10A and COQ10B

Each of the following plasmids, pQM (empty vector), pQM COQ10A, pQM COQ10B, pRCM (empty vector), pRCM COQ10A, and pRCM COQ10B was transformed into wild-type W303 or *coq10Δ*, and the transformed cells were selected on SD-Ura plates as described (29). A single colony from each SD-Ura plate was inoculated in SD-Ura liquid medium. Wild-type W303 and *coq10Δ* were each inoculated in SD-Complete liquid medium. Cultures were incubated overnight at 30°C 250 rpm. The overnight cultures were diluted to 0.2 OD_{600}/mL with sterile H_2O, from which a series of five-fold dilutions were prepared. An aliquot of 2 µL of sample from the dilution series was plated onto YPD and YPG plate medium and incubated at 30°C. Pictures were taken after three to four days.

Fatty acid sensitivity assay

Fatty acid sensitivity assay was performed as described (30, 31) with slight modifications. Briefly, yeast W303 wild type, *cor1Δ*, *coq9Δ*, and *coq10Δ* were inoculated in SD-Complete liquid medium, and *coq10Δ* harboring the designated plasmids were inoculated in SD−Ura liquid medium and incubated overnight at 30°C 250 rpm. Overnight cultures were back diluted to 0.2 OD_{600}/mL with fresh SD-Complete or SD−Ura liquid medium and incubated for six hours at 30°C 250 rpm to logarithmic phase. The cells were harvested, washed twice with sterile H_2O, and suspended in 0.1 M phosphate buffer with 0.2% dextrose, pH 6.2 to a cell density of 0.2 OD_{600}/mL. To test yeast sensitivity to PUFA induced oxidative stress, ethanol-diluted oleic acid (Nu-Chek Prep), or α-linolenic acid (Nu-Check Prep), were added to aliquots of 5 mL cell suspension in phosphate buffer with 0.2% dextrose to a final concentration of 200 µM. Identical 5 mL cell suspensions were prepared with 0.1% (vol/vol) ethanol as a vehicle control. After a

four hours incubation at 30°C 250 rpm, cell viability was assessed with plate dilution assay by spotting 2 µL of sample from a series of five-fold dilution onto YPD plates. Cell viability was also ascertained before addition of fatty acids, and labeled as zero hour.

Mitochondria isolation from yeast *coq10Δ* expressing human COQ10A or COQ10B

Precultures of yeast *coq10Δ* transformed with pQM COQ10A, pQM COQ10B, pRCM COQ10A, or pRCM COQ10B in YPD were back diluted with YPGal and grown overnight at 30°C 250 rpm until the cell density had reached ~3.0 OD_{600}/mL. Preparation of spheroplasts with Zymolyase-20T (MP Biomedicals) and extraction of mitochondria in the presence of Complete EDTA-free protease inhibitor mixture (Roche), phosphatase inhibitor cocktail set II (EMD Millipore) and phosphatase inhibitor cocktail set 3 (Sigma-Aldrich) over Nycodenz (Sigma-Aldrich) density gradient were previously described (32). Purified mitochondria were flash frozen in liquid nitrogen and stored at −80°C until use.

Immunoblot analysis of steady state Coq polypeptide levels

Protein concentration in gradient purified mitochondria was measured by the bicinchoninic acid (BCA) assay (Thermo Fisher Scientific). Purified mitochondria were resuspended in SDS sample buffer (50 mM Tris, pH 6.8, 10% glycerol, 2% SDS, 0.1% bromophenol blue, and 1.33% β-mercaptoethanol), and an aliquot of 25 µg of mitochondrial protein from each sample was loaded in individual lanes and separated by SDS gel electrophoresis on 12% Tris-glycine polyacrylamide gels. Proteins were subsequently transferred to 0.45 µm nitrocellulose membrane (Bio-Rad), and blocked with blocking buffer (0.5% BSA, 0.1% Tween 20, 0.02% SDS in phosphate-buffered saline). Representative Coq polypeptides and mitochondrial malate dehydrogenase Mdh1 (loading control) were detected with rabbit polyclonal antibodies prepared in blocking buffer at dilutions listed in Table 3. Polyclonal antibodies against human COQ10A (Proteintech) and COQ10B (Abcam) were

commercially obtained, and used at dilutions recommended by the companies. The secondary IRDye 680LT goat anti-rabbit IgG antibody (LiCOR) was used at 1:10,000 dilution in the same blocking buffer. Immunoblot images were visualized with LiCOR Odyssey Infrared Scanner (LiCOR), and relative protein levels were quantified by band densitometry using Image J software (https://imagej.nih.gov/ij/).

Analysis of high molecular weight complexes with two-dimensional Blue Native/SDS-PAGE

Two-dimensional Blue Native/SDS-PAGE was performed as described (33-35). Purified mitochondria at 4 mg/mL were solubilized for one hour in ice-cold solubilization buffer (11 mM HEPES, pH 7.4, 0.33 M sorbitol, 1X NativePAGE sample buffer (Thermo Fisher Scientific), 16 mg/mL digitonin (Biosynth)) in the presence of the previously described mixtures of protease and phosphatase inhibitors. After centrifugation (100,000 × *g*, ten minutes), the protein concentration in the soluble fraction was measured by BCA assay and NativePAGE 5% G-250 sample additive (Thermo Fisher Scientific) was added to the soluble fraction to a final concentration of 0.25%. Soluble protein from each sample (80 µg) was separated on NativePAGE 4-16% Bis-Tris gel (Thermo Fisher Scientific) in the first dimension, followed by separation on 12% Tris-glycine polyacrylamide gel in the second dimension. The molecular weight standards for Blue Native gel electrophoresis and SDS gel electrophoresis were obtained from GE Healthcare (Sigma-Aldrich) and Bio-Rad, respectively. Immunoblot analysis of the CoQ synthome was performed as described above using antibodies against Coq4 and Coq9. A separate COQ10A- or COQ10B-containing complex was detected using commercial antibodies against COQ10A and COQ10B, respectively.

Analyses of de novo and steady state levels of CoQ_6 and CoQ_6-intermediates

Metabolic labeling with $^{13}C_6$-labeled ring precursors and subsequent analyses of labeled and unlabeled CoQ_6 and CoQ_6-intermediates in yeast whole cell lipid extract by RP-HPLC tandem mass spectrometry were previously described (9, 36). Briefly, overnight cultures of yeast wild type, *coq10Δ* in SD-Complete medium, and *coq10Δ* expressing pQM, pQM COQ10A, pQM COQ10B, pRCM, pRCM COQ10A, or pRCM COQ10B in SD−Ura medium were back diluted with fresh SD-Complete or SD−Ura medium to 0.1 OD_{600}/mL and grown to 0.5 OD_{600}/mL (early-log phase) at 30°C 250 rpm. The $^{13}C_6$-labeled precursors pABA or 4HB were dissolved in ethanol and added to yeast cultures at a final concentration of 5 µg/mL (equivalent to 34.9 µM $^{13}C_6$-pABA and 34.7 µM $^{13}C_6$-4HB). Vehicle control samples contained a final concentration of 0.1% (vol/vol) ethanol. The cultures were incubated with the labeled precursors or ethanol for five hours at 30°C 250 rpm before triplicates of 5 mL culture were harvested for lipid extraction. The cell density measured by OD_{600} at the time of harvest was recorded.

For lipid extraction, collected yeast cell pellets were dissolved in 2 mL methanol, and lipids were extracted twice in the presence of internal standard CoQ_4, each time with 2 mL petroleum ether followed by vigorous vortex. The organic phase from two extractions were combined and dried under a stream N_2 gas. A series of CoQ_6 standards (Avanti) containing CoQ_4 were prepared and lipid extracted concurrently with yeast samples to construct a CoQ_6 standard curve. The dried lipids were reconstituted in 200 µL of 0.5 mg/mL benzoquinone prepared in ethanol to oxidize all lipid species for mass spectrometry analysis with a 4000 QTRAP linear MS/MS spectrometer (Applied Biosystems). Aliquots (20 µL) of each reconstituted lipid extract were injected into a Luna phenyl-hexyl column (100 x 4.6 mm, 5 µm; Phenomenex). The HPLC mobile phase consisted of solvent A (95:5 methanol/isopropanol, 2.5 mM ammonium formate) and solvent B (isopropanol, 2.5 mM ammonium formate). As the percentage of solution B was increased linearly from 0 to 10%, representative CoQ_6 and CoQ_6-intermediates eluted off the column at distinct retention times and were monitored under

multiple reaction monitoring mode (MRM) scanning precursor to product ion transitions listed in Table 4. For each analyte, the precursor to product ion transitions of both protonated ion species and its ammonium adduct ion species were tracked. The ammonium adducts provide much stronger ion signals for detection of isoprenoids by positive-ion electrospray ionization mass spectrometry. Analyst 1.4.2 software (Applied Biosystems) was used for data acquisition and processing. In each sample, the amount of CoQ_6 and CoQ_6-intermediates was calculated from the sum of peak areas of each analyte and its corresponding ammonium adduct at a specific retention time, corrected for the recovery of internal standard CoQ_4. Statistical analyses were performed using GraphPad Prism with two-way ANOVA multiple comparisons comparing the mean of each sample to the mean of its corresponding empty vector control, and comparing the mean of wild type to the mean of *coq10Δ*.

Homology modeling of human COQ10A and COQ10B

Secondary structural elements and disordered regions within the COQ10A and COQ10B ORFs were predicted using PsiPred (37) and DisoPred (38). Secondary structural alignments and initial model generation were performed using the SwissModel server (39). Using COQ10A as the query sequence, 50 homologous protein templates were identified with sequence identities ranging from 6.94% to 28.68%, and sequence similarity between 25-30%. Nine templates with the best alignment of the secondary structural elements were selected for model building in SwissModel. Of the nine models generated, four models with either low QMEAN scores or high identity to the template were selected for further improvement. As the sequence coverage of the models differs from each other, a combination of all four models was used to generate the final model that covers residues 87-228 of COQ10A. The final steps of model refinement, rebuilding strange loops, and improvement of side chain packing and backbone distortion were completed using custom script in PyRosetta (40). A total of 16,000 decoys were generated and the convergence of the refinement was assessed by checking RMSD of all

decoys to the lowest energy decoy versus Rosetta energy. The top five decoys with the lowest Rosetta energy were selected and model quality was assessed via Qmean (41), Verify3D (42), Errat (43) and MolProbity (44). The decoy that scored equally well in all four metrics was chosen as the final model of COQ10A. A similar approach was used to create homology model of COQ10B from a combination of six models that covered residues 79-219 of COQ10B.

Molecular docking of CC1736

Molecular docking was completed using Autodock vina (45), and substrate molecules were produced using phenix.ELBOW (46) and verified with phenix.REEL (46). Docking of each substrate was executed with a 20x20x20 Å grid box that encompassed the entirety of the hydrophobic pocket of CC1736. Docking was performed with an exhaustiveness of 18 and 9 docking solutions were produced per run.

Yeast Coq10 ortholog similarity clustering and Coq10 co-expression analysis

The protein similarity network was constructed using the EFI-EST tool (http://efi.igb.illinois.edu/efi-est/) (47) with an alignment score of 30, with human COQ10A as the BLASTp seed sequence, retrieving 8,095 hits. Protein nodes were collapsed at >75% identity. The network was visualized with the yFiles organic layout provided with the Cytoscape software (48). The nodes in the network were colored by taxonomy as provided by the UniProt database (49). Information associated with proteins included in this analysis can be found in Supplemental Table S2. Gene neighborhoods of bacterial homologs were retrieved with the EFI-GNT tool (https://efi.igb.illinois.edu/efi-gnt/). The phylogenetic analysis was performed using MAFFT (50) for sequence alignment and IQ Tree (51) as implemented on the CIPRES (52, 53) web portal with 1000 bootstrap replicates (54). Before tree reconstruction, the multiple sequence alignment (MSA) was trimmed to remove poorly aligned sequence at the N-terminus, and the edited MSA can be found in Supplemental Table S2.

RESULTS

Expression of either COQ10A or COQ10B from human restores respiratory growth of the yeast *coq10Δ* mutant

Human *COQ10A* and *COQ10B* are co-orthologs of yeast *COQ10* located on human chromosome 12 and chromosome 2, respectively (55). The polymorphisms in COQ10A (P79H, P231S) and COQ10B (L48F) are thought to be one of the genetic factors predisposing patients to statin-associated myopathy (56, 57). The underlying molecular mechanisms of statin-associated myopathy are proposed to be isoprenoid depletion, inhibition of CoQ biosynthesis, disruption of cholesterol homeostasis, or disturbance of calcium metabolism (58). *COQ10A* and *COQ10B* each contain six exons, which give rise to two isoforms of COQ10A and four isoforms of COQ10B as a result of alternative splicing and translation initiation (Figure 1A). Each of the two *COQ10A* mRNA transcripts contains a unique 5' UTR and translation initiation site (Figure 1A, Supplemental Table S1). According to the UniProt database (49), *COQ10A* mRNA #1 encodes the longer isoform of COQ10A, with the first 15 residues predicted to be the mitochondrial targeting sequence (Supplemental Table S1). *COQ10A* mRNA #2 encodes COQ10A isoform 2 with a unique N-terminus. Two of the *COQ10B* mRNA transcripts share an identical 5' UTR and translation initiation site, whereas the other two *COQ10B* mRNA transcripts each has a unique 5' UTR and translation initiation site (Figure 1A, Supplemental Table S1). Based on the UniProt database, *COQ10B* mRNA #1 encodes the longest isoform, and its mitochondrial targeting sequence consists of the first 37 residues (Supplemental Table S1). COQ10B isoform 2 encoded by mRNA #2 lacks one of the exons present in mRNA #1 (Figure 1A). COQ10B isoforms 3 and 4 contain distinct N-terminal sequences and their subcellular localization are unknown (Figure 1A, Supplemental Table S1). Although RNA processing predicts several isoforms of COQ10A and COQ10B, both isoforms of COQ10A and all four isoforms of COQ10B retain amino acid residues important for START domain formation.

Expression of human COQ10A from a multi-copy vector was previously shown to complement respiratory growth of the yeast *coq10Δ* mutant on non-fermentable carbon source (10, 16). Here, we examined the functional complementation of the yeast c*oq10Δ* by both single-copy (pQM) and multi-copy (pRCM) expression of human COQ10A or COQ10B. The cDNA expressed for COQ10A corresponded to residues 44 to 247 of isoform 1 (*COQ10A* mRNA #1), and the cDNA expressed for COQ10B corresponded to residues 1 to 238 of isoform 1 (*COQ10B* mRNA #1). Yeast *coq10Δ*, and *coq10Δ* with empty vectors pQM or pRCM show slow growth on non-fermentable glycerol-containing medium (Figure 1B). Expression of either COQ10A or COQ10B in single-copy or multi-copy rescued the glycerol growth of the *coq10Δ* mutant (Figure 1B). Interestingly, single-copy COQ10A, and both single- and multi-copy COQ10B seem to complement the defective growth of the *coq10Δ* mutant better as compared to multi-copy COQ10A (Figure 1B). These results identify human COQ10A and COQ10B as functional co-orthologs of yeast Coq10.

Human COQ10A and COQ10B share low sequence identity but high structural similarity with other Coq10 orthologs

In vitro lipid binding assays have shown that the *C. crescentus* Coq10 ortholog CC1736 binds to isoforms of CoQ_n with varying polyisoprenoid chain length (n = 2, 3, 6, or 10) and to a farnesylated analog (n = 3) of a late-stage CoQ intermediate DMQ_3 (9). CC1736 does not bind to a farnesylated analog of an early-stage CoQ intermediate farnesyl-hydroxybenzoate (FHB) (9). This observation strongly implies that the quinone moiety, but not the polyisoprenoid chain, is the structural determinant of Coq10 ligand interaction. Several amino acid residues have been identified through site-directed mutagenesis, and a substitution of these residues on Coq10 orthologs result in altered ligand-binding affinity and respiratory defects (9, 16, 21, 59). Among these residues, a combination of positive charge provided by residue K8, paired hydrophobic residues A55 and V70, and salt bridge formed by E64 and K115 are thought to

confer the ligand specificity of CC1736 (11). Mutations in the equivalent residues in *S. cerevisiae* Coq10 result in defects in respiration as measured by oxygen consumption, H_2O_2 release, or NADH-cytochrome *c* reductase activity (9, 59). Here, we constructed sequence alignment of four Coq10 orthologs and mapped these residues relative to positions in isoform 1 of human COQ10A and COQ10B amino acid sequence (Figure 2A). From the multiple sequence alignment, we noticed several additional conserved residues (shaded blue and lilac in Figure 2A) besides those previously identified. Most noticeably, aromatic amino acids (tyrosine, phenylalanine, and tryptophan), and nonpolar amino acids (valine, leucine and alanine) are highly enriched among these conserved residues (Figure 2A). Residues F39 and P41 of *S. pombe* Coq10 are believed to be within the region for CoQ binding, and mutation of F39A and P41A reduces the photolabeling yield with azido-quinone to about 50% of the wild-type control (21). Replacement of L63 or W104 with alanine on *S. pombe* Coq10 reduces CoQ binding affinity to about 50%, and a double point mutant further reduces the binding affinity to only 25% (16). Based on homology modeling, the N-terminal regions of human COQ10A and COQ10B do not seem to form defined secondary structure and were excluded from the predicted secondary structures shown in Figure 2A. Thus, exon skipping in COQ10B isoform 2 (Figure 1A), as well as variable N-terminal sequences on all COQ10A and COQ10B isoforms that result from alternative splicing and translation initiation (Figure 1A) are not expected to change the secondary structural elements of the START domain of COQ10A and COQ10B.

Based on the multiple sequence alignment, we also noticed that although human COQ10A and COQ10B exhibit relatively low sequence identity with other Coq10 orthologs (~26-31%), they are predicted to share similar helix-grip structures (Figure 2B). The predicted structures of COQ10A and COQ10B are almost identical to each other (Figure 2B) and similar to the solved structure of CC1736 (Figure 2C). The core of both COQ10A and COQ10B consists of two α-helices and seven antiparallel β-sheets, and is predicted to form a

hydrophobic cavity shielding its CoQ lipid ligand from the aqueous environment (Figure 2B). The structural feature of a helix-grip fold identifies both COQ10A and COQ10B as distinctive members of the START domain protein family.

In order to reveal the most likely binding site for the CoQ lipid ligand and to identify additional residues that may confer CoQ lipid ligand binding specificity in COQ10A and COQ10B, we attempted to dock CoQ_6 to the known structure of CC1736. Consistent with previous in vitro binding assay results, we observed that docking of FHB to CC1736 occurred with free energy values significantly higher (more positive, and less favorable) than CoQ_6 docked at the central cavity of CC1736 (Figure 3A, B). The docking solutions of CoQ_6 to CC1736 consistently showed that the CoQ_6 folds into a boomerang-like structure, with its hexaprenyl tail making contacts with resides A55, V70, and W95 lining the surface inside the cavity (Figure 3A). However, the orientation of the benzoquinone head group was slightly more variable between docking solutions. Several START domain proteins have been reported to undergo ligand-induced conformational change such that the readily accessible entryway to the central cavity becomes partially constricted, shielding the ligand from the aqueous environment (60-62). Thus, it is highly likely that the flexible orientation of the quinone head group may be a result of a less compact conformation of the central cavity in the structure of a ligand-free CC1736. Further studies that would allow a more in-depth characterization of the conformational change of Coq10 or its orthologs are needed to decipher the CoQ ligand binding interaction.

Expression of either human COQ10A or COQ10B restores steady state levels of Coq polypeptides

Coq polypeptide components of the CoQ synthome serve as enzymes required for CoQ biosynthesis, and/or play structural roles necessary for formation or stability of the CoQ synthome (5, 34, 63). Yeast Coq10 has not been detected as part of the CoQ synthome, but its

absence causes destabilization of Coq3, Coq4, Coq6, Coq7 and Coq9, as well as the overall CoQ synthome (34, 63). We tested the ability of human COQ10A or COQ10B to restore steady state levels of Coq polypeptides when expressed in the yeast *coq10Δ* mutant. We noticed that the steady state level of Coq5 is slightly reduced and the level of Coq8 is slightly increased in the *coq10Δ* mutant, in addition to other affected Coq polypeptide levels shown previously (63). The presence of single-copy pQM COQ10A fully restores steady state levels of Coq5 and Coq6 (Figure 4, S1), partially restores steady state levels of Coq3, Coq4, Coq7, and Coq9 (Figure 4, S1). The single-copy pQM COQ10B fully restores the steady state level of Coq5 (Figure 4, S1), restores steady-state level of Coq4, Coq7, and Coq9 to a minimal degree (Figure 4, S1), but seems to have a negative effect on the levels of Coq3, Coq6, and Coq8 (Figure 4, S1). Neither COQ10A nor COQ10B expressed on a multi-copy pRCM vector function as well as the corresponding single-copy pQM vector, despite the fact that COQ10A and COQ10B are barely detected when expressed from a single-copy vector (Figure 4). The multi-copy pRCM COQ10A restores the steady state level of Coq6, partially restores the levels of Coq5, and Coq9 (Figure 4, S1) while the steady state levels of Coq3, Coq4, and Coq7 remain similar to the *coq10Δ* mutant, if not lower (Figure 4, S1). Yeast cells expressing COQ10A from a multi-copy vector show a nearly 50% reduction of Coq8 content compared to the wild-type control (Figure 4, S1). Overexpression of Coq8 promotes assembly of sub-complexes of the CoQ synthome (34), and Coq8 deficit may explain the ineffective rescue of *coq10Δ* by the multi-copy COQ10A and its corresponding poor growth phenotype on YPG plate medium (Figure 1B). The multi-copy pRCM COQ10B restores Coq5 and Coq9 (Figure 4, S1), but has no effect on the Coq3, Coq4, Coq6, and Coq7 levels (Figure 4, S1). Opposite from the effect of expressing multi-copy pRMC COQ10A, presence of multi-copy pRCM COQ10B leads to 50% increase of Coq8 compared to the wild type cells (Figure 4, S1). It is quite intriguing that pRCM COQ10B results in a slight reduction of Coq1 level while the level of Coq11 is nearly 2.5-fold more compared to the wild type cells (Figure 4, S1). The anti-COQ10A antibody specifically recognizes COQ10A and does

not cross react with human COQ10B (Figure 4). Anti-COQ10B antibody is also antigen-specific, but it gives two intense bands, migrating at ~30 kDa and ~17 kDa (Figure 4). In human cells, only the higher molecular weight band is detected, and the lower molecular weight band may correspond to a processed form of COQ10B unique to the yeast cells.

Expression of human COQ10A or COQ10B fails to restore the CoQ synthome in the yeast *coq10Δ* mutant

The decreased steady state levels of component Coq polypeptides in the yeast *coq10Δ* mutant are directly related to the destabilization of the CoQ synthome (34). Here, we assessed the stability of CoQ synthome in c*oq10Δ* expressing single- or multi-copy COQ10A or COQ10B by two-dimensional Blue Native/SDS-PAGE (BN/SDS-PAGE). In the first dimension, multi-subunit protein complexes are resolved under non-denaturing native conditions, followed by separation into individual polypeptide constituents in the second dimension by traditional SDS-PAGE under denaturing conditions. Proteins that represent subunits from the same multi-subunit complex are found in one vertical line, and a designated polypeptide component that is present in several distinct complexes or sub-complexes is indicated by a horizontal signal. Thus the CoQ synthome that is represented by its component Coq4 or Coq9 polypeptide is shown by two horizontal lines that align with the Coq4 and Coq9 bands present in the sample of intact mitochondria from each sample in the lane labeled as “M” (Figure 5). In wild-type yeast cells, the CoQ synthome is represented by a complex array of high molecular mass signals, spanning a range of about 400 kDa to > 1 MDa for Coq4 and from ~140 kDa to > 1 MDa for Coq9 (Figure 5A). In contrast, the CoQ synthome in the *coq10Δ* mutant appears destabilized, indicated by the disappearance of complexes much larger than 669 kDa, and an appearance of complexes limited to a distribution between 140 kDa and slightly greater than 669 kDa for both Coq4 and Coq9 signals (Figure 5A). Although expression of single-copy pQM COQ10A restored the steady state polypeptide levels of both Coq4 and Coq9 (Figure 4), the distribution of high

molecular mass signals for Coq4 and Coq9 remains limited to a range similar to that of the *coq10Δ* mutant (Figure 5A). Single-copy pQM COQ10B reinforced the CoQ synthome assemblies below 440 kDa, as shown by intense Coq9 signal (Figure 5A), but it also failed to restore the CoQ synthome at a much greater molecular mass (Figure 5A). Neither multi-copy COQ10A nor COQ10B expression appears to confer a stabilization effect on the CoQ synthome (Figure 5A). Thus, the expression of either COQ10A or COQ10B, while having a rather dramatic effect on steady state Coq polypeptide levels, exerts a negligible effect on the high molecular mass signals that characterize efficient CoQ synthesis and the presence of the CoQ synthome.

Coq10 co-migrates with Coq2 and Coq8 on two-dimensional BN/SDS-PAGE (64), but so far there is no direct evidence showing Coq10 interaction with other known Coq polypeptides or with the CoQ synthome. On a sucrose gradient, native Coq10 from yeast mitochondrial extract sediments at a fraction that corresponds to a molecular weight of approximately 140 kDa (10). Given that the monomeric molecular weight of mature Coq10 is 20 kDa, Coq10 must be present in a complex that consists of an oligomeric form of Coq10, and/or with other partner proteins (10). We tested whether human COQ10A or COQ10B might also assemble into complexes. Because the signal intensities of both COQ10A and COQ10B expressed from single-copy vectors are quite weak, we decided to examine their complex formation when expressed from the multi-copy vector. On the two-dimensional BN/SDS-PAGE, wild-type yeast Coq10-containing complex is distributed across the entire range of high molecular weight standards, but predominantly concentrated between 66 kDa and 232 kDa (Figure 5B), and the Coq10-containing complex is absent in the *coq10Δ* mutant (Figure 5B). Although the signal intensities of COQ10A and COQ10B are low, it appears that COQ10A forms a discrete complex at ~140 kDa (Figure 5B), and COQ10B is dispersed across between 232 kDa and 440 kDa (Figure 5B). Knowing the total amount of protein subjected to analysis by BN/SDS-PAGE, it is possible that a

significant amount of COQ10A and COQ10B may migrate at a much smaller size corresponding to its monomeric molecular weight, not observed by the first dimension gel matrix.

Expression of human COQ10A or COQ10B fails to restore CoQ biosynthesis in the yeast c*oq10Δ* mutant

In yeast, CoQ is produced from two distinct quinone ring precursors, pABA or 4HB (5). Early-stage intermediates 4-amino-3-hexaprenylbenzoic acid (HAB) and 4-hydroxy-3-hexaprenylbenzoic acid (HHB) are the first polyisoprenylated intermediates emerging from pABA and 4HB, respectively (5). Subsequent modifications of the ring of HAB or HHB give rise to late-stage intermediates 4-imino-demethoxy-Q_6H_2 ($IDMQ_6H_2$) or demethoxy-Q_6H_2 (DMQ_6H_2). It is believed that only DMQ_6H_2 gets directly converted to CoQ_6H_2, whereas $IDMQ_6H_2$ represents a dead-end late-stage product; the deamination of HAB is mediated by the Coq6/Coq9 step in the pABA pathway (5). To examine how well single- and multi-copy COQ10A or COQ10B rescues yeast *coq10Δ* de novo CoQ biosynthesis, we labeled the cells with $^{13}C_6$-pABA or $^{13}C_6$-4HB in order to measure the efficiency of CoQ production from both pathways.

Consistent with previously published results (9), we observed that the yeast *coq10Δ* mutant produced less $^{13}C_6$-CoQ_6 (Figure 6A), but significantly higher amounts of early intermediates $^{13}C_6$-HAB (Figure S2A) and $^{13}C_6$-HHB (Figure S2B) during log phase growth. The yeast *coq10Δ* mutant also makes less late-stage intermediates $^{13}C_6$-DMQ_6 (Figure S2C) and $^{13}C_6$-$IDMQ_6$ (Figure S2D) de novo compared to the wild-type cells. One caveat to this result is that when the yeast c*oq10Δ* mutant is transformed with empty vector pQM or pRCM, these empty vectors seem to make significant difference on the levels of all representative CoQ_6-intermediates as well as in CoQ_6 when compared to the *coq10Δ* mutant (Figure 6, S2). We suspected this might be a result of different medium used to culture the *coq10Δ* mutant (SD-Complete) and *coq10Δ* mutant with empty vectors (SD−Ura). Therefore, we compared the yeast

coq10Δ expressing single- or multi-copy COQ10A or COQ10B to their respective empty vector controls for the statistical analyses. If COQ10A or COQ10B were to restore efficient de novo CoQ biosynthesis, we would expect lower amounts of $^{13}C_6$-HAB, $^{13}C_6$-HHB, and higher amount of $^{13}C_6$-CoQ_6. However, expression of either COQ10A or COQ10B has only a minimal effect on the de novo biosynthesis of $^{13}C_6$-CoQ_6. Single-copy COQ10A seems to make slightly more $^{13}C_6$-CoQ_6 from labeled pABA and 4HB (Figure 6A), and has slightly higher levels of total CoQ_6 (Figure 6B) when compared to the empty vector control. In contrast, expression of COQ10B, particularly in multi-copy, decreases de novo $^{13}C_6$-CoQ_6, as well as the total CoQ_6 content (Figure 6A, B). While single- and multi-copy of COQ10A, and multi-copy COQ10B synthesize $^{13}C_6$-DMQ_6 (Figure S2C) and $^{13}C_6$-$IDMQ_6$ (Figure S2D), the conversion from early-stage intermediates to late-stage intermediates is slow as indicated by a buildup of the labeled $^{13}C_6$-HAB (Figure S2A) and $^{13}C_6$-HHB (Figure S2B).

In addition to $^{13}C_6$-labeled CoQ_6 and CoQ_6-intermediates, we also quantified the unlabeled CoQ_6 and CoQ_6-intermediates (Figure 6B, S2E-H). Similar to what we observed with the $^{13}C_6$-labeled CoQ_6 and CoQ_6-intermediates, the yeast *coq10Δ* mutant expressing single- or multi-copy COQ10A or COQ10B has only a negligible effect on the steady state levels of CoQ_6 and CoQ_6-intermediates. To summarize, neither single- nor multi-copy expression of COQ10A or COQ10B functionally restores de novo CoQ biosynthesis to the wild-type level, and has negligible effects on the synthesis of early stage CoQ_6-intermediates relative to the empty vector control. Given that the high molecular weight CoQ synthome is known to be necessary for efficient CoQ_6 biosynthesis in yeast, it is not surprising that each of the human COQ10 orthologs fails to restore the yeast de novo CoQ_6 production.

Human COQ10A rescues PUFA sensitivity of the yeast *coq10Δ* mutant

PUFAs are particularly susceptible to oxidative damage caused by ROS-dependent abstraction of hydrogen atoms at bis-allylic positions, generating carbon centered free radicals (65). In the presence of oxygen, the resulting peroxyl radicals trigger a chain reaction of lipid peroxidation, and propagate oxidative damage to other macromolecules. Collectively, this oxidative damage results in DNA mutations, protein fragmentation, and formation of protein-protein cross links (66). As shown in Figure 7, the yeast CoQ-less mutant (*coq9Δ*) is sensitive to α-linolenic acid due to the absence of antioxidant protection offered by CoQ (30, 31). The yeast *coq10Δ* mutant is also sensitive to treatment with α-linolenic acid presumably because the chaperone function of the Coq10 polypeptide is necessary for the ability of CoQ to function as an antioxidant (9). This chaperone function of Coq10 is independent of its role in respiration per se, because a CoQ-replete respiratory deficient mutant lacking a subunit of complex III (*cor1Δ*) is resistant to α-linolenic acid (Figure 7). Thus, we assessed whether the sensitivity to PUFA treatment of yeast *coq10Δ* was rescued by the expression of single- or multi-copy human COQ10A or COQ10B. Expression of either single- or multi-copy COQ10A rescued yeast *coq10Δ* sensitivity to treatment with α-linolenic acid (Figure 7). Multi-copy COQ10B partially rescued yeast *coq10Δ* sensitivity to α-linolenic acid, while single-copy COQ10B did not have a significant effect (Figure 7). As expected, yeast strains tested were resistant to monounsaturated oleic acid (Figure 7). Thus, our data suggest that COQ10A and COQ10B are only partially able to complement the yeast *coq10Δ* mutant; both human co-orthologs are capable of rescuing defective respiration and PUFA sensitivity in the yeast *coq10Δ* mutant, but fail to rescue the defect in CoQ_6 biosynthesis.

COQ10 family analysis

A protein sequence similarity network analysis reveals that the COQ10-like family can be divided into six main similarity clusters that are generally grouped by taxonomy (Figure 8A). The COQ10-like proteins from land plants and green algae (with the exception of prasinophyte

homologs) are closely related to animal homologs, and in the phylogenetic tree reconstruction are nestled within the metazoan clade (Figure 8B). Two groups of bacterial proteins are found in the COQ10-like family. Proteins encoded by genes (referred to as *yfjG*/*ratA* in *E. coli*) in the highly conserved *smpB-ratA-yfjF* gene neighborhood (67, 68) dominate bacterial cluster 1. RatA from *E. coli* (see sequence alignment in Fig 2A) has a proposed role in cell cycle arrest as a response to stresses such as nutrient starvation (69). Upon induction, RatA blocks 70S ribosome association, and inhibits the translation initiation step (69). The first gene in the neighborhood, *smpB*, also encodes a protein that interacts with the ribosome through a complex formed with tmRNA that is essential for rescuing stalled ribosomes (70, 71). The third gene in the conserved operon, *yfjF*, encodes a protein of unknown function, which was renamed RatB, an assumed antitoxin of RatA, but evidence suggests that RatB does not function as an antitoxin to RatA (69). YfjF is homologous to RnfH, a *Rhodobacter capsulatus* homolog encoded by a gene at the end of the *rnf* operon (72). Rnf is an enzyme complex homologous to but distinct from the bacterial respiratory complex Na^+-dependent NADH: ubiquinone oxidoreductase (Na^+-NQR) (73). However, a role for RnfH in the Rnf complex is unsubstantiated and many *rnf* operons do not encode an RnfH orthologs (74).

Proteins encoded by genes that are often physically clustered with *lipA* orthologs, which encode lipoyl synthases, dominate bacterial cluster 2. Mining co-expression databases revealed that the characterized *COQ10* from *S. pombe* is co-expressed with *AIM22* (second-ranked co-expressed gene) (75), encoding a putative lipoate-protein ligase A. These two functional inferences (conserved gene clusters in bacteria and co-expression in *S. pombe*) may point to a yet uncharacterized role of COQ10 in lipoic acid biosynthesis or regulation; lipoic acid is a prosthetic group covalently attached to several dehydrogenases within the mitochondria. We also note that the top-ranked co-expressed gene in *S. cerevisiae*, *MDM12,* is positioned head-to-head with *COQ10 (75),* suggesting that the two genes share a bi-directional promoter. The mitochondrial distribution and morphology protein (Mdm12) is the cytosolic subunit of the ER-

mitochondria encounter structure (ERMES) for establishing the ER-mitochondria contact sites, the absence of which causes severe mitochondrial morphological defects, defects in respiration, and rapid loss of mitochondrial DNA (76, 77).

The Coq10-Coq11 fusion proteins found in genomes from *Ustilaginaceae* (78) are also shown in Figure 8. Additional domains found in the present analysis fused to the COQ10 domain (PF03364) (encoded by at least two different species) include PF00098 (zinc-finger domain), PF00227/PF10584 (proteasome subunits), and PF00378 (enoyl-CoA hydratase/isomerase family). Additionally, both COQ10A and COQ10B were previously found to interact with the enoyl-CoA hydratase ECH1, which in turn, has been observed to interact with COQ2, COQ3, COQ4, COQ6, COQ7 and COQ8A (79, 80). Mining co-expression databases, both *COQ3* and *COQ8A* also co-express with *COQ10A* (81). The human ECH1 localizes to the matrix of mitochondria and participates in β-oxidation of unsaturated fatty acids (82), and the interaction of ECH1 with both COQ10A and COQ10B aligns well with their roles as chaperones to deliver CoQ as a cofactor for the reaction.

DISCUSSION

This study provides another piece of evidence supporting the functional conservation of yeast and human proteins involved in CoQ biosynthesis. Unlike yeast, humans have two isoforms of COQ10, which may have evolved by a duplication event during chordate evolution (Figure 8B). RNA-seq analysis of different human tissues suggests that although both COQ10A and COQ10B are universally expressed, COQ10A seems predominantly expressed in heart and skeletal muscle cells (83, 84). Knowing that COQ10A and COQ10B share 66% sequence identity (84% similarity), the enrichment of COQ10A in human heart and skeletal muscle implies a functional specialization of the protein. From our experimental results, it is curious to note that single-copy COQ10A performs the best in terms of restoring steady state Coq polypeptide levels (Figure 4), stabilizing CoQ synthome (Figure 5), and restoring resistance against PUFAs (Figure 7), despite the finding that single-copy COQ10A seems to restore respiratory growth phenotype just as well as both single- and multi-copy COQ10B on YPG plate medium (Figure 1B). In contrast, neither COQ10A nor COQ10B expression restores de novo CoQ synthesis in yeast when compared to the *coq10Δ* empty vector control (Figure 6, S2). Efficient CoQ biosynthesis requires properly assembled CoQ synthome, but neither COQ10A nor COQ10B expression fully restores the CoQ synthome assembly (Figure 5). Importantly, neither COQ10A nor COQ10B expression restores the steady state levels of Coq4, which is known to be the central organizer protein of the CoQ synthome (34). Additionally, the assembly and stability of the CoQ synthome relies on the presence of CoQ_6 and CoQ_6-intermediates. Studies have shown that reestablishment of de novo CoQ_6 biosynthesis and the levels of certain CoQ_6-intermediates restore CoQ synthome assembly and CoQ domain formation (34, 85). The CoQ synthome is responsible for efficient de novo CoQ biosynthesis, and the resulting CoQ and CoQ-intermediates are in turn necessary to stabilize the CoQ synthome. Because neither COQ10A nor COQ10B rescues the defect in de novo CoQ_6 production, the amounts of CoQ_6 or CoQ_6-intermediates may not be sufficient to restore and stabilize the CoQ synthome. However,

expression of either the human COQ10A or COQ10B orthologs complemented the *coq10Δ* glycerol growth (Figure 1B). Thus, human COQ10A and COQ10B fulfill two independent functions in yeast: 1) both facilitate the function of CoQ in respiration; and 2) both enable CoQ to function as a chain-terminating antioxidant. However, neither COQ10A nor COQ10B function to restore the efficient CoQ biosynthesis in yeast.

One possibility is that a coordinated action of both yeast Coq10 and Coq11 is necessary to restore efficient CoQ biosynthesis in yeast *coq10Δ* mutant. In mammalian cells, it is common that the START domain may be coupled with other motifs/domains on the same protein, offering additional functions such as localization, enzymatic activity, or signaling (12, 13, 86). For instance, the metastatic lymph node 64 (MLN64) is a cholesterol-specific START protein, and it contains a conserved membrane-spanning (MLN64 N-terminal) MENTAL domain in addition to the START domain (87). The NMENTAL domain anchors MLN64 to the late endosome membranes, from which the MENTAL domain can capture cholesterol and subsequently transfer it to cytoplasmic START domain (14, 87, 88). Yeast Coq11 belongs to the short-chain dehydrogenase/reductase (SDR) superfamily, which contains a conserved Rossmann fold with N-terminal binding site for NAD(H) or NADP(H) (89). The *S. cerevisiae coq11Δ* does not exhibit apparent growth defect on non-fermentable carbon source, but its de novo $^{13}C_6$-CoQ_6 production is significantly lower compared to the wild-type cells (78). *S. cerevisiae coq10Δ* shares very similar phenotype except that its growth on non-fermentable carbon sources is impaired but not completely abolished. Thus, it may be possible that in yeast, the Coq10 and Coq11 functions need to be coordinated in order to achieve wild-type level efficiency for de novo CoQ_6 biosynthesis. The presence of Coq10-Coq11 fusion protein in several *Ustilaginaceae* species (Figure 8) further consolidates a potential functional link conferred by their physical interaction and/or function in the same biological pathway. In mammalian cells, the closest but distinct homolog to yeast Coq11 is NDUFA9, a NADH dehydrogenase and a Complex I

ubiquinone reduction-module (Q-module) subunit (78, 90). However, because humans do not have Coq11, a similar interaction between Coq10 and Coq11 either never evolved or was lost during evolution. Therefore, we postulate that neither human COQ10A nor COQ10B was able to interact with yeast Coq11, hence failing to restore de novo CoQ biosynthesis (Figure 6, S2). In contrast, plants and algae do have orthologs of yeast Coq11 and have evolved to use Coq11 or Coq11-like proteins (78). The *Arabidopsis thaliana* genome encodes four Coq11 orthologs (At1g32220, At5g15910, At5g15480, and At5g10730), and the chloroplast-localized flavin reductase-related protein At1g32220 is thought to be involved in plastoquinone biosynthesis (49, 78). In COXPRESdb, *COQ10A* is co-expressed with SDR39U1, which like Coq11 belongs to the SDR superfamily (75), and SDR39U1 was found co-eluting with human COQ9 from a hydroxyapatite column in mitochondria solubilized with Triton X-100 (91). These functional inferences may supply a link between human COQ10 and Coq11-like proteins in CoQ production.

So far, most of the publications on yeast Coq10 are focused on its putative function as a CoQ chaperone for its function in respiration and as a lipophilic antioxidant. The Coq10 similarity network analysis (Figure 8A) suggests that Coq10 homologs may be functionally linked to lipoic acid synthesis and/or regulation. Lipoic acid is a sulfur-containing co-factor and is essential for enzymatic functions of pyruvate dehydrogenase, α-ketoglutarate dehydrogenase, as well as the glycine cleavage system (92). Lipoic acid is assembled on its cognate proteins from precursor octanoic acid from the fatty acid biosynthesis pathway to a specific lysine residue of the cognate protein by octanoyl transferase (LipB), followed by insertion of sulfur by lipoyl synthetase (LipA) (92). Eukaryotes contain a conserved mitochondrial fatty acid synthetic pathway, independent from cytosolic fatty acid biosynthesis machinery (93). The respiratory competence in yeast is dependent on the ability of mitochondria to synthesize fatty acids, and yeast deletion mutants of enzymes involved in mitochondrial fatty acid synthesis exhibit

respiratory deficient phenotype and small mitochondria, possibly mediated by inefficient tRNA processing by RNase P cleavage (93). A role for Coq10 or Coq10 homologs in fatty acid synthesis has not been substantiated, but because yeast *coq10Δ* is respiratory-defective, it would be interesting to examine the mitochondrial morphology in this particular mutant and assess the lipoic acid-dependent enzyme activities.

Another possible functional role of Coq10 relates to the co-expression of *COQ10* and *MDM12* from a shared promoter in *S. cerevisiae* (Figure 8A) (94). The arrangement and co-regulation of different genes via promoter sharing is indicative of functional connection and/or physical interactions between the two gene products. In yeast, Mdm12 is positioned on the mitochondrial outer membrane as part of the ERMES complex subunit; Mdm12 bridges Mmm1 localized at the ER membrane with Mdm10 and Mdm34 at the cytosolic site (76). The ERMES complex mediates ER-mitochondrial contacts, essential for lipid exchange between the two organelles (76). Recently, polypeptide members of the CoQ synthome (Coq3-Coq7, Coq9, and Coq11) have been shown to localize selectively to multiple domains (CoQ domains) (85, 95). These CoQ domains are marked by ER-mitochondria contact sites, and are established by START-like domain containing, ER membrane sterol transporter protein Ltc1 in complex with the mitochondrial outer membrane protein Tom71, as well as by the ERMES complex (85, 95). Presence of the CoQ domain relies on the cooperative assembly of the CoQ synthome components (85). Absence of any one subunit of the ERMES complex also elicits a dramatic effect on the overall stability of the CoQ synthome and CoQ domain formation, but only negligible effect on the steady state levels of the constituent Coq polypeptides of the CoQ synthome (85, 95). Deletion of *LTC1* in the *mmm1Δ* mutant further enhanced the defect of CoQ domain formation, suggesting a redundant functional role of these two ER-mitochondria tethers for domain positioning in the mitochondria (85). The *ERMESΔ* mutants accumulate steady state and $^{13}C_6$-labeled CoQ_6-intermediates as a result of inefficient CoQ_6 biosynthesis from

destabilized CoQ synthome (95). Interestingly, these *ERMESΔ* mutants retain more $^{13}C_6$-labeled CoQ_6 even though their steady state CoQ_6 levels inside the mitochondria are lower compared to the wild-type cells (95). The disruption of CoQ_6 homeostasis presumably results from the reduced sequestration of CoQ_6 within the mitochondria and/or compromised degradation of CoQ_6 at the peroxisomes, which have been reported to co-localize with the ERMES complex at specific mitochondrial subdomains (95, 96). Inside the yeast mitochondria, two separate studies have observed a reduced number of CoQ synthome domain formation in the yeast *coq10Δ* mutant, which is likely contributed by the partial destabilization of the CoQ synthome, as well as component Coq polypeptides in the absence of Coq10 (63, 85, 95). The establishment of CoQ domains within mitochondria relies on CoQ-intermediates, and substrate flux (85), which seems to correlate well with the role of Coq10 in mediating efficient CoQ production. However, the exact mechanism underlying the role of Coq10 in coordination of the ER-mitochondria contact sites and CoQ biosynthesis remains to be elucidated.

Similar CoQ domains are also observed in human cells (85). However, mammalian cells do not have orthologs of ERMES polypeptides, and the physical contact between ER and mitochondria is established by homo- or hetero-dimerization of ER-localized mitofusin 2 (MFN2) with MFN1 or MFN2 on the mitochondrial outer membrane (97). Loss of MFN2 impairs respiration capacity, originating from a depletion of mitochondrial CoQ content and reduced CoQ-dependent NADH-cytochrome *c* reductase and succinate-cytochrome *c* reductase activities (98). Proteomic and metabolic analyses suggest that loss of MFN2 likely affects the isoprene biosynthesis pathway that is upstream of both CoQ and cholesterol biosynthesis, but the effect is only observed as decreased CoQ but not cholesterol levels (98). Similar to the yeast system, the enzymes involved in the isoprene biosynthetic pathway exist in different organelles, including mitochondria, ER, and peroxisomes (98), however the functional implications of the involvement of human COQ10A and COQ10B in physical coordination of these organelles remain to be uncovered.

In summary, this study indicates that although expression of the human COQ10A or COQ10B orthologs failed to restore efficient de novo synthesis of CoQ_6, they nonetheless rescue the respiratory deficiency and the sensitivity to oxidative stress of the yeast *coq10Δ* mutant. These results indicate that the Coq10 START domain functions as a CoQ chaperone, necessary for respiration dependent cellular bioenergetics and defense mechanisms against oxidative stress. The COQ10 family protein analyses provide additional insights into the possible roles of Coq10-dependent transport of CoQ, necessary for its function as a cofactor in biological pathways and trafficking between organelles.

Table 1. Genotype and source of yeast strains

Strain	Genotype[a]	Source
W303 1B	MAT α, *ade2-1 can1-100 his3-11,15 leu2-3,112 trp1-1 ura3-1*	R. Rothstein[b]
W303 *coq1Δ*	MAT α, *ade2-1 can1-100 his3-11,15 leu2-3,112 trp1-1 ura3-1 coq1::LEU2*	(99)
CC303	MAT α, *ade2-1 can1-100 his3-11,15 leu2-3,112 trp1-1 ura3-1 coq3::LEU2*	(100)
W303 *coq4Δ*	MAT **a**, *ade2-1 can1-100 his3-11,15 leu2-3,112 trp1-1 ura3-1 coq4::TRP1*	(101)
W303 *coq5Δ*	MAT α, *ade2-1 can1-100 his3-11,15 leu2-3,112 trp1-1 ura3-1 coq5::HIS3*	(27)
W303 *coq6Δ*	MAT **a**, *ade2-1 can1-100 his3-11,15 leu2-3,112 trp1-1 ura3-1 coq6::LEU2*	(102)
W303 *coq7Δ*	MAT α, *ade2-1 can1-100 his3-11,15 leu2-3,112 trp1-1 ura3-1 coq7::LEU2*	(103)
W303 *coq8Δ*	MAT **a**, *ade2-1 can1-100 his3-11,15 leu2-3,112 trp1-1 ura3-1 coq8::HIS3*	(101)
W303 *coq9Δ*	MAT α, *ade2-1 can1-100 his3-11,15 leu2-3,112 trp1-1 ura3-1 coq9::URA3*	(104)
W303 *coq10Δ*	MAT **a**, *ade2-1 can1-100 his3-11,15 leu2-3,112 trp1-1 ura3-1 coq10::HIS3*	(10)
W303 *coq11Δ*	MAT **a**, *ade2-1 can1-100 his3-11,15 leu2-3,112 trp1-1 ura3-1 coq11::HIS3*	This study

[a]Mating type **a** (MAT **a**) is in bold to distinguish it from mating type alpha (MAT α).
[b]Dr. Rodney Rothstein, Department of Human Genetics, Columbia University. New York, NY.

Table 2. Yeast expression vectors

Plasmid	Relevant genes/markers	Source
pQM	pAH01 with *COQ3* mito leader, single-copy	(28)
pQM COQ10A	pQM with human *COQ10A*; single-copy	This work
pQM COQ10B	pQM with human *COQ10B*; single-copy	This work
pRCM	pCH1 with *COQ3* mito leader; multi-copy	(9)
pRCM COQ10A	pRCM with human *COQ10A*; multi-copy	This work
pRCM COQ10B	pRCM with human *COQ10B*; multi-copy	This work

Table 3. Description and source of antibodies

Antibody	Working dilution	Source
Coq1	1:10,000	(99)
Coq3	1:200	(105)
Coq4	1:2,000	(106)
Coq5	1:5,000	(107)
Coq6	1:200	(102)
Coq7	1:1,000	(108)
Coq8	Affinity purified, 1:30	(63)
Coq9	1:1,000	(109)
Coq10	Affinity purified, 1:400	This work
Coq11	1:500	This work
Mdh1	1:10,000	Lee McAlister-Henn[c]
COQ10A	1:500	Proteintech
COQ10B	1 µg/mL	Abcam

[c] Dr. Lee McAlister-Henn, Department of Molecular Biophysics and Biochemistry, University of Texas Health Sciences Center, San Antonio, TX

Table 4. Precursor-to-product ion transitions

	m/z $[M+H]^+$	m/z $[M+NH_4]^+$
HAB	546.4/150.0	563.0/150.0
$^{13}C_6$-HAB	552.4/156.0	569.0/156.0
HHB	547.4/151.0	564.0/151.0
$^{13}C_6$-HHB	553.4/157.0	570.4/157.0
DMQ_6	561.4/167.0	578.0/167.0
$^{13}C_6$-DMQ_6	567.4/173.0	584.0/173.0
$IDMQ_6$	560.6/166.0	577.0/166.0
$^{13}C_6$-$IDMQ_6$	566.6/172.0	583.0/172.0
CoQ_4	455.4/197.0	472.0/197.0
CoQ_6	591.4/197.0	608.0/197.0
$^{13}C_6$-CoQ_6	597.4/203.0	614.0/203.0

Supplemental Table S1. Predicted human COQ10A and COQ10B mitochondrial targeting sequence[d]

Protein	N-terminal sequence[e]
COQ10A isoform 1	**MAWAGSRRVPAGTRA**AAERCCRLSLSPGAQPAPPPGPLPPPRPMR[46]FLTSCS…
COQ10A isoform 2	MLLQVVREGKFSG[14]FLTSCS…
COQ10B isoform 1	**MAARTGHTALRRVVSGCRPKSATAAGAQAPVRNGRYL**ASCGILMSRTLPLHTSILPKEICARTFFKITAPLINKRKEYSERRILG[86]YSMQEM…
COQ10B isoform 2	**MAARTGHTALRRVVSGCRPKSATAAGAQAPVRNGR**----------[36]YSMQEM...
COQ10B isoform 3	MGVCVWR----------YLASCGILMSRTLPLHTSILPKEICARTFFKITAPLINKRKEYSERRILG[58]YSMQEM…
COQ10B isoform 4	MSRTLPLHTSILPKEICARTFFKITAPLINKRKEYSERRILG[43]YSMQEM…

[d]UniprotKB, https://www.uniprot.org

[e]NCBI, https://www.ncbi.nlm.nih.gov

The N-terminal sequence of the human COQ10A and COQ10B isoforms were aligned with their predicted mitochondrial targeting sequence highlighted in bold. The amino acid residue number in superscript represented the beginning of the shared amino acid sequences among isoforms of either COQ10A or COQ10B.

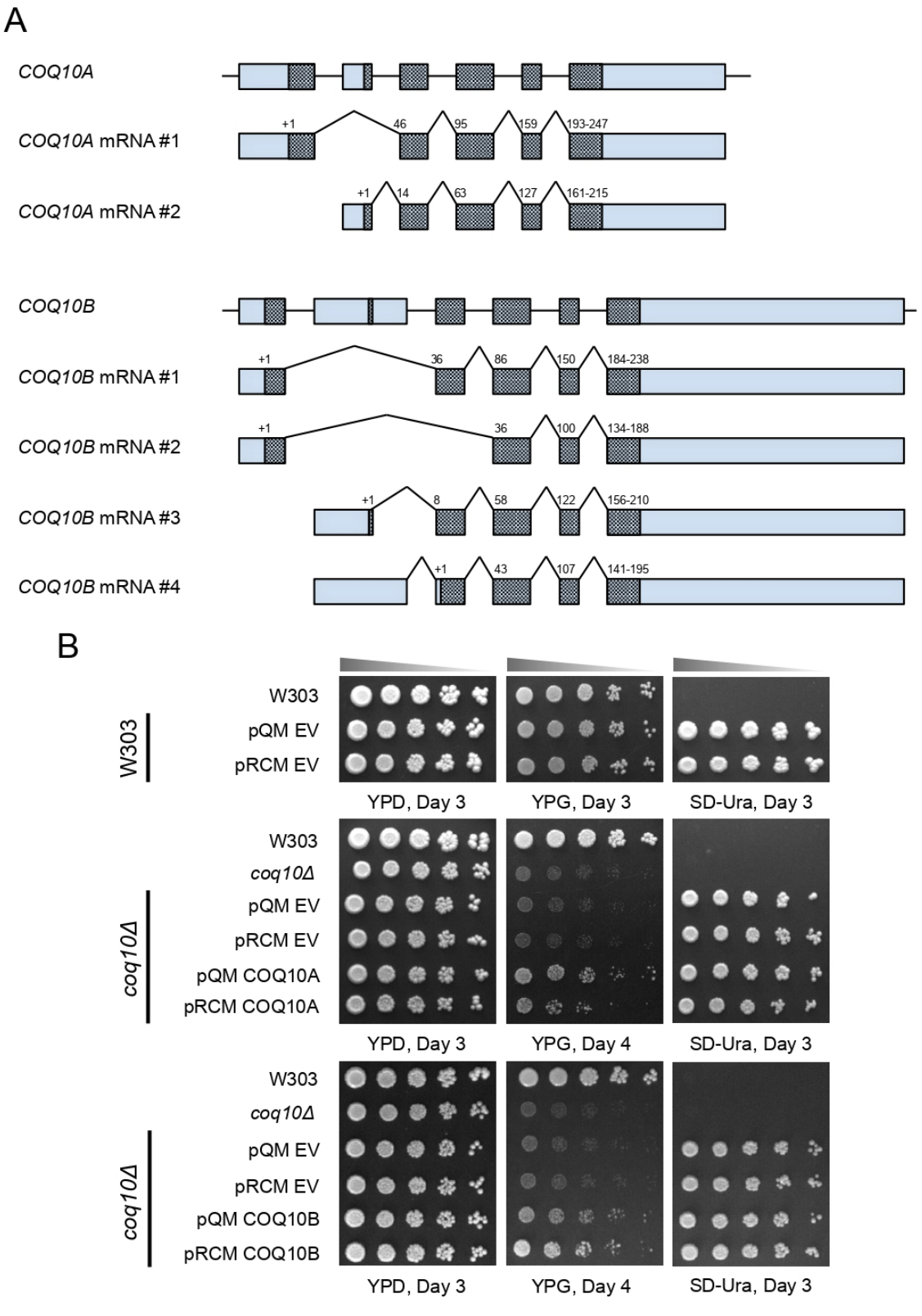
A
COQ10A
COQ10A mRNA #1
+1
46
95
159
193-247
COQ10A mRNA #2
+1
14
63
127
161-215
COQ10B
COQ10B mRNA #1
+1
36
86
150
184-238
COQ10B mRNA #2
+1
36
100
134-188
COQ10B mRNA #3
+1
8
58
122
156-210
COQ10B mRNA #4
+1
43
107
141-195
B
W303
W303
pQM EV
pRCM EV
YPD, Day 3
YPG, Day 3
SD-Ura, Day 3
coq10Δ
W303
coq10Δ
pQM EV
pRCM EV
pQM COQ10A
pRCM COQ10A
YPD, Day 3
YPG, Day 4
SD-Ura, Day 3
coq10Δ
W303
coq10Δ
pQM EV
pRCM EV
pQM COQ10B
pRCM COQ10B
YPD, Day 3
YPG, Day 4
SD-Ura, Day 3

Figure 1. Expression of either human COQ10A or COQ10B restores respiratory growth of the yeast *coq10Δ* mutant. A) A schematic representation of alternative splicing of human *COQ10A* and *COQ10B* mRNA. Alternative splicing and different translation initiation sites result in two isoforms of COQ10A and four isoforms of COQ10B. Boxes represent the exons, and the protein coding sequences are shaded within the exons. Both exons and the protein coding sequences were drawn relative to their corresponding number of base pairs. The introns are represented by horizontal lines and are not drawn to scale. The translation initiation sites were marked as "+1" on top of the protein coding sequence, and the numbers denote the amino acid residue numbers at the beginning of the coding sequence within each exon. The amino-terminal sequences of all isoforms of COQ10A and COQ10B are listed in Supplemental Table S1, with predicted mitochondria targeting sequence highlighted in bold. **B)** Wild-type W303, *coq10Δ* mutant, *coq10Δ* expressing single-copy (pQM), multi-copy (pRCM) human COQ10A, COQ10B, or their respective empty vectors were inoculated in SD-Complete or SD−Ura liquid medium overnight, from which a series of five-fold dilutions of the overnight culture were prepared and plated on to YPD, YPG, and SD−Ura plate medium. Aliquots of 2 µL of samples from serial dilutions were plated in each spot, starting at 0.2 OD_{600}/mL in the first spot to the left. Pictures were taken three or four days after incubation at 30°C.

A

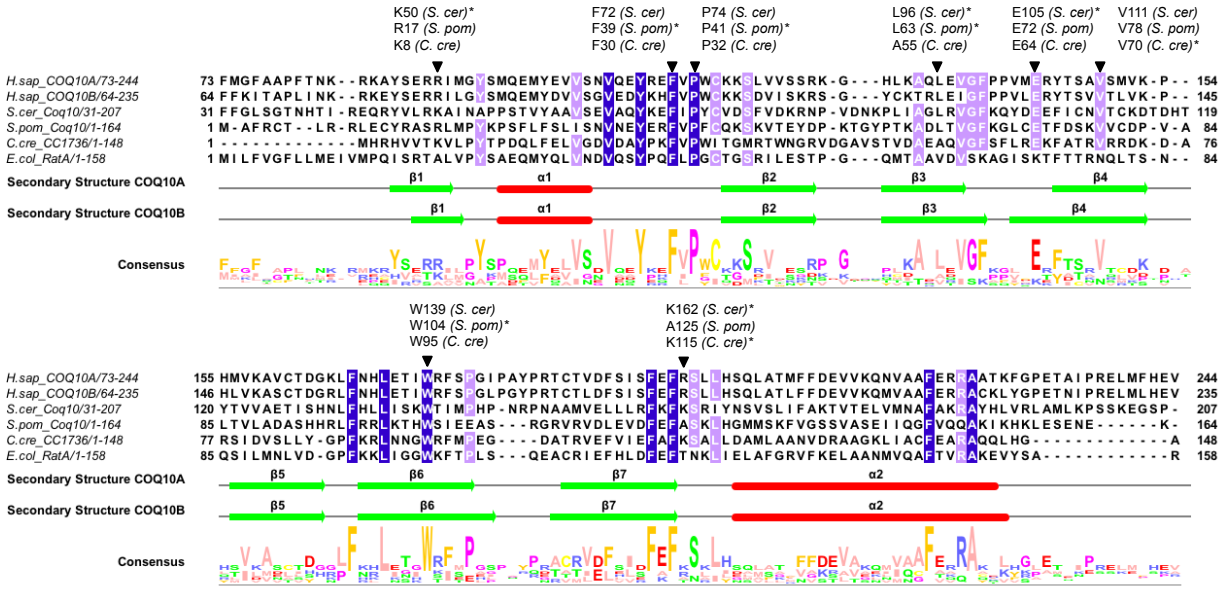

B

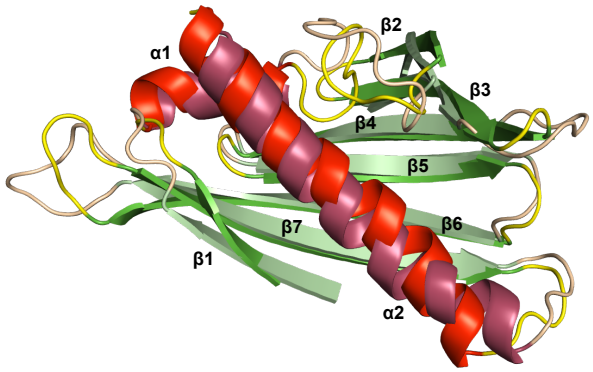

C

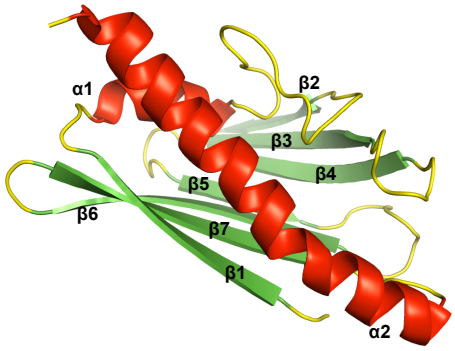

	RMSD (Å)	
Model Pair	Backbone	All Atom
COQ10A:COQ10B	2.205	2.614
CC1736:COQ10A	2.685	3.045
CC1736:COQ10B	2.526	2.915

Figure 2. Human COQ10A and COQ10B share low sequence identity with Coq10 orthologs, but are predicted to contain conserved START domain structures for lipid binding. A) Sequence alignment of human COQ10A (residue 73-244) and COQ10B (residue 64-235) with Coq10 orthologs in *S. cerevisiae*, *S. pombe*, *C. crescentus*, and *E. coli*. Multiple sequence alignment was constructed using Tcoffee, with identical residues shaded in blue and highly conserved residues shaded in lilac. Residues that have been previously tested and deemed critical for ligand binding are indicated with an inverted triangle, and the asterisk indicates the organism in which the site-directed mutagenesis study was performed. The secondary structures of COQ10A and COQ10B were predicted using JPred and adjusted based on their refined models in **B)**. Alpha-helices are shown in red and labeled α1-α2, and β-sheets are shown in green and labeled β1-β7. The figure was assembled in Jalview. **B)** Overlay of predicted homologous models of human COQ10A and COQ10B were generated using the structures of MSMEG_0129 from *Mycobacterium smegmatis* (pdb ID: 5Z8O) as a template. The predicted structures of COQ10A (dark shade) and COQ10B (bright shade) were colored respectively, based on their predicted secondary structures. The COQ10A and COQ10B share a similar START domain, a hydrophobic cavity consists of α-helix (red) and anti-parallel β-sheets (green). **C)** NMR structure of CC1736 (pdb ID: 1T17), a Coq10 ortholog in *C. crescentus* (11). Structures in **B)** and **C)** were generated using PyMOL.

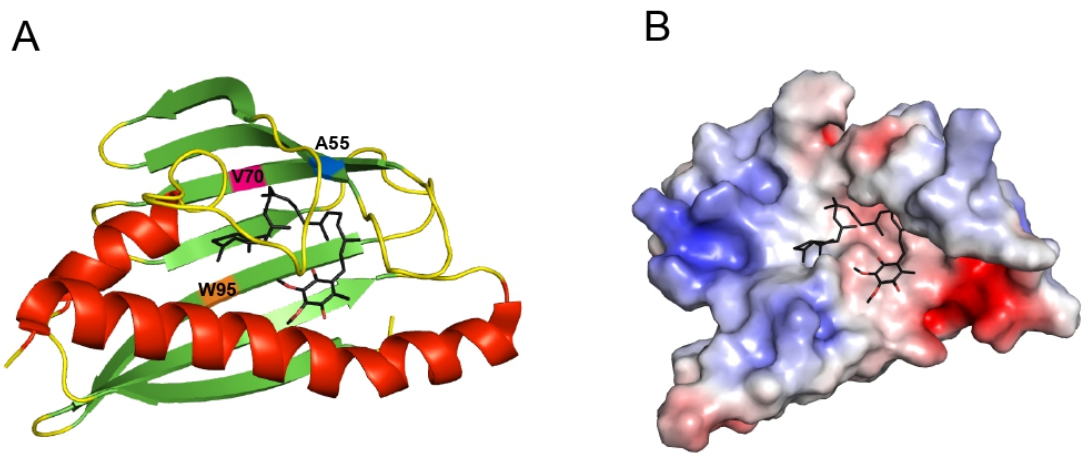

Figure 3. CoQ_6 docks in the hydrophobic cavity of CC1736. **A)** CoQ_6 (colored in black) was docked to the NMR structure of CC1736 using AutoDock. The α-helices are shown in red and β-sheets are shown in green. Docking structures were produced using Autodock vina (45). **B)** Electrostatic surface of CC1736 showing the cavity docked with CoQ_6 with some residues hidden for clarity (red, negative, and blue, positive). The polyisoprenoid chain is threaded through the hydrophobic cleft crated by residues Ala55, Val70, and Trp95.

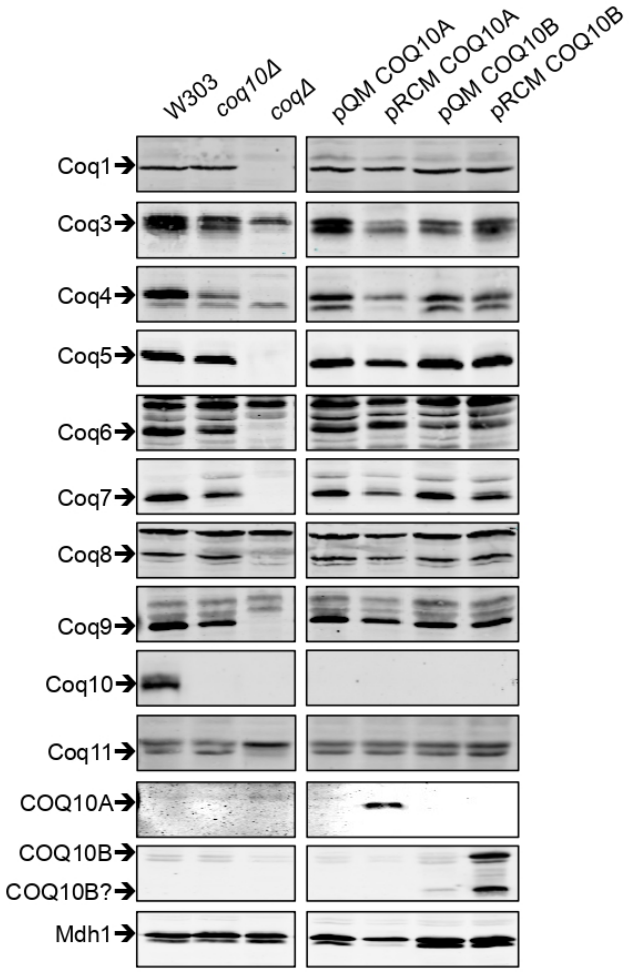

Figure 4. Expression of either human COQ10A or COQ10B restores steady state levels of Coq polypeptides. An aliquot of 25 µg of purified mitochondrial protein from wild type, *coq10Δ*, or *coq10Δ* expressing single- or multi-copy COQ10A or COQ10B was applied to each lane and separated on 12% Tris-Glycine SDS-PAGE gels. Purified mitochondria from *coq1Δ*, and *coq3Δ* - *coq11Δ* mutants were included as negative controls for Western blotting against each of the Coq polypeptide. Purified mitochondria from *coq10Δ* were used as *coqΔ* control for blotting against human COQ10A and COQ10B. Yeast mitochondrial malate dehydrogenase (Mdh1) was included as loading control. Two panels (left and right) were immunoblots derived from the same nitrocellulose membrane. Relative protein levels were quantified by band densitometry in Supplemental Figure S1 using Image J software.

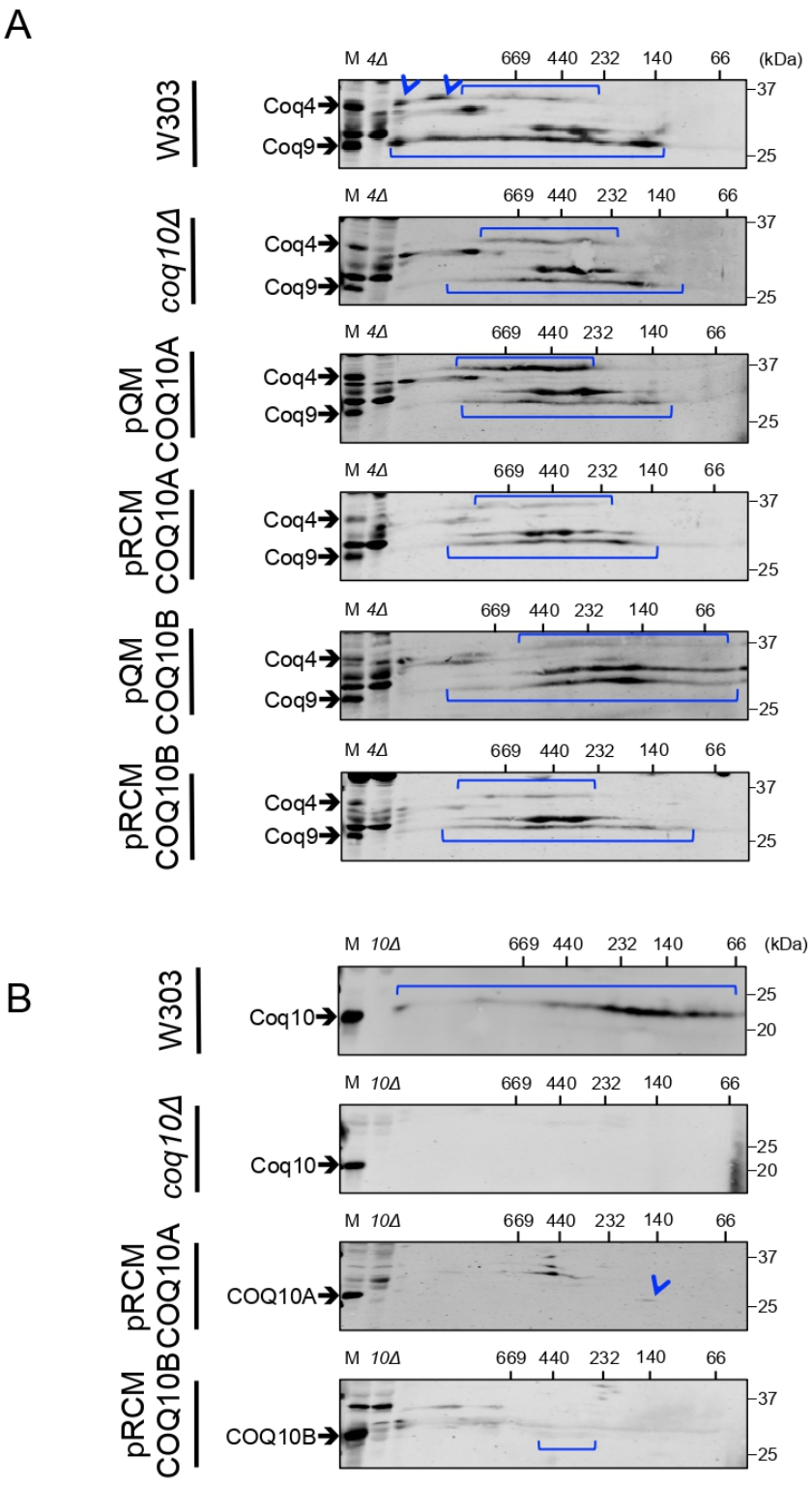
A
W303
coq10Δ
pQM COQ10A
pRCM COQ10A
pQM COQ10B
pRCM COQ10B
M 4Δ
669 440 232 140 66 (kDa)
Coq4
Coq9
37
25
B
M 10Δ
669 440 232 140 66 (kDa)
Coq10
COQ10A
COQ10B
25
20
37

Figure 5. Expression of either human COQ10A or COQ10B partially restores the yeast CoQ synthome. An aliquot of 80 µg of purified mitochondrial protein from wild type, *coq10Δ*, or *coq10Δ* expressing single- or multi-copy COQ10A or COQ10B was resolved on a two-dimensional BN/SDS-PAGE, and blotted against **A)** Coq4 and Coq9, or against **B)** Coq10, COQ10A, or COQ10B. An aliquot of 25 µg of un-solubilized intact mitochondrial from each designated sample was loaded in the lane labeled "M", and same amount of intact *coq4Δ* or *coq10Δ* mitochondria were included as negative controls. The yeast *coq4Δ* mutant lacks both Coq4 and Coq9 polypeptides (63), and was used as a negative control for blotting against both proteins on the same membrane.

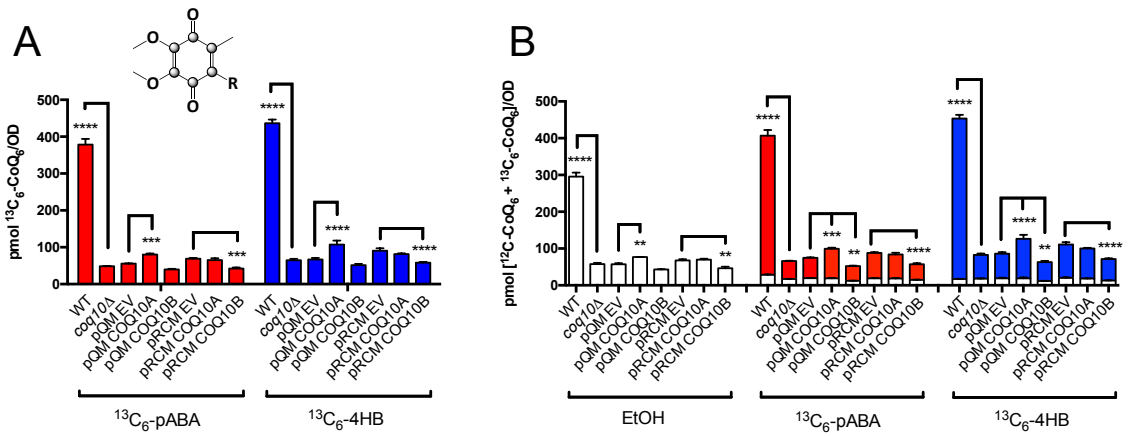

Figure 6. Expression of either human COQ10A or COQ10B has minimal effect on de novo CoQ_6 biosynthesis and total CoQ_6 content. The de novo production of CoQ_6 was measured from yeast whole cell lipid extracts from wild type, *coq10Δ*, *coq10Δ* expressing single- or multi-copy COQ10A or COQ10B, or their respective empty vector labeled with $^{13}C_6$-pABA (red) or $^{13}C_6$-4HB (blue) for 5 hours. Expression of single- or multi-copy COQ10A or COQ10B has almost negligible effect on both **A)** de novo $^{13}C_6$-CoQ_6 and **B)** total CoQ_6 when compared to their respective empty vector controls. The statistical analyses were performed using two-way ANOVA multiple comparisons from three biological replicates, comparing yeast *coq10Δ* expressing single- or multi-copy COQ10A or COQ10B to their respective empty vector controls, and comparing yeast *coq10Δ* mutant to the wild-type control. The error bar indicates mean ±SD, and the statistical significance is represented by *p < 0.05, **p < 0.01, ***p < 0.001 and ****p < 0.0001.

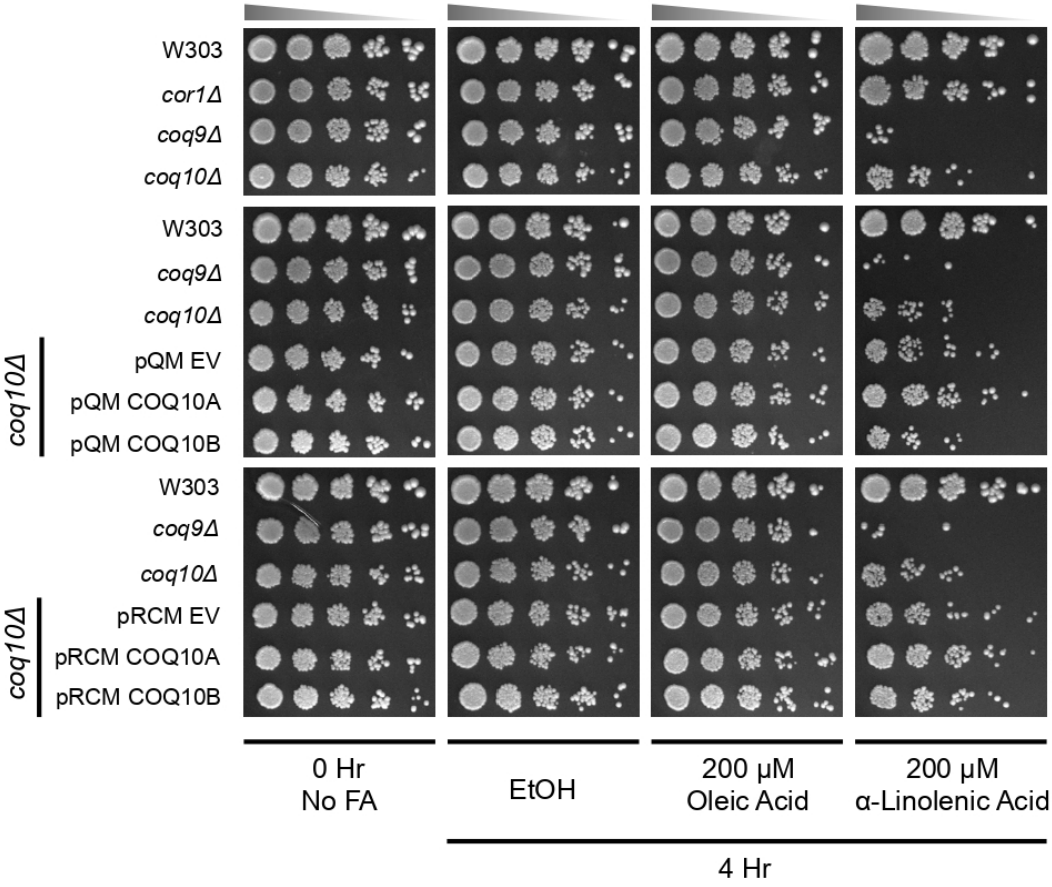

Figure 7. Human COQ10A rescues PUFA sensitivity of the yeast *coq10Δ* mutant. Wild-type W303, respiratory deficient mutant *cor1Δ*, CoQ-less mutant *coq9Δ*, *coq10Δ*, and *coq10Δ* expressing single- or multi-copy COQ10A or COQ10B, or their respective empty vector were grown in SD-Complete, or SD-Ura liquid medium to log phase. Harvested cells were washed twice with sterile H_2O, and resuspended in phosphate buffer with 0.2% dextrose, pH 6.2 to 0.2 OD_{600}/mL. The resuspended cells were incubated with oleic acid, or α-linolenic acid prepared in ethanol at a final concentration of 200 μM for 4 hours. Cells were also incubated with only ethanol as vehicle control. Aliquots of cell suspension from each sample were removed before addition of fatty acids (0 Hr, no fatty acids), and 4 hours post fatty acids incubation to assess cell viability by plate dilution assay. An aliquot of 2 μL of series of five-fold diluted sample was plated in each spot, starting at 0.2 OD_{600}/mL in the first spot on YPD plate medium. Pictures were taken two days after incubation at 30°C.

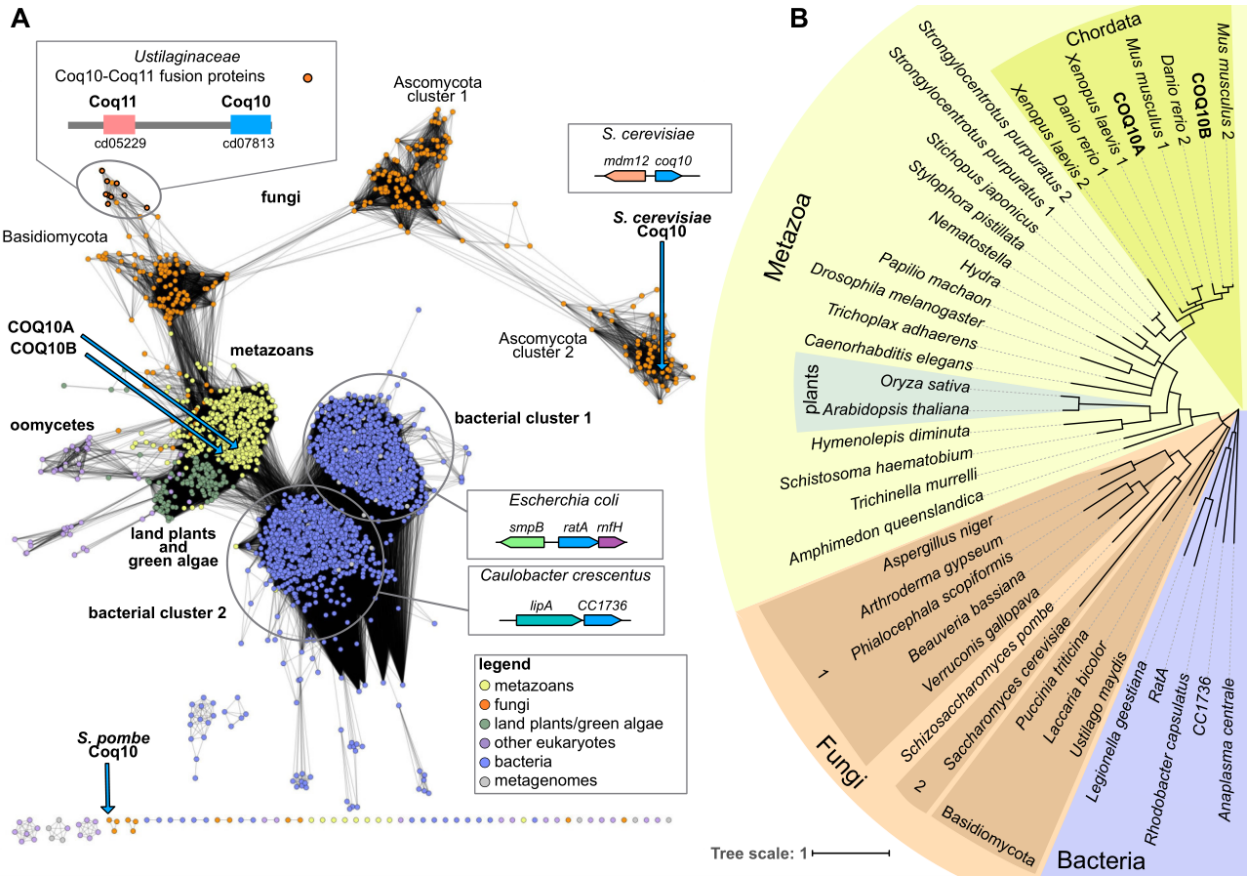
A
Ustilaginaceae
Coq10-Coq11 fusion proteins
Coq11
Coq10
cd05229
cd07813
fungi
Basidiomycota
Ascomycota cluster 1
Ascomycota cluster 2
S. cerevisiae
mdm12 coq10
S. cerevisiae Coq10
COQ10A
COQ10B
metazoans
oomycetes
land plants and green algae
bacterial cluster 1
bacterial cluster 2
Escherchia coli
smpB ratA mfH
Caulobacter crescentus
lipA CC1736
legend
metazoans
fungi
land plants/green algae
other eukaryotes
bacteria
metagenomes
S. pombe Coq10
B
Chordata
Metazoa
plants
Fungi
Bacteria
Basidiomycota
Mus musculus 2
Mus musculus 1
COQ10B
COQ10A
Danio rerio 2
Danio rerio 1
Xenopus laevis 1
Xenopus laevis 2
Strongylocentrotus purpuratus 1
Strongylocentrotus purpuratus 2
Stichopus japonicus
Stylophora pistillata
Nematostella
Hydra
Papilio machaon
Drosophila melanogaster
Trichoplax adhaerens
Caenorhabditis elegans
Oryza sativa
Arabidopsis thaliana
Hymenolepis diminuta
Schistosoma haematobium
Trichinella murrelli
Amphimedon queenslandica
Aspergillus niger
Arthroderma gypseum
Phialocephala scopiformis
Beauveria bassiana
Verruconis gallopava
Schizosaccharomyces pombe
Saccharomyces cerevisiae
Puccinia triticina
Laccaria bicolor
Ustilago maydis
Legionella geestiana
RatA
Rhodobacter capsulatus
CC1736
Anaplasma centrale
1
2
Tree scale: 1

Figure 8. The COQ10 family of proteins. A) A protein similarity network of proteins similar to COQ10 is shown. Each node (circle) represents one or more protein sequences, and each edge (solid line) represents similarity between two proteins (threshold set at an alignment score of 30). Nodes are colored by taxonomy as indicated in the legend. The locations of nodes representing human COQ10A and COQ10B as well as previously characterized Coq10 orthologs from *S. cerevisiae* and *S. pombe* are indicated with blue arrows. The disconnection of *S. pombe* Coq10 from the rest of the network is due to the low similarity (as measured by the BLASTp Evalue) between *S. pombe* Coq10 and other COQ10 homologs (with the exception of Coq10 from other *Schizosaccharomyces* species). The predominant operons observed for the two distinct bacterial clusters, represented by *E. coli* and *C. crescentus*, are shown as cartoons. A schematic of the Coq11-Coq10 protein fusion observed in genomes from *Ustilaginaceae* is also shown, and corresponding nodes are indicated with a thick border. Coq11 contains the cd05229 domain, an atypical SDR domain, and Coq10 contains the cd07813 domain, a SRPBCC (START/RHO_alpha_C/PITP/Bet_v1/CoxG/CalC) domain with a deep hydrophobic ligand-binding pocket. Protein and organism information for each node is available in Supplemental Table S2. **B)** A phylogenetic tree of selected COQ10 homologs from each of the sequence similarity network protein clusters. Background shading corresponds to taxonomy as indicated. Branches with less than 50% bootstrap support were deleted.

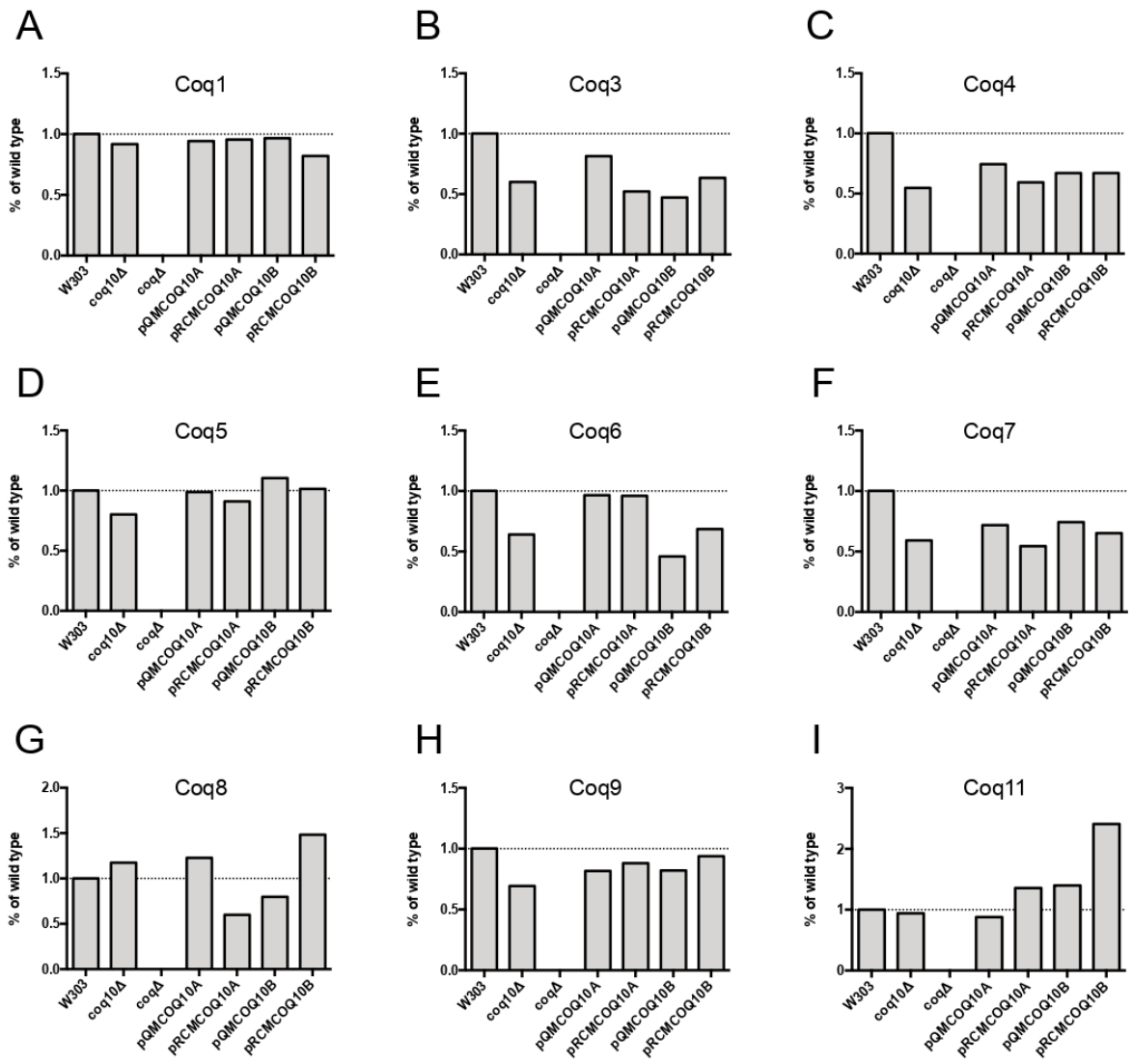

Supplemental Figure S1. Expression of either human COQ10A or COQ10B restores steady state levels of Coq polypeptides. Relative Coq polypeptide levels shown in Figure 4 were quantified by band densitometry using Image J software. The densitometry reading of each *coqΔ* control was first subtracted from the reading of each sample blotted against the corresponding specific Coq polypeptide, then normalized by the reading of the loading control Mdh1. The percentage of signal intensity from each sample relative to the wild type control was plotted in the y-axis.

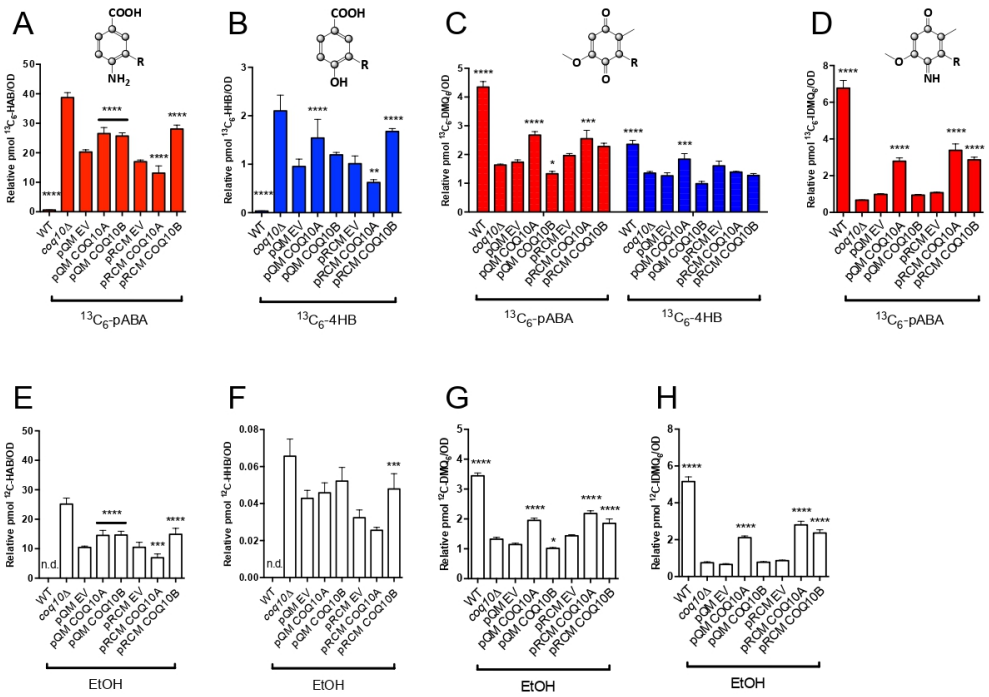

Supplemental Figure S2. Expression of either human COQ10A or COQ10B has minimal effect on de novo and steady state levels of CoQ_6-intermediates. The de novo production $^{13}C_6$-CoQ_6-intermediates, including **A)** $^{13}C_6$-HAB, **B)** $^{13}C_6$-HHB, **C)** $^{13}C_6$-DMQ_6, **D)** $^{13}C_6$-$IDMQ_6$ were measured from yeast whole cell lipid extracts from wild type, *coq10Δ*, *coq10Δ* expressing single- or multi-copy COQ10A or COQ10B, or their respective empty vector labeled with $^{13}C_6$-pABA (red) or $^{13}C_6$-4HB (blue) for 5 hours. The steady state levels of **E)** HAB, **F)** HHB, **G)** DMQ_6, **H)** $IDMQ_6$ were measured from designated samples treated with ethanol as vehicle control. The statistical analyses were performed using two-way ANOVA multiple comparisons from three biological replicates, comparing yeast *coq10Δ* expressing single- or multi-copy COQ10A or COQ10B to their respective empty vector controls, and comparing yeast *coq10Δ* mutant to the wild-type control. The error bar indicates mean ±SD, and the statistical significance is represented by *p < 0.05, **p < 0.01, ***p < 0.001 and ****p < 0.0001.

REFERENCES

1. Alcazar-Fabra, M., E. Trevisson, and G. Brea-Calvo. 2018. Clinical syndromes associated with coenzyme Q_{10} deficiency. *Essays Biochem* **62**: 377-398.

2. Turunen, M., J. Olsson, and G. Dallner. 2004. Metabolism and function of coenzyme Q. *Biochim Biophys Acta* **1660**: 171-199.

3. Desbats, M. A., G. Lunardi, M. Doimo, E. Trevisson, and L. Salviati. 2015. Genetic bases and clinical manifestations of coenzyme Q_{10} (CoQ_{10}) deficiency. *J Inherit Metab Dis* **38**: 145-156.

4. Stefely, J. A., and D. J. Pagliarini. 2017. Biochemistry of mitochondrial coenzyme Q biosynthesis. *Trends Biochem Sci* **42**: 824-843.

5. Awad, A. M., M. C. Bradley, L. Fernández-del-Río, A. Nag, H. S. Tsui, and C. F. Clarke. 2018. Coenzyme Q_{10} deficiencies: pathways in yeast and humans. *Essays Biochem* **62**: 361-376.

6. Hajj Chehade, M., L. Pelosi, C. D. Fyfe, L. Loiseau, B. Rascalou, S. Brugière, K. Kazemzadeh, C.-D.-T. Vo, L. Ciccone, L. Aussel, Y. Couté, M. Fontecave, F. Barras, M. Lombard, and F. Pierrel. 2019. A soluble metabolon synthesizes the isoprenoid lipid ubiquinone. *Cell Chemical Biology* **26**: 1-11.

7. Okada, K., K. Suzuki, Y. Kamiya, X. Zhu, S. Fujisaki, Y. Nishimura, T. Nishino, T. Nakagawa, M. Kawamukai, and H. Matsuda. 1996. Polyprenyl diphosphate synthase essentially defines the length of the side chain of ubiquinone. *Biochim Biophys Acta* **1302**: 217-223.

8. Kawamukai, M. 2016. Biosynthesis of coenzyme Q in eukaryotes. *Biosci Biotechnol Biochem* **80**: 23-33.

9. Allan, C. M., S. Hill, S. Morvaridi, R. Saiki, J. S. Johnson, W. S. Liau, K. Hirano, T. Kawashima, Z. Ji, J. A. Loo, J. N. Shepherd, and C. F. Clarke. 2013. A conserved START domain coenzyme Q-binding polypeptide is required for efficient Q biosynthesis, respiratory electron transport, and antioxidant function in *Saccharomyces cerevisiae*. *Biochim Biophys Acta* **1831**: 776-791.

10. Barros, M. H., A. Johnson, P. Gin, B. N. Marbois, C. F. Clarke, and A. Tzagoloff. 2005. The *Saccharomyces cerevisiae COQ10* gene encodes a START domain protein required for function of coenzyme Q in respiration. *J Biol Chem* **280**: 42627-42635.

11. Shen, Y., S. Goldsmith-Fischman, H. S. Atreya, T. Acton, L. Ma, R. Xiao, B. Honig, G. T. Montelione, and T. Szyperski. 2005. NMR structure of the 18 kDa protein CC1736 from *Caulobacter crescentus* identifies a member of the START domain superfamily and suggests residues mediating substrate specificity. *Proteins* **58**: 747-750.

12. Ponting, C. P., and L. Aravind. 1999. START: a lipid-binding domain in StAR, HD-ZIP and signalling proteins. *Trends Biochem Sci* **24**: 130-132.

13. Iyer, L. M., E. V. Koonin, and L. Aravind. 2001. Adaptations of the helix-grip fold for ligand binding and catalysis in the START domain superfamily. *Proteins* **43**: 134-144.

14. Alpy, F., and C. Tomasetto. 2014. START ships lipids across interorganelle space. *Biochimie* **96**: 85-95.

15. Martin, L. A., B. E. Kennedy, and B. Karten. 2016. Mitochondrial cholesterol: mechanisms of import and effects on mitochondrial function. *J Bioenerg Biomembr* **48**: 137-151.

16. Cui, T. Z., and M. Kawamukai. 2009. Coq10, a mitochondrial coenzyme Q binding protein, is required for proper respiration in *Schizosaccharomyces pombe*. *FEBS J* **276**: 748-759.

17. Wikstrom, M. K., and J. A. Berden. 1972. Oxidoreduction of cytochrome *b* in the presence of antimycin. *Biochim Biophys Acta* **283**: 403-420.

18. Starkov, A. A., and G. Fiskum. 2001. Myxothiazol induces H_2O_2 production from mitochondrial respiratory chain. *Biochem Biophys Res Commun* **281**: 645-650.

19. Drose, S., and U. Brandt. 2008. The mechanism of mitochondrial superoxide production by the cytochrome *bc1* complex. *J Biol Chem* **283**: 21649-21654.

20. Busso, C., E. B. Tahara, R. Ogusucu, O. Augusto, J. R. Ferreira-Junior, A. Tzagoloff, A. J. Kowaltowski, and M. H. Barros. 2010. *Saccharomyces cerevisiae coq10* null mutants are

responsive to antimycin A. *FEBS J* **277**: 4530-4538.

21. Murai, M., K. Matsunobu, S. Kudo, K. Ifuku, M. Kawamukai, and H. Miyoshi. 2014. Identification of the binding site of the quinone-head group in mitochondrial Coq10 by photoaffinity labeling. *Biochemistry* **53**: 3995-4003.

22. Montini, G., C. Malaventura, and L. Salviati. 2008. Early coenzyme Q_{10} supplementation in primary coenzyme Q_{10} deficiency. *N Engl J Med* **358**: 2849-2850.

23. Marcoff, L., and P. D. Thompson. 2007. The role of coenzyme Q_{10} in statin-associated myopathy: a systematic review. *J Am Coll Cardiol* **49**: 2231-2237.

24. Ayer, A., P. Macdonald, and R. Stocker. 2015. CoQ_{10} function and role in heart failure and ischemic heart disease. *Annu Rev Nutr* **35**: 175-213.

25. Mortensen, S. A., F. Rosenfeldt, A. Kumar, P. Dolliner, K. J. Filipiak, D. Pella, U. Alehagen, G. Steurer, G. P. Littarru, and Q. S. S. Investigators. 2014. The effect of coenzyme Q_{10} on morbidity and mortality in chronic heart failure: results from Q-SYMBIO: a randomized double-blind trial. *JACC Heart Fail* **2**: 641-649.

26. Burke, D., Dawson, D., and Stearns, T. . 2000. Methods in yeast genetics. *Cold spring Harbor Laboratory Press*.

27. Barkovich, R. J., A. Shtanko, J. A. Shepherd, P. T. Lee, D. C. Myles, A. Tzagoloff, and C. F. Clarke. 1997. Characterization of the *COQ5* gene from *Saccharomyces cerevisiae*. Evidence for a C-methyltransferase in ubiquinone biosynthesis. *J Biol Chem* **272**: 9182-9188.

28. Hsu, A. Y., W. W. Poon, J. A. Shepherd, D. C. Myles, and C. F. Clarke. 1996. Complementation of *coq3* mutant yeast by mitochondrial targeting of the *Escherichia coli* UbiG polypeptide: evidence that UbiG catalyzes both O-methylation steps in ubiquinone biosynthesis. *Biochemistry* **35**: 9797-9806.

29. Elble, R. 1992. A simple and efficient procedure for transformation of yeasts. *Biotechniques* **13**: 18-20.

30. Hill, S., K. Hirano, V. V. Shmanai, B. N. Marbois, D. Vidovic, A. V. Bekish, B. Kay, V. Tse,

J. Fine, C. F. Clarke, and M. S. Shchepinov. 2011. Isotope-reinforced polyunsaturated fatty acids protect yeast cells from oxidative stress. *Free Radic Biol Med* **50**: 130-138.

31. Hill, S., C. R. Lamberson, L. Xu, R. To, H. S. Tsui, V. V. Shmanai, A. V. Bekish, A. M. Awad, B. N. Marbois, C. R. Cantor, N. A. Porter, C. F. Clarke, and M. S. Shchepinov. 2012. Small amounts of isotope-reinforced polyunsaturated fatty acids suppress lipid autoxidation. *Free Radic Biol Med* **53**: 893-906.

32. Glick, B. S., and L. A. Pon. 1995. Isolation of highly purified mitochondria from *Saccharomyces cerevisiae*. *Methods Enzymol* **260**: 213-223.

33. Schagger, H., W. A. Cramer, and G. von Jagow. 1994. Analysis of molecular masses and oligomeric states of protein complexes by blue native electrophoresis and isolation of membrane protein complexes by two-dimensional native electrophoresis. *Anal Biochem* **217**: 220-230.

34. He, C. H., L. X. Xie, C. M. Allan, U. C. Tran, and C. F. Clarke. 2014. Coenzyme Q supplementation or over-expression of the yeast Coq8 putative kinase stabilizes multi-subunit Coq polypeptide complexes in yeast *coq* null mutants. *Biochim Biophys Acta* **1841**: 630-644.

35. Wittig, I., H. P. Braun, and H. Schagger. 2006. Blue native PAGE. *Nat Protoc* **1**: 418-428.

36. Marbois, B., L. X. Xie, S. Choi, K. Hirano, K. Hyman, and C. F. Clarke. 2010. *para*-Aminobenzoic acid is a precursor in coenzyme Q_6 biosynthesis in *Saccharomyces cerevisiae*. *J Biol Chem* **285**: 27827-27838.

37. Buchan, D. W., F. Minneci, T. C. Nugent, K. Bryson, and D. T. Jones. 2013. Scalable web services for the PSIPRED Protein Analysis Workbench. *Nucleic Acids Res* **41**: W349-357.

38. Jones, D. T., and D. Cozzetto. 2015. DISOPRED3: precise disordered region predictions with annotated protein-binding activity. *Bioinformatics* **31**: 857-863.

39. Waterhouse, A., M. Bertoni, S. Bienert, G. Studer, G. Tauriello, R. Gumienny, F. T. Heer, T. A. P. de Beer, C. Rempfer, L. Bordoli, R. Lepore, and T. Schwede. 2018. SWISS-MODEL: homology modelling of protein structures and complexes. *Nucleic Acids Res* **46**: W296-W303.

40. Chaudhury, S., S. Lyskov, and J. J. Gray. 2010. PyRosetta: a script-based interface for implementing molecular modeling algorithms using Rosetta. *Bioinformatics* **26**: 689-691.

41. Benkert, P., S. C. Tosatto, and D. Schomburg. 2008. QMEAN: a comprehensive scoring function for model quality assessment. *Proteins* **71**: 261-277.

42. Luthy, R., J. U. Bowie, and D. Eisenberg. 1992. Assessment of protein models with three-dimensional profiles. *Nature* **356**: 83-85.

43. Colovos, C., and T. O. Yeates. 1993. Verification of protein structures: patterns of nonbonded atomic interactions. *Protein Sci* **2**: 1511-1519.

44. Chen, V. B., W. B. Arendall, 3rd, J. J. Headd, D. A. Keedy, R. M. Immormino, G. J. Kapral, L. W. Murray, J. S. Richardson, and D. C. Richardson. 2010. MolProbity: all-atom structure validation for macromolecular crystallography. *Acta Crystallogr D Biol Crystallogr* **66**: 12-21.

45. Trott, O., and A. J. Olson. 2010. AutoDock Vina: improving the speed and accuracy of docking with a new scoring function, efficient optimization, and multithreading. *J Comput Chem* **31**: 455-461.

46. Adams, P. D., P. V. Afonine, G. Bunkoczi, V. B. Chen, I. W. Davis, N. Echols, J. J. Headd, L. W. Hung, G. J. Kapral, R. W. Grosse-Kunstleve, A. J. McCoy, N. W. Moriarty, R. Oeffner, R. J. Read, D. C. Richardson, J. S. Richardson, T. C. Terwilliger, and P. H. Zwart. 2010. PHENIX: a comprehensive Python-based system for macromolecular structure solution. *Acta Crystallogr D Biol Crystallogr* **66**: 213-221.

47. Gerlt, J. A., J. T. Bouvier, D. B. Davidson, H. J. Imker, B. Sadkhin, D. R. Slater, and K. L. Whalen. 2015. Enzyme Function Initiative-Enzyme Similarity Tool (EFI-EST): a web tool for generating protein sequence similarity networks. *Biochim Biophys Acta* **1854**: 1019-1037.

48. Shannon, P., A. Markiel, O. Ozier, N. S. Baliga, J. T. Wang, D. Ramage, N. Amin, B. Schwikowski, and T. Ideker. 2003. Cytoscape: a software environment for integrated models of biomolecular interaction networks. *Genome Res* **13**: 2498-2504.

49. UniProt Consortium, T. 2018. UniProt: the universal protein knowledgebase. *Nucleic Acids Res* **46**: 2699.

50. Katoh, K., and D. M. Standley. 2013. MAFFT multiple sequence alignment software version 7: improvements in performance and usability. *Mol Biol Evol* **30**: 772-780.

51. Nguyen, L. T., H. A. Schmidt, A. von Haeseler, and B. Q. Minh. 2015. IQ-TREE: a fast and effective stochastic algorithm for estimating maximum-likelihood phylogenies. *Mol Biol Evol* **32**: 268-274.

52. Miller, M. A., T. Schwartz, B. E. Pickett, S. He, E. B. Klem, R. H. Scheuermann, M. Passarotti, S. Kaufman, and M. A. O'Leary. 2015. A RESTful API for access to phylogenetic tools via the CIPRES science gateway. *Evol Bioinform Online* **11**: 43-48.

53. Miller, M. A., W. Pfeiffer, and T. Schwartz. 2010. Creating the CIPRES Science Gateway for inference of large phylogenetic trees. *Gateway Computing Environments Workshop (GCE) in New Orleans, LA*: 1-8.

54. Hoang, D. T., O. Chernomor, A. von Haeseler, B. Q. Minh, and L. S. Vinh. 2018. UFBoot2: improving the Ultrafast Bootstrap approximation. *Mol Biol Evol* **35**: 518-522.

55. Sayers, E. W., R. Agarwala, E. E. Bolton, J. R. Brister, K. Canese, K. Clark, R. Connor, N. Fiorini, K. Funk, T. Hefferon, J. B. Holmes, S. Kim, A. Kimchi, P. A. Kitts, S. Lathrop, Z. Lu, T. L. Madden, A. Marchler-Bauer, L. Phan, V. A. Schneider, C. L. Schoch, K. D. Pruitt, and J. Ostell. 2018. Database resources of the National Center for Biotechnology Information. *Nucleic Acids Res*.

56. Vrablik, M., L. Zlatohlavek, T. Stulc, V. Adamkova, M. Prusikova, L. Schwarzova, J. A. Hubacek, and R. Ceska. 2014. Statin-associated myopathy: from genetic predisposition to clinical management. *Physiol Res* **63 Suppl 3**: S327-334.

57. Peterson, T. A., A. Adadey, I. Santana-Cruz, Y. Sun, A. Winder, and M. G. Kann. 2010. DMDM: domain mapping of disease mutations. *Bioinformatics* **26**: 2458-2459.

58. Abd, T. T., and T. A. Jacobson. 2011. Statin-induced myopathy: a review and update.

Expert Opin Drug Saf **10**: 373-387.

59. Busso, C., L. Bleicher, J. R. Ferreira-Junior, and M. H. Barros. 2010. Site-directed mutagenesis and structural modeling of Coq10p indicate the presence of a tunnel for coenzyme Q_6 binding. *FEBS Lett* **584**: 1609-1614.

60. Gatta, A. T., A. C. Sauerwein, A. Zhuravleva, T. P. Levine, and S. Matthews. 2018. Structural insights into a StART-like domain in Lam4 and its interaction with sterol ligands. *Biochem Biophys Res Commun* **495**: 2270-2274.

61. Horenkamp, F. A., D. P. Valverde, J. Nunnari, and K. M. Reinisch. 2018. Molecular basis for sterol transport by StART-like lipid transfer domains. *EMBO J* **37**.

62. Jentsch, J. A., I. Kiburu, K. Pandey, M. Timme, T. Ramlall, B. Levkau, J. Wu, D. Eliezer, O. Boudker, and A. K. Menon. 2018. Structural basis of sterol binding and transport by a yeast StARkin domain. *J Biol Chem* **293**: 5522-5531.

63. Hsieh, E. J., P. Gin, M. Gulmezian, U. C. Tran, R. Saiki, B. N. Marbois, and C. F. Clarke. 2007. *Saccharomyces cerevisiae* Coq9 polypeptide is a subunit of the mitochondrial coenzyme Q biosynthetic complex. *Arch Biochem Biophys* **463**: 19-26.

64. Tauche, A., U. Krause-Buchholz, and G. Rodel. 2008. Ubiquinone biosynthesis in *Saccharomyces cerevisiae*: the molecular organization of O-methylase Coq3p depends on Abc1p/Coq8p. *FEMS Yeast Res* **8**: 1263-1275.

65. Yin, H., L. Xu, and N. A. Porter. 2011. Free radical lipid peroxidation: mechanisms and analysis. *Chem Rev* **111**: 5944-5972.

66. Porter, N. A. 1986. Mechanisms for the autoxidation of polyunsaturated lipids. *Accounts Chem Res* **19**: 262-268.

67. Iyer, L. M., A. M. Burroughs, and L. Aravind. 2006. The prokaryotic antecedents of the ubiquitin-signaling system and the early evolution of ubiquitin-like beta-grasp domains. *Genome Biol* **7**: R60.

68. Hudson, C. M., B. Y. Lau, and K. P. Williams. 2014. Ends of the line for tmRNA-SmpB.

Front Microbiol **5**: 421.

69. Zhang, Y., and M. Inouye. 2011. RatA (YfjG), an *Escherichia coli* toxin, inhibits 70S ribosome association to block translation initiation. *Mol Microbiol* **79**: 1418-1429.

70. Karzai, A. W., M. M. Susskind, and R. T. Sauer. 1999. SmpB, a unique RNA-binding protein essential for the peptide-tagging activity of SsrA (tmRNA). *EMBO J* **18**: 3793-3799.

71. Karzai, A. W., E. D. Roche, and R. T. Sauer. 2000. The SsrA-SmpB system for protein tagging, directed degradation and ribosome rescue. *Nat Struct Biol* **7**: 449-455.

72. Jouanneau, Y., H. S. Jeong, N. Hugo, C. Meyer, and J. C. Willison. 1998. Overexpression in *Escherichia coli* of the *rnf* genes from *Rhodobacter capsulatus*--characterization of two membrane-bound iron-sulfur proteins. *Eur J Biochem* **251**: 54-64.

73. Reyes-Prieto, A., B. Barquera, and O. Juarez. 2014. Origin and evolution of the sodium-pumping NADH: ubiquinone oxidoreductase. *PLoS One* **9**: e96696.

74. Biegel, E., S. Schmidt, J. M. Gonzalez, and V. Muller. 2011. Biochemistry, evolution and physiological function of the Rnf complex, a novel ion-motive electron transport complex in prokaryotes. *Cell Mol Life Sci* **68**: 613-634.

75. Okamura, Y., Y. Aoki, T. Obayashi, S. Tadaka, S. Ito, T. Narise, and K. Kinoshita. 2015. COXPRESdb in 2015: coexpression database for animal species by DNA-microarray and RNAseq-based expression data with multiple quality assessment systems. *Nucleic Acids Res* **43**: D82-86.

76. Murley, A., and J. Nunnari. 2016. The emerging network of mitochondria-organelle contacts. *Mol Cell* **61**: 648-653.

77. Kornmann, B., E. Currie, S. R. Collins, M. Schuldiner, J. Nunnari, J. S. Weissman, and P. Walter. 2009. An ER-mitochondria tethering complex revealed by a synthetic biology screen. *Science* **325**: 477-481.

78. Allan, C. M., A. M. Awad, J. S. Johnson, D. I. Shirasaki, C. Wang, C. E. Blaby-Haas, S. S. Merchant, J. A. Loo, and C. F. Clarke. 2015. Identification of Coq11, a new coenzyme Q

biosynthetic protein in the CoQ-synthome in *Saccharomyces cerevisiae*. *J Biol Chem* **290**: 7517-7534.

79. Floyd, B. J., E. M. Wilkerson, M. T. Veling, C. E. Minogue, C. Xia, E. T. Beebe, R. L. Wrobel, H. Cho, L. S. Kremer, C. L. Alston, K. A. Gromek, B. K. Dolan, A. Ulbrich, J. A. Stefely, S. L. Bohl, K. M. Werner, A. Jochem, M. S. Westphall, J. W. Rensvold, R. W. Taylor, H. Prokisch, J. P. Kim, J. J. Coon, and D. J. Pagliarini. 2016. Mitochondrial protein interaction mapping identifies regulators of respiratory chain function. *Mol Cell* **63**: 621-632.

80. Chatr-Aryamontri, A., R. Oughtred, L. Boucher, J. Rust, C. Chang, N. K. Kolas, L. O'Donnell, S. Oster, C. Theesfeld, A. Sellam, C. Stark, B. J. Breitkreutz, K. Dolinski, and M. Tyers. 2017. The BioGRID interaction database: 2017 update. *Nucleic Acids Res* **45**: D369-D379.

81. Zhu, Q., A. K. Wong, A. Krishnan, M. R. Aure, A. Tadych, R. Zhang, D. C. Corney, C. S. Greene, L. A. Bongo, V. N. Kristensen, M. Charikar, K. Li, and O. G. Troyanskaya. 2015. Targeted exploration and analysis of large cross-platform human transcriptomic compendia. *Nat Methods* **12**: 211-214, 213 p following 214.

82. Kovalyov, L. I., M. A. Kovalyova, P. L. Kovalyov, M. V. Serebryakova, S. A. Moshkovskii, and S. S. Shishkin. 2006. Polymorphism of delta3,5-delta2,4-dienoyl-coenzyme A isomerase (the *ECH1* gene product protein) in human striated muscle tissue. *Biochemistry (Mosc)* **71**: 448-453.

83. Uhlen, M., L. Fagerberg, B. M. Hallstrom, C. Lindskog, P. Oksvold, A. Mardinoglu, A. Sivertsson, C. Kampf, E. Sjostedt, A. Asplund, I. Olsson, K. Edlund, E. Lundberg, S. Navani, C. A. Szigyarto, J. Odeberg, D. Djureinovic, J. O. Takanen, S. Hober, T. Alm, P. H. Edqvist, H. Berling, H. Tegel, J. Mulder, J. Rockberg, P. Nilsson, J. M. Schwenk, M. Hamsten, K. von Feilitzen, M. Forsberg, L. Persson, F. Johansson, M. Zwahlen, G. von Heijne, J. Nielsen, and F. Ponten. 2015. Proteomics. Tissue-based map of the human proteome. *Science* **347**: 1260419.

84. Fagerberg, L., B. M. Hallstrom, P. Oksvold, C. Kampf, D. Djureinovic, J. Odeberg, M.

Habuka, S. Tahmasebpoor, A. Danielsson, K. Edlund, A. Asplund, E. Sjostedt, E. Lundberg, C. A. Szigyarto, M. Skogs, J. O. Takanen, H. Berling, H. Tegel, J. Mulder, P. Nilsson, J. M. Schwenk, C. Lindskog, F. Danielsson, A. Mardinoglu, A. Sivertsson, K. von Feilitzen, M. Forsberg, M. Zwahlen, I. Olsson, S. Navani, M. Huss, J. Nielsen, F. Ponten, and M. Uhlen. 2014. Analysis of the human tissue-specific expression by genome-wide integration of transcriptomics and antibody-based proteomics. *Mol Cell Proteomics* **13**: 397-406.

85. Subramanian, K., A. Jochem, M. Le Vasseur, S. Lewis, B. R. Paulson, T. R. Reddy, J. D. Russell, J. J. Coon, D. J. Pagliarini, and J. Nunnari. 2019. Coenzyme Q biosynthetic proteins assemble in a substrate-dependent manner into domains at ER-mitochondria contacts. *J Cell Biol* **In Press. DOI: 10.1083/jcb.201808044**.

86. Clark, B. J. 2012. The mammalian START domain protein family in lipid transport in health and disease. *J Endocrinol* **212**: 257-275.

87. Alpy, F., C. Wendling, M. C. Rio, and C. Tomasetto. 2002. MENTHO, a MLN64 homologue devoid of the START domain. *J Biol Chem* **277**: 50780-50787.

88. Alpy, F., and C. Tomasetto. 2006. MLN64 and MENTHO, two mediators of endosomal cholesterol transport. *Biochem Soc Trans* **34**: 343-345.

89. Persson, B., and Y. Kallberg. 2013. Classification and nomenclature of the superfamily of short-chain dehydrogenases/reductases (SDRs). *Chem Biol Interact* **202**: 111-115.

90. Baertling, F., L. Sanchez-Caballero, M. A. M. van den Brand, C. W. Fung, S. H. Chan, V. C. Wong, D. M. E. Hellebrekers, I. F. M. de Coo, J. A. M. Smeitink, R. J. T. Rodenburg, and L. G. J. Nijtmans. 2018. *NDUFA9* point mutations cause a variable mitochondrial complex I assembly defect. *Clin Genet* **93**: 111-118.

91. Yamamoto, T., H. Tamaki, C. Katsuda, K. Nakatani, S. Terauchi, H. Terada, and Y. Shinohara. 2013. Molecular basis of interactions between mitochondrial proteins and hydroxyapatite in the presence of Triton X-100, as revealed by proteomic and recombinant techniques. *J Chromatogr A* **1301**: 169-178.

92. Cronan, J. E. 2014. Biotin and lipoic acid: synthesis, attachment, and regulation. *EcoSal Plus* **6**.

93. Hiltunen, J. K., M. S. Schonauer, K. J. Autio, T. M. Mittelmeier, A. J. Kastaniotis, and C. L. Dieckmann. 2009. Mitochondrial fatty acid synthesis type II: more than just fatty acids. *J Biol Chem* **284**: 9011-9015.

94. Hibbs, M. A., D. C. Hess, C. L. Myers, C. Huttenhower, K. Li, and O. G. Troyanskaya. 2007. Exploring the functional landscape of gene expression: directed search of large microarray compendia. *Bioinformatics* **23**: 2692-2699.

95. Eisenberg-Bord, M., H. S. Tsui, D. Antunes, L. Fernández-del-Río, M. C. Bradley, C. D. Dunn, T. P. T. Nguyen, D. Rapaport, C. F. Clarke, and M. Schuldiner. 2019. The ER-Mitochondria Encounter Structure (ERMES) complex coordinates coenzyme Q biosynthesis. *Contact* **2**: 1-14.

96. Cohen, Y., Y. A. Klug, L. Dimitrov, Z. Erez, S. G. Chuartzman, D. Elinger, I. Yofe, K. Soliman, J. Gartner, S. Thoms, R. Schekman, Y. Elbaz-Alon, E. Zalckvar, and M. Schuldiner. 2014. Peroxisomes are juxtaposed to strategic sites on mitochondria. *Mol Biosyst* **10**: 1742-1748.

97. Merkwirth, C., and T. Langer. 2008. Mitofusin 2 builds a bridge between ER and mitochondria. *Cell* **135**: 1165-1167.

98. Mourier, A., E. Motori, T. Brandt, M. Lagouge, I. Atanassov, A. Galinier, G. Rappl, S. Brodesser, K. Hultenby, C. Dieterich, and N. G. Larsson. 2015. Mitofusin 2 is required to maintain mitochondrial coenzyme Q levels. *J Cell Biol* **208**: 429-442.

99. Gin, P., and C. F. Clarke. 2005. Genetic evidence for a multi-subunit complex in coenzyme Q biosynthesis in yeast and the role of the Coq1 hexaprenyl diphosphate synthase. *J Biol Chem* **280**: 2676-2681.

100. Do, T. Q., J. R. Schultz, and C. F. Clarke. 1996. Enhanced sensitivity of ubiquinone-deficient mutants of *Saccharomyces cerevisiae* to products of autoxidized polyunsaturated fatty

acids. *Proc Natl Acad Sci U S A* **93**: 7534-7539.

101. Hsu, A. Y., T. Q. Do, P. T. Lee, and C. F. Clarke. 2000. Genetic evidence for a multi-subunit complex in the O-methyltransferase steps of coenzyme Q biosynthesis. *Biochim Biophys Acta* **1484**: 287-297.

102. Gin, P., A. Y. Hsu, S. C. Rothman, T. Jonassen, P. T. Lee, A. Tzagoloff, and C. F. Clarke. 2003. The *Saccharomyces cerevisiae COQ6* gene encodes a mitochondrial flavin-dependent monooxygenase required for coenzyme Q biosynthesis. *J Biol Chem* **278**: 25308-25316.

103. Marbois, B. N., and C. F. Clarke. 1996. The *COQ7* gene encodes a protein in *Saccharomyces cerevisiae* necessary for ubiquinone biosynthesis. *J Biol Chem* **271**: 2995-3004.

104. Johnson, A., P. Gin, B. N. Marbois, E. J. Hsieh, M. Wu, M. H. Barros, C. F. Clarke, and A. Tzagoloff. 2005. *COQ9*, a new gene required for the biosynthesis of coenzyme Q in *Saccharomyces cerevisiae*. *J Biol Chem* **280**: 31397-31404.

105. Poon, W. W., R. J. Barkovich, A. Y. Hsu, A. Frankel, P. T. Lee, J. N. Shepherd, D. C. Myles, and C. F. Clarke. 1999. Yeast and rat Coq3 and *Escherichia coli* UbiG polypeptides catalyze both O-methyltransferase steps in coenzyme Q biosynthesis. *J Biol Chem* **274**: 21665-21672.

106. Belogrudov, G. I., P. T. Lee, T. Jonassen, A. Y. Hsu, P. Gin, and C. F. Clarke. 2001. Yeast *COQ4* encodes a mitochondrial protein required for coenzyme Q synthesis. *Arch Biochem Biophys* **392**: 48-58.

107. Baba, S. W., G. I. Belogrudov, J. C. Lee, P. T. Lee, J. Strahan, J. N. Shepherd, and C. F. Clarke. 2004. Yeast Coq5 C-methyltransferase is required for stability of other polypeptides involved in coenzyme Q biosynthesis. *J Biol Chem* **279**: 10052-10059.

108. Tran, U. C., B. Marbois, P. Gin, M. Gulmezian, T. Jonassen, and C. F. Clarke. 2006. Complementation of *Saccharomyces cerevisiae coq7* mutants by mitochondrial targeting of the *Escherichia coli* UbiF polypeptide: two functions of yeast Coq7 polypeptide in coenzyme Q

biosynthesis. *J Biol Chem* **281**: 16401-16409.

109. Hsieh, E. J., J. B. Dinoso, and C. F. Clarke. 2004. A $tRNA^{TRP}$ gene mediates the suppression of *cbs2-223* previously attributed to *ABC1/COQ8*. *Biochem Biophys Res Commun* **317**: 648-653.

CHAPTER 3

The endoplasmic reticulum-mitochondria encounter structure complex coordinates coenzyme Q biosynthesis

Original Research

The Endoplasmic Reticulum-Mitochondria Encounter Structure Complex Coordinates Coenzyme Q Biosynthesis

Contact
Volume 2: 1–14

DOI: 10.1177/2515256418825409
journals.sagepub.com/home/ctc
SAGE

Michal Eisenberg-Bord[1,#], Hui S. Tsui[2,#], Diana Antunes[3,#], Lucía Fernández-del-Río[2,#], Michelle C. Bradley[2], Cory D. Dunn[4,5], Theresa P. T. Nguyen[6], Doron Rapaport[3], Catherine F. Clarke[2], and Maya Schuldiner[1]

Abstract

Loss of the endoplasmic reticulum (ER)-mitochondria encounter structure (ERMES) complex that resides in contact sites between the yeast ER and mitochondria leads to impaired respiration; however, the reason for that is not clear. We find that in *ERMES* null mutants, there is an increase in the level of mRNAs encoding for biosynthetic enzymes of coenzyme Q_6 (CoQ_6), an essential electron carrier of the mitochondrial respiratory chain. We show that the mega complexes involved in CoQ_6 biosynthesis (CoQ synthomes) are destabilized in ERMES mutants. This, in turn, affects the level and distribution of CoQ_6 within the cell, resulting in reduced mitochondrial CoQ_6. We suggest that these outcomes contribute to the reduced respiration observed in ERMES mutants. Fluorescence microscopy experiments demonstrate close proximity between the CoQ synthome and ERMES, suggesting a spatial coordination. The involvement of the ER-mitochondria contact site in regulation of CoQ_6 biogenesis highlights an additional level of communication between these two organelles.

Keywords

coenzyme Q, endoplasmic reticulum, ER-mitochondrial encounter structure, mitochondrion (mitochondria)

Introduction

Over the past two decades, our initial conception of eukaryotic cell architecture has been gradually altered. The original idea of solitary organelles scattered sparsely in the cytosol has been replaced by an appreciation of the close cooperation that exists between organelles. Indeed, organelles are tightly packed together and are anything but solitary. All organelles appear to have the capacity to be tethered to one another by designated structures termed membrane contact sites, and these contact sites are generated by use of tethering molecules (Kakimoto et al., 2018; Shai et al., 2018; Valm et al., 2017). Such areas of close membrane apposition allow for the transfer of metabolites, lipids, and other molecules between the two organelles (Eisenberg-Bord, Shai, Schuldiner, & Bohnert, 2016). One of the most studied contact sites is formed between the endoplasmic reticulum (ER) and mitochondria. In the budding yeast *Saccharomyces cerevisiae* (hereafter termed yeast),

[1]Department of Molecular Genetics, Weizmann Institute of Science, Rehovot, Israel
[2]Department of Chemistry and Biochemistry and the Molecular Biology Institute, UCLA, Los Angeles, CA, USA
[3]Interfaculty Institute of Biochemistry, University of Tübingen, Tübingen, Germany
[4]Institute of Biotechnology, Helsinki Institute of Life Science, University of Helsinki, Helsinki, Finland
[5]Department of Molecular Biology and Genetics, Koç University, İstanbul, Turkey
[6]Department of Chemistry, Loyola University Maryland, Baltimore, MD, USA

[#]The first four authors contributed equally to this work.

Received July 29, 2018. Revised December 27, 2018. Accepted December 27, 2018.

Corresponding Authors:
Maya Schuldiner, Weizmann Institute, 234 Herzl St, Rehovot 7610001, Israel.
Email: maya.schuldiner@weizmann.ac.il
Catherine F. Clarke, Department of Chemistry and Biochemistry and the Molecular Biology Institute, UCLA, Los Angeles, CA, USA 90095-1569.
Email: cathy@chem.ucla.edu
Doron Rapaport, University of Tübingen Hoppe-Seyler-Str. 4 Tübingen, 72076 Germany.
Email: doron.rapaport@uni-tuebingen.de

a prominent complex promoting association of the ER and mitochondria is the ER-mitochondria encounter structure (ERMES; Kornmann et al., 2009). ERMES is composed of four subunits: two mitochondrial subunits (Mdm10 and Mdm34), an ER localized subunit (Mmm1), and a soluble subunit (Mdm12).

One of the most closely examined roles of ERMES is the transfer of phospholipids. As mitochondria cannot synthesize most of the lipids that they require, phospholipids, sterols, and ceramide/sphingolipids must be imported from the ER. Hence, ER-mitochondria contact sites accommodate many lipid transfer factors and proteins that are involved in lipid metabolism (Dimmer & Rapaport, 2017). Recently, it was shown that the Mmm1-Mdm12 complex can mediate phospholipid transfer *in vitro* and that mutations in *MMM1* or *MDM12* lead to impaired phospholipid transfer through the ERMES complex *in vivo* (Kawano et al., 2018). Surprisingly, ERMES mutants typically exhibit only a mild decrease in specific phospholipids at mitochondria due to the existence of compensatory mechanisms for phospholipid transfer (González Montoro et al., 2018; John Peter et al., 2017; Kojima, Endo, & Tamura, 2016; Lang, Peter, Walter, & Kornmann, 2015; Tan et al., 2013). Despite the moderate effects on lipid transfer between organelles, ERMES disruption leads to a wide array of cellular phenotypes, including loss of mitochondrial morphology, increased loss of mitochondrial DNA, and reduced respiratory capacity (Berger, Sogo, & Yaffe, 1997; Hobbs, Srinivasan, McCaffery, & Jensen, 2001; Kornmann et al., 2009; Youngman et al., 2004). Why loss of ERMES causes these adverse phenotypes, including respiratory deficiency, has not yet been fully elucidated. Hence, we have focused our attention on the role of ERMES in regulating respiration.

Here, we show that cells lacking ERMES components exhibit increased mRNA levels for proteins that participate in the coenzyme Q_6 (CoQ_6) biosynthetic pathway. CoQ_6 is a polyisoprenylated benzoquinone lipid that functions within the electron transport chain of the inner mitochondrial membrane of yeast. CoQ_6 can also act as a lipophilic antioxidant (Awad et al., 2018; Tran & Clarke, 2007). All of the steps required for the assembly of the polyisoprenoid diphosphate tail of CoQ, its ligation to aromatic ring precursors, and modification of the ring precursor are catalyzed by Coq enzymes associated with the matrix side of the mitochondrial inner membrane (Awad et al., 2018; Bentinger, Tekle, & Dallner, 2010). Many of the these Coq polypeptides (Coq3-Coq9 and Coq11) assemble within a mega complex termed the CoQ synthome (Allan et al., 2015; Belogrudov et al., 2001; He, Xie, Allan, Tran, & Clarke, 2014; Marbois et al., 2005; Marbois, Gin, Gulmezian, & Clarke, 2009). Synthesis of the polyisoprenoid tail of CoQ_6 originates from compounds that derive from the mevalonate pathway associated with the ER, suggesting that the ER-mitochondria contact site might promote movement of CoQ_6, or its biochemical intermediates and precursors, between these two organelles.

Indeed, we show that the CoQ synthome is destabilized in ERMES mutants, and this results in transcriptionally upregulated, yet inefficient, *de novo* CoQ_6 biosynthesis. Such compromised synthesis results in an increase of CoQ_6-intermediates as well as accumulation of CoQ_6 at non-mitochondrial cellular membranes. We further demonstrate that ERMES mutants harbor decreased steady-state levels of CoQ_6 and CoQ_6-intermediates within mitochondria. This reduced level may contribute to the respiratory deficiency. Furthermore, ERMES-mediated contacts seem to be located in proximity to specialized matrix niches where the CoQ synthome is enriched, suggesting a spatially regulated process. Our study provides new insights into the relevance of ER-mitochondria contacts to CoQ_6 homeostasis and, more broadly, to cellular respiration.

Materials and Methods

Strains and Plasmids

Saccharomyces cerevisiae strains and plasmids used in this study are listed in Table S1 and Table S2, respectively. Yeast strains were based on strains S288C (BY4741; Brachmann et al., 1998) or W303 (Thomas & Rothstein, 1989). Transformations of polymerase chain reaction (PCR) products into yeast cells were performed using the Li-acetate method (Gietz & Woods, 2006; Janke et al., 2004; Longtine et al., 1998). Primers were designed using Primers-4-Yeast: http://www.weizmann.ac.il/Primers-4-Yeast/ (Yofe & Schuldiner, 2014).

RNA-Sequencing

S288C (BY4741) cells were cultured overnight in a synthetic medium SD (2% [wt/vol] glucose, 0.67% [wt/vol] yeast nitrogen base with ammonium sulfate and amino acid supplements) at 30°C. W303 cells were cultured overnight in a synthetic medium SGly (3% [wt/vol] glycerol, 0.67% [wt/vol] yeast nitrogen base with ammonium sulfate and amino acid supplements) at 30°C. In the morning, cells were back-diluted to $OD_{600}\sim$ 0.01 and followed until reaching $OD_{600}\sim$ 0.2. Cells were centrifuged (3,000 *g*, 3 min), and the pellet was frozen in liquid nitrogen and stored at −80°C until further analysis.

For all samples, RNA was purified as described (Voichek, Bar-Ziv, and Barkai, 2016). Briefly, RNA was extracted according to a protocol of Nucleospin® 96 RNA Kit (Machery-Nagel) with two modifications: Lysis was performed by adding 450 µl of lysis buffer containing 1 M sorbitol, 100 mM EDTA, and 0.45 µl

lyticase (10 IU/μl) to cells in a 96 deep-well plate. The plate was then incubated for 30 min at 30°C, centrifuged (3,000 *g*, 10 min) and the supernatant was removed. In addition, dithiothreitol was used as a replacement for β-mercaptoethanol.

For S288C (BY4741) cells, RNA was fragmented, RNA molecules harboring a poly(A) were enriched, and this was followed by cDNA preparation, barcoding, and sequencing using Illumina HiSeq 2500, as described in Voichek et al. (2016). For W303 cells, RNA libraries were created by reverse transcription with a barcoded poly(T). DNA-RNA hybrids were pooled, followed by use of a hyperactive variant of the Tn5 transposase for fragmentation. SDS (0.2%) was used to strip Tn5 from DNA. Following SDS treatment, samples were purified using Solid Phase Reversible Immobilization (Beckman Coulter) Beads. cDNA was then amplified using PCR and sequenced using the Illumina NextSeq 500.

Single end reads were mapped to *S. cerevisiae* genome (R64 in SGD; Cherry et al., 2012) using bowtie (parameters: –best –a –m 2 –strata –5 10; Liu et al., 2005). Following alignment, reads mapped to rRNA were excluded. For S288C samples, reads were down sampled to 400,000 reads and normalized for PCR bias using the unique molecular identifier (Kivioja et al., 2012). For all samples, expression of each gene was the summary of reads aligned between 400 bp upstream and 200 bp downstream of the predicted open reading frame. The gene expression summary was normalized to be 1,000,000 and a gene with an expression below 10 was excluded from further analysis (Voichek et al., 2016). Each sample was analyzed twice, and values shown are typically the average of the two. However, if only one sample had a value, that value was utilized.

Mitochondrial Purification

Yeast wild-type and ERMES mutant cultures were cultured in YPGly (3% [wt/vol] glycerol, 1% [wt/vol] Bacto yeast extract, and 2% [wt/vol] Bacto peptone) at 30°C. Cells were harvested at $OD_{600} < 4.0$, and mitochondria were purified with discontinuous Nycodenz as described (Glick & Pon, 1995). Protease inhibitor mixture (Roche Complete EDTA-free), phosphatase inhibitor cocktail set II (EMD Millipore), and phosphatase inhibitor cocktail set 3 (Sigma-Aldrich) were added to the solutions. Gradient-purified mitochondria were frozen in liquid nitrogen and stored at −80°C until further analysis. Mitochondria from yeast Δ*coq* mutants were purified in the same manner from cultures expanded in YPGal medium (2% [wt/vol] galactose, 0.1% [wt/vol] dextrose, 1% [wt/vol] Bacto yeast extract, and 2% [wt/vol] Bacto peptone).

SDS-PAGE Analysis of Steady-State Levels of Coq Polypeptides

Purified mitochondria were resuspended in SDS sample buffer consisting of 50 mM Tris, pH 6.8, 10% glycerol, 2% SDS, 0.1% bromophenol blue, and 1.33% β-mercaptoethanol and proteins were separated by SDS-PAGE on 12% Tris-glycine polyacrylamide gels. An aliquot of 25 μg of purified mitochondria, as measured by the bicinchoninic acid assay standardized using bovine serum albumin, was loaded in each lane.

Two-Dimensional Blue Native- and SDS-PAGE Analysis of CoQ Synthome

Analyses of protein complexes by blue native (BN) gel electrophoresis were performed as previously described (Schagger, Cramer, & Vonjagow, 1994; Wittig, Braun, & Schägger, 2006). Briefly, an aliquot of 200 μg protein of purified mitochondria was pelleted by centrifugation (14,000 *g*, 10 min) and solubilized at a concentration of 4 mg protein/ml on ice for 1 h with BN solubilization buffer containing 11 mM HEPES, pH 7.4, 0.33 M sorbitol, 1× NativePAGE sample buffer (Thermo Fisher Scientific), 16 mg/ml digitonin (Biosynth), Roche Complete EDTA-free protease inhibitor mixture (Roche Complete EDTA-free), phosphatase inhibitor cocktail set II, and phosphatase inhibitor cocktail set 3. The soluble fraction was obtained by centrifugation (100,000 *g,* 10 min) and the protein concentration in the supernatant was determined by bicinchoninic acid assay. NativePAGE 5% G-250 sample additive (Thermo Fisher Scientific) was added to the supernatant to a final concentration of 0.25%. The first-dimension BN gel electrophoresis was performed using NativePAGE 4-16% Bis-Tris gel 1.0 mm x 10 wells (Thermo Fisher Scientific). First-dimension gel slices were soaked in hot SDS sample buffer for 15 min before loading them onto second dimension 12% Tris-glycine polyacrylamide gels. The high molecular weight standards for first-dimension BN gel electrophoresis were obtained from GE Healthcare (Sigma-Aldrich) and the molecular weight standards for the second dimension SDS-PAGE were obtained from Bio-Rad.

Immunoblot Analyses

Proteins were transferred onto 0.45 μm nitrocellulose membrane (Bio-Rad). Membranes were blocked in 0.5% bovine serum albumin, 0.1% Tween 20, 0.02% SDS in phosphate-buffered saline. Membranes were probed with primary antibodies in the same blocking buffer at the dilutions listed in Table S3. IRDye 680LT goat anti-rabbit IgG secondary antibody or IRDye 800CW goat anti-mouse IgG secondary antibody

(LiCOR) was used at 1:10,000 dilutions. Blot images were recorded using LiCOR Odyssey Infrared Scanner (LiCOR).

BN-PAGE and Analysis of ATP Synthase

Wild type and Δ*mdm10* of the W303 background were grown in SLac (2% [wt/vol] lactate, 0.67% [wt/vol] Bacto yeast nitrogen base without amino acids), harvested at $OD_{600} < 2.0$ and isolated by differential centrifugation as described (Daum, Bohni, and Schatz (1982). BN-PAGE was performed as described earlier (Schägger, 2002). Briefly, 100 μg mitochondria were lysed in 40 μl buffer containing digitonin (1% digitonin, 20 mM Tris-HCl, 0.1 mM EDTA, 50 mM NaCl, 10% [vol/vol] glycerol, 1 mM PMSF, pH 7.2). After incubation on ice for 15 min and a clarifying spin (30,000 *g*, 15 min, 2°C), 5 μl sample buffer (5% (w/v) Coomassie blue G, 500 mM 6-amino-N-caproic acid, 100 mM Bis-Tris, pH 7.0) was added. The native complexes were analyzed by electrophoresis in a 6–14% gradient of acrylamide blue native gel. Proteins were transferred to polyvinylidene fluoride membranes and proteins were further analyzed by immunodecoration.

Stable Isotope Labeling

Cells were shaken overnight at 30°C in 100 ml of YPGly and diluted the next morning to an OD_{600} ~0.1 with fresh YPGly. The cultures were incubated as before until they reached an OD_{600} of 0.6. Then ethanol (as vehicle control) or 8 μg/ml of the stable isotopes $^{13}C_6$-pABA or $^{13}C_6$-4HB were added, and the cultures were expanded for an additional 5 h. At each time point, triplicates of 10 ml culture were harvested by centrifugation (3,000 *g*, 5 min). Cell pellets were stored at −20°C.

Lipid Extractions and Analysis of CoQ_6 and CoQ_6 Intermediates

For lipid extractions, approximately 100 μg of purified mitochondria from each strain were prepared in triplicates. The same amount of internal standard CoQ_4 was added to all samples and standards, followed by the addition of 2 ml methanol. Lipids were extracted twice, each time with 2 ml petroleum ether. Extracted lipids were dried down with N_2 and stored at −20°C. Lipid extraction from isotopically labeled whole cell was performed in the same way from frozen cell pellets in triplicate.

For lipid analyses, dried lipids were reconstituted in 200 μl of 0.5 mg/ml benzoquinone in order to oxidize hydroquinones to quinones. An aliquot of 20 μl of each sample was injected into a 4000 QTRAP linear MS/MS spectrometer (Applied Biosystems). Applied Biosystems software, Analyst version 1.4.2, was used for data acquisition and processing. The chromatographic separation was carried out using a Luna 5 μm phenyl-hexyl column (100 × 4.6 mm, 5 μm; Phenomenex) and a mobile phase consisted of 95:5 methanol/isopropanol solution with 2.5 mM ammonium formate as solution A and 100% isopropanol solution with 2.5 mM ammonium formate as solution B. The percentage of solution B was increased linearly from 0 to 10% over 7 min, whereby the flow rate was increased from 650 to 800 μl/min. Each sample was analyzed using multiple reaction monitoring mode. The precursor-to-product ion transitions monitored for each sample are listed in Table S4. The area value of each peak, normalized with the correspondent standard curve and internal standard, was referred to the total mitochondrial protein present in the sample or total OD of cells in each cell pellet. Statistical analysis was performed with GraphPad Prism with one-way analysis of variance Bonferroni's multiple comparisons test, with the Greenhouse-Geisser correction for mitochondrial lipid analyses, and with two-way analysis of variance Dunnett's multiple comparisons test for whole cell lipid analyses.

Microscopy

Yeast were cultured overnight at 30°C in either SGly for W303 cells or SD for S288C strain. In the morning, cells were back-diluted to OD_{600}~0.2 and cultured until reaching mid-logarithmic phase. Cells were then moved to glass-bottom, 384-well microscope plates (Matrical Bioscience) coated with Concanavalin A. After 20 min incubation at room temperature to enable adherence of cells to the matrix, the wells were washed with medium. Cells were then imaged at room temperature using a 60× oil lens (NA 1.4) in the VisiScope Confocal Cell Explorer system, which is composed of a Zeiss Yokogawa spinning disk scanning unit (CSU-W1) coupled with an inverted IX83 microscope (Olympus). Single–focal-plane images were taken using a PCO-Edge sCMOS camera, controlled by VisiView software (GFP-488 nm, RFP-561 nm, or BFP-405 nm). Images were reviewed using ImageJ, where brightness adjustment and cropping were performed.

Results

Yeast Lacking ERMES Have Higher Levels of Transcripts for Coenzyme Q Biosynthesis Enzymes

To investigate how ERMES contributes to the respiratory capacity of yeast cells, we measured the transcriptional response prompted by deletion of genes encoding ERMES subunits. We performed RNA sequencing on ERMES mutants from two different yeast genetic backgrounds: W303 yeast that were cultured on medium

containing glycerol (a nonfermentable carbon source), to ensure preservation of their mitochondrial DNA (Hobbs et al., 2001), or S288C (BY4741) yeast, in which the ERMES mutants harbor reduced levels of mitochondrial DNA, and were therefore cultured on medium containing glucose to enable fermentation (the complete list of mRNA levels in ERMES mutants is in Table S5).

When surveying transcripts which are associated with mitochondrial respiration, we noticed that the mRNA levels of most *COQ* genes involved in the biosynthesis of CoQ_6 were elevated relative to those in the respective control, in both genetic backgrounds and irrespective of the medium used (Figure 1(a) for W303 and Figure S1(a) for S288C). Of note, the mRNA levels of genes encoding for subunits of the respiration complexes did not show a consistent trend of either up- or downregulation (Figure S1(b).

We therefore tested whether the higher mRNA levels of the *COQ* genes resulted in higher protein levels of those polypeptides, in mitochondria purified from W303 cells (Figure 1(b)). We examined the steady-state levels of Coq proteins that have previously been identified as members of the CoQ synthome, as well as Coq10, which is not part of the CoQ synthome but is thought to chaperone CoQ_6 from the synthome to sites of function (Allan et al., 2013; Barros et al., 2005). Surprisingly, we observed that the steady-state levels of all Coq proteins in the mutant cells were either similar, or even slightly reduced, relative to their amounts in control cells (Figure 1(b)).

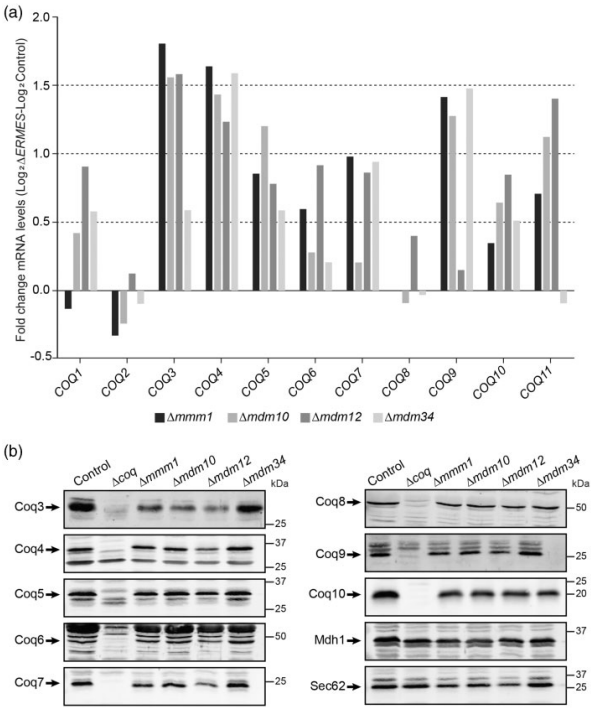

Figure 1. Cells lacking ERMES show higher levels of *COQ* mRNAs without alterations to Coq proteins. (a) Levels of mRNAs of the indicated *COQ* genes were measured in different W303-based strains deleted for ERMES subunits (Δ*mmm1*, Δ*mdm10*, Δ*mdm12* Δ*mdm34*), and a control strain, during growth in medium containing glycerol. The majority of *COQ* biosynthetic genes show higher mRNA levels compared to the control. Values are averages of two biological repeats. (b) Immunoblotting for steady-state levels of Coq polypeptides in purified mitochondria isolated from the indicated W303-based strains. Shown are mutants of the ERMES complex (Δ*mmm1*, Δ*mdm10*, Δ*mdm12*, and Δ*mdm34*), Δ*coq* (Δ*coq3*-Δ*coq10*) and a control, demonstrating that steady-state levels of the different Coq polypeptides were not dramatically altered in the ERMES deletion strains. Immunoblotting was performed with antisera against designated yeast Coq polypeptides (Coq3-Coq10), Mdh1 as a mitochondrial marker, and Sec62 as an ER marker. Arrows denote the corresponding protein in their respective blots. Images are representative gels from at least two biological replicates.

The CoQ Synthome Is Destabilized in the Absence of ERMES Subunits

As the overall mRNA levels of the *COQ* transcripts were higher in ERMES deletions, yet there was no major difference in protein levels, it seems that Coq proteins might be less stable in cells lacking the ERMES complex. Since most of the Coq polypeptides assemble in the CoQ synthome (Belogrudov et al., 2001; He et al., 2014; Marbois et al., 2005; Marbois et al., 2009) and proteins may become unstable when not assembled properly into their natural complexes, we examined the CoQ synthome by two-dimensional BN-PAGE (Figures 2 and S2(a)). Previously, the CoQ synthome was studied when galactose was used as a carbon source (He et al., 2014; Nguyen et al., 2014). However, to match the conditions we previously used for our assays, we followed Coq4, Coq5, and Coq9 in mitochondrial lysates from glycerol-cultured W303 cells. As expected, in control cells, the CoQ synthome was represented by high molecular weight signals, spanning a size range of 140 kDa to >1 MDa for both Coq4 and Coq9 (Figures 2(a) and (b) and S2(a)) and between 440 kDa to >1 MDa for Coq5 (Figure 2(b)). However, in the ERMES mutant strains, the majority of very large species ($>$MDa), representing the CoQ synthome, was replaced by subcomplexes with apparent migration equal to or less than $\sim$440 kDa (Figures 2 and S2(a)), indicating that the CoQ synthome is indeed destabilized in the absence of the ERMES complex. This is not due to a general destabilization of mitochondrial complexes, as the ATP synthase (complex V) was not affected by the absence of the ERMES subunit Mdm10 (Figure S2(b)). Furthermore, previous work did not reveal any change in the migration behavior of porin oligomers and the Tim22 complex in Δ*mdm10* strains (Meisinger et al., 2004). Collectively, our current results, alongside previous observations, suggest that the effect of ERMES mutants on the CoQ synthome is specific.

ERMES Deletion Strains Show Elevated De Novo *Synthesis of CoQ_6 and Accumulate CoQ_6 and CoQ_6-Intermediates in Whole Cells*

To quantify how the biosynthesis of CoQ_6 is affected by destabilization of the CoQ synthome in ERMES mutants,

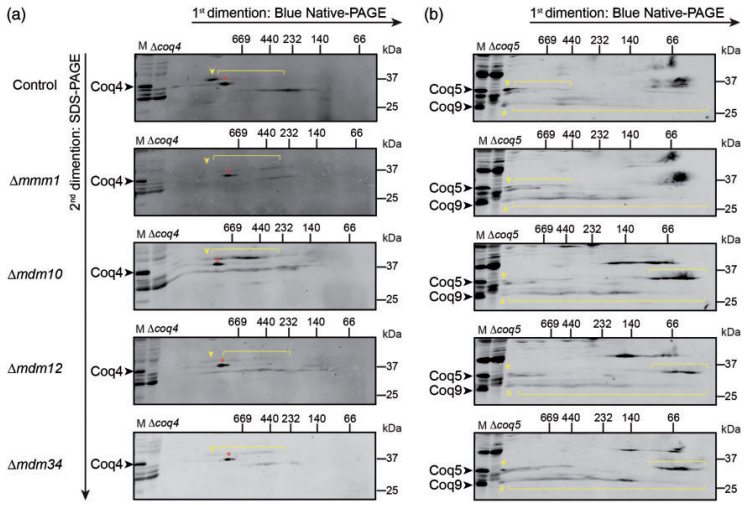

Figure 2. The CoQ synthome is destabilized in the absence of ERMES subunits. (a) Two-dimensional Blue Native-SDS-PAGE gel electrophoresis analysis of the CoQ synthome in mitochondria from ERMES mutants or from a wild-type (WT) control strain. Gels were immunoblotted against Coq4. In the control sample, the CoQ synthome appears as complexes ranging from 232 kDa to >1 MDa (the positions of the synthome is marked by the yellow arrow), while in the Δ*ERMES* strains, the high molecular weight signal is replaced by a signal dispersed over a range of smaller molecular weights (indicated by brackets). The relevant band was identified by comparing the bands in the WT and Δ*coq4* lanes. The red asterisk (*) indicates a discrete nonspecific signal observed with the antisera to Coq4. (b) Two-dimensional Blue Native-SDS-PAGE gel electrophoresis was performed as described in (a). Mitochondria from Δ*coq5* strain were used to identify specific bands (Coq9 is also destabilized and undetectable in the Δ*coq5* strain). Gels were immunoblotted against Coq5 and Coq9. The strong Coq5 and Coq9 bands in the higher molecular weight ($>$669 kDa) in the control sample (indicated by yellow arrows) are weaker in the Δ*ERMES* strains and are replaced by an additional diffuse signal in the lower molecular weights (indicated by brackets).

we measured *de novo* synthesis of CoQ_6 *in vivo*. Yeast cells may utilize either para-aminobenzoic acid (pABA) or 4-hydroxybenzoic acid (4HB) as ring precursors of CoQ_6 (Marbois et al., 2010; Pierrel et al., 2010). Early-stage intermediates, hexaprenyl-aminobenzoic acid (HAB) and hexaprenyl-hydroxybenzoic acid (HHB) are derived from prenylation of pABA or 4HB, respectively. Subsequent modifications of the aromatic ring produce late-stage intermediates such as demethyl-demethoxy-Q_6H_2 ($DDMQ_6$), and demethoxy-Q_6H_2 (DMQ_6), which eventually lead to production of Q_6H_2 (for a schematic of the pathway, see Figure 3(a)). The amino substituent on the pABA ring is removed by a combination of Arh1, Yah1, Coq6, and Coq9 (He et al., 2015; Ozeir et al., 2015) and 4-imino-demethyl-demethoxy-Q_6H_2 ($IDDMQ_6$) and 4-imino-demethoxy-Q_6H_2 ($IDMQ_6$) likely represent dead-end products.

To determine whether CoQ_6 production was altered in the ERMES deletion strains, we analyzed *de novo* biosynthesis of $^{13}C_6$-CoQ_6 with ^{13}C ring-labeled precursors, namely, $^{13}C_6$-pABA and $^{13}C_6$-4HB. Surprisingly,

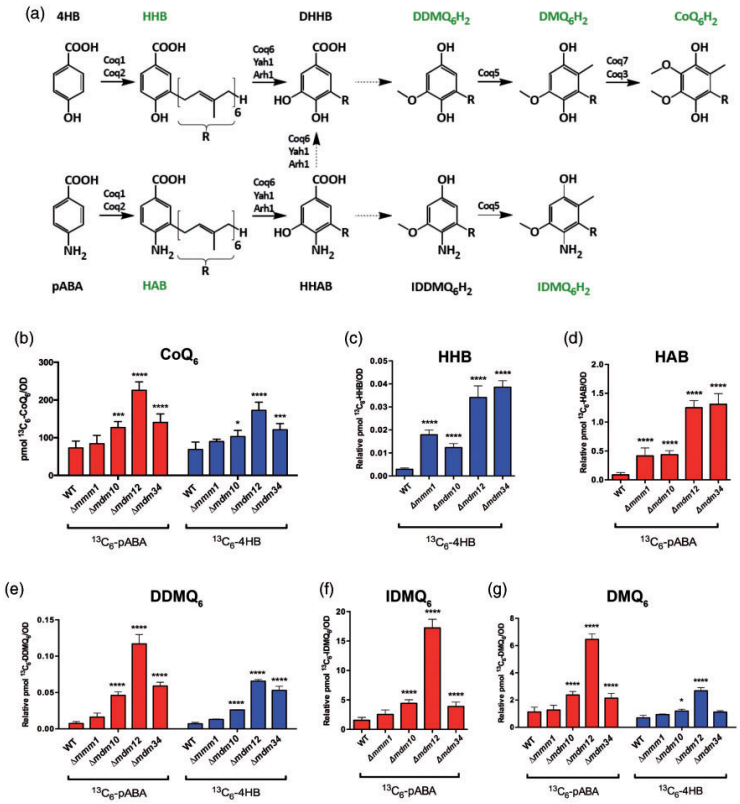

Figure 3. Biosynthesis of CoQ_6 and CoQ_6-intermediates is increased in cells lacking the ERMES complex. (a) Schematic representation of selected steps of the CoQ_6 biosynthesis pathway. CoQ_6-intermediates that were analyzed using mass spectrometry (MS) are indicated in green text. (b-g) MS-MS analysis for CoQ_6 and CoQ_6-intermediates in whole cell lipid extracts from W303 control, Δ*mmm1*, Δ*mdm10*, Δ*mdm12*, and Δ*mdm34* strains. $^{13}C_6$-CoQ_6 and $^{13}C_6$-CoQ_6-intermediates derived from $^{13}C_6$-pABA are depicted in red, while the $^{13}C_6$-CoQ_6 and $^{13}C_6$-CoQ_6-intermediates derived from $^{13}C_6$-4HB are depicted in blue. The biosynthesis of $^{13}C_6$-CoQ_6 (b) is increased in Δ*mdm10*, Δ*mdm12*, and Δ*mdm34* strains labeled with $^{13}C_6$-pABA or $^{13}C_6$-4HB. The biosynthesis of $^{13}C_6$-HHB (c) and $^{13}C_6$-HAB (d) is significantly higher in all the ERMES deletion strains. The *de novo* levels of demethyl-demethoxy-Q_6 ($^{13}C_6$-$DDMQ_6$) (e), 4-imino-DMQ_6 ($^{13}C_6$-$IDMQ_6$) (f), and demethoxy-Q_6 ($^{13}C_6$-DMQ_6) (g) are significantly increased in Δ*mdm10*, Δ*mdm12*, and Δ*mdm34* strains, with the exception of $^{13}C_6$-DMQ_6 in Δ*mdm34* that did not change after the labeling with $^{13}C_6$-4HB. Values are the mean of three repeats. The error bar indicates ±SD. Statistically significant differences between control (WT) and each of the ERMES mutants are represented by *, $p < .05$; **, $p < .01$; ***, $p < .001$, and ****, $p < .0005$. HHB = hexaprenyl-hydroxybenzoic acid; HAB = hexaprenyl-aminobenzoic acid; CoQ = Coenzyme Q; DDMQ = demethyl-demethoxy-Q; DMQ = demethoxy-Q; IDMQ = 4-imino-demethoxy-Q.

we saw that Δ*mdm10*, Δ*mdm12*, and Δ*mdm34* cells showed enhanced *de novo* synthesis of $^{13}C_6$-CoQ_6 (Figure 3(b)). These mutants also accumulated CoQ_6-intermediates emanating from $^{13}C_6$-pABA and $^{13}C_6$-4HB, whereas Δ*mmm1* cells only contained significantly higher amount of $^{13}C_6$-labeled HAB and HHB, but not the other intermediates (Figure 3(c) to (g)). We also measured the levels of unlabeled CoQ_6 (which correspond to the steady-state levels) in the same samples and observed an accumulation of unlabeled CoQ_6 and CoQ_6-intermediates in most of the ERMES deletion mutants, regardless of the presence or absence of ^{13}C-labeled precursor (Figure S3). The results suggest that the destabilized CoQ synthome in ERMES mutants results in an aberrant accumulation of CoQ_6 as well as CoQ_6-intermediates.

ERMES Deletion Strains Show Decreased Steady-State Levels of CoQ_6 and CoQ_6-Intermediates in Isolated Mitochondria

Although the biosynthesis of yeast CoQ_6 occurs exclusively within mitochondria, CoQ_6 is present in all cellular membranes (Bentinger et al., 2010). To focus on the status of CoQ_6 in mitochondria, we compared the steady-state content of CoQ_6 in mitochondria isolated from the ERMES deletion mutants to mitochondria obtained from a control strain. Although the overall cellular levels of CoQ_6 in these mutants were increased, the steady-state levels of CoQ_6 per unit of mitochondrial protein were significantly reduced in mitochondria isolated from Δ*mmm1*, Δ*mdm10*, or Δ*mdm12* strains (Figure 4(a)). Only strains lacking Mdm34 appeared to have nearly normal levels of CoQ_6. Isolated mitochondria from all of the ERMES deletion strains also contained lower levels of the late-stage intermediates $IDMQ_6$ and DMQ_6 (Figure 4(b) and (c), respectively). The levels of the late-stage intermediate $DDMQ_6$ were reduced in all strains, though the reduction was not statistically significant (Figure 4(d)). Our finding of decreased steady-state levels of CoQ_6 and its late intermediates in isolated mitochondria suggests that the accumulation of these molecules in whole cell lipid extracts (Figures 3 and S3) must reside in non-mitochondrial membranes. Moreover, reduced levels of pathway product in vicinity to the enzymes may reduce feedback

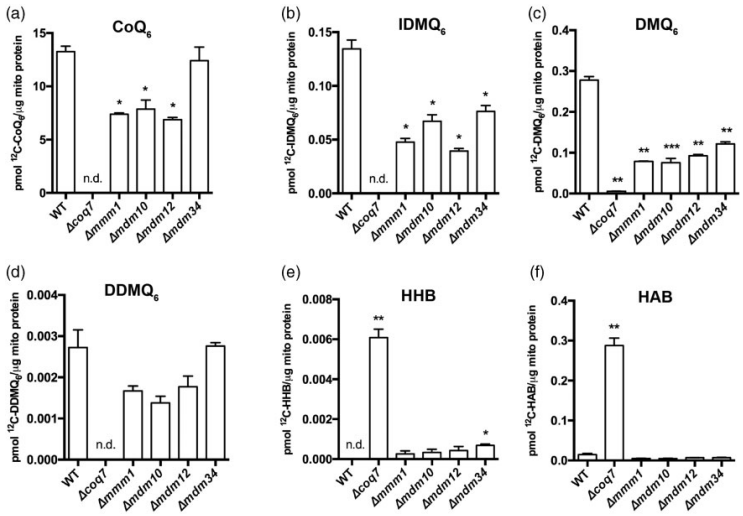

Figure 4. Mitochondria from ERMES mutants show less CoQ_6 and CoQ_6-intermediates. (a-f) Targeted MS-MS analyses for CoQ_6 and CoQ_6-intermediates from purified mitochondria from W303 wild-type (WT) control, ERMES mutants (Δ*mmm1*, Δ*mdm10*, Δ*mdm12*, and Δ*mdm34*) as well as Δ*coq7*, which was included as a negative control. Levels of (a) CoQ_6 were significantly reduced in all ERMES deletion strains except for Δ*mdm34*. Levels of (b) $IDMQ_6$ and (c) DMQ_6 were significantly reduced in all ERMES deletion strains. Levels of (d) $DDMQ_6$ were not significantly changed. Levels of (e) HHB and (f) HAB were significantly higher in the Δ*coq7* strain; however, ERMES deletion strains did not show an accumulation of either HHB or HAB (with the exception of Δ*mdm34* accumulating HHB). Values are means of three biological repeats. The error bar indicates ±SD. Statistically significant differences between the control and each of the ERMES mutants are represented by *, $p < .05$; **, $p < .01$; ***, $p < .001$; and ****, $p < .0005$. n.d. = not detected. HHB = hexaprenyl-hydroxybenzoic acid; HAB = hexaprenyl-aminobenzoic acid; CoQ = Coenzyme Q; DDMQ = demethyl-demethoxy-Q; DMQ = demethoxy-Q; IDMQ = 4-imino-demethoxy-Q.

inhibition (Berg, Tymoczko, & Stryer, 2002; Gehart & Pardee, 1962; Umbarger, 1961), providing an explanation for the increased rate of synthesis observed in ERMES mutants. However, feedback inhibition has not yet been reported for Coq enzymes.

In the complete absence of the CoQ synthome, strains fail to make CoQ_6 and can only carry out the first two steps of the biosynthetic pathway, producing HAB or HHB from the prenylation reaction of pABA or 4HB, respectively, using precursors derived from the mevalonate pathway in the ER (He et al., 2014). Indeed, deletion of the *COQ7* gene resulted in a dramatic accumulation of HHB and HAB (Figure 4(e) and (f)), as observed previously (Tran & Clarke, 2007). Interestingly, in the strains deleted for ERMES subunits, this accumulation of early CoQ_6-intemediates did not occur (with the exception of HHB slightly accumulating in the Δ*mdm34* strain (Figure 4(e))). The difference in the accumulation phenotypes between the ERMES-deletion strains and Δ*coq7* suggests that in addition to stabilizing the CoQ synthome, ERMES has a role at an earlier stage of the pathway.

The CoQ Synthome Resides in Specific Membrane Niches in Proximity to ERMES Contacts

Strains lacking ERMES subunits exhibit increased levels of cellular CoQ_6 and CoQ_6-intermediates, yet mitochondrial CoQ_6 and CoQ_6-intermediates are decreased and the CoQ synthome is destabilized. In addition, early pathway intermediates do not accumulate, suggesting a reduced flux of precursors from the ER. We wondered whether the ERMES complex may play a role in organizing the CoQ synthome and the trafficking of CoQ_6-related metabolites near ER-mitochondria contacts. As tagging Coq polypeptides with green fluorescent protein (GFP) does not impair their function (Figure S4(a)), we tagged Coq3, Coq4, Coq6, Coq9, and Coq11 with GFP and performed fluorescence microscopy. We noticed that these proteins are not distributed evenly throughout the mitochondrial matrix, but rather manifest a more punctate distribution (data not shown), suggesting that there might be discrete areas inside the mitochondrial matrix that are dedicated to the synthesis of CoQ_6. If the assembly of the CoQ synthome depends on ERMES, in a strain deleted for ERMES the punctate pattern of the GFP-tagged Coq polypeptide should disappear. Indeed, when we GFP-tagged Coq6 and Coq9 in a strain harboring a deletion for *MDM34*, the Coq-GFP punctate pattern was lost and the GFP signal was now spread throughout the entire mitochondrion (Figure S4(b)). However, as these mutants show dramatic alteration in mitochondrial morphology (Kornmann et al., 2009), it is hard to determine whether this effect is direct. To better understand the spatial relationship between ERMES and the CoQ synthome, we tagged Coq6 and Coq9 with GFP in a strain expressing Mdm34 fused to mCherry. Analyses of these cells revealed that more than 70% of the Mdm34-mCherry-marked contacts colocalized with Coq6-GFP or Coq9-GFP puncta (Figure 5(a) and quantification in Figure 5(b)). This colocalization was independent of genetic background and was also evident in a S288C background strain (Figure S4(c)). Our results strongly suggest that the localization of the CoQ synthome is coordinated with the position of the ER-mitochondria contact site.

Interestingly, in the yeast genome, the *COQ10* and *MDM12* genes are adjacent and likely to share a promoter (Cherry et al., 2012). Indeed, SPELL analysis of transcriptional co-regulation (Hibbs et al., 2007) demonstrates that these two genes are co-expressed. We therefore tested whether Coq10 is involved in the positioning of the CoQ synthome next to ERMES. To this end, we removed *COQ10*, then assessed colocalization between Coq6-GFP and Mdm34-mCherry. The Coq6-GFP signal was dramatically reduced upon *COQ10* deletion, consistent with previous findings (Hsieh et al., 2007). Nevertheless, several Coq6-GFP-containing puncta were observed. Quantification of the colocalization between these Coq6-GFP puncta and Mdm34-mCherry revealed that the positioning of the CoQ synthome next to the ERMES complex was reduced in the *coq10* null mutant (Figure 5(c) and quantification in Figure 5(d)). Our results suggest that the positioning of the CoQ synthome within mitochondria is a regulated process which depends upon the presence of Coq10.

Discussion

Contact sites play a critical role in shaping cellular architecture, and their facilitation of small molecule transfer between organelles enables tight regulation of biochemical pathways. In this study, we show that ERMES, an ER-mitochondria contact site tether, plays a key role in regulating CoQ_6 biosynthesis and distribution.

The ERMES complex appears to impact CoQ_6 synthesis on two levels. First, absence of the ERMES complex leads to destabilization of the CoQ synthome, perturbed CoQ_6 synthesis, and altered distribution of CoQ_6 and its precursors. Second, there is a clear spatial coordination of the ERMES complex with the CoQ synthome (Figure 5(e)). It is possible that ERMES may directly impact the CoQ synthome; however, there is no evidence showing direct interaction of ERMES subunits with known members of the CoQ synthome. We also note that the effects of ERMES disruption on the synthome and CoQ_6 biogenesis may be, at least in part, indirectly prompted by changes to phospholipid metabolism (Elbaz-Alon et al., 2014; Hönscher et al., 2014; Kawano et al., 2018; Lahiri et al., 2014) or by alteration

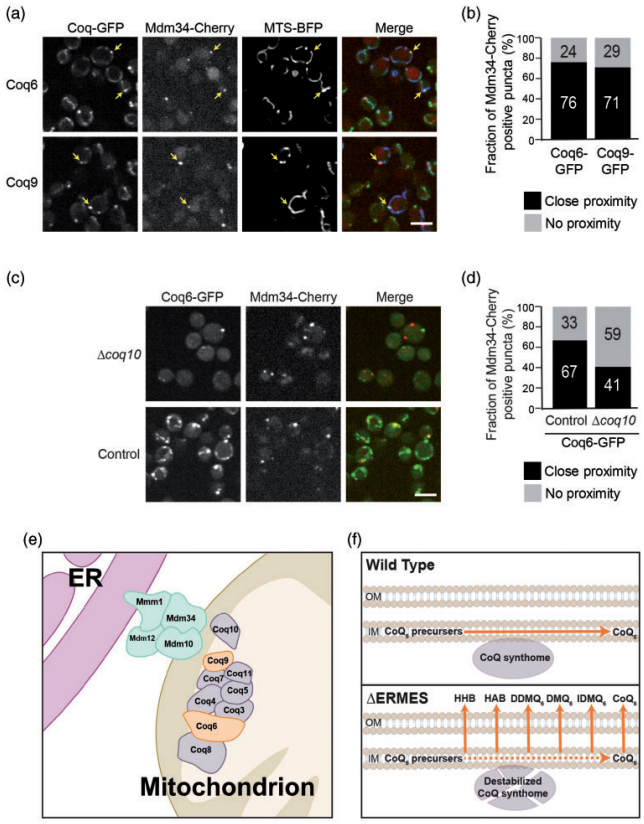

Figure 5. Members of the CoQ synthome reside in a matrix niche that underlies the ERMES complex. (a) Yeast cells expressing the indicated GFP-tagged Coq protein, the ERMES component Mdm34 tagged with mCherry, and a marker for the mitochondrial matrix (blue fluorescent protein [BFP] fused to a mitochondrial targeting sequence [MTS]) were imaged using fluorescence microscopy. Mitochondrial Coq foci that underlie ERMES are indicated by arrows. Scale bar = 5 μM. (b) Quantification of (a), for each cell, the Coq-GFP foci were identified. Then the proximity between each Mdm34-mCherry puncta and Coq-GFP was assessed. $n = 100$ Mdm34-mCherry puncta. (c) Yeast cells expressing Coq6-GFP, Mdm34-mCherry, and a MTS-BFP were imaged using fluorescence microscopy on either control or Δ*coq10* background. Scale bar = 5 μM. (d) Quantification of (c). The proximity between each Mdm34-mCherry puncta and the Coq6-GFP signal was examined. $n = 100$ Mdm34-mCherry puncta. (e) Schematic representation of the colocalization of ERMES and the CoQ synthome. Coq6 and Coq9, which were visualized in (a), are highlighted in orange. (f) A suggested model for the retention of CoQ_6 and CoQ_6-intermediates inside mitochondria: Under normal conditions, the CoQ synthome is well assembled and CoQ_6 biosynthesis (represented by the red arrow) occurs efficiently inside mitochondria. This catalytic efficiency ensures that early- and late-stage CoQ_6-intermediates do not accumulate, and optimal funneling through the pathway reduces loss across the mitochondrial outer membrane and into the rest of the cell. When the ERMES complex is absent, the stability of the CoQ synthome is compromised. A partially destabilized CoQ synthome underlies inefficient CoQ biosynthesis, leading to leakage of early- and late-stage CoQ_6-intermediates. OM = outer membrane, IM = inner membrane; GFP = green fluorescent protein; BFP = blue fluorescent protein; MTS = mitochondrial targeting sequence; ER = endoplasmic reticulum; ERMES = ER mitochondria encounter structure; HHB = hexaprenyl-hydroxybenzoic acid; HAB = hexaprenyl-aminobenzoic acid; CoQ = Coenzyme Q; DDMQ = demethyl-demethoxy-Q; DMQ = demethoxy-Q; IDMQ = 4-imino-demethoxy-Q.

of the shape and size of mitochondria (Hanekamp et al., 2002; Tan et al., 2013; Youngman et al., 2004).

We have shown that Coq10 is involved in the coordination of CoQ_6 synthesis across the ER-mitochondria interface (Figure 5(c) and (d)). *COQ10* encodes a membrane-spanning protein harboring a putative steroidogenic acute regulatory-related lipid transfer (StART) domain and a lipid-binding pocket for CoQ_6

and late-stage CoQ_6-intermediates (Allan et al., 2013) . Although Coq10 has not been shown to be part of the CoQ synthome, it is necessary for efficient *de novo* CoQ_6 biosynthesis and respiration (Allan et al., 2013). The co-expression of the *COQ10* and *MDM12* genes (Hibbs et al., 2007) might help coordinate the levels of Coq10 and ERMES to allow a better positioning of the CoQ synthome next to ER-mitochondria contact sites as they fluctuate in amount with changing cellular needs. Intriguingly, when overexpressed, Mdm12 is capable of entering the nucleus (Weill et al., 2018), raising the possibility of feedback control of the CoQ synthome-ERMES interaction. Moreover, the specific mechanism by which COQ genes are transcriptionally upregulated by ERMES disruption remains to be determined, but extensive communication exists between mitochondria and the nucleus (Eisenberg-Bord & Schuldiner, 2017), and at least one pathway by which CoQ biosynthesis can be upregulated by CoQ deficiency has been revealed in metazoans (Oks, Lewin, Goncalves, & Sapir, 2018).

How do CoQ_6 and CoQ_6-intermediates escape from mitochondria and accumulate in non-mitochondrial membranes in the ERMES deletion mutants? This might be due to a direct or indirect effect. Given that many Coq proteins of the CoQ synthome can bind to CoQ_6 or its biosynthetic intermediates, we propose that a destabilized CoQ synthome causes reduced sequestration of CoQ_6 within mitochondria (Figure 5(f)). In an alternative, yet not mutually exclusive model, disruption of ERMES mutants leads to reduced degradation of CoQ_6 outside of mitochondria. Although CoQ_6 degradation has not been studied extensively, it is believed that degradation of the polyisoprene tail of CoQ_6 may be carried out in peroxisomes via both α- and β-oxidation (Wanders, 2014). Indeed, we have previously shown that peroxisome-mitochondria (PERMIT) contact sites reside in proximity to ER-mitochondria contact sites (Cohen et al., 2014), raising the possibility that loss of ERMES may also affect the capacity to degrade escaped CoQ_6.

Excitingly, our findings are likely to have relevance to human health and disease. In mammals, the mitofusin 2 (MFN2) protein acts as a tether between the ER and mitochondria (de Brito & Scorrano, 2008), and conditional *MFN2* knock-out mice exhibit impaired respiration linked to a decrease in mitochondrial levels of the mammalian ubiquinones, CoQ_9 and CoQ_{10} (Mourier et al., 2015). It is hypothesized that this phenotype is not directly related to the role of MFN2 in mitochondrial fusion as the CoQ deficiency was not linked to the morphology of the mitochondrial network. These findings further suggest that a reduction in ER-mitochondria tethering can perturb CoQ biosynthesis, suggesting parallels between the yeast and mammalian cells.

Acknowledgments

We thank Rodney Rothstein for strains, we thank Christian Ungermann, Jodi Nunnari and Naama Barkai for plasmids, we thank Lee McAlister-Henn and David Meyer for antibodies, and we thank Ido Amit for the transposase required for the sequencing. We thank Yoav Voichek and Yulia Gordon for producing and analyzing the RNA-sequencing data. We thank Alexander Brandis and Tevi Mehlman from the Targeted Metabolomics unit of the Life Sciences Core Facilities of the Weizmann Institute for Mass-Spectrometry analysis.

Declaration of Conflicting Interests

The author(s) declared no potential conflicts of interest with respect to the research, authorship, and/or publication of this article.

Funding

The author(s) disclosed receipt of the following financial support for the research, authorship, and/or publication of this article: CDD acknowledges funding from an EMBO Installation Grant (2138) and from an European Research Council Starting Grant (RevMito 637649). MEB is grateful to the Azrieli Foundation for the award of an Azrieli Fellowship. This work was supported by the Deutsche Forschungsgemeinschaft (DIP to MS and DR), and the IMPRS "From Molecules to Organisms" (DA). Work in the Schuldiner lab is additionally supported by an SFB1190 from the DFG as well as a "Life" grant from the Volkswagen foundation. MS is an incumbent of the Dr. Gilbert Omenn and Martha Darling Professorial Chair in Molecular Genetics. This work is supported by the National Science Foundation Grant MCB-1330803 (to CFC) and by the National Institutes of Health Grant T32 GM 008496 to HST and MCB.

Supplemental material

Supplemental material for this article is available online.

References

Allan, C. M., Awad, A. M., Johnson, J. S., Shirasaki, D. I., Wang, C., Blaby-Haas, C. E., Clarke, C. F. (2015). Identification of Coq11, a new coenzyme Q biosynthetic protein in the CoQ-synthome in *Saccharomyces cerevisiae*. *Journal of Biological Chemistry*, *290*, 7517–7534.

Allan, C. M., Hill, S., Morvaridi, S., Saiki, R., Johnson, J. S., Liau, W. S., Clarke, C. F. (2013). A conserved START domain coenzyme Q-binding polypeptide is required for efficient Q biosynthesis, respiratory electron transport, and antioxidant function in *Saccharomyces cerevisiae*. *Biochimica et Biophysica Acta – Molecular and Cell Biology of Lipids*, *1831*, 776–791.

Awad, A. M., Bradley, M. C., Fernández-Del-Río, L., Nag, A., Tsui, H. S., & Clarke, C. F. (2018). Coenzyme Q10 deficiencies: Pathways in yeast and humans. *Essays in Biochemistry*, *62*, 361–376.

Barros, M. H., Johnson, A., Gin, P., Marbois, B. N., Clarke, C.F., & Tzagoloff, A. (2005). The *Saccharomyces cerevisiae COQ10* gene encodes a START domain protein required for function of coenzyme Q in respiration. *Journal of Biological Chemistry*, *280*, 42627–42635.

Belogrudov, G. I., Lee, P. T., Jonassen, T., Hsu, A. Y., Gin, P., & Clarke, C. F. (2001). Yeast *COQ4* encodes a mitochondrial protein required for coenzyme Q synthesis. *Archives of Biochemistry and Biophysics*, *392*, 48–58.

Bentinger, M., Tekle, M., & Dallner, G. (2010). Coenzyme Q – Biosynthesis and functions. *Biochemical and Biophysical Research Communication*, *396*, 74–79.

Berg, J. M., Tymoczko, J. L., & Stryer, L. (2002). *The biosynthesis of amino acids*. New York: W H Freeman.

Berger, K. H., Sogo, L. F., & Yaffe, M. P. (1997). Mdm12p, a component required for mitochondrial inheritance that is conserved between budding and fission yeast. *Journal of Cell Biology*, *136*, 545–553.

Brachmann, C. B., Davies, A., Cost, G. J., Caputo, E., Li, J., Hieter, P., & Boeke, J. D. (1998). Designer deletion strains derived from *Saccharomyces cerevisiae* S288C: A useful set of strains and plasmids for PCR-mediated gene disruption and other applications. *Yeast*, *14*, 115–132.

Cherry, J. M., Hong, E. L., Amundsen, C., Balakrishnan, R., Binkley, G., Chan, E. T., Wong, E. D. (2012). Saccharomyces Genome Database: The genomics resource of budding yeast. *Nucleic Acids Research*, *40*, D700–D705.

Cohen, Y., Klug, Y. A., Dimitrov, L., Erez, Z., Chuartzman, S. G., Elinger, D., Schuldiner, M. (2014). Peroxisomes are juxtaposed to strategic sites on mitochondria. *Molecular Biosystems*, *10*, 1742–1748.

Daum, G., Bohni, P. C., & Schatz, G. (1982). Import of proteins into mitochondria. *Journal of Biological Chemistry*, *257*, 13028–13033.

de Brito, O. M., & Scorrano, L. (2008). Mitofusin 2 tethers endoplasmic reticulum to mitochondria. *Nature*, *456*, 605–610.

Dimmer, K. S., & Rapaport, D. (2017). Mitochondrial contact sites as platforms for phospholipid exchange. *Biochimica et Biophysica Acta – Molecular and Cell Biology of Lipids*, *1862*, 69–80.

Eisenberg-Bord, M., & Schuldiner, M. (2017). Ground control to major TOM: Mitochondria-nucleus communication. *FEBS Journal*, *284*, 196–210.

Eisenberg-Bord, M., Shai, N., Schuldiner, M., & Bohnert, M. (2016). A tether is a tether is a tether: Tethering at membrane contact sites. *Developmental Cell*, *39*, 395–409.

Elbaz-Alon, Y., Rosenfeld-Gur, E., Shinder, V., Futerman, A. H., Geiger, T., & Schuldiner, M. (2014). A dynamic interface between vacuoles and mitochondria in yeast. *Developmental Cell*, *30*, 95–102.

Gehart, J. C., & Pardee, A. B. (1962). The enzymology of control by feedback inhibition. *Journal of Biological Chemistry*, *237*, 891–896.

Gietz, R. D., & Woods, R. A. (2006). Yeast transformation by the LiAc/SS Carrier DNA/PEG method. *Methods in Molecular Biology*, *313*, 107–120.

Glick, B. S., & Pon, L. A. (1995). Isolation of highly purified mitochondria from *Saccharomyces cerevisiae*. *Methods in Enzymology*, *260*, 213–223.

González Montoro, A., Auffarth, K., Hönscher, C., Bohnert, M., Becker, T., Warscheid, B., Ungermann, C. (2018). Vps39 interacts with Tom40 to establish one of two functionally distinct vacuole-mitochondria contact sites. *Developmental Cell*, *45*, 621.e7–636.e7.

Hanekamp, T., Thorsness, M. K., Rebbapragada, I., Fisher, E. M., Seebart, C., Darland, M. R., Thorsness, P. E. (2002). Maintenance of mitochondrial morphology is linked to maintenance of the mitochondrial genome in *Saccharomyces cerevisiae*. *Genetics*, *162*, 1147–1156.

He, C. H., Black, D. S., Nguyen, T. P. T., Wang, C., Srinivasan, C., & Clarke, C. F. (2015). Yeast Coq9 controls deamination of coenzyme Q intermediates that derive from para-aminobenzoic acid. *Biochimica et Biophysica Acta*, *1851*, 1227–1239.

He, C. H., Xie, L. X., Allan, C. M., Tran, U. C., & Clarke, C. F. (2014). Coenzyme Q supplementation or overexpression of the yeast Coq8 putative kinase stabilizes multi-subunit *Coq* polypeptide complexes in yeast coq null mutants. *Biochimica et Biophysica Acta – Molecular and Cell Biology of Lipids*, *1841*, 630–644.

Hibbs, M. A., Hess, D. C., Myers, C. L., Huttenhower, C., Li, K., & Troyanskaya, O. G. (2007). Exploring the functional landscape of gene expression: Directed search of large microarray compendia. *Bioinformatics*, *23*, 2692–2699.

Hobbs, A. E., Srinivasan, M., McCaffery, J. M., & Jensen, R. E. (2001). Mmm1p, a mitochondrial outer membrane protein, is connected to mitochondrial DNA (mtDNA) nucleoids and required for mtDNA stability. *Journal of Cell Biology*, *152*, 401–410.

Hönscher, C., Mari, M., Auffarth, K., Bohnert, M., Griffith, J., Geerts, W., Ungermann, C. (2014). Cellular metabolism regulates contact sites between vacuoles and mitochondria. *Developmental Cell*, *30*, 86–94.

Hsieh, E. J., Gin, P., Gulmezian, M., Tran, U. C., Saiki, R., Marbois, B. N., & Clarke, C. F. (2007). *Saccharomyces cerevisiae* Coq9 polypeptide is a subunit of the mitochondrial coenzyme Q biosynthetic complex. *Archives of Biochemistry and Biophysics*, *463*, 19–26.

Janke, C., Magiera, M. M., Rathfelder, N., Taxis, C., Reber, S., Maekawa, H., Knop, M. (2004). A versatile toolbox for PCR-based tagging of yeast genes: New fluorescent proteins, more markers and promoter substitution cassettes. *Yeast*, *21*, 947–962.

John Peter, A. T., Herrmann, B., Antunes, D., Rapaport, D., Dimmer, K. S., & Kornmann, B. (2017). Vps13-Mcp1 interact at vacuole-mitochondria interfaces and bypass ER-mitochondria contact sites. *Journal of Cell Biology*, *216*, 3219–3229.

Kakimoto, Y., Tashiro, S., Kojima, R., Morozumi, Y., Endo, T., & Tamura, Y. (2018). Visualizing multiple inter-organelle contact sites using the organelle-targeted split-GFP system. *Scientific Reports*, *8*, 6175.

Kawano, S., Tamura, Y., Kojima, R., Bala, S., Asai, E., Michel, A. H., Endo, T. (2018). Structure–function insights into direct lipid transfer between membranes by Mmm1–Mdm12 of ERMES. *Journal of Cell Biology*, *217*, 1–22.

Kivioja, T., Vähärautio, A., Karlsson, K., Bonke, M., Enge, M., Linnarsson, S., & Taipale, J. (2012). Counting absolute

numbers of molecules using unique molecular identifiers. *Nature Methods*, *9*, 72–74.

Kojima, R., Endo, T., & Tamura, Y. (2016). A phospholipid transfer function of ER-mitochondria encounter structure revealed *in vitro*. *Scientific Reports*, *6*, 30777.

Kornmann, B., Currie, E., Collins, S. R., Schuldiner, M., Nunnari, J., Weissman, J. S., & Walter, P. (2009). An ER-mitochondria tethering complex revealed by a synthetic biology screen. *Science*, *325*, 477–481.

Lahiri, S., Chao, J. T., Tavassoli, S., Wong, A. K. O., Choudhary, V., Young, B. P., Loewen, C. J., Prinz, W. A. (2014). A conserved endoplasmic reticulum membrane protein complex (EMC) facilitates phospholipid transfer from the ER to mitochondria. *PLoS Biology*, *12*, e1001969.

Lang, A. B., Peter, A. T. J., Walter, P., & Kornmann, B. (2015). ER-mitochondrial junctions can be bypassed by dominant mutations in the endosomal protein Vps13. *Journal of Cell Biology*, *210*, 883–890.

Liu, C. L., Kaplan, T., Kim, M., Buratowski, S., Schreiber, S. L., Friedman, N., & Rando, O. J. (2005). Single-nucleosome mapping of histone modifications in *S. cerevisiae*. *PLoS Biology*, *3*, e328.

Longtine, M. S., McKenzie, A., Demarini, D. J., Shah, N. G., Wach, A., Brachat, A. Philippsen, P., … Pringle, J. R. (1998). Additional modules for versatile and economical PCR-based gene deletion and modification in *Saccharomyces cerevisiae*. *Yeast*, *14*, 953–961.

Marbois, B., Gin, P., Faull, K. F., Poon, W. W., Lee, P. T., Strahan, J., Clarke, C. F. (2005). Coq3 and Coq4 define a polypeptide complex in yeast mitochondria for the biosynthesis of coenzyme Q. *Journal of Biological Chemistry*, *280*, 20231–20238.

Marbois, B., Gin, P., Gulmezian, M., … Clarke, C. F. (2009). The yeast Coq4 polypeptide organizes a mitochondrial protein complex essential for coenzyme Q biosynthesis. *Biochimica et Biophysica Acta – Molecular and Cell Biology of Lipids*, *1791*, 69–75.

Marbois, B., Xie, L. X., Choi, S., Hirano, K., Hyman, K., & Clarke, C. F. (2010). Para-aminobenzoic acid is a precursor in coenzyme Q6 biosynthesis in *Saccharomyces cerevisiae*. *Journal of Biological Chemistry*, *285*, 27827–27838.

Meisinger, C., Rissler, M., Chacinska, A., Szklarz, L. K. S., Milenkovic, D., Kozjak, V., Schonfisch, B., Lohaus, C., Meyer, H.E., Yaffe, M.P., Guiard, B., Wiedemann, N., Pfanner, N. (2004). The mitochondrial morphology protein Mdm10 functions in assembly of the preprotein translocase of the outer membrane. *Developmental Cell*, *7*, 61–71.

Mourier, A., Motori, E., Brandt, T., Lagouge, M., Atanassov, I., Galinier, A. Rappl, G., Brodesser, S., Hultenby, K., Dieterich, C. Larsson, N. G. (2015). Mitofusin 2 is required to maintain mitochondrial coenzyme Q levels. *Journal of Cell Biology*, *208*, 429–442.

Nguyen, T. P. T., Casarin, A., Desbats, M. A., Doimo, M., Trevisson, E., Santos-Ocaña, C., Salviati, L. (2014). Molecular characterization of the human COQ5 C-methyltransferase in coenzyme Q10 biosynthesis. *Biochimica et Biophysica Acta—Molecular and Cell Biology of Lipids*, *1841*, 1628–1638.

Oks, O., Lewin, S., Goncalves, I. L., & Sapir, A. (2018). The UPRmt protects *Caenorhabditis elegans* from mitochondrial dysfunction by upregulating specific enzymes of the mevalonate pathway. *Genetics*, *209*, 457–473.

Ozeir, M., Pelosi, L., Ismail, A., Mellot-Draznieks, C., Fontecave, M., & Pierrel, F. (2015). Coq6 is responsible for the C4-deamination reaction in coenzyme Q biosynthesis in *Saccharomyces cerevisiae*. *Journal of Biological Chemistry*, *290*, 24140–24151.

Pierrel, F., Hamelin, O., Douki, T., Kieffer-Jaquinod, S., Mühlenhoff, U., Ozeir, M., … Fontecave, M. (2010). Involvement of mitochondrial ferredoxin and para-aminobenzoic acid in yeast coenzyme Q biosynthesis. *Chemistry & Biology*, *17*, 449–459.

Schägger, H. (2002). Respiratory chain supercomplexes of mitochondria and bacteria. *Biochimica et Biophysica Acta—Bioenergetics*, *1555*, 154–159.

Schagger, H., Cramer, W. A., & Vonjagow, G. (1994). Analysis of molecular masses and oligomeric states of protein complexes by blue native electrophoresis and isolation of membrane protein complexes by two-dimensional native electrophoresis. *Analytical Biochemistry*, *217*, 220–230.

Shai, N., Yifrach, E., van Roermund, C. W. T., Cohen, N., Bibi, C., IJlst, L., Cavellini, L., Meurisse, J., Schuster, R., Zada, L., Mari, M.C., Reggiori, F.M., Hughes, A.L., Escobar-Henriques, M., Cohen, M.M., Waterham, H.R., Wanders, R.J.A., Schuldiner, M., … Zalckvar, E. (2018). Systematic mapping of contact sites reveals tethers and a function for the peroxisome-mitochondria contact. *Nature Communications*, *9*, 1761.

Tan, T., Ozbalci, C., Brügger, B., Rapaport, D., & Dimmer, K. S. (2013). Mcp1 and Mcp2, two novel proteins involved in mitochondrial lipid homeostasis. *Journal of Cell Science*, *126*, 3563–3574.

Thomas, B. J., & Rothstein, R. (1989). Elevated recombination rates in transcriptionally active DNA. *Cell*, *56*, 619–630.

Tran, U. C., & Clarke, C. F. (2007). Endogenous synthesis of coenzyme Q in eukaryotes. *Mitochondrion*, *7* Suppl, S62–S71.

Umbarger, H. E. (1961). Feedback control by endproduct inhibition. *Cold Spring Harbor Symposia on Quantitative Biology*, *26*, 301–312.

Valm, A. M., Cohen, S., Legant, W. R., Melunis, J., Hershberg, U., Wait, E., Cohen, A.R., Davidson, M.W., Betzig, E., Lippincott-Schwartz, J. (2017). Applying systems-level spectral imaging and analysis to reveal the organelle interactome. *Nature*, *546*, 162–167.

Voichek, Y., Bar-Ziv, R., & Barkai, N. (2016). Expression homeostasis during DNA replication. *Science*, *351*, 1087–1090.

Wanders, R. J. A. (2014). Metabolic functions of peroxisomes in health and disease. *Biochimie*, *98*, 36–44.

Weill, U., Yofe, I., Sass, E., Stynen, B., Davidi, D., Natarajan, J., Ben-Menachem, R., Avihou, Z., Goldman, O., Harpaz, N., Chuartzman, S., Kniazev, K., Knoblach, B., Laborenz, J., Boos, F., Kowarzyk, J., Ben-Dor, S., Zalckvar, E., Herrmann, J.M., Rachubinski, R.A., Pines, O., Rapaport, D., Michnick, S.W., Levy, E.D., Schuldiner, M. (2018).

Genome-wide SWAp-Tag yeast libraries for proteome exploration. *Nature Methods*, *15*, 617–622.
Wittig, I., Braun, H.-P., & Schägger, H. (2006). Blue native PAGE. *Nature Protocols*, *1*, 418–428.
Yofe, I., & Schuldiner, M. (2014). Primers-4-Yeast: A comprehensive web tool for planning primers for *Saccharomyces cerevisiae*. *Yeast*, *31*, 77–80.
Youngman, M. J., Hobbs, A. E. A., Burgess, S. M., Srinivasan, M., & Jensen, R. E. (2004). Mmm2p, a mitochondrial outer membrane protein required for yeast mitochondrial shape and maintenance of mtDNA nucleoids. *Journal of Cell Biology*, *164*, 677–688.

CHAPTER 4

Isotope-reinforced polyunsaturated fatty acids protect mitochondria from oxidative stress

Free Radical Biology and Medicine 82 (2015) 63–72

Contents lists available at ScienceDirect

Free Radical Biology and Medicine

journal homepage: www.elsevier.com/locate/freeradbiomed

Original Contribution

Isotope-reinforced polyunsaturated fatty acids protect mitochondria from oxidative stress

Alexander Y. Andreyev [a], Hui S. Tsui [b], Ginger L. Milne [c], Vadim V. Shmanai [d], Andrei V. Bekish [e], Maksim A. Fomich [d], Minhhan N. Pham [b], Yvonne Nong [b], Anne N. Murphy [a], Catherine F. Clarke [b], Mikhail S. Shchepinov [f,*]

[a] Department of Pharmacology, University of California at San Diego, La Jolla, CA 92093-0636, USA
[b] Department of Chemistry and Biochemistry and Molecular Biology Institute, University of California at Los Angeles, Los Angeles, CA 90095-1569, USA
[c] Division of Clinical Pharmacology, Vanderbilt University, Nashville, TN 37232-6602, USA
[d] Institute of Physical Organic Chemistry, National Academy of Science of Belarus, Minsk 220072, Belarus
[e] Department of Chemistry, Belarusian State University, Minsk 220020, Belarus
[f] Retrotope, Inc., Los Altos Hills, CA 94022, USA

ARTICLE INFO

Article history:
Received 24 October 2014
Received in revised form
11 December 2014
Accepted 24 December 2014
Available online 8 January 2015

Keywords:
Chain reaction
Coenzyme Q
Kinetic isotope effect
Lipid peroxidation
Mitochondria respiration
Polyunsaturated fatty acid
Free radicals

ABSTRACT

Polyunsaturated fatty acid (PUFA) peroxidation is initiated by hydrogen atom abstraction at bis-allylic sites and sets in motion a chain reaction that generates multiple toxic products associated with numerous disorders. Replacement of bis-allylic hydrogens of PUFAs with deuterium atoms (D-PUFAs), termed site-specific isotope reinforcement, inhibits PUFA peroxidation and confers cell protection against oxidative stress. We demonstrate that structurally diverse deuterated PUFAs similarly protect against oxidative stress-induced injury in both yeast and mammalian (myoblast H9C2) cells. Cell protection occurs specifically at the lipid peroxidation step, as the formation of isoprostanes, immediate products of lipid peroxidation, is drastically suppressed by D-PUFAs. Mitochondrial bioenergetics function is a likely downstream target of oxidative stress and a subject of protection by D-PUFAs. Pretreatment of cells with D-PUFAs is shown to prevent inhibition of maximal uncoupler-stimulated respiration as well as increased mitochondrial uncoupling, in response to oxidative stress induced by agents with diverse mechanisms of action, including *t*-butylhydroperoxide, ethacrynic acid, or ferrous iron. Analysis of structure–activity relationships of PUFAs harboring deuterium at distinct sites suggests that there may be a mechanism supplementary to the kinetic isotope effect of deuterium abstraction off the bis-allylic sites that accounts for the protection rendered by deuteration of PUFAs. Paradoxically, PUFAs with partially deuterated bis-allylic positions that retain vulnerable hydrogen atoms (e.g., monodeuterated 11-D_1-Lin) protect in a manner similar to that of PUFAs with completely deuterated bis-allylic positions (e.g., 11,11-D_2-Lin). Moreover, inclusion of just a fraction of deuterated PUFAs (20–50%) in the total pool of PUFAs preserves mitochondrial respiratory function and confers cell protection. The results indicate that the therapeutic potential of D-PUFAs may derive from the preservation of mitochondrial function.

Lipids containing polyunsaturated fatty acids (PUFAs) make up a large fraction of vital cellular membranes, especially in specialized cells, such as neurons and photoreceptor cells, as well as in specific organelles, such as synaptic vesicles and photoreceptor discs, in which they are essential for membrane performance [1]. Mitochondria are particularly rich in PUFAs that are indispensable for maintaining optimal function of membrane enzymes and transporters and in modulating mitophagy and apoptosis [2–5]. However, the very structural features that make PUFAs essential for membrane function also render them vulnerable to oxidation. Lipid peroxidation is an important factor in the etiology of numerous neurological, ophthalmic, and other diseases. Unlike stoichiometric oxidative damage to DNA and proteins, nonenzymatic lipid peroxidation is a chain reaction; consequently, a process initiated by a single free radical moiety causes oxidation of many PUFA residues [6,7] and leads to rearrangements and scissions that give rise to variable carbonyl compounds [7–9] and other toxic species [9,10]. These products of lipid peroxidation show variable hydrophobicity and are highly reactive, irreversibly damaging proteins [9,11], DNA bases [9,12], and other biomolecules, and elicit electrophilic redox signaling [13]. The remaining PUFA ester "stubs" protrude from the lipid membranes, forming "lipid whiskers" that can participate in apoptotic,

* Corresponding author.
E-mail address: misha@retrotope.com (M.S. Shchepinov).

http://dx.doi.org/10.1016/j.freeradbiomed.2014.12.023
0891-5849/

inflammatory, and other signaling [5,14,15]. Moreover, peroxidized membrane lipids compromise physical–chemical properties of membranes (such as membrane fluidity [16]) and their barrier function. Antioxidants, which are consumed on interaction with radicals and therefore require a continuous supply to keep reactive oxygen species (ROS) in check, are generally inefficient at preventing the process and sometimes even exacerbate it [9,17].

Site-specific isotope-reinforced PUFAs (D-PUFAs), such as 11,11-D_2-linoleic acid (11,11-D_2-Lin; Scheme 1), harbor deuterium atoms at the bis-allylic positions and are protected against lipid peroxidation in comparison to natural PUFAs [18,19]. The abstraction of bis-allylic atoms (D versus H) exhibits an isotope effect and acts to slow the rate-limiting step of the peroxidation chain reaction. For peroxidation mediated by the linoleyl peroxyl radical, the kinetic isotope effect (KIE) for abstraction of bis-allylic D atoms compared to H atoms is 12.8 [19]. Even higher KIEs are observed when the tocopheroxyl radical mediates the peroxidation [20]. D-PUFAs within cells are more resistant to lipid peroxidation as monitored with the C11-BODIPY fluorescent probe [19]. Surprisingly, inclusion of only a relatively small fraction of D-PUFAs is needed to inhibit the lipid peroxidation of the larger nondeuterated PUFA pool [19,21].

Previous studies have shown that yeast lacking coenzyme Q (Q or ubiquinone) are exquisitely sensitive to PUFA treatment [22,23]. This is due to the loss of action of Q/QH_2 as a lipid-soluble, chain-terminating antioxidant [24]. D-PUFAs compensate for the loss of Q/QH_2 function and rescue the Q-less *coq* mutant yeast [18]. Site-specific reinforcement at the bis-allylic position (e.g., 11,11-D_2-Lin; Scheme 1), compared to other methylene positions, was found to be essential for this protection, because treatment with monoallylic 8,8-D_2-Lin failed to protect Q-less yeast [19]. The sensitivity of the *coq* yeast mutants to PUFA treatment is not due to their inability to respire, because the respiratory-deficient *cor1*-null mutant lacking complex III does not show sensitivity to PUFA treatment [18,19]. The D-PUFAs are incorporated into cellular membranes in the same way as normal, nondeuterated PUFAs, but are highly resistant to the chain reaction [18,19].

Oxidative stress and lipid peroxidation play major roles in many neurodegenerative diseases, including Parkinson and Alzheimer diseases, for which a critical involvement of mitochondria is demonstrated [25,26]. We have earlier observed a mitigating effect of D-PUFAs in models of several such disorders, including Parkinson disease [27] and Friedreich ataxia [28].

Here we further investigate the dramatic cellular mechanisms of protection afforded by D-PUFAs in both yeast and mammalian cells. We present direct evidence that the protective mechanisms function by inhibiting the lipid peroxidation step in the cascade of cellular oxidative stress. Structure–activity analysis of various deuterated PUFAs shows that KIE on abstraction at the initiation step of the chain reaction may not be the only factor influencing the stability of D-PUFAs toward lipid peroxidation. We also probe for potential effects of D-PUFAs on mitochondrial function using oxygen consumption measurements in combination with various mitochondrial inhibitors [29]. The results indicate that preservation of mitochondrial function may be one mechanism of cell protection against oxidative stress conditions. Overall, this study suggests the therapeutic potential of the isotope-reinforced PUFAs for applications in a broad spectrum of diseases with a strong oxidative stress component.

Experimental methods

Fatty acids

The fatty acids used in this study are shown in Scheme 1. Ole, Lin, α-Lnn, and Ara (99% pure) were from Sigma-Aldrich or Nu-chek Prep (Elysian, MN, USA). The synthesis of 8,8-D_2-Lin, 11,11-D_2-Lin, 11-D-Lin, 11,11-D_2-α-Lnn, 14,14-D_2-α-Lnn, and 11,11,14,14-D_4-α-Lnn was described previously [18–20]. The synthesis of 14-D-α-Lnn, 11,14-D_2-α-Lnn, and 9,10,12,14-D_4-Lin is described in the supplementary material. ^{1}H, ^{13}C NMR and mass spectrometry were used to confirm the structures and purity of the deuterated PUFAs (supplementary material).

Yeast strains and growth media

Yeast strains used in this study are described in Table 1. Yeast growth media were prepared as described [30] and included YPD (1% yeast extract, 2% yeast peptone, 2% dextrose). Solid plate medium contained 2% Bacto agar. Components for the growth media were obtained from Difco, Fisher, and Sigma.

Fatty acid sensitivity assays

Fatty acid sensitivity assays were performed as described [18]. Yeast cells were inoculated overnight in 5 ml YPD with aeration (250 rpm at

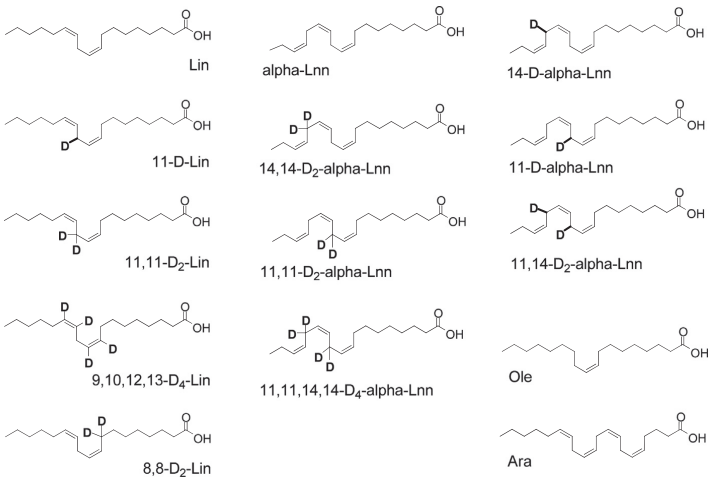

Scheme 1. Structures of fatty acids used in this study. Ara, arachidonic acid; Lin, linoleic acid; α-Lnn, α-linolenic acid; Ole, oleic acid.

Table 1
Genotype and source of yeast strains.

Strain	Genotype	Source
W303–1B	MAT α *ade2–1 his3–1, 15 leu2–3, 112 trp1–1 ura3–1*	[42]
W303*cor1*Δ	MAT α *ade2–1 his3–11, 15 leu2–3, 112 ura3–1 trp-1 can1–110 cor1: HIS3*	[42]
W303*coq9*Δ	MAT α *ade2–1 his3–1, 15 leu2–3, 112 trp1–1 ura3–1 coq9: URA3*	[43]

30 °C). Yeast cultures were diluted to 0.2 OD_{600} in fresh YPD medium and were grown to midlog phase (< 1.0 OD_{600}). Yeast cells were collected by centrifugation (5 min at 1000 *g*) followed by two washes with sterile water. Yeast cells were diluted to 0.2 OD_{600} in 0.10 M phosphate buffer (0.2% dextrose, pH 6.2). Aliquots (5 ml) were placed in overnight tubes and treated with the designated fatty acids and incubated at 30 °C with aeration (250 rpm). Aliquots were removed at the designated times and viability was assessed by spotting 2 μl of 1:5 serial dilutions (starting at 0.20 OD_{600}) onto the YPD plate medium. Pictures were taken after 2 days of growth at 30 °C.

Measurement of F_2-isoprostanes (F_2-IsoP's)

To each yeast cell pellet, 5 ml of chloroform:methanol (2:1, v/v) containing butylated hydroxytoluene (BHT; 50 mg/ml) was added and the samples were mixed with a vortex. Ice-cold 0.9% aqueous NaCl was added (2 ml) and samples were vortexed 1 min. The organic layer was transferred to a clean tube and dried under a stream of nitrogen. Samples were reconstituted in 0.5 ml of methanol containing BHT (50 μg/ml) followed by the addition of 0.5 ml of 15% aqueous KOH and vortexed again. The samples were incubated at 37 °C 30 min and then diluted to a volume of 10 ml with deionized water and acidified to pH 3 with 1 N HCl, and 1.0 ng of [D_4]-15-F_{2t}-IsoP ([D_4]-8-iso-$PGF_{2\alpha}$; Cayman Chemical, Ann Arbor, MI, USA) was added as an internal standard. The sample was then applied to a C-18 Sep-Pak cartridge that had been prewashed with 5 ml of methanol and 5 ml of 0.01 N HCl. The cartridge was then washed with 10 ml of 0.01 N HCl, followed by 10 ml of heptane, and compounds were eluted with 10 ml of ethyl acetate:heptane (50:50, v/v). The eluate was applied to a silica Sep-Pak cartridge prewashed with ethyl acetate (5 ml). It was rinsed with 5 ml of ethyl acetate and compounds were eluted with 5 ml of ethyl acetate:methanol (50:50, v/v), and the eluate was dried under nitrogen. Compounds were converted to the pentafluorobenzyl (PFB) esters by the addition of 40 μl of a 10% solution of pentafluorobenzyl bromide in acetonitrile and 20 μl of a solution of 10% di-isopropylethanolamine in acetonitrile and allowed to incubate for 30 min at 37 °C. Reagents were dried under nitrogen and the residue was reconstituted in 30 μl of chloroform and 20 μl of methanol and chromatographed on a silica TLC plate to 13 cm in a solvent system of chloroform:methanol (93:7, v/v). The methyl ester of $PGF_{2\alpha}$ was chromatographed on a separate lane and visualized with 10% phosphomolybdenic acid in ethanol by heating. The R_f of $PGF_{2\alpha}$ methyl ester in this solvent system was 0.15. Compounds migrating in the region 1 cm below the $PGF_{2\alpha}$ standard to 1.0 cm above the standard were scraped from the TLC plate, extracted with 1 ml of ethyl acetate, and dried under nitrogen. After TLC purification, compounds were converted to trimethylsilyl (TMS) ether derivatives by addition of 20 μl of *N,O*-bis(trimethylsilyl)trifluoroacetamide and 10 μl of dimethylformamide. The sample was incubated at 37 °C for 10 min and then dried under nitrogen. The residue was redissolved for GC/MS analysis in 20 μl of undecane that had been stored over a bed of calcium hydride.

Mass spectrometric methods for F_2-IsoP analysis

GC/NICI–MS was carried out on an Agilent 5973 inert mass selective detector, coupled with an Agilent 6890n Network GC system (Agilent Laboratories, Torrance, CA, USA) and interfaced with an Agilent computer. GC was performed with a 15-m, 0.25-μm film thickness, DB-1701 fused silica capillary column (J&W Scientific, Folsom, CA, USA). The column temperature was programmed from 190 to 300 °C at 20 °C per minute. The major ion generated in the NICI mass spectrum of the PFB ester, TMS ether derivative of F_2-IsoP's is the *m/z* 569 carboxylate anion (M-181 (M-$CH_2C_6F_5$)). The corresponding ion generated by the [D_4]-15-F_{2t}-IsoP internal standard is *m/z* 573. Levels of endogenous F_2-IsoP's in a biological sample are calculated from the ratio of intensities of the ions *m/z* 569 to *m/z* 573. Employing this assay, the lower limit of detection of F_2-IsoP's is in the range of 4 pg using an internal standard with a blank of 3 parts per thousand. The precision of this assay in biological fluids is ± 6% and the accuracy 94%.

Cell preparation for respiration measurements

H9C2 myoblasts [31] were maintained in growth medium containing Dulbecco's modified Eagle's medium (DMEM; with glucose and glutamine) supplemented with 10% fetal bovine serum, 1 × GlutaMax (Life Technologies), and 100 units/ml penicillin and 100 μg/ml streptomycin at 37 °C in an incubator with an atmosphere containing 5% CO_2.

Assays of respiration of H9C2 myoblasts

Respiration of H9C2 cells was measured with Seahorse Bioscience XF24, XF96, or XF^e96 flux analyzers. Cells were plated on the Seahorse cell culture plates in their growth medium 48 h before the experiment at a density of 2×10^4 or 10^4 cells per well for 24- and 96-well plates, respectively. At 24 h before the experiment the medium was supplemented with an equal volume of the same medium containing 2 × concentrations of various PUFAs. At the start of the experiment cells were treated with various pro-oxidants from 100 × stock solutions and incubated for an additional 1–3 h in a CO_2 incubator. The pro-oxidant iron(II) stock solution was prepared with water that was deoxygenated by streaming argon over it for 30 min to slow the rapid oxidation of iron(II). Immediately before measurement the medium was removed, and the cells were gently washed with assay buffer (unbuffered DMEM prepared according to Seahorse protocols supplemented with 10 mM glucose, 10 mM sodium pyruvate, and 1 × GlutaMax, pH 7.4). Wells were filled with 450 or 100 μl/well assay buffer for 24- and 96-well plates, respectively, and the measurements were performed in the Seahorse apparatus according to the manufacturer's recommendations.

Data and statistical analysis

Statistical analysis of oxygen consumption data from individual plates is presented; these results are typical for cells harvested at, at least, three different passages (3 to 10 plates total for each figure). Two-way ANOVA (analysis of variance) followed by Bonferroni's post hoc test was performed using GraphPad Prism. Where differences are noted, analysis of variance detected significant variance at $p < 0.001$, $p < 0.01$, or $p < 0.05$ for pairwise comparisons shown on Figs. 4–7. See the figure legend for special labels used in Fig. 7.

Results

Partial isotope reinforcement of D-PUFAs protects Q-less yeast from cell death compared to treatment with natural α-Lnn

Yeast *coq9*Δ mutants lack Q and are hypersensitive to treatment with PUFAs, compared to either wild-type yeast or respiratory-deficient mutants that retain Q (*cor1*Δ) [18,19]. Treatment of the *coq9*Δ mutant with 200 μM α-Lnn for 4 h results in a significant loss of viability, as determined either by plate dilution assay (Fig. 1A) or by

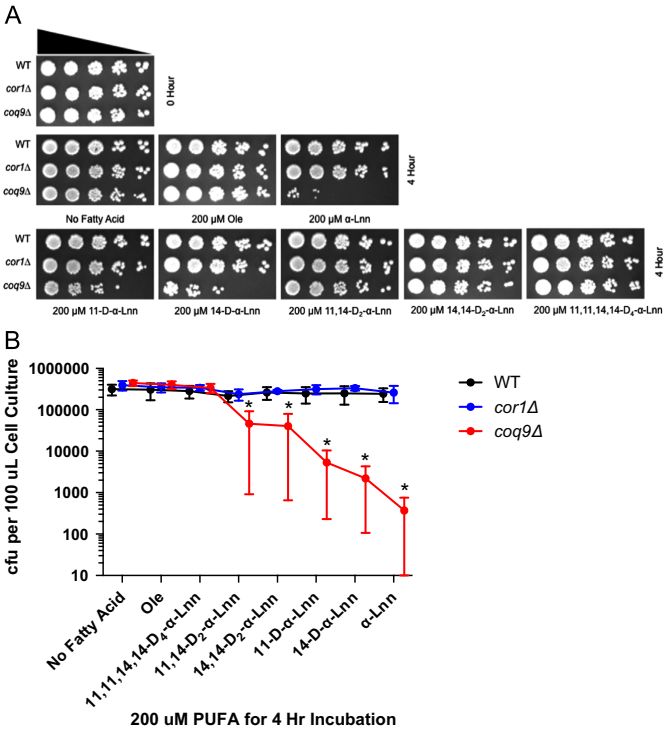

Fig. 1. Differently deuterated α-Lnn renders variable degrees of protection for Q-deficient *coq9*Δ mutant yeast. Fatty acid sensitivity assays were performed as described under Experimental methods. (A) Yeast strains (W303–1B wild type (WT), W303*cor1*Δ, and W303*coq9*Δ) were treated with 200 μM designated PUFA at 0.2 OD_{600} for 4 h at 30 °C, 250 rpm, before an aliquot was removed for plate dilution assay. Serial dilutions (1:5) starting at 0.2 OD_{600} were spotted on YPD plates, and pictures were taken after 2 days growth at 30 °C. (B) After 4 h incubation with 200 μM designated PUFA, a small aliquot of yeast culture was removed and diluted 1000-fold before 100 μl was plated in triplicate on YPD. For yeast *coq9*Δ treated with α-Lnn, aliquots of 100 μl were plated directly without any dilution, and yeast *coq9*Δ mutants treated with 11-D-α-Lnn, 14-D-α-Lnn, 11,14-D_2-α-Lnn, or 14,14-D_2-α-Lnn were diluted 10-fold before 100 μl was plated. Yeast colonies were counted after 2 days of growth at 30 °C. The graph plots the average number (±SD) of colonies counted on the YPD plates per 100 μl of cell culture plated. The average numbers of cfu were significantly less (*$p < 0.0001$) with yeast *coq9*Δ mutants treated with α-Lnn, 11-D-α-Lnn, 14-D-α-Lnn, 11,14-D_2-α-Lnn, or 14,14-D_2-α-Lnn compared with either wild-type yeast or *cor1*Δ mutants or compared with *coq9*Δ mutants without fatty acids or with Ole or 11,11,14,14-D_4-α-Lnn. The cfu counts shown are representative of two independent experiments. Statistical analyses were performed with two-way ANOVA multiple comparison test by GraphPad Prism version 6.

determination of colony-forming units (cfu) (Fig. 1B). To further examine the effects of site-specific D-PUFAs, we treated yeast with the D-PUFAs shown in Scheme 1. The protective effect of deuteration roughly corresponds to the number of deuterated bis-allylic C–D bonds. The effect does not seem to depend on the exact position of D at the bis-allylic sites. Indeed, monodeuterated 11-D and 14-D derivatives seem to exert similar toxicity. Likewise, the toxicity of 14,14-D_2-α-Lnn is very close to that of 11,14-D_2-α-Lnn. This correlates with our earlier finding that 11,11-D_2-α-Lnn and 14,14-D_2-α-Lnn render similar degrees of protection to *coq* mutant yeast [18].

Q-less yeast are protected by Lin deuterated at double bonds only

We have previously established the importance of deuteration at the bis-allylic positions. Surprisingly, deuteration at the double bonds but retaining H atoms at the bis-allylic site also made Lin less toxic to Q-less yeast, as shown by the viability of the *coq9*Δ Q-less yeast after serial dilution and plating onto rich growth medium (Fig. 2). This provides another indication that steps other than abstraction of a bis-allylic site may be affected by the presence of deuterium, playing an important role in PUFA catabolism.

Inclusion of small amounts of D-PUFAs inhibits isoprostane formation from arachidonic acid

Nonenzymatic oxidation of Ara gives rise to a large class of bioactive prostaglandin-like compounds called isoprostanes [32,33]. F_2-IsoP's are a validated biomarker of oxidative stress generated from the free radical-catalyzed peroxidation of Ara. We wished to investigate the ability of 11,11-D_2-Lin and 11,11,14,14-D_4-α-Lnn to inhibit this process within cells. Yeast *coq9*Δ mutant cells were treated with Ara (100 μM), in the absence or presence of either 11,11-D_2-Lin (25 μM) or 11,11,14,14-D_4-α-Lnn (25 μM). As shown in Fig. 3, levels of IsoP's were highest in the *coq9*Δ yeast mutant treated with 100 μM Ara. Levels of IsoP's decreased dramatically by including small amounts (25 μM) of either 11,11-D_2-Lin or 11,11,14,14-D_4-α-Lnn in combination with 100 μM Ara. These findings demonstrate that inclusion of small amounts (20 mol%) of isotope-reinforced D-PUFAs slows down the free radical lipid peroxidation processes that occur within whole cells.

Treatment with D-PUFA (11,11-D_2-Lin) protects mitochondria from oxidative stress

PUFAs are essential nutrients and when provided to yeast or mammalian cells they are rapidly assimilated into phospholipids,

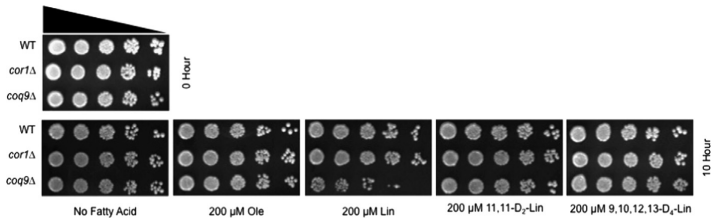

Fig. 2. Yeast *coq9*Δ mutants are protected by Lin deuterated at non-bis-allylic positions. Yeast fatty acid sensitivity assays were performed as described under Experimental methods. Yeast cells were treated with 200 μM designated PUFAs for 10 h before an aliquot was removed for plate dilution assay. Pictures were taken after 2 days growth at 30 °C.

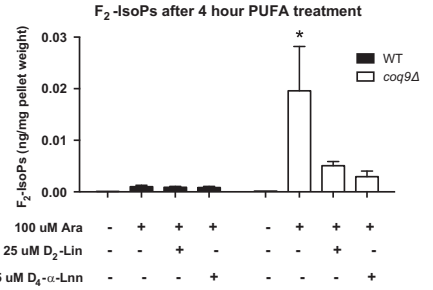

Fig. 3. Small amounts of deuterated Lin or α-Lnn suppress isoprostane formation from Ara. Yeast PUFA treatment was similar to the fatty acid sensitivity assays as described under Experimental methods with the following modifications. Aliquots of 100 ml of mid-log-phase yeast cells were placed in sterile flasks and PUFAs were added to a final concentration of 100 μM Ara in the absence or presence of 25 μM 11,11-D_2-Lin or 11,11,14,14-D_4-α-Lnn (from stocks prepared in ethanol). After incubation at 30 °C, 250 rpm, for 4 h, aliquots were removed to collect pellets and yeast cell viability was assessed by plate dilution assay. Cell pellets were collected by centrifugation for 5 min at 1000*g*, followed by two washes with sterile water. A total of 10 OD_{600} cell pellet was prepared in duplicates for each yeast strain for each PUFA treatment condition. Measurements of F_2-IsoP's by mass spectrometry were as described under Experimental methods. The amount of F_2-IsoP's was significantly ($^*p < 0.05$) higher in Ara-treated yeast *coq9*Δ mutants compared to *coq9*Δ mutants with no added fatty acids or with additional 11,11-D_2-Lin or 11,11,14,14-D_4-α-Lnn. The statistical analyses were performed with two-way ANOVA multiple comparison test by GraphPad Prism version 6.

including mitochondrial phosphatidylethanolamine and cardiolipin [34,35]. Mitochondria are enriched in PUFAs [36,37,44], rendering them a particularly vulnerable target of oxidative stress. Furthermore, mitochondria harbor a plethora of redox carriers (such as quinones and iron–sulfur centers) that are prone to single-electron oxidation that is accompanied by single-electron reduction of oxygen, i.e., generation of ROS. A positive feedback loop from mitochondrial oxidative damage to mitochondrial ROS production may lead to amplification of injury. Consequently, treatments that preserve mitochondrial function would be expected to protect viability and normal functioning of cells under the stress.

Thus, we investigated whether incorporation of D-PUFA would preserve mitochondrial function. The most quantitative and noninvasive assay of mitochondrial function/dysfunction is the measurement of mitochondrial oxygen consumption (respiration) rate (OCR). Oxygen is irreversibly consumed in the terminal reaction of catabolic pathways and therefore the rate of its disappearance is a direct measure of total metabolic flux through the system. This is an advantage over other commonly used measures of bioenergetic function of the cell (ATP levels, membrane potential, pyridine nucleotide redox status, metabolite levels, etc.), which are all intermediates that depend on a balance of two metabolic branches, i.e., production and utilization pathways. Therefore these parameters may change in either direction or remain unchanged, depending on to what extent, if any, these two branches suffer an injury. To assess respiration in a physiologically relevant adherent state we performed mitochondrial OCR measurements in intact H9C2 myoblast cells and used a plate-based technology (Seahorse Biosciences) [38].

A typical Seahorse respiration experiment is shown in Fig. 4A. After the basal respiration rate was determined, respiratory State 4 was induced by the addition of 1 μg/ml oligomycin, followed by sequential additions of the protonophoric uncoupler FCCP to induce maximal uncoupled (or State 3 u) respiration. This titration of FCCP was essential because, depending on the degree of mitochondrial injury, cells may attain maximal rates at different concentrations of FCCP. For example, cells supplemented with natural Lin approached maximal respiration (State 3 u) at 900 nM FCCP, whereas cells treated with *tert*-butylhydroperoxide (t-ButOOH) reached a maximal rate at only 300 nM FCCP, and the rate started to decline at higher doses. The necessity for three-point FCCP titration precluded Seahorse-recommended systematic assessment of the background OCR insensitive to respiratory inhibitors. We performed this test in separate experiments using 2 μM myxothiazol and found that the background OCR was low and did not exceed 5% of maximal respiration (data not shown). This background rate did not interfere with the comparative assessment of protective effects of deuterated versus natural PUFAs.

State 3u and State 4 respiration rates are direct indicators of mitochondrial function and can be used to monitor mitochondrial injury. The State 3u rate is a measure of maximal respiratory capacity of mitochondria, whereas the State 4 rate is a reciprocal measure of intactness of the mitochondrial membrane. Healthy mitochondria possess high respiratory capacity and intact membranes, necessary for robust energy conversion with minimal losses, i.e., high State 3u and low State 4 rates. Mitochondrial injury may cause a drop in State 3u (respiratory inhibition due to damage to respiratory chain complexes, matrix dehydrogenases, and/or substrate transporters) and/or an increase in State 4 (increased membrane leak due to perturbation of the lipid bilayer, activation of specific transporters, or mitochondrial permeability transition). Treatment with t-ButOOH causes both increased membrane leak (increased State 4) and respiratory inhibition (decreased State 3u). For clarity, the two relevant rates, State 4 and State 3u, are derived from the entire array of data (as shown in Fig. 4A) and depicted as separate bar graphs (Fig. 4B and C, respectively).

The basal respiration rate of healthy cells is a measure of cellular ATP turnover reflective of cellular energy demand rather than the capacity of mitochondria to produce ATP. Cells possess spare respiratory capacity necessary to meet increased energy demand under stress conditions; this is manifested in Fig. 4A as the excess of maximal respiration rate (State 3u) over the basal respiration rate. Oxidative stress induced by t-ButOOH decreased the spare capacity, but the mitochondria still were able to maintain their basal rate unchanged, indicating their ability to meet the basal demand for ATP. This is a common scenario for other oxidative stress paradigms explored in this study, and for purposes of assessing mitochondrial dysfunction the unchanged basal rate is not informative.

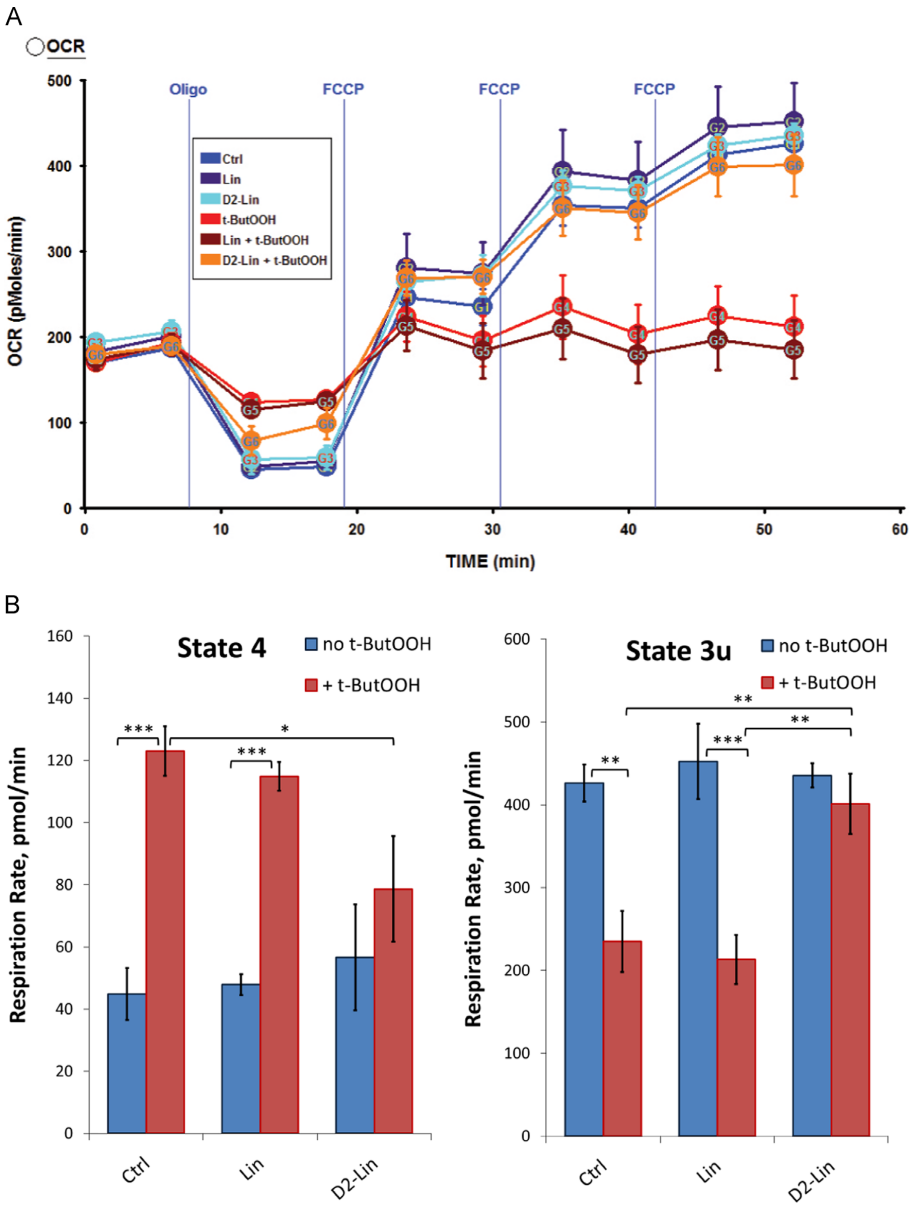

Fig. 4. D-PUFAs protect against oxidative stress induced by organic hydroperoxide. (A) Principle of the assessment of mitochondrial function (output panel of the Seahorse XF24 analyzer is shown). H9C2 myoblasts were allowed 24 h before the experiment to incorporate a bolus of 25 μM (5 nmol) 11,11-D_2-Lin (D2-Lin) or nondeuterated Lin. Oxidative stress was induced by the addition of 200 μM *tert*-butylhydroperoxide (t-ButOOH) 1 h before assay. After measurement of the basal respiration rate (OCR), the intactness of the mitochondrial membrane was assessed after addition of 1 μg/ml oligomycin (Oligo). Maximal respiratory capacity of the mitochondria was assessed using sequential additions of the uncoupler FCCP at 300 nM; the resulting total dose of $3 \times 300 = 900$ nM allowed the approach to saturation. The vertical lines indicate the time of addition. All readings were obtained twice. Data are the mean ± SEM of three or four wells per group. (B) State 4 respiratory rate (the reciprocal measure of intactness of the membrane) was derived from the data in (A). For each experimental group the minimal value from the two readings in the presence of Oligo was taken as the State 4 rate. Data are the mean ± SEM, $n = 3$ or 4. 11,11-D_2-Lin but not nondeuterated Lin largely prevented t-ButOOH-induced injury (increased membrane leak). (C) Maximal respiratory capacity of mitochondria expressed as maximal or State 3 u OCR was derived from the data in (A). For each experimental group the maximal value from the six readings in the presence of FCCP was taken as the State 3 u rate. Note that these rates were attained at different doses of FCCP. Data are the mean ± SEM, $n = 3$ or 4. 11,11-D_2-Lin but not nondeuterated Lin nearly completely prevented t-ButOOH-induced injury (decreased respiratory capacity). $^{***}p < 0.001$, $^{**}p < 0.01$, $^{*}p < 0.05$.

Fig. 4 also demonstrates that cellular incorporation of exogenously added PUFAs (either Lin or 11,11-D_2-Lin) does not significantly affect mitochondrial bioenergetics. However, in stark contrast to natural Lin, 11,11-D_2-Lin almost completely protects mitochondrial function from oxidative stress caused by t-ButOOH: maximal respiration (Fig. 4C) is nearly completely preserved, whereas the increase in membrane leak (Fig. 4B) is substantially diminished (from 250–300% stimulation of State 4 respiration in control or Lin-supplemented cells to a 25% stimulation in 11,11-D_2-Lin-supplemented cells).

To demonstrate whether the protective effects are generalized in nature, we tested several other oxidative stress paradigms in addition to t-ButOOH, which oxidizes and depletes the pool of reduced glutathione in a reversible manner. Similarly, ethacrynic acid, which depletes the glutathione pool via irreversible chemical derivatization, and severely inhibits respiration, was partially protected by 11,11-D_2-Lin but not by Lin (Fig. 5A). The redox cycling catalyst iron(II) caused inhibition of maximal respiration (State 3u) that was completely prevented by 11,11-D_2-Lin but not Lin (Fig. 5B). We found iron(II) to be a much more reproducible inducer of oxidative stress than t-ButOOH or ethacrynic acid. These two agents both work through a glutathione-depletion mechanism and suffer from a threshold (all-or-none) manner of action, which manifests in variability of both dose and time dependence of cell responses (data not shown). Therefore we chose iron(II) treatment as the model of oxidative stress for testing effects of other D-PUFAs.

Treatments with small amounts of 11,11,14,14-D_4-α-Lnn or other D-PUFAs protect mitochondria from oxidative stress

Addition of 11,11,14,14-D_4-α-Lnn (D_4-α-Lnn) was protective against oxidative stress induced by Fe(II). H9C2 myoblasts were treated, and data were derived as described for Fig. 4. Either D_4-α-Lnn or natural α-Lnn was added as indicated, and State 4 (Fig. 6A) and State 3u (maximal respiration, Fig. 6B) were determined. Natural α-Lnn acted as a pro-oxidant, exacerbating injury caused by iron(II)-induced oxidative stress (Fig. 6B), whereas the same amount of D_4-α-Lnn afforded significant protection. In contrast to the yeast plate dilution assay survival data (Fig. 2), the effects of 9,10,12,13-D_4-Lin on the bioenergetics were not different from the pro-oxidant action of nondeuterated Lin (Fig. 7A). However, monodeuterated 11-D_1-Lin appeared to be protective (Fig. 7A and B).

We further tested whether substitution of only a fraction of the total pool of PUFAs can provide mitochondrial protection against oxidative stress [19]. Incorporation into the cells of just 5 μM D_4-α-Lnn, added to 20 μM nondeuterated α-Lnn (20% of total PUFA pool), provided significant protection against a very severe oxidative stress induced by 1.2 mM iron(II) (Fig. 7C). Similarly, substitution of 50% Lin pool even with monodeuterated D_1-Lin also protected against oxidative stress (Fig. 7B).

Discussion

Oxidative stress is considered a critical contributor to the etiology of diverse grave diseases and pathologic conditions, such as neurodegeneration (Alzheimer disease, Parkinson disease, Friedrich ataxia, stroke, etc.), metabolic syndrome (cardiovascular disease, diabetes, and obesity), inflammatory, and autoimmune diseases [9]. Lipid peroxidation, as a key propagation step in the cascade of oxidative stress processes, presents an attractive target for potential therapeutic interventions to combat these disorders. In this study we assessed the potential of isotope-reinforced D-PUFAs to counteract oxidative stress-inflicted damage to cell function and viability in both yeast and mammalian cells. We found similar structure–activity relationships that indicate a common mechanism across the taxonomic kingdoms.

Because mitochondria are considered both a major source and a critical target of oxidative stress, we specifically tested PUFAs with

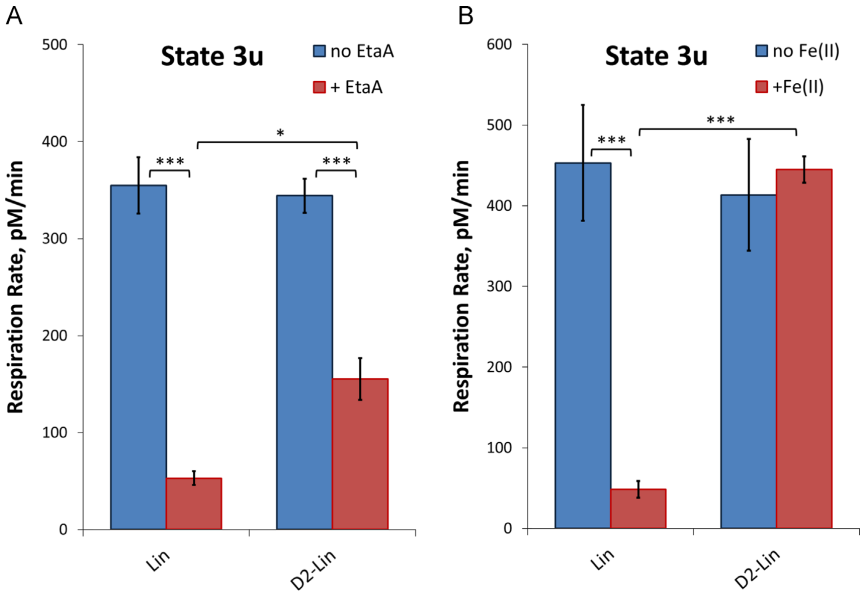

Fig. 5. 11,11-D_2-Lin partially protects against oxidative stress induced by ethacrynic acid or Fe(II). (A) Oxidative stress was induced by the glutathione-depleting agent ethacrynic acid (EtaA); 320 μM EtaA was added 4 h before the assay. H9C2 myoblasts were treated, and data were derived as described for Fig. 4. 50 μM (10 nmol) 11,11-D_2-Lin (D2-Lin) or Lin was added as indicated. Data are the mean ± SEM, $n=5$ or 6. (B) Oxidative stress was induced by Fe(II), through addition of 1 mM $FeSO_4$ made 90 min before assay. H9C2 myoblasts were treated, and data were derived as described for Fig. 4. 25 μM (5 nmol) D2-Lin or Lin was added as indicated. Data are the mean ± SEM, $n=5$. $^{***}p < 0.001$, $^{*}p < 0.05$.

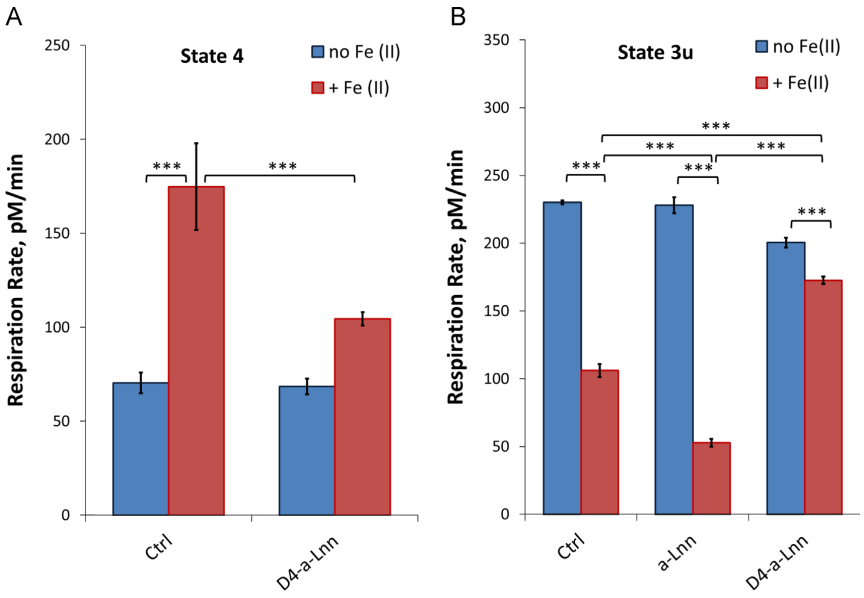

Fig. 6. 11,11,14,14-D_4-α-Lnn protects against oxidative stress induced by Fe(II). Either (A) 0.8 or (B) 1.2 mM $FeSO_4$ was added 3 h before the assay. H9C2 myoblasts were treated, and data were derived as described for Fig. 4. 25 μM (5 nmol) 11,11,14,14-D_4-α-Lnn (D4-α-Lnn) or α-Lnn (α-Lnn) was added as indicated. Data are the mean ± SEM, $n=5$. $^{***}p < 0.001$.

deuterated bis-allylic positions. Here we provide the first evidence that D-PUFAs protect mammalian cell mitochondrial function from pro-oxidant and iron-induced injury. Indicators of membrane integrity (respiratory State 4) and enzyme activity (respiratory State 3u) were protected; protection of membrane integrity is consistent with prevention of lipoperoxidation.

It should be noted that, although the ultimate measure of mitochondrial function is respiratory State 3 (phosphorylating respiration), its measurement in intact cells cannot be achieved at the current state of the art. We used State 3u as the next best parameter that could report damage to the immense complexity of metabolic pathways necessary for maintaining maximal respiration: from cellular uptake of nutrients through their cytoplasmic conversions to mitochondrial substrate transport, Krebs cycle activity, and respiratory chain function. By taking this approach, we might have missed potential damage to a limited number of components constituting the phosphorylation machinery (ATP synthase and transporters of phosphate and adenine nucleotides).

Protection was observed under diverse oxidative stress paradigms (organic peroxide, GSH-derivatizing agent and redox cycling pro-oxidant treatments in H9C2 cells or, in yeast, deficiency in coenzyme Q, an endogenous antioxidant). The extent of this protection varied, most likely owing to different severities of the various pro-oxidant insults, but was qualitatively consistent, indicative of a specific effect at a common step in the process. This step can be directly localized to an initial phase of lipid peroxidation cascade given suppression of its early products, isoprostanes (Fig. 3). Isoprostanes are proinflammatory and serve as sensitive markers of oxidative stress [32,33]. It is tempting to speculate that mitochondrial oxidative injury may be the underlying cause of loss of cell survival (as seen in our yeast experiments) and that D-PUFAs protect cells via mitochondria-centered mechanisms.

A standing paradox in our studies of D-PUFAs is that PUFAs harboring D atoms at just one (11-D_1-Lin) or two sites (e.g., 11,11-D_2-Lnn) remain protective [18,19]. It is also intriguing that inclusion of small amounts of D-PUFAs, for example 20 mol%, along with natural PUFAs affords significant protection to both yeast and rat myoblast cells (Figs. 3 and 7C). Here we tested a series of α-Lnn derivatives containing variable numbers of the bis-allylic C–D bonds (Scheme 1), from one (11-D-α-Lnn; 14-α-D-Lnn), to two (11,14-D_2-α-Lnn; 11,11-D_2-α-Lnn; 14,14-α-D_2-Lnn), to four (11,11,14,14-α-D_4-Lnn). The partially reinforced D-PUFAs proved to be protective although with quantitatively different potencies. We observed the increase in the total number of bis-allylic C–D groups to increase protection, which roughly correlates with the number of bis-allylic hydrogens available for abstraction. Indeed, a similar correlation exists between the free radical peroxidation propagation rate constants for Lin (one bis-allylic site; $k_P = 62\ M^{-1}\ s^{-1}$), Ara (three bis-allylic sites; $k_P = 201 \pm 12$), Eicosapentaenoic acid (EPA) (four bis-allylic sites, $k_P = 249 \pm 14$), and Docosahexaenoic acid (DHA) (five bis-allylic sites, $k_P = 321 \pm 32$) [2], from which it follows that each bis-allylic site makes a similar, approximately linear contribution to the overall propagation rate.

In general, however, protective effects associated with partial replacement of bis-allylic hydrogens in the system are not due to simple mass-action law (i.e., decreased concentration of the reactive sites). As is evident from Fig. 7B and C a mere decrease in concentration of natural PUFAs (from 50 to 25 μM Lin or from 25 to 20 μM Lnn, see Fig. 7B and C, respectively) does not show significant protection, whereas replacement of the balance with D-PUFA (25 μM 11,11-D_2-Lin or 5 μM 11,11,14,14-α-D_4-Lnn, respectively) is highly protective. Similarly, an addition of D-PUFAs to Ara suppresses isoprostane production (Fig. 3) although the level of reactive (bis-allylic) sites does not change as the concentration of Ara is preserved. Similarly, simple 11,11-D_2-Lin: Lin (1:1) and Ole:Lin (1:1) mixtures did not result in equal resistance to oxidation even though the same number of available bis-allylic C–H groups were present [19]. Instead, the Ole:Lin pair is highly oxidizable, whereas the 11,11-D_2-Lin:Lin mixture is resistant, suggesting an active role for the D-containing moieties in the process.

Most intriguingly, 11,11-D_2-α-Lnn and 14,14-D_2-α-Lnn, with one bis-allylic position completely blocked by deuteration, may be expected to behave very similar to nondeuterated Lin and to be toxic. However, they are actually almost as protective as 11,11,14,14-D_4-α-Lnn (Fig. 1 and [18]). Another indication that the bis-allylic C–H abstraction may not be the only factor comes from protection rendered by 9,10,12,13-D_4-Lin, which is deuterated at the double bonds but not at the bis-allylic site (Fig. 2), although we note that 9,10,12,13-D_4-Lin was not protective in HC92 cells. We speculate that the protective effects of partial isotope reinforcement might be due to the presence of D's in the conjugated radical system [39,40], playing a role important for either the progress of the chain reaction or, as might be the case for 9,10,12,13-D_4-Lin, for the formation of the toxic end-products [41] downstream of the chain process.

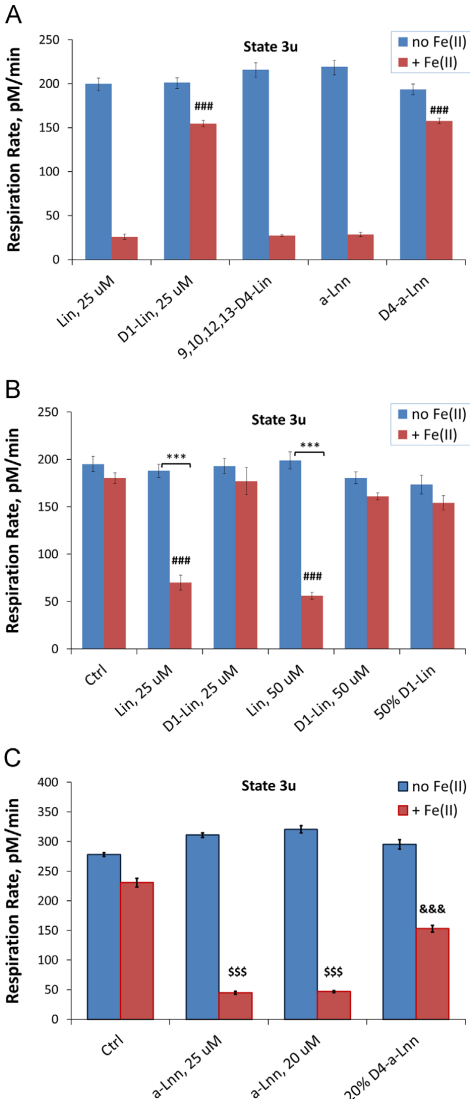

PUFAs harboring bis-allylic D's inhibit the chain process irrespective of their exact position [19]. The fact that partially deuterated PUFAs (11-D_1-α-Lnn versus 14-D_1-α-Lnn; 14,14-D_2-α-Lnn versus 11,11-D_2-α-Lnn versus 11,14-D_2-α-Lnn) are similarly protective argues against specific reactive carbonyls being responsible for cytotoxicity. However, lipid peroxidation results in the production of a complex array of electrophilic reactive lipid species; thus there are multiple vectors of toxicity potentially affected by the presence of D-PUFAs.

It is also possible that the observed protective effects may be due to D-PUFA-mediated inhibition of enzymes or cytochromes capable of initiating the chain process. Although lipoxygenase genes are not evident in the *Saccharomyces cerevisiae* genome, it does contain P450s, β-oxidation enzymes, copper oxidases, and iron-containing enzymes, and these enzymes have been implicated in the production of arachidonic acid-derived eicosanoids in a variety of pathogenic yeasts [45]. In this scenario, inclusion of small amounts of D-PUFAs may act to inhibit the action of a lipid oxidase from metabolizing normal H-PUFAs. This may explain, at least in part, the nature of protection by partially deuterated PUFAs and/or the protection afforded by including just 20% D-PUFAs. Both observations suggest an active role for the D atoms in protection that would in this event be due to inhibition of lipid peroxidation initiation.

Potential therapeutic applications of D-PUFA require better understanding of their influence on mitochondrial function in mammalian systems. Our findings suggest that D-PUFA-rendered protection, at least in part, proceeds through stabilization of mitochondrial performance at elevated levels of oxidative stress.

Acknowledgments

We thank Ned A. Porter and Henry J. Forman for their advice and helpful discussions. This work was supported by a grant from the National Science Foundation (Grant MCB-1330803 to C.F.C.) and by funds from Retrotope. Mikhail S. Shchepinov holds stock in Retrotope, Inc. The other authors have no conflicts to declare.

Appendix A. Supporting information

Supplementary data associated with this article can be found in the online version at http://dx.doi.org/10.1016/j.freeradbiomed.2014.12.023.

Fig. 7. Addition of small amounts of D-PUFAs or partial deuteration of PUFAs at some but not all bis-allylic positions is protective. (A) Comparison of effects of various PUFAs (50 μM) on oxidative stress induced over 3 h by addition of 0.8 mM Fe(II). Note protective effect of monodeuterated linoleic acid, 11-D_1-Lin (D1-Lin), compared to nondeuterated Lin and lack of protection by complete deuteration at the double bonds (9,10,12,13-D_4-Lin). 11,11,14,14-α-D_4-Lnn (D4-α-Lnn) and nondeuterated linolenic (α-Lnn) acid served as internal negative and positive controls for the experiment. H9C2 myoblasts were treated and data were derived as described for Fig. 4. Data are the mean ± SE, $n=5$. (B) Partial replacement of Lin with 11-D_1-Lin (50% D1-Lin) is protective. Cells were supplemented as indicated with 25 or 50 μM Lin or 11-D_1-Lin or with both at 25 μM simultaneously, for the total of 50 μM (50% D1-Lin). The data were derived as described for Fig. 4. Note that the effect of 11-D_1-Lin is much more than just dilution of the PUFA pool; in fact, 25 μM 11-D_1-Lin counteracts the pro-oxidant effect of 25 μM nondeuterated Lin present in the 50% mixture (compare to the effect of 25 μM Lin alone [19]). Data are the mean ± SE, $n=5$. (C) Partial replacement of α-Lnn with 11,11,14,14-α-D_4-Lnn (20% D4-α-Lnn) is protective. Cells were supplemented as indicated with 20 or 25 μM α-Lnn or a mixture of 20 μM α-Lnn and 5 μM 11,11,14,14-α-D_4-Lnn for the total of 25 μM (20% D4-α-Lnn). Oxidative stress was induced by addition of 1.2 mM $FeSO_4$ 3 h before assay. The data were derived as described for Fig. 4. Note that the effect of 11,11,14,14-α-D_4-Lnn is much more than just a dilution of the PUFA pool; in fact, 5 μM 11,11,14,14-α-D_4-Lnn counteracts the pro-oxidant effect of 20 μM nondeuterated α-Lnn present in the 20% mixture (compare to the effect of 20 μM α-Lnn alone). Data are the mean ± SE, $n=4$. ###, $$$, &&&, significantly different from all other +Fe(II) groups, from the +Fe(II) control group, or from the α-Lnn alone group, respectively (***$p < 0.001$).

References

[1] Pinot, M; Vanni, S; Pagnotta, S; Lacas-Gervais, S; Payet, L-A; Ferreira, T; Gautier, R; Goud, B; Antonny, B; Barelli, H. Polyunsaturated phospholipids facilitate membrane deformation and fission by endocytic proteins. *Science* **345:**693–697; 2014.

[2] McMillin, JB; Dowhan, W. Cardiolipin and apoptosis. *Biochim. Biophys. Acta* **1585:**97–107; 2002.

[3] Ardail, D; Privat, JP; Egret-Charlier, M; Levrat, C; Lerme, F; Louisot, P. Mitochondrial contact sites: lipid composition and dynamics. *J. Biol. Chem.* **265:**18797–18802; 1990.

[4] Stanley, WC; Khairallah, RJ; Dabkowski, ER. Update on lipids and mitochondrial function: impact of dietary n-3 polyunsaturated fatty acids. *Curr. Opin. Clin. Nutr. Metab. Care* **15:**122–126; 2012.

[5] Tyurina, YY; Poloyac, SM; Tyurin, VA; Kapralov, AA; Jiang, J; Anthonymuthu, TS; Kapralova, VI; Vikulina, AS; Jung, MY; Epperly, MW; Mohammadyani, D; Klein-Seetharaman, J; Jackson, TC; Kochanek, PM; Pitt, BR; Greenberger, JS; Vladimirov, YA; Bayir, H; Kagan, VE. A mitochondrial pathway for biosynthesis of lipid mediators. *Nat. Chem* **6:**542–552; 2014.

[6] Porter, NA; Caldwell, SE; Mills, KA. Mechanisms of free radical oxidation of unsaturated lipids. *Lipids* **30:**277–290; 1995.

[7] Yin, H; Xu, L; Porter, NA. Free radical lipid peroxidation: mechanisms and analysis. *Chem. Rev.* **111:**5944–5972; 2011.

[8] Esterbauer, H; Schaur, RJR; Zollner, H. Chemistry and biochemistry of 4-hydroxynonenal, malonaldehyde and related aldehydes. *Free Radic. Biol. Med.* **11:**81–128; 1991.

[9] Halliwell, B; Gutteridge, JMC. *Free Radicals in Biology and Medicine*. New York: Oxford Univ. Press; 2007.

[10] Roberts, LJII; Fessel, JP. The biochemistry of the isoprostane, neuroprostane, and isofuran pathways of lipid peroxidation. *Chem. Phys. Lipids* **128:**173–186; 2004.

[11] Negre-Salvayre, A; Coatrieux, C; Inguenau, C; Salvayre, R. Advanced lipid peroxidation end products in oxidative damage to proteins: potential role in diseases and therapeutic prospects for the inhibitors. *Br. J. Pharmacol.* **153:**6–20; 2008.

[12] Blair, IA. DNA adducts with lipid peroxidation products. *J. Biol. Chem.* **283 :**15545–15549; 2008.

[13] Higdon, AN; Landar, A; Barnes, S; Darley-Usmar, VM. The electrophile responsive proteome: integrating proteomics and lipidomics with cellular function. *Antioxid. Redox Signaling* **17:**1580–1589; 2012.

[14] Kagan, VE; Borisenko, GG; Tyurina, YY; Tyurin, VA; Jiang, J; Potapovich, AI; Kini, V; Amoscato, AA; Fujii, Y. Oxidative lipidomics of apoptosis: redox catalytic interactions of cytochrome *c* with cardiolipin and phosphatidylserine. *Free Radic. Biol. Med.* **37:**1963–1985; 2004.

[15] Greenberg, ME; Li, XM; Guqiu, BG; Gu, X; Qin, J; Salomon, RG; Hazen, SL. The lipid whisker model of the structure of oxidized cell membranes. *J. Biol. Chem.* **283:**2385–2396; 2008.

[16] Dobretsov, GE; Borschevskaya, TA; Petrov, VA; Vladimirov, YA. The increase of phospholipid bilayer rigidity after lipid peroxidation. *FEBS Lett.* **84:**125–128; 1977.

[17] Bowry, VW; Stocker, R. Tocopherol-mediated peroxidation: the prooxidant effect of vitamin E on the radical-initiated oxidation of human low-density lipoprotein. *J. Am. Chem. Soc.* **115:**6029–6044; 1993.

[18] Hill, S; Hirano, K; Shmanai, VV; Marbois, BN; Vidovic, D; Bekish, AV; Kay, B; Tse, V; Fine, J; Clarke, CF; Shchepinov, MS. Isotope-reinforced polyunsaturated fatty acids protect yeast cells from oxidative stress. *Free Radic. Biol. Med.* **50:**130–138; 2011.

[19] Hill, S; Lamberson, CR; Xu, L; To, R; Tsui, HS; Shmanai, VV; Bekish, AV; Awad, AM; Marbois, BN; Cantor, CR; Porter, NA; Clarke, CF; Shchepinov, MS. Small amounts of isotope-reinforced polyunsaturated fatty acids suppress lipid autoxidation. *Free Radic. Biol. Med.* **53:**893–906; 2012.

[20] Lamberson, CR; Xu, L; Muchalski, H; Montenegro-Burke, JR; Shmanai, VV; Bekish, AV; McLean, JA; Clarke, CF; Shchepinov, MS; Porter, NA. Unusual kinetic isotope effects of deuterium reinforced polyunsaturated fatty acids in tocopherol mediated free radical chain oxidations. *J. Am. Chem. Soc.* **136:**838–841; 2014.

[21] Shchepinov, MS; Roginsky, VA; Brenna, JT; Molinari, RJ; To, R; Tsui, H; Clarke, CF; Manning-Bog, AB. *Deuterium protection of polyunsaturated fatty acids against lipid peroxidation: a novel approach to mitigating mitochondrial neurological diseases. Omega-3 Fatty Acids in Brain and Neurological Health*. San Diego: Elsevier; 2014.

[22] Do, TQ; Schultz, JR; Clarke, CF. Enhanced sensitivity of ubiquinone deficient mutants of Saccharomyces cerevisiae to products of autooxidized polyunsaturated fatty acid. *Proc. Natl. Acad. Sci. USA* **93:**7534–7539; 1996.

[23] Poon, WW; Do, TQ; Marbois, BN; Clarke, CF. Sensitivity to treatment with polyunsaturated fatty acids is a general characteristic of the ubiquinone-deficient yeast *coq* mutants. *Mol. Aspects Med.* **18:**s121–s127; 1997.

[24] Bentinger, M; Brismar, K; Dallner, G. The antioxidant role of coenzyme Q. *Mitochondrion* **7 S:**S41–S50; 2007.

[25] Beal, MF. Mitochondria take center stage in aging and neurodegeneration. *Ann. Neurol.* **58:**495–505; 2005.

[26] DiMauro, S; Schon, EA. Mitochondrial disorders in the nervous system. *Annu. Rev. Neurosci.* **31:**91–123; 2008.

[27] Shchepinov, MS; Chou, VP; Pollock, E; Langston, JW; Cantor, CR; Molinari, RJ; Manning-Bog, AB. Isotopic reinforcement of essential polyunsaturated fatty acids diminishes nigrostriatal degeneration in a mouse model of Parkinson's disease. *Toxicol. Lett.* **207:**97–103; 2011.

[28] Cotticelli, MG; Crabbe, AM; Wilson, RB; Shchepinov, MS. Insights into the role of oxidative stress in the pathology of Friedreich ataxia using peroxidation resistant polyunsaturated fatty acids. *Redox Biol* **1:**398–404; 2013.

[29] Dranka, BP; Hill, BG; Darley-Usmar, VM. Mitochondrial reserve capacity in endothelial cells: the impact of nitric oxide and reactive oxygen species. *Free Radic. Biol. Med.* **48:**905–914; 2010.

[30] Burke, D; Dawson, D; Stearns, T. *Methods in Yeast Genetics*. Plainview (NY): Cold Spring Harbor Laboratory Press; 2000.

[31] Kimes, BW; Brandt, BL. Properties of a clonal muscle cell line from rat heart. *Exp. Cell Res.* **98:**367–381; 1976.

[32] Milne, GL; Yin, H; Hardy, KD; Davies, SS; Roberts 2nd LJ. Isoprostane generation and function. *Chem. Rev.* **111:**5973–5996; 2011.

[33] Milne, GL; Gao, B; Terry, ES; Zackert, WE; Sanchez, SC. Measurement of F_2-isoprostanes and isofurans using gas chromatography–mass spectrometry. *Free Radic. Biol. Med.* **59:**36–44; 2013.

[34] Trivedi, A; Fantin, DJ; Tustanoff, ER. Role of phospholipid fatty acids on the kinetics of high and low affinity sites of cytochrome c oxidase. *Biochem. Cell Biol.* **64:**1195–1210; 1986.

[35] Hoch, FL. Cardiolipins and biomembrane function. *Biochim. Biophys. Acta* **1113:**71–133; 1992.

[36] Stanley, WC; Keehan, KH. Update on innovative initiatives for the American Journal of Physiology–Heart and Circulatory Physiology. *Am. J. Physiol. Heart Circ. Physiol* **304:**H1045–H1049; 2013.

[37] Mayr, JA. Lipid metabolism in mitochondrial membranes. *J. Inherit. Metab. Dis.* **38:**137–144; 2014.

[38] Yamazaki, KG; Andreyev, AY; Ortiz-Vilchis, P; Petrosyan, S; Divakaruni, AS; Wiley, SE; De La Fuente, C; Perkins, G; Ceballos, G; Villarreal, F; Murphy, AN. Intravenous (−)-epicatechin reduces myocardial ischemic injury by protecting mitochondrial function. *Int. J. Cardiol.* **175:**297–306; 2014.

[39] Halevi, EA; Nussim, M. *Bull. Res. Counc. Isr* **6 A:**167; 1957.

[40] Elison, C; Rapoport, H; Laursen, R; Elliott, HW. Effect of deuteration of N–CH_3 group on potency and enzymatic N-demethylation of morphine. *Science* **134:**1078–1079; 1961.

[41] Frenette, M; Scaiano, JC. Evidence for hydroxyl radical generation during lipid (linoleate) peroxidation. *J. Am. Chem. Soc.* **130:**9634–9635; 2008.

[42] Tzagoloff, A; Wu, MA; Crivellone, M. Assembly of the mitochondrial membrane system: characterization of *COR1*, the structural gene for the 44-kilodalton core protein of yeast coenzyme QH_2-cytochrome *c* reductase. *J. Biol. Chem.* **261:**17163–17169; 1986.

[43] Johnson, A; Gin, P; Marbois, BN; Hsieh, EJ; Wu, M; Barros, MH; Clarke, CF; Tzagoloff, A. *COQ9*, a new gene required for the biosynthesis of coenzyme Q in *Saccharomyces cerevisiae*. *J. Biol. Chem.* **280:**31397–31404; 2005.

[44] Harkewicz, R; Fahy, E; Andreyev, AY; Dennis, EA. Arachidonate-derived dihomoprostaglandin production observed in endotoxin-stimulated macrophage-like cells. *J. Biol. Chem.* **282:**2899–2910; 2007.

[45] Ells, R; Kock, JLF; Albertyn, J; Pohl, CH. Arachidonic acid metabolites in pathogenic yeasts. *Lipids Health Dis.* **11:**100–107; 2012.

CHAPTER 5

Disturbed cardiolipin metabolism impairs coenzyme Q biosynthesis

ABSTRACT

Cardiolipin (CL) is a structurally unique phospholipid that optimizes mitochondrial function in part by stabilizing proteins and protein complexes. Nascent CL is remodeled to incorporate unsaturated fatty acyl chains. Although unmodified CL functions almost identically to remodeled CL, remodeling of CL has been shown to mitigate oxidative damage caused by lipid peroxidation. Recent evidence suggests a functional relationship between CL and coenzyme Q (CoQ). CoQ is an essential lipid quinone necessary for respiratory electron transport and also functions as a lipid soluble antioxidant. An inner mitochondrial membrane protein complex termed the CoQ synthome is required for CoQ biosynthesis. Here we show that the assembly and/or stability of the CoQ synthome is impaired in *Saccharomyces cerevisiae* mutants with defects in CL biosynthesis or remodeling. Interestingly, the CoQ synthome, but not its component Coq polypeptide subunits, was less abundant in the absence of CL or when CL remodeling is prevented. Destabilization of the CoQ synthome resulted in elevated levels of early CoQ-intermediates, a hallmark of inefficient de novo biosynthesis of CoQ_6. Inefficient CoQ biosynthesis was observed in yeast CL mutants cultured under either fermentation or respiration growth conditions. Similar changes in steady state CoQ content were observed in a loss-of-function human HEK 293 cell line with genetically perturbed CL remodeling. Collectively, our results establish a novel link between the metabolism of two important mitochondrial lipids and provide novel mechanistic insight into Barth syndrome, an inherited childhood cardiomyopathy caused by defective CL remodeling.

INTRODUCTION

Cellular membranes are physical barriers that have unique chemical compositions and enable specific chemical reactions to occur within subcellular organelle compartments. They store energy in the form of transmembrane ion gradients and allow the anchoring of protein receptors, transporters, and multi-subunit complexes that perform various functions. Phospholipids serve as the fundamental structural elements of biological membranes. Cardiolipin (CL) is a minor phospholipid species, constituting approximately 10-15% of the total phospholipid content in mitochondria (1). CL has a unique molecular structure and is specifically enriched within the mitochondrial inner membrane. Therein, CL serves a multitude of functions that are collectively indispensable for optimal mitochondrial bioenergetics (2-4).

CL is composed of a glycerol head that provides a bridge for two phosphatidyl groups with four total fatty acyl chains. The biosynthesis of CL occurs in the mitochondrion. In *Saccharomyces cerevisiae*, CL arises from phosphatidyl transfer from cytidine diphosphate diacylglycerol (CDP-DAG) to phosphatidylglycerol (PG), catalyzed by CL synthase Crd1 (5-7). Acyl chain remodeling enzymes process the nascent CL post de novo synthesis, whereby the saturated acyl chains on immature CL are replaced with unsaturated fatty acyl chains (8, 9). During this process, nascent CL is de-acylated to form monolyso-CL (MLCL) by the CL-specific deacylase Cld1, followed by re-acylation via transacylation of MLCL by tafazzin, Taz1, which uses phosphatidylcholine (PC) or phosphatidylethanolamine (PE) as acyl chain donor (7, 8, 10). While the four stereochemically distinct acyl positions on CL may give rise to very diverse CL species, the remodeling process generates only a few species of CL with predominantly one or two unsaturated acyl chains (11). In *S. cerevisiae,* the end product of CL remodeling contains CL with predominantly mono-unsaturated fatty acyl chains of 16 and 18 carbons in length (12).

Although the fatty acyl composition of mature CL and the degree of unsaturation in these fatty acyl chains vary considerably in different organisms, the biosynthetic pathway for CL is largely conserved among eukaryotes (11, 12). One distinctive difference is that the CL remodeling in higher eukaryotes can be accomplished by alternative mechanisms. More specifically, de-acylation of nascent CL to MLCL is executed by phospholipases other than Cld1 (metazoans lack a Cld1 ortholog) and subsequent re-acylation of MLCL can be achieved by CoA-dependent re-acylation catalyzed by MLCL acyltransferase 1 (MLCLAT1) or acyl-CoA:lysocardiolipin acyltransferase 1 (ALCAT1) in addition to tafazzin-dependent transacylation (9).

It is still under debate whether the acyl specificity of the Taz1 reaction is accountable for maintaining the unique molecular species of CL present in different tissues and organisms (7, 9). In vitro experiments have shown that Taz1 catalyzes promiscuous acyl chain transfer from various phospholipids (13, 14), and the substrate specificity of Taz1 observed in vivo may depend on the lipid packing arrangement of the substrate (15), or assembly of protein complexes and supercomplexes (e.g. mitochondrial contact site and cristae organizing system, respiratory electron transport complexes, and prohibitin complexes) surrounding the Taz1 enzyme (7). Patients with mutations in *TAZ* exhibit clinical phenotype of Barth syndrome (BTHS), a disease associated with low CL content of altered acyl chain composition and elevated MLCL, and the increased MLCL/CL ratio results in cardiomyopathy, skeletal myopathy, neutropenia, 3-methylglutaconic aciduria, growth retardation, and respiratory chain defects (10, 16-18).

The functional implications of CL remodeling are not completely understood. The incorporation of unsaturated fatty acyl chains into CL is postulated to mitigate lipid curvature stress that arises from the protein-rich, highly folded cristae of the inner membrane (1, 16). The

structural integrity of mitochondrial cristae is key to the organization of respiratory complexes, establishment of the proton gradient that drives oxidative phosphorylation, mitochondrial fusion/fission, as well as apoptosis (19). Additionally, the expression of Cld1 to initiate the CL remodeling pathway is found to be important to mitigate oxidative damage originated from CL peroxidation (20). Deletion of *CLD1* in genetically engineered polyunsaturated fatty acid (PUFA)-producing yeast results in dramatic reductions of mitochondrial membrane potential, respiratory capacity, and overall chronological lifespan (20).

As a non-bilayer-forming phospholipid, CL is almost exclusively found in energy-transducing membranes, such as the cytoplasmic membrane in prokaryotes and the mitochondrial inner membrane in eukaryotes (4, 11). Due to its unique molecular geometry and the presence of two unshielded negative charges, CL interacts with many mitochondrial proteins and protein complexes to provide architectural support important for optimal mitochondrial energy metabolism (7, 21). CL is found to associate with complexes III, IV, and V, with its acyl chains interacting with surfaces of respiratory protein complexes at multiple sites (22-25). CL is necessary for respiratory supercomplex assembly and stability, which is crucial for efficient substrate channeling between respiratory complexes (26, 27). CL also regulates the proton gradient across the mitochondrial inner membrane maintaining the mitochondrial membrane potential (22). Disrupted CL synthesis results in dissipated membrane potential, decreased ATP production, and inefficient mitochondrial bioenergetics (17, 28).

Conversely, the protein complexes of the mitochondrial inner membrane may stabilize CL (7, 29). Studies have shown that almost all of the CL is bound to proteins in isolated mitochondria, and the sequestration of CL in protein complexes contributes to a much longer half-life of CL relative to other phospholipids (7, 29). Thus, CL promotes assembly of protein complexes, which in turn protect CL from degradation (7, 29).

Several lines of evidence suggest a functional relationship between CL and coenzyme Q biosynthesis. Coenzyme Q (ubiquinone or CoQ) is an essential lipid quinone in the respiratory electron transport chain. Complexes I and II donate electrons and protons to CoQ, forming the CoQ hydroquinone ($CoQH_2$) which is then oxidized by complex III. Biosynthesis of CoQ depends on the Coq polypeptides in yeast and analogous COQ polypeptides in human cells (30, 31). Recent genetic evidence suggests that Cld1, a phospholipase A2 family protein that deacylates CL, may modulate CoQ biosynthesis at the penultimate step mediated by Coq7 (32). Over-expression of *CLD1* rescues the CoQ deficiency of *coq7* mutants with mutations in its predicted membrane-binding domain and increases the abundance of MLCL species with longer unsaturated acyl chains (32). This latter affect is postulated to facilitate the interaction of the membrane-anchor mutant Coq7 with the inner membrane (32). CoQ synthesis also depends on the activity of Coq8, a putative ancient kinase (33, 34). Lipid membranes containing CL regulate the ATPase activity of human COQ8A via its KxGQ domain in combination with phenolic compounds that are structurally analogous to CoQ-intermediates (35). Human COQ9 is also shown to associate with CL via electrostatic interaction mediated by two lysine residues in the α9-α10 loop at its C-terminus (36). Membrane interaction of COQ9 is necessary for its access to the membrane-embedded isoprene groups on polyprenylated CoQ-intermediates, which are subsequently handed over to COQ7 for enzymatic modification (36).

Because of its ability to survive via fermentation and ease of genetic manipulation of nuclear and mitochondrial DNA, yeast is a powerful model system for studying CoQ biology, CL biosynthesis, and mitochondria-related diseases. In this work, we investigate the effects of yeast mutations known to disrupt CL biosynthesis (*crd1Δ*) or CL remodeling (*taz1Δ*) on the biosynthesis of CoQ under both respiration and fermentation growth conditions. We demonstrate that the yeast *crd1Δ* and *taz1Δ* mutants each disrupt de novo CoQ biosynthesis,

primarily by impairing the assembly of the CoQ synthome, a multi-subunit complex necessary for CoQ biosynthesis. We further extend our study to show that the disruption of CoQ metabolism in yeast *taz1Δ* mutant recapitulates what occurs in a human BTHS cell model.

MATERIALS AND METHODS

Yeast strains and growth media

S. cerevisiae strains used in this study are listed in Table 1. Growth media were prepared as described (37) and included YPD (1% Bacto yeast extract, 2% Bacto peptone, 2% dextrose), YPG (1% Bacto yeast extract, 2% Bacto peptone, 3% glycerol), and YPGal (1% Bacto yeast extract, 2% Bacto peptone, 2% galactose, 0.1% dextrose). Synthetic Dextrose-Complete (0.18% Difco yeast nitrogen base without amino acids and ammonium sulfate, 0.5% ammonium sulfate, 0.14% NaH_2PO_4, 2% dextrose, 0.008% adenine hemisulfate, 0.004% arginine hydrochloride, 0.01% aspartic acid, 0.008% cysteine hydrochloride, 0.01% glutamic acid, 0.008% histidine hydrochloride, 0.006% isoleucine, 0.012% leucine, 0.006% lysine hydrochloride, 0.008% methionine, 0.006% phenylalanine, 0.04% serine, 0.02% threonine, 0.008% tryptophan, 0.004% tyrosine, 0.008% uracil, and 0.015% valine, final pH ~6.0 adjusted by NaOH pellets) was prepared as described (38). Drop out Dextrose-Complete (0.68% yeast nitrogen base with ammonium sulfate without folic acid without pABA (MP Biomedicals), 2% dextrose, 0.14% NaH_2PO_4, and complete amino acid mix as described above, final pH ~6.0 adjusted by NaOH pellets) was prepared as described (39). Plate medium contained additional 2% Bacto agar.

Cell culture

Wild-type human embryonic kidney (HEK) 293 Flp-In (Invitrogen) cells and *taz*^{TALEN} clones (*taz*^{TALEN}.2 and *taz*^{TALEN}.19) (40) were grown and maintained in DMEM with 4.5 g/L glucose (Cellgro), supplemented with 10% fetal bovine serum (FBS, Hyclone), 2 mM L-glutamine (Gibco), and 100 µg/mL zeocin (Invitrogen) in six-well plates at 37°C, 5% CO_2. Once expanded to confluency, cells were washed with 1x phosphate buffered saline (PBS) and subjected to trypsinization. Cells were collected by centrifugation at 600 *g* for 2 min followed by

removal of the supernatant. Cell pellets were stored at −80°C until further analysis. Four biological replicates were prepared for each cell line.

Yeast mitochondrial isolation

Mitochondria were isolated from yeast cells grown under fermentation and respiration condition, respectively. To culture yeast cells in fermentation supportive medium, the designated yeast strains were grown in YPD for 10 h and sub-inoculated into YPGal in large volumes for overnight growth in a shaking incubator at 30°C, 250 rpm. To culture yeast cells in respiration supportive medium, the starter cultures of designated yeast strains were prepared in YPG for 10 h and back diluted with fresh YPG in large volumes for overnight growth in a shaking incubator at 30°C, 250 rpm. Cells grown under both conditions were harvested at OD_{600} < 4.0 per mL, and mitochondria were purified as described (41). Briefly, yeast spheroplasts were obtained after incubating cells with 2.5 mg Zymolyase-20T (MP Biomedicals) per gram cell pellet at 30°C for 60 min in buffer A (20 mM potassium phosphate, pH 7.4, 1.2 M sorbitol). Crude mitochondria were isolated from manual douncing of spheroplasts suspension in buffer B (20 mM MES, pH 6.0, 0.6 M sorbitol) with addition of complete EDTA-free protease inhibitor mixture (Roche), phosphatase inhibitor cocktail set II (EMD Millipore) and phosphatase inhibitor cocktail set 3 (Sigma-Aldrich), followed by fractionation. Crude mitochondria were resuspended in buffer B and further purified over Nycodenz (Sigma-Aldrich) density gradient, and were collected at the interface between 14.5% and 20% (wt/vol) Nycodenz layers after ultracentrifugation at 25,000 *g* at 4°C for 90 min. Gradient purified mitochondria were washed and resuspended in buffer C (20 mM HEPES, pH 7.4, 0.6 M sorbitol) with protease inhibitor mixture and phosphatase inhibitor cocktails described above. Purified mitochondria were flash frozen in liquid nitrogen and stored at −80°C until further analysis. Total mitochondrial protein concentration was measured with the bicinchoninic acid (BCA) assay (Thermo Fisher Scientific) using bovine serum albumin (BSA) as the standard.

SDS-PAGE and immunoblot analyses

Purified mitochondria samples were resuspended in SDS sample buffer (50 mM Tris, pH 6.8, 10% glycerol, 2% SDS, 0.1% bromophenol blue, and 1.33% β-mercaptoethanol), and same amount total mitochondrial protein from each sample was loaded and separated by SDS-PAGE on 12% Tris-glycine polyacrylamide gels. Proteins were subsequently transferred to 0.45 μm nitrocellulose membrane (Bio-Rad), and membranes were blocked in blocking buffer (0.5% BSA, 0.1% Tween 20, 0.02% SDS in 1x PBS). Proteins of interest were probed with primary rabbit polyclonal antibodies in blocking buffer at dilutions listed in Table 2, followed by IRDye 680LT goat anti-rabbit IgG secondary antibody (LiCOR) at 1:10,000 dilutions. Blot images were obtained using LiCOR Odyssey Infrared Scanner (LiCOR).

Two-dimensional Blue Native/SDS-PAGE

Two-dimensional Blue Native/SDS-PAGE was performed as described (42, 43). Aliquots of 200 μg of purified mitochondria were solubilized at 4 mg/mL in solubilization buffer (11 mM HEPES, pH 7.4, 0.33 M sorbitol, 1x NativePAGE sample buffer (Thermo Fisher Scientific)) with 16 mg/mL digitonin (Biosynth) and protease inhibitor mixture, phosphatase inhibitor cocktails described above on ice for one hour. The soluble fraction was separated from the insoluble pellets by ultracentrifugation at 100,000 *g* for 10 min, and the protein concentration in the soluble fraction was determined by BCA assay. NativePAGE 5% G-250 sample additive (Thermo Fisher Scientific) was added to the soluble fraction to a final concentration of 0.25%. A total of 80 μg protein in the soluble fraction were loaded and separated on the first dimension NativePAGE 4-16% Bis-Tris gel (Thermo Fisher Scientific). First-dimension gel slices were soaked in hot SDS sample buffer for 15 min before loading onto the second dimension 12% Tris-glycine polyacrylamide gels. The high molecular weight standards for first dimension Blue Native electrophoresis were obtained from GE Healthcare (Sigma-Aldrich), and the molecular

weight standards for second dimension SDS-PAGE were obtained from Bio-Rad. Subsequent immunoblot analyses were performed as described above.

Metabolic labeling of CoQ_6 and CoQ_6-intermediates with $^{13}C_6$-labeled ring precursors

Labeling of CoQ_6 and CoQ_6-intermediates was carried out in yeast cells grown under both fermentation and respiration conditions. Overnight yeast cultures grown in SD-Complete or YPG medium were back diluted to 0.1 OD_{600}/mL with fresh DoD-Complete medium or YPG medium respectively, and growth continued in a shaking incubator at 30°C, 250 rpm to 0.5 OD_{600}/mL. To early-log phase cell cultures, $^{13}C_6$-pABA, $^{13}C_6$-4HB, or ethanol as vehicle control, were added to a final concentration of 5 µg/mL, and the cultures were allowed to grow for up to 5 h. At each 1-, 3-, and 5-hour time point, triplicates of 5 mL culture were collected by centrifugation at 3,000 *g* for 5 min, and the cell density measured at OD_{600} at each harvesting time point was recorded. Cell pellets were stored at −20 °C until further analysis.

Yeast CoQ_6 and CoQ_6-intermediates analysis by RP-HPLC tandem mass spectrometry

Yeast whole cell lipid extraction and LC-MS/MS analyses with CoQ_4 as internal standard were performed as described (44). Yeast cell pellets were disrupted with 2 mL methanol in the presence of CoQ_4. Lipids were extracted with 2 mL petroleum ether followed by vigorous vortexing. The top organic layer was removed and lipids were extracted again from the bottom aqueous layer one more time with addition of 2 mL petroleum ether. The top layer from two extractions were combined and dried under a stream N_2 gas. The dried lipids were reconstituted in 200 µL of 0.5 mg/mL benzoquinone prepared in ethanol to oxidize all lipid species for mass spectrometry analysis.

A 4000 QTRAP linear MS/MS spectrometer (Applied Biosystems) was used for sample analysis, and Analyst version 1.4.2 software (Applied Biosystems) was used for data acquisition

and processing. Reconstituted lipid extract was separated on a Luna 5 µm phenyl-hexyl column (100 x 4.6 mm, 5 µm; Phenomenex) with a mobile phase consisting of solvent A (95:5 methanol/isopropanol, 2.5 mM ammonium formate) and solvent B (isopropanol, 2.5 mM ammonium formate). The representative CoQ_6 and CoQ_6-intermediates were eluted at distinct retention times as the percentage of solution B was increased linearly from 0 to 10% over 7 min as the flow rate was increased from 650 to 800 µl/min. Analytes eluting from the column were monitored with multiple reaction monitoring mode (MRM) scanning the precursor to product ion transitions of each analyte and their respective ammonium adducts listed in Table 3. The amounts of CoQ_6 and CoQ_6-intermediates were calculated from the sum of peak areas of each analyte and its corresponding ammonium adduct at a specific retention time, normalized against the internal standard CoQ_4, and quantified using a standard curve constructed with varying amounts of CoQ_6. Statistical analysis made use of GraphPad Prism with two-way ANOVA Dunnett's multiple comparison test.

Human cell CoQ_9 and CoQ_{10} analysis by RP-HPLC tandem mass spectrometry

Lipid extract from HEK cells was prepared as described previously (45) by first resuspending the frozen cell pellets from each sample in 100 µL of 1x PBS, pH 7.3, from which 10 µL of the cell suspension was used to measure protein concentration by Bradford assay (Invitrogen), and the remaining 90 µL of the cell suspension was subjected to lipid extraction using methanol and petroleum ether in the presence of internal standard dipropoxy-CoQ_{10} as described above. A series of CoQ_9 and CoQ_{10} standards containing dipropoxy-CoQ_{10} were prepared and lipid extracted concurrently with HEK cell samples to construct CoQ_9 and CoQ_{10} standard curves. Measurements of CoQ_9 and CoQ_{10} contents by RP-HPLC MS/MS were performed in the same manner as described above, except that the reconstituted lipid extract was separated on a Luna 5 µm PFP(2) 100A column (100 x 4.6 mm, 5 µm; Phenomenex) in 10% solvent B at a constant flow rate of 1 mL/min. The precursor to product ion transitions of

CoQ_9, CoQ_{10}, and their ammonium adducts are listed in Table 3. Similarly, the amounts of CoQ_9 and CoQ_{10} were quantified based on the total peak areas corresponding to each analyte and their respective ammonium adduct, normalized against the internal standard dipropoxy-CoQ_{10}, and calculated using the CoQ_9 and CoQ_{10} standard curves. Statistical analysis was performed using GraphPad Prism with two-tailed nonparametric t-test.

RESULTS

Steady-state levels of Coq polypeptides are altered in *crd1Δ* or *taz1Δ* mutants under growth conditions requiring respiration

CL biosynthesis and remodeling modulate the enzymatic activities of at least three Coq polypeptides (Coq7, Coq8, and Coq9) (32, 35, 36). To examine whether steady state levels of other Coq polypeptides might be affected in *crd1Δ* and *taz1Δ* mutants, we performed immunoblot analyses against known members of the CoQ synthome, Coq3-Coq9, as well as Coq1 and Coq10 polypeptides that are independent of the CoQ synthome. When cultured in fermentation-supportive medium (YPGal), the steady state levels of most of the Coq polypeptides examined remain unchanged in both *crd1Δ* and *taz1Δ* mutants compared to the wild-type cells (Fig. 1A, supplemental Fig. S1A). While the steady state level of Coq6 appeared to be marginally reduced in the *crd1Δ* mutant, the abundance of Coq8 dropped to nearly 50% of the wild-type level in the *crd1Δ* mutant (Fig. 1A, supplemental Fig. S1A). When cultured in respiration-requiring medium (YPG), we noticed that the absence of CL in the *crd1Δ* mutant and defects in CL remodeling in the *taz1Δ* mutant have opposite effects on many Coq polypeptides. When cultured under conditions requiring respiration, the steady state levels of Coq5, Coq6, and Coq7 were slightly decreased in the *crd1Δ* mutant, and approximately 50% reductions of Coq1, Coq8, and Coq10 were observed in the *crd1Δ* mutant when compared to the wild-type cells (Fig. 1B, supplemental Fig. S1B). Under the same respiration-requiring conditions, evident up-regulated expressions of Coq3 and Coq9 were detected in the *crd1Δ* mutant cells, and up-regulation of Coq3, Coq4, Coq6, Coq7, Coq9 and Coq10 were detected in the *taz1Δ* mutant cells (Fig. 1B, supplemental Fig. S1B). Elevated level of Coq6 was also observed in the *taz1Δ* mutant cells grown under fermentation conditions (Fig. 1A, supplemental Fig. S1A). These results are consistent with previous findings that Coq8 was more susceptible to changes in cells lacking CL (*crd1Δ*) (35). Coq6 may represent another candidate protein whose level is

dependent on the changes of CL abundance regardless of the fermentative or respiratory growth conditions.

Absence of CL or disturbance of CL maturation affects the stability of the CoQ synthome

So far, at least 14 nuclear encoded genes (*COQ1-COQ11, YAH1, ARH1* and *HFD1*) are recognized to be important for CoQ biosynthesis and its fundamental role in the electron transport chain (30, 31). Many of the encoded gene products serve as enzymes involved in the CoQ biosynthetic pathway and assemble into a high molecular weight complex known as the CoQ synthome (also known as complex Q) (30, 31, 46). In addition to catalyzing reactions in CoQ biosynthesis, many of the Coq proteins have structural functions stabilizing other members of the CoQ synthome. Previous work has shown that the absence of certain Coq polypeptides disrupts the CoQ synthome, and decreases steady state levels of certain Coq subunits of the CoQ synthome (46, 47). The downstream effect of such *coq* mutations is the abolishment of CoQ production and lack of growth on non-fermentable carbon sources. Based on the known capacity of CL to stabilize respiratory complexes and other proteins within the mitochondrial inner membrane (16), we hypothesized that CL may play a similar role in the assembly or stability of the CoQ synthome. Thus, the stability of CoQ synthome under fermentation-supportive or respiration-requiring growth conditions was examined in wild-type yeast, and in *crd1Δ,* and *taz1Δ* mutants, by two-dimensional Blue Native (BN)/SDS-PAGE. Detection of Coq4 and Coq9 served as indicator polypeptides of the CoQ synthome (46).

Under fermentation growth conditions (YPGal), the CoQ synthome represented by Coq4 and Coq9 signals manifested as a heterogeneous mixture of complexes distributed from ~66 kDa to >669 kDa (Fig. 2A). Under these same YPGal growth conditions, a similar distribution pattern of Coq4 and Coq9 was also apparent in *crd1Δ* and *taz1Δ* mutants (Fig. 2A). The signals of Coq4 and Coq9 partially overlap, and the different appearance of the CoQ synthome on 2D

BN/SDS-PAGE as detected by Coq4 and Coq9 may be contributed by presence of sub-complexes of CoQ synthome, and/or the affinity of Coq4 and Coq9 to the CoQ synthome. Under the respiration growth conditions (YPG), the CoQ synthome in the wild-type yeast appeared to be similar to the wild-type yeast cultured under the fermentation condition (Fig. 2B). Although direct quantitative comparisons between different blots shown in Figure 2 are not possible, within each blot the dispersed Coq4 and Coq9 signals of the CoQ synthome can be related to the respective Coq4 and Coq9 signals present in the lanes containing the sample of intact mitochondria (labeled as M). Hence, the overall abundance of the CoQ synthome seemed to be less in the wild-type cells grown in glycerol-containing YPG medium (Fig. 2B) than if they were grown in galactose-containing YPGal medium (Fig. 2A). Under the respiration-requiring growth conditions, the CoQ synthome becomes further destabilized in both *crd1Δ* and *taz1Δ* mutants. The CoQ synthome at molecular weight >669 kDa of the wild type cells was replaced by sub-complexes predominantly at 440 kDa represented by the Coq4 signal, or by sub-complexes migrating between 140 kDa to 440 kDa represented by the Coq9 signal in the *crd1Δ* and *taz1Δ* mutants (Fig. 2B). The increased signal of the lower mass complexes may account for the observation that the steady-state levels of most of the Coq polypeptides *taz1Δ* mutants were unaltered or even slightly increased (Fig. 1B, supplemental Fig. S1B).

CoQ biosynthesis and turnover is less efficient in the *crd1Δ* and *taz1Δ* mutants

In yeast, CoQ biosynthesis derives from 4-hydroxybenzoic acid (4HB) or *para*-aminobenzoic acid (pABA) (Fig. 3) (30). Polyisoprenylation of the ring precursors 4HB and pABA gives rise to early-stage intermediates 3-hexaprenyl-4-hydroxybenzoic acid (HHB) and 3-hexaprenyl-4-aminobenzoic acid (HAB), each of which is subsequently converted to late-stage intermediates demethoxy-Q_6H_2 (DMQ_6H_2) and CoQ_6H_2 (Fig. 3) (30). The 4-imino-demethoxy-Q_6H_2 ($IDMQ_6H_2$) likely represents a pABA-specific dead-end product (Fig. 3) (30). To gauge the efficiency of CoQ_6 production, de novo CoQ_6 biosynthesis was tracked in wild type, *crd1Δ,* and

taz1Δ yeast with either $^{13}C_6$-4HB or $^{13}C_6$-pABA over the course of 5 h under both fermentation-supportive and respiration-requiring conditions.

Under fermentation growth conditions, the *crd1Δ* mutant cells produced significantly decreased amounts of $^{13}C_6$-CoQ_6 emanating from $^{13}C_6$-pABA, but not from $^{13}C_6$-4HB (Fig. 4A). The *crd1Δ* mutant cells also generated lower amounts of the penultimate intermediate $^{13}C_6$-DMQ_6 as compared to wild-type control (Fig. 4D). The *crd1Δ* mutant cells accumulated significantly higher amounts of $^{13}C_6$-labeled early intermediates $^{13}C_6$-HHB and $^{13}C_6$-HAB (Fig. 4B, and C). The accumulation of HHB and HAB is indicative of inefficient biosynthesis, as HHB and HAB accumulate in the *coq* null mutants (*coq3Δ – coq11Δ*) (30). In contrast, the *taz1Δ* mutant behaved more like wild-type in terms of the levels of $^{13}C_6$-labeled HHB, HAB, and DMQ_6 (Fig. 4B, C, and D), but it made less $^{13}C_6$-$IDMQ_6$ (Fig. 4E), as well as less $^{13}C_6$-CoQ_6 from pABA at the 3- and 5-h time points (Fig. 4A).

In the same experiment performed with $^{13}C_6$-labeled ring precursors, we also measured the content of unlabeled CoQ_6 and CoQ_6-intermediates. For the samples treated with a $^{13}C_6$-ring labeled precursor, this gives a rough approximation of the turnover of CoQ_6. Most noticeably, the steady state levels of unlabeled CoQ_6 were significantly higher in *crd1Δ* at every time point regardless of whether a $^{13}C_6$-ring labeled precursor was added or not (Fig. 5A). Although the steady state levels of CoQ_6 in *taz1Δ* mutant was only sporadically higher (Fig. 5A), the levels of the unlabeled penultimate intermediate DMQ_6 was consistently elevated at every time point with or without $^{13}C_6$-labeled precursors (Fig. 5C). While unlabeled HAB was not detected (data not shown), the steady state levels of unlabeled HHB were significantly higher in *crd1Δ* at 3- and 5-h time point in the ethanol control treatment (Fig. 5B). The steady state levels of $IDMQ_6$ were higher in *crd1Δ* and *taz1Δ* mutants in the first hour, but these differences were lost over time (Fig. 5D). We also plotted the levels of total CoQ_6 as the sum of de novo $^{13}C_6$-CoQ_6 and steady

state unlabeled CoQ_6 (Fig. 6). Even though the steady state CoQ_6 levels were consistently higher in *crd1Δ* (Fig. 5A), the total CoQ_6 content in *crd1Δ* mutant was only higher in a few samples (Fig. 6), while the amount of total CoQ_6 in the remaining samples was offset by inefficient de novo CoQ_6 synthesis (Fig. 6A). In *taz1Δ* mutant, the higher steady state levels of CoQ_6 in $^{13}C_6$-4HB treated sample at 3 h led to a higher total CoQ_6 content (Fig. 6), since the de novo CoQ_6 synthesis in *taz1Δ* mutant is not too different from the corresponding wild-type controls (Fig. 4A).

Under the respiration-requiring growth conditions, the CoQ synthome was further destabilized in both *crd1Δ* and *taz1Δ* mutants, yet the efficiency of de novo CoQ_6 biosynthesis appeared to be more disturbed in the *taz1Δ* mutant. The levels of $^{13}C_6$-CoQ_6 in both *crd1Δ* and *taz1Δ* mutants were not statistically different from the wild-type cells at almost all time points, except that the *taz1Δ* mutant unexpectedly produced more $^{13}C_6$-CoQ_6 from both $^{13}C_6$-pABA and $^{13}C_6$-4HB at the 5-h time point (Fig. 7A). Accumulations of $^{13}C_6$-HHB, $^{13}C_6$-HAB, $^{13}C_6$-DMQ_6 from $^{13}C_6$-pABA, and $^{13}C_6$-$IDMQ_6$ in the *taz1Δ* mutant at 5-h time point (Fig. 7B, C, D, and E) suggested inefficient de novo CoQ biosynthesis. On the contrary, although the *crd1Δ* mutant had a buildup of $^{13}C_6$-HAB and $^{13}C_6$-$IDMQ_6$ at 5-h time point (Fig. 7C, and E), its $^{13}C_6$-CoQ_6 content originating from $^{13}C_6$-labeled pABA was indistinguishable from the wild-type cells (Fig. 7A). The *crd1Δ* mutant experienced a setback on $^{13}C_6$-DMQ_6 production at the 3-h time point (Fig. 7D), which explained a drop in the amount $^{13}C_6$-CoQ_6 observed at the same time point (Fig. 7A). However, the mutant cells were able to catch up on de novo CoQ_6 synthesis at a later time point.

Consistent with our observation of high levels of de novo $^{13}C_6$-CoQ_6 and $^{13}C_6$-CoQ_6-intermediates at the 5-h time point, the *taz1Δ* mutant also contained elevated steady state levels of unlabeled CoQ_6, HAB, HHB, DMQ_6 and $IDMQ_6$ at the 5-h time point (Fig. 8A-E). The steady

state levels of $IDMQ_6$ were considerably higher in the *crd1Δ* mutant at all times compared to the wild-type control (Fig. 8E), whereas levels of CoQ_6 and other CoQ_6-intermediates were only sporadically high in the *crd1Δ* mutant at 5-h time point (Fig. 8A, B, and D). A combination of increased levels of de novo $^{13}C_6$-CoQ_6 and steady state CoQ_6 resulted in an overall higher total CoQ_6 in the *taz1Δ* mutant at the 5-h time point (Fig. 9), and the higher levels of total CoQ_6 in the *crd1Δ* mutant at 5-h time point was mainly contributed by the steady state accumulation of unlabeled CoQ_6 (Fig. 9).

Collectively, under fermentation-supportive conditions, absence of CL or defects in CL remodeling has a mild effect on de novo CoQ biosynthesis, consistent with the fact that both mutants had negligible changes on the assembly of the CoQ synthome. However, both the de novo biosynthesis and turnover of CoQ appeared to be less efficient in the *crd1Δ* mutant, presumably due to the decreased Coq6 and Coq8 levels rather than destabilized CoQ synthome. Under respiration-requiring conditions, destabilized CoQ synthome impacted the *taz1Δ* mutant to a greater extent regardless of the elevated levels of individual Coq polypeptide, which was reflected by impeded de novo CoQ synthesis and CoQ turnover. In summary, the elevated levels of early CoQ-intermediates and the dead-end IDMQ intermediate are hallmarks of inefficient CoQ biosynthesis in the *crd1Δ* and *taz1Δ* mutants.

Mammalian BTHS cell model shows elevated steady state level of CoQ

Yeast has been the go-to organism to model the disease pathogenicity caused by BTHS patient-associated missense alleles. Recently, a mammalian BTHS cell model was established and characterized biochemically to mimic a loss of function BTHS allele (40). The *taz*^{TALEN}.2 and *taz*^{TALEN}.19 HEK 293 cell lines contain genetic lesions within *TAZ* exon 1, and produce no detectable levels of TAZ protein (40). Thus, to extend our study of CoQ metabolism to include a human BTHS disease model, we examined the CoQ content in the *taz*^{TALEN}.2 and *taz*^{TALEN}.19

HEK 293 cell lines. Human cells contain two different isoforms of CoQ. CoQ_{10}, which contains ten isoprene units in the tail, is the predominant form of CoQ in humans, and CoQ_9 constitutes only a small portion of the total CoQ in humans. While the *taz*^{TALEN}.2 HEK 293 cells contained less CoQ_9, since it is the minor CoQ species, its decrease did not impact the total amount of CoQ (Fig. 10A-C). The *taz*^{TALEN}.19 HEK 293 cells had significantly higher amounts of CoQ_9, CoQ_{10}, and total CoQ (Fig. 10A-C), and this result was similar to the observation of increased amounts of steady state CoQ_6 (Fig. 8A), and total CoQ_6 (Fig. 9) in yeast *taz1Δ* mutant at 5-h time point under the respiration condition. While the basis for the differences observed between *taz*^{TALEN}.2 and *taz*^{TALEN}.19 293 cells is presently unclear, our results suggest that alterations in CoQ levels may also occur in human cells with impaired CL remodeling.

DISCUSSION

The importance of CL is highlighted by its ability to structurally stabilize proteins and protein complexes in the mitochondrial inner membrane thereby optimizing their function. This work supports a new role for CL in optimizing the function of the CoQ synthome, a multi-subunit protein complex that is required for efficient CoQ biosynthesis (Fig. 11). Our results show that both yeast *crd1Δ* and *taz1Δ* mutant cells exhibit inefficient CoQ_6 biosynthesis as a result of the destabilized CoQ synthome (Fig. 11). The *crd1Δ* and *taz1Δ* mutations affect the corresponding yeast mutant cells differently depending on the growth conditions. Growth under fermentation-permissive conditions affects the de novo CoQ_6 biosynthesis in the *crd1Δ* mutant to a greater extent (Fig. 4), whereas growth in respiration-requiring conditions results in higher de novo CoQ_6 biosynthesis and also higher accumulation of early CoQ-intermediates in the *taz1Δ* mutant (Fig. 7). Detection of more CoQ in the HEK 293 *taz*^{TALEN}.19 cells mirrors our observation in the *taz1Δ* mutant under respiratory condition, and implies that a disturbance of CoQ synthome assembly and CoQ homeostasis may be a previously unidentified clinical phenotype in human BTHS patients. We think several considerations may explain the observed inefficient CoQ biosynthesis that results from a lack of CL in the *crd1Δ* mutant, or disruption of CL acyl chain composition in the *taz1Δ* mutant.

First, most of the Coq polypeptides are peripheral membrane proteins organized along the mitochondrial inner membrane facing the matrix side (30, 48), and absence of CL or disturbance of CL homeostasis may have a direct impact on the stability and/or enzymatic activity of individual Coq polypeptides involved in CoQ biosynthesis. Indeed, diminished steady state levels of Coq8 were found in the *crd1Δ* mutant under both fermentation and respiration conditions (Fig. 1), in support of a functional connection between CL and Coq8 activity (35). Although the steady state levels of some Coq polypeptides were not prominently influenced by the absence of CL or alteration of its acyl chain composition (Fig. 1, supplemental Fig. S1), it is

tempting to speculate that the enzymatic activity of individual Coq proteins may benefit from the presence of CL, given that in vitro assays often indicate that CL enhances protein function. For example, the mitochondrial matrix protein rhodanese folds into a more native conformation with greatly enhanced in vitro activity when it is bound to CL-containing liposomes (49). Reconstitution of in vitro activities of complex IV and the ADP/ATP carrier both require the presence of CL (50, 51). The ATPase activity of human COQ8A also requires its membrane association with CL-containing liposomes, mediated by the positively charged surface residues of COQ8A at the KxGQ domain and conserved Gly-zipper motif at the transmembrane domain (35, 52). Overexpression of yeast Coq8 restores CoQ synthome in yeast *coqΔ* mutants (46), and the Coq8 ATPase activity depends on the presence of CL (35). Thus, it is possible that the destabilized CoQ synthome in *crd1Δ* mutant is a result of a combination of both decreased abundance of Coq8 and impaired Coq8 function in the absence of CL.

Recently, membrane interaction of human COQ9, mediated by its amphipathic C-terminal helix 10 was shown to be involved in accessing the membrane embedded CoQ-intermediates and presenting them to human COQ7 for the penultimate step in CoQ biosynthesis (36). Molecular dynamics simulations and liposome floatation assays revealed that CL aids stable COQ9 membrane association, and a CL-enriched sub-domain within the mitochondrial inner membrane is necessary for establishing COQ7-COQ9 interaction during CoQ biosynthesis (36). Coincidently, we observed an up-regulation of both Coq7 and Coq9 in yeast *taz1Δ* mutant (Fig. 1B, supplemental Fig. S1B), that had an increased MLCL to CL ratio (53), and a more disrupted CoQ synthome assembly represented by Coq9 (Fig. 2) specifically under the respiration growth conditions. A slight increase of steady-state levels of the Coq9 polypeptide was also observed in the *crd1Δ* mutant under the respiration condition (Fig. 1B, supplemental Fig. S1B). Presumably, when respiration is necessary, an up-regulated expression of Coq9 is required to neutralize the loss of interaction between Coq9 and the

membrane in cells that are deficient or devoid of CL. Moreover, Coq9 is required for removal of the amino group at the C4 position of CoQ-intermediates derived from pABA (54), and Coq9 is likely to function together with Coq6 for coordinated deamination at C4 and hydroxylation at C5 of CoQ-intermediates (Fig. 3) (30). Indeed, elevated expressions of both Coq7 and Coq9 were observed in the *taz1Δ* mutant under the respiration condition (Fig. 1B, supplemental Fig. S1B). We also noticed that both *crd1Δ* and *taz1Δ* mutants made less $^{13}C_6$-CoQ_6 from $^{13}C_6$-pABA than from $^{13}C_6$-4HB (Fig. 4A) under the fermentation growth conditions; accumulations of $^{13}C_6$-HAB (Fig. 7C), $^{13}C_6$-DMQ_6 (Fig. 7D) and $^{13}C_6$-$IDMQ_6$ (Fig. 7E) were also more evident in both *crd1Δ* and *taz1Δ* mutants labeled with$^{13}C_6$-pABA. It seems highly likely that Coq9 membrane interaction is also crucial for subsequent Coq6-Coq9 interaction, and compromised Coq6-Coq9 interaction impairs CoQ_6 biosynthesis specifically from the pABA pathway.

Many of the Coq polypeptides organize into a high molecular weight complex, possibly for efficient substrate channeling, catalytic enhancement, and sequestration of toxic reactive intermediates generated during CoQ biosynthesis. Absence of CL and changes in its acyl chain composition may have an impact on proper assembly of the multi-subunit CoQ synthome essential for efficient CoQ biosynthesis. This may be more evident under the respiration-requiring conditions when CoQ is playing an essential role of relaying protons and electrons between respiratory complexes. Under the fermentation growth conditions, although the CoQ synthome assembly was only mildly affected (Fig. 2), the accumulation of early-stage $^{13}C_6$-CoQ_6-intermediates (Fig. 4B, C) and decreased late-stage $^{13}C_6$-CoQ_6-intermediates (Fig. 4D, E) and $^{13}C_6$-CoQ_6 (Fig. 4A) in the *crd1Δ* and *taz1Δ* mutants is indicative of a catalytically inefficient CoQ synthome. However, the CoQ synthome assembly was visibly more disrupted in the *crd1Δ* and *taz1Δ* mutants under respiration growth conditions (Fig. 2). Our BN/SDS-PAGE results examining the CoQ synthome assembly suggest that both the presence of CL, as well as MLCL to CL ratio were important for the overall stability of the CoQ synthome complex (Fig. 2) when

active cellular respiration is needed. Particularly, preserving a proper ratio of MLCL to CL appears to be more critical for maintaining the CoQ synthome, as the increased levels of component Coq polypeptide (Fig. 1B, supplemental Fig. S1B) failed to restore the high molecular weight complex of the CoQ synthome (Fig. 2) in the *taz1Δ* mutant under the respiration conditions. Interestingly, while de novo CoQ biosynthesis from the pABA pathway under the fermentation condition was similarly affected in both *crd1Δ* and *taz1Δ* mutants (Fig. 4A), the decreased efficiency of de novo CoQ production was more affected in the *taz1Δ* mutant under respiration growth conditions (Fig. 7A).

In yeast, Cld1 and Taz1 together mediate CL remodeling (8). Unlike the *crd1Δ* mutant that has completely abolished CL synthesis, yeast lacking Cld1 or Taz1 accumulate CL (in *cld1Δ* mutant) (8), or MLCL (in *taz1Δ* mutant) (55) with saturated fatty acyl chains instead of monounsaturated C18:1 and C16:1 acyl chain species that normally predominate (8, 55). In particular, the *taz1Δ* mutant contains 10-25% or 30-60% less CL than wild-type cells under fermentation or respiration condition, respectively, whereas the CL content in *cld1Δ* mutant is not significantly different from the wild-type control (55, 56). Unremodeled CL appears to function the same as remodeled CL in supporting mitochondrial functions measured by oxygen consumption rate and mitochondrial membrane potential (56). In addition to aberrant CL composition, yeast *taz1Δ* mutant cells exhibit decreased mitochondrial membrane potential and increased proton leak (57), which are mainly caused by increased MLCL to CL ratio rather than the absence of remodeled CL (56, 58). It is tempting to speculate that the elevated CoQ in yeast *taz1Δ* mutant and *taz*^{TALEN}.19 HEK 293 cells may act to mitigate an increase in CL oxidation when the CL remodeling-mediated CL repair pathway is defective. Indeed, previous studies have shown pretreatment with CoQ_{10} substantially reduced rotenone-induced mitochondrial depolarization and preserved mitochondrial membrane potential in primary neuronal cells (59-61).

In humans, CL is highly susceptible to oxidative damage due to its high content of polyunsaturated fatty acyl chains and its exclusive location inside the mitochondria, which are the primary source of ROS production. The CL acyl chain composition is readily modulated by exogenous lipid species in mammalian cells (62). Yeast cells do not make polyunsaturated fatty acids (PUFAs), but they readily take up exogenous PUFAs and incorporate them into CL (63). Yeast CoQ-less *coq* mutants are hypersensitive to exogenously supplemented PUFAs, including linoleic acid (C18:2), linolenic acid (C18:3), eicosapentaenoic acid (C22:5), and arachidonic acid (C20:4) (64, 65). This is due to the loss of CoQ as a lipophilic chain-terminating antioxidant (64, 65). Yeast *coq9Δ* supplemented with exogenous arachidonic acid resulted in significantly elevated amounts of F2-isoprostanes, indicating non-enzymatic, free radical-catalyzed lipid peroxidation/oxidation (65). Protein carbonylation as a result of ROS production under respiration conditions is elevated in both *crd1Δ* and *taz1Δ* mutants and the increase of oxidative stress is likely not due to a lack of antioxidant defense mechanisms as measured by cellular and mitochondrial superoxide dismutase activities (66). In response to oxidative stress, *CLD1* expression is upregulated to possibly deacylate peroxidized CL (58). Thus, one postulated functional outcome of CL remodeling is to remove and/or repair damaged CL (20, 58). It is tempting to speculate that *CLD1* upregulation may stabilize the CoQ synthome, thus prompting more efficient CoQ biosynthesis in an effort to ameliorate damages caused by lipid peroxidation.

Neurotoxicity induced by CL oxidation is implicated in the development of neurodegenerative diseases (67-69). Mitochondrial targeted antioxidants, including a derivative of CoQ have shown great efficacy protecting CL from oxidative damage and attenuating disease pathogenesis (70-72). Supplementation of a CoQ derivative (MitoQ) increases *CRD1* gene expression and overall CL content in hepatic mitochondria in rat models (70). The studies

reported here provide the framework to extend the functional link between CL homeostasis, CoQ metabolism and its function as an antioxidant to BTHS as well as neurodegenerative diseases. It will be particularly interesting to see if dietary supplementation of CoQ or other strategies (i.e. deuterium reinforced-PUFA) that protect CL from autoxidation (64, 65) can ameliorate or reverse the pathogenic phenotypes of these diseases in clinical studies,

Table 1. Genotype and source of yeast strains

Strain	Genotype	Source
W303 1B	MAT α, *ade2-1 can1-100 his3-11,15 leu2-3,112 trp1-1 ura3-1*	R. Rothstein[a]
W303 *crd1Δ*	MAT **a**, *his3 -11,15, leu2, ura3, ade8, Δcrd1::TRP*	(56)
W303 *taz1Δ*	MAT **a**, *leu2, ura3, trp1, ade8, Δtaz1::HISMX6*	(56)
W303 *coq1Δ*	MAT α*, ade2-1 can1-100 his3-11,15 leu2-3,112 trp1-1 ura3-1 coq1::LEU2*	(73)
CC303	MAT α*, ade2-1 can1-100 his3-11,15 leu2-3,112 trp1-1 ura3-1 coq3::LEU2*	(74)
W303 *coq4Δ*	MAT **a***, ade2-1 can1-100 his3-11,15 leu2-3,112 trp1-1 ura3-1 coq4::TRP1*	(75)
W303 *coq5Δ*	MAT α, *ade2-1 can1-100 his3-11,15 leu2-3,112 trp1-1 ura3-1 coq5::HIS3*	(38)
W303 *coq6Δ*	MAT **a***, ade2-1 can1-100 his3-11,15 leu2-3,112 trp1-1 ura3-1 coq6::LEU2*	(76)
W303 *coq7Δ*	MAT α*, ade2-1 can1-100 his3-11,15 leu2-3,112 trp1-1 ura3-1 coq7::LEU2*	(77)
W303 *coq8Δ*	MAT **a***, ade2-1 can1-100 his3-11,15 leu2-3,112 trp1-1 ura3-1 coq8::HIS3*	(75)
W303 *coq9Δ*	MAT α*, ade2-1 can1-100 his3-11,15 leu2-3,112 trp1-1 ura3-1 coq9::URA3*	(78)
W303 *coq10Δ*	MAT **a**, *ade2-1 can1-100 his3-11,15 leu2-3,112 trp1-1 ura3-1 coq10::HIS3*	(79)

[a]Dr. Rodney Rothstein. Department of Human Genetics, Columbia University, New York, NY.

Mating type a (MAT **a**) is in bold to distinguish it from mating type alpha (MAT α).

Table 2. Description and source of antibodies

Antibody	Working dilution	Source
Coq1	1:10,000	(73)
Coq3	1:200	(80)
Coq4	1:2,000	(81)
Coq5	1:5,000	(82)
Coq6	1:200	(76)
Coq7	1:1,000	(83)
Coq8	Affinity purified; 1:30	(47)
Coq9	1:1,000	(84)
Coq10	Affinity purified, 1:400	(85)
Mdh1	1:10,000	L. McAlister-Henn[b]

[b]Dr. Lee McAlister-Henn, Department of Molecular Biophysics and Biochemistry, University of Texas Health Sciences Center, San Antonio, TX.

Table 3. Precursor-to-product ion transitions

	m/z $[M+H]^+$	*m/z* $[M+NH_4]^+$
HAB	546.4/150.0	563.0/150.0
$^{13}C_6$-HAB	552.4/156.0	569.0/156.0
HHB	547.4/151.0	564.4/151.0
$^{13}C_6$-HHB	553.4/157.0	570.4/157.0
DMQ_6	561.4/167.0	578.0/167.0
$^{13}C_6$-DMQ_6	567.6/173.0	584.0/173.0
$IDMQ_6$	560.6/166.0	577.0/166.0
$^{13}C_6$-$IDMQ_6$	566.6/172.0	583.0/172.0
CoQ_4	455.4/197.0	472.0/197.0
CoQ_6	591.4/197.0	608.0/197.0
$^{13}C_6$-CoQ_6	597.4/203.0	614.0/203.0
Dipropoxy-CoQ_{10}	919.7/253.1	936.7/253.1
CoQ_9	795.6/197.08	812.6/197.08
CoQ_{10}	863.6/197.08	880.6/197.08

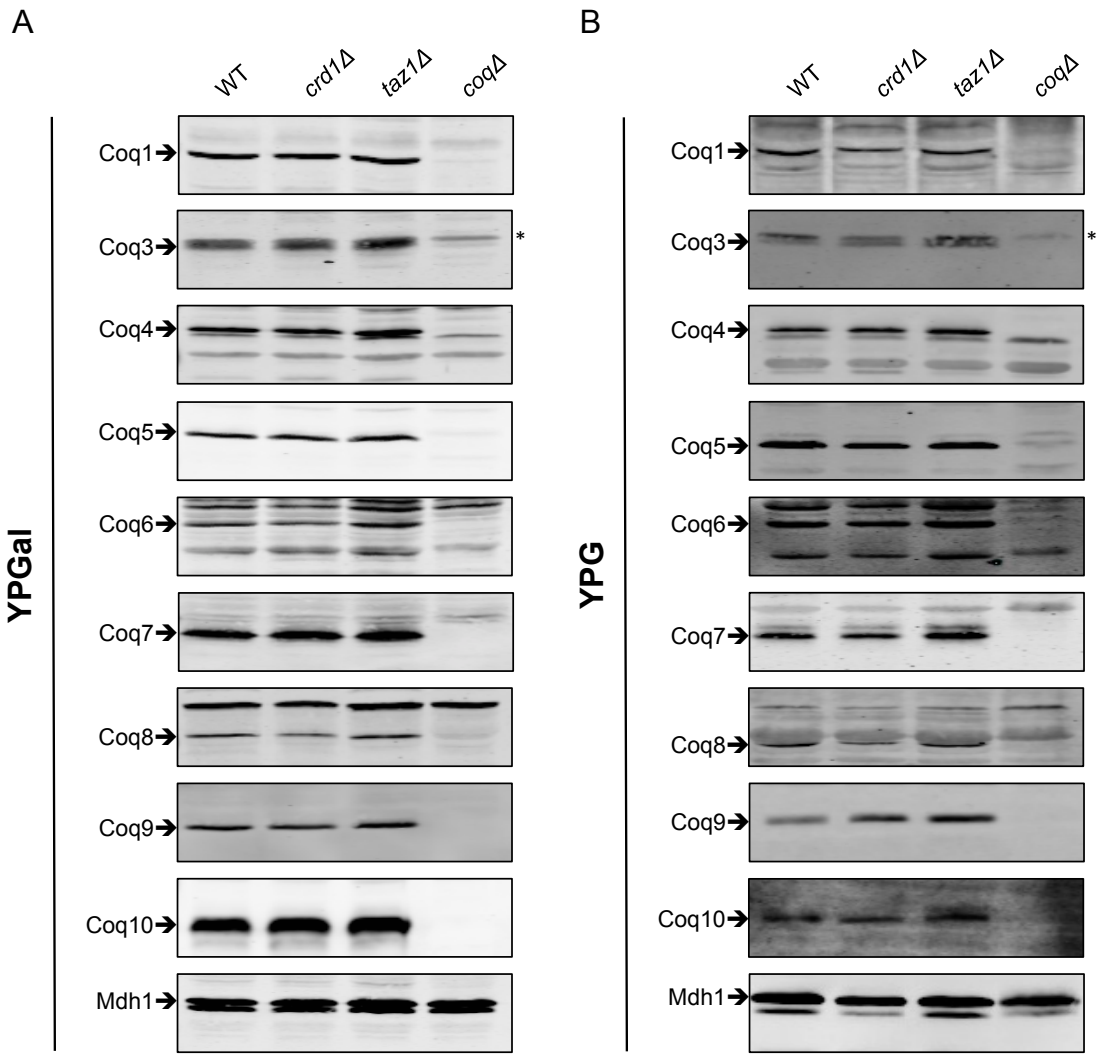

Figure 1. Steady state levels of Coq polypeptides are altered in *crd1Δ* or *taz1Δ* mutants under growth conditions requiring respiration. Aliquots (25 µg) of purified mitochondrial protein from wild-type, *crd1Δ*, or *taz1Δ* yeast cultured in **A)** galactose-containing medium, or **B)** glycerol-containing medium were separated on 12% Tris-Glycine SDS-PAGE gels. Purified mitochondria from the appropriate *coqΔ* mutant (*coq1Δ*, *coq3Δ* - *coq10Δ*) were included as negative controls for Western blotting with antisera to each of the Coq polypeptides. Mitochondrial malate dehydrogenase (Mdh1) was included as loading control, and a representative blot with mitochondria from wild-type, *crd1Δ*, *taz1Δ* and *coq1Δ*, blotted against Mdh1 is shown.

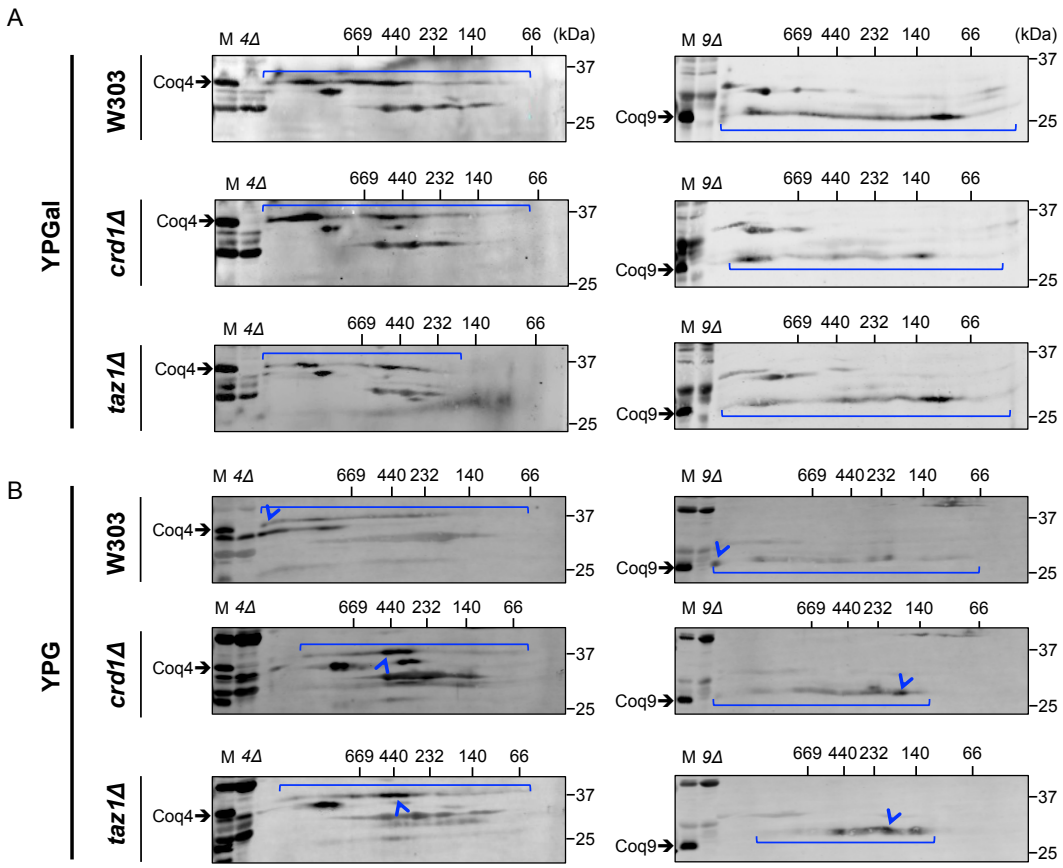

Figure 2. Absence of CL or disturbance of its acyl-chain composition affects the stability of the CoQ synthome. Aliquots (80 µg) of purified mitochondrial protein from wild-type, *crd1Δ*, or *taz1Δ* mutant yeast cultured in **A)** galactose-containing medium, or **B)** glycerol-containing medium were solubilized with digitonin and resolved on a two-dimensional BN/SDS-PAGE, transferred to membranes, and visualized with antibodies to Coq4 or Coq9, respectively. As represented by the Coq4 and Coq9 signals, the CoQ synthome appears as a heterogeneous signal from ~66 kDa to >669 kDa in wild-type control (W303) under both growth conditions. "M" denotes an aliquot of intact mitochondria from wild-type, *crd1Δ*, or *taz1Δ*. Aliquots of *coq4Δ* and *coq9Δ* mitochondria were included as negative controls for the antisera to Coq4 and Coq9, respectively.

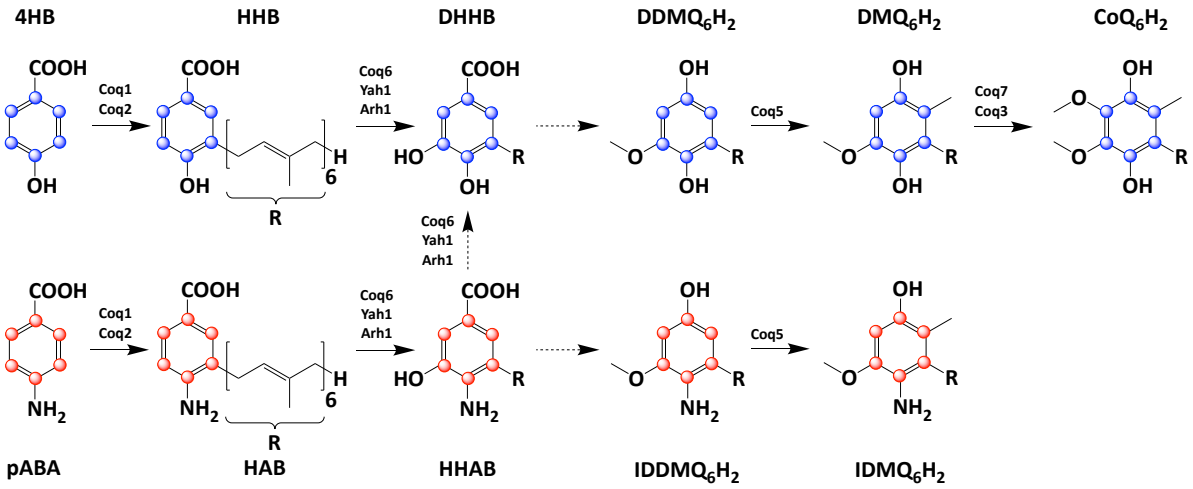

Figure 3. A schematic representation of CoQ_6 biosynthetic pathway. The efficiency of de novo CoQ_6 biosynthesis was measured by the incorporation of ^{13}C-labeled aromatic precursors, $^{13}C_6$-4HB (blue) and $^{13}C_6$-pABA (red) into CoQ_6-intermediates in the pathway.

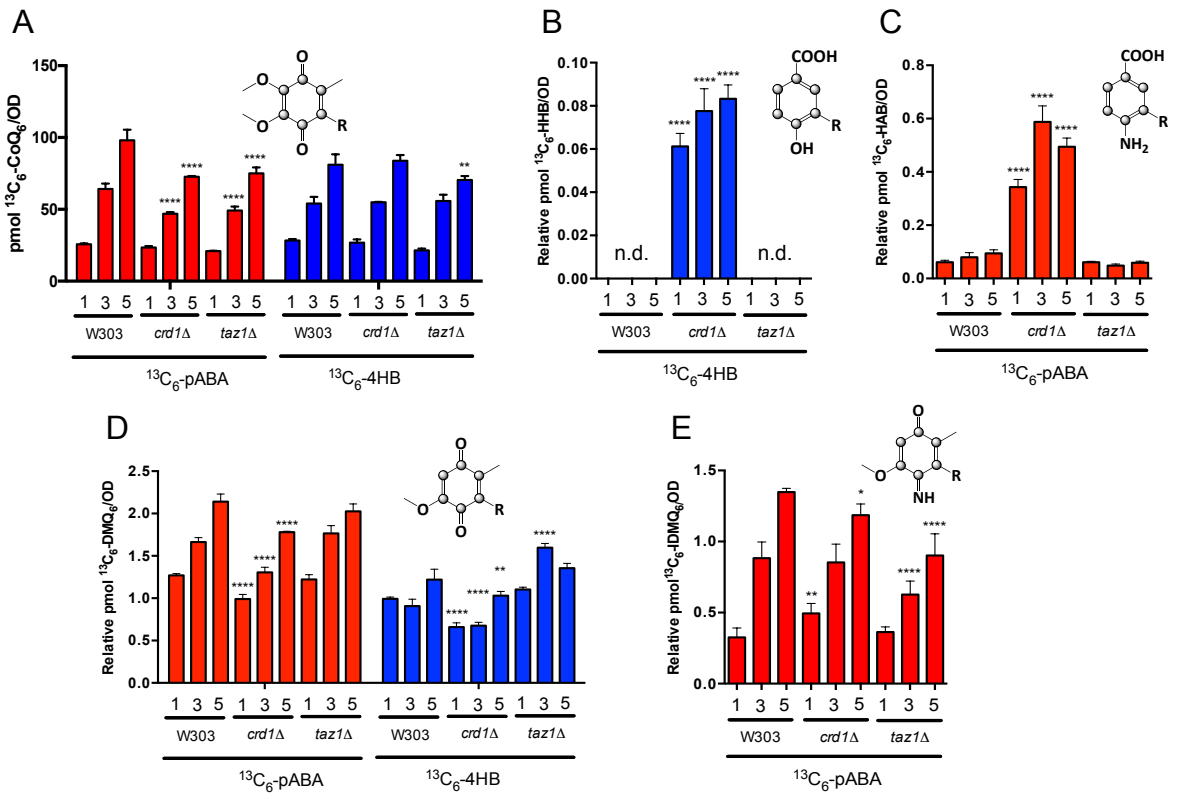

Figure 4. Absence of CL or disturbance of its acyl-chain composition results in inefficient de novo CoQ_6 biosynthesis under fermentation condition. The de novo production of CoQ_6 and CoQ_6-intermediates were measured from yeast whole cell lipid extracts from wild-type, *crd1Δ*, or *taz1Δ* mutants labeled with 5 µg/mL $^{13}C_6$-pABA (red) or $^{13}C_6$-4HB (blue), or 0.1% ethanol in DoD-Complete for 1, 3, or 5 hours. Triplicates of 5 mL culture were collected as pellets, lipid extracted, and analyzed by RP-HPLC-MS/MS. Multiple reaction monitoring (MRM) detected the precursor-product transitions described in Table 3 and enabled the detection and quantitation of **A)** $^{13}C_6$-CoQ_6; **B)** $^{13}C_6$-HHB; **C)** $^{13}C_6$-HAB; **D)** $^{13}C_6$-DMQ_6; and **E)** $^{13}C_6$-$IDMQ_6$. The statistical analyses were performed using two-way ANOVA Dunnett's multiple comparison test from three biological replicates, comparing *crd1Δ* or *taz1Δ* mutants to their corresponding wild-type control. The error bar indicates mean ± SD, and the statistical significance is represented by *p < 0.05, **p < 0.01, ***p < 0.001 and ****p < 0.0001. Label "n.d." denotes not detected.

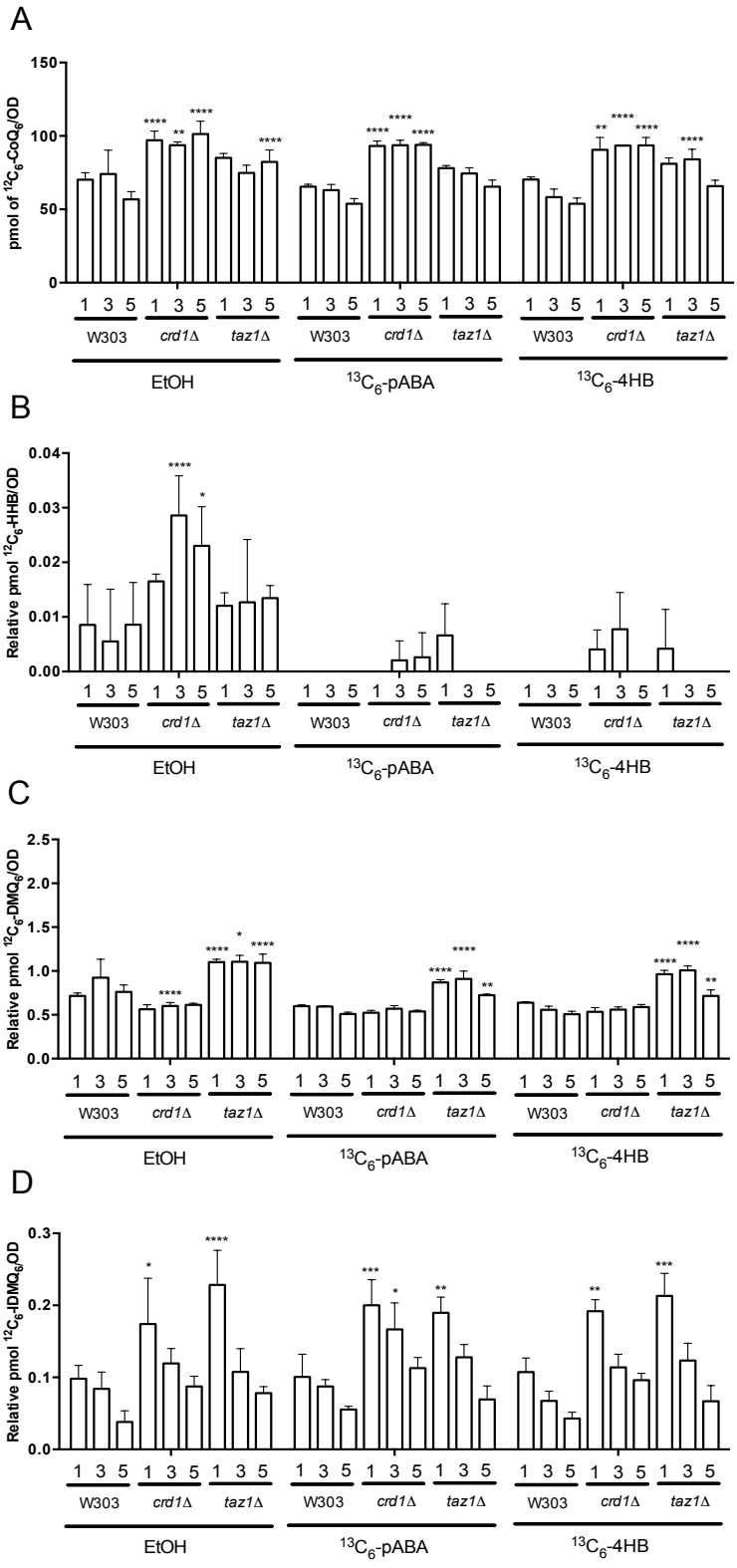
A
pmol of $^{12}C_6$-CoQ$_6$/OD
150
100
50
0
1 3 5 1 3 5 1 3 5
W303 crd1Δ taz1Δ
EtOH
$^{13}C_6$-pABA
$^{13}C_6$-4HB
B
Relative pmol $^{12}C_6$-HHB/OD
0.04
0.03
0.02
0.01
0.00
C
Relative pmol $^{12}C_6$-DMQ$_6$/OD
2.5
2.0
1.5
1.0
0.5
0.0
D
Relative pmol $^{12}C_6$-DDMQ$_6$/OD
0.3
0.2
0.1
0.0

Figure 5. Absence of CL or disturbance of its acyl-chain composition leads to changes in steady state levels of CoQ_6 and CoQ_6-intermediates under the fermentation condition. Steady state levels of **A)** CoQ_6, **B)** HHB, **C)** DMQ_6, and **D)** $IDMQ_6$ were measured in whole cell lipid extracts from wild-type, *crd1Δ*, or *taz1Δ* mutants upon addition of $^{13}C_6$-4HB, $^{13}C_6$-pABA, or ethanol as vehicle control. No HAB was detected (data not shown). The statistical analyses were performed using two-way ANOVA Dunnett's multiple comparison test from three biological replicates, comparing *crd1Δ* or *taz1Δ* mutants to their corresponding wild-type control. The error bar indicates mean ± SD, and the statistical significance is represented by *p < 0.05, **p < 0.01, ***p < 0.001 and ****p < 0.0001.

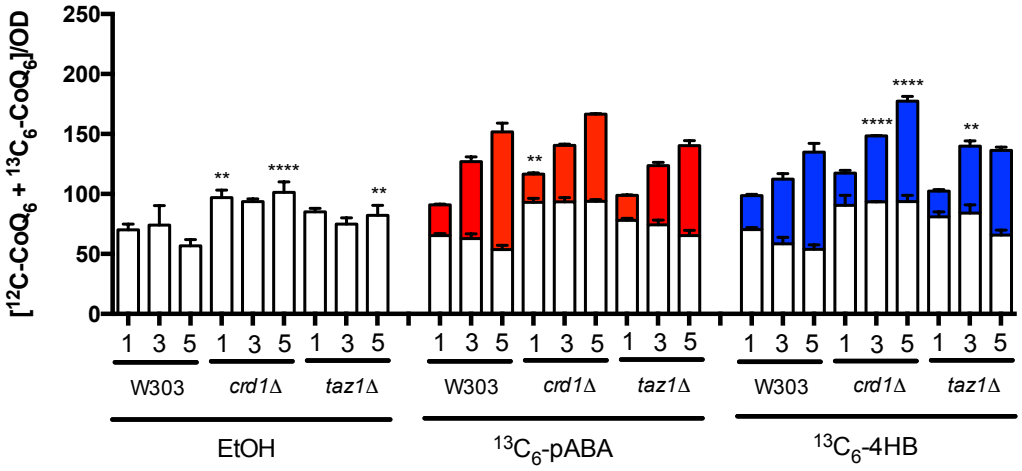

Figure 6. Absence of CL or disturbance of its acyl-chain composition results in minor changes in total CoQ_6 content under fermentation condition. Total amount of CoQ_6 was plotted as the sum of de novo $^{13}C_6$-CoQ_6 and steady state CoQ_6 levels measured in whole cell lipid extracts from wild-type, *crd1Δ*, or *taz1Δ* mutants supplemented with $^{13}C_6$-4HB, $^{13}C_6$-pABA, or ethanol. The statistical analyses were performed using two-way ANOVA Dunnett's multiple comparison test from three biological replicates, comparing *crd1Δ* or *taz1Δ* mutants to their corresponding wild-type control. The error bar indicates mean ± SD, and the statistical significance is represented by *p < 0.05, **p < 0.01, ***p < 0.001 and ****p < 0.0001.

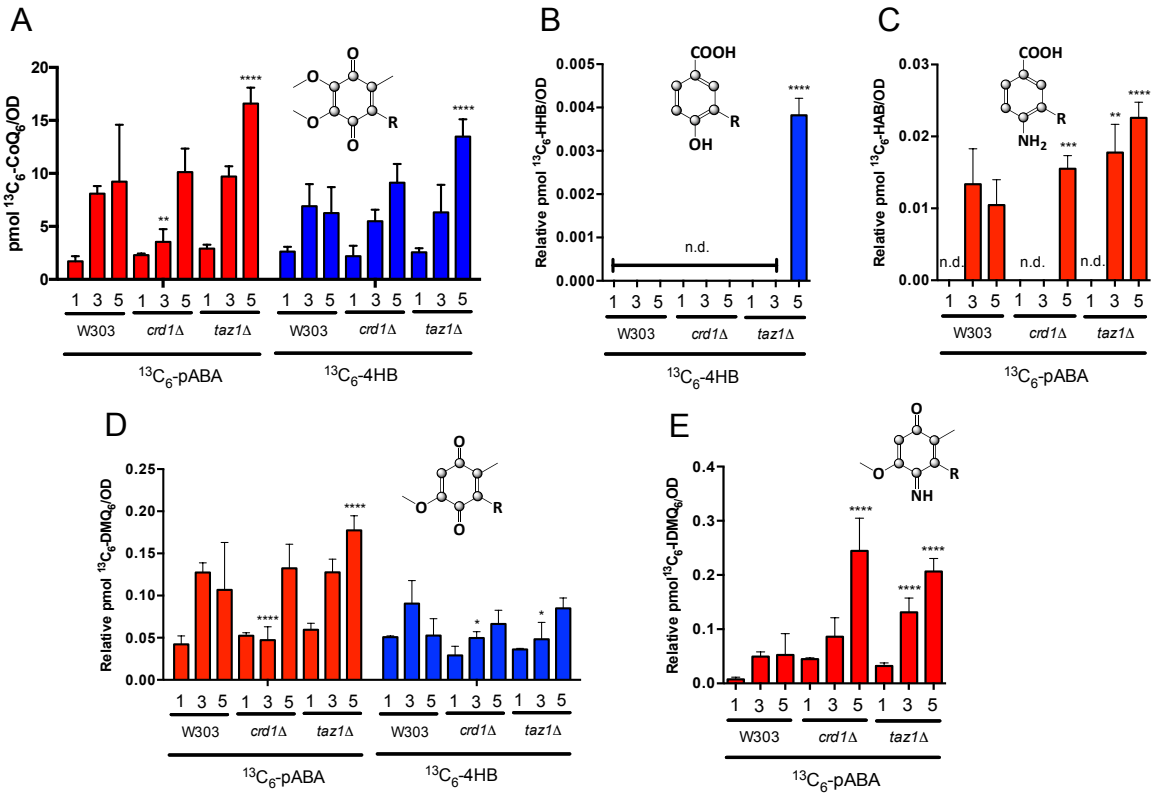

Figure 7. The de novo CoQ_6 biosynthesis is more disrupted in the *taz1Δ* mutant under respiration condition. The de novo production of CoQ_6 and CoQ_6-intermediates were measured from yeast whole cell lipid extracts from wild-type, *crd1Δ*, or *taz1Δ* mutants labeled with 5 μg/mL $^{13}C_6$-pABA (red) or $^{13}C_6$-4HB (blue), or 0.1% ethanol in YPG for 1, 3, or 5 hours. Triplicates of 5 mL culture were collected as pellets, lipid extracted, and analyzed for the levels of **A)** $^{13}C_6$-CoQ_6; **B)** $^{13}C_6$-HHB; **C)** $^{13}C_6$-HAB; **D)** $^{13}C_6$-DMQ_6; and **E)** $^{13}C_6$-$IDMQ_6$ by RP-HPLC-MS/MS. The statistical analyses were performed using two-way ANOVA Dunnett's multiple comparison test from three biological replicates, comparing *crd1Δ* or *taz1Δ* mutants to their corresponding wild-type control. The error bar indicates mean ± SD, and the statistical significance is represented by *p < 0.05, **p < 0.01, ***p < 0.001 and ****p < 0.0001. Label "n.d." denotes not detected.

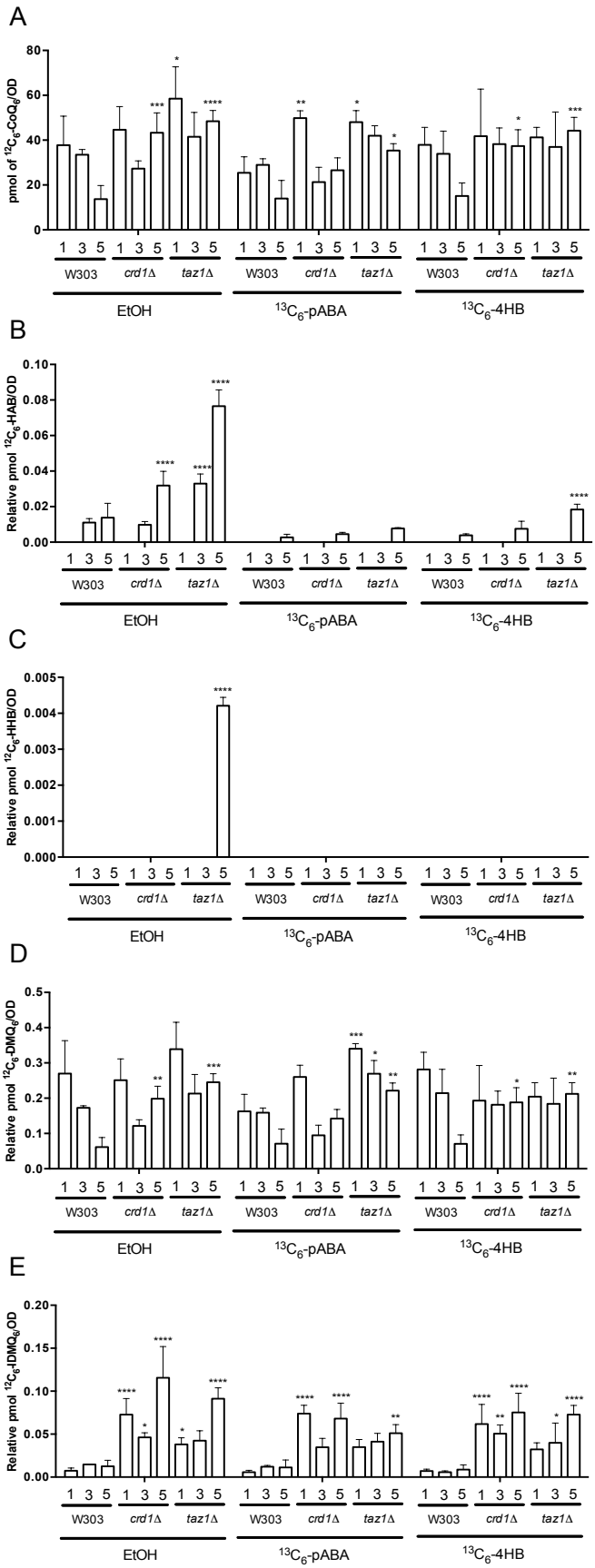
A
pmol of $^{12}C_6$-CoQ$_6$/OD
B
Relative pmol $^{12}C_6$-HAB/OD
C
Relative pmol $^{12}C_6$-HHB/OD
D
Relative pmol $^{12}C_6$-DMQ$_6$/OD
E
Relative pmol $^{12}C_6$-IDMQ$_6$/OD
1 3 5
W303
crd1Δ
taz1Δ
EtOH
$^{13}C_6$-pABA
$^{13}C_6$-4HB

Figure 8. Absence of CL or disturbance of its acyl-chain composition leads to impaired turnover of CoQ_6 and CoQ_6-intermediates under respiration condition. Steady state levels of **A)** CoQ_6, **B)** HAB, **C)** HHB, **D)** DMQ_6, and **E)** $IDMQ_6$ were measured in whole cell lipid extracts from wild-type, *crd1Δ*, or *taz1Δ* mutants upon addition of $^{13}C_6$-4HB, $^{13}C_6$-pABA, or ethanol as vehicle control cultured in YPG medium. The statistical analyses were performed using two-way ANOVA Dunnett's multiple comparison test from three biological replicates, comparing *crd1Δ* or *taz1Δ* mutants to their corresponding wild-type control. The error bar indicates mean ± SD, and the statistical significance is represented by *p < 0.05, **p < 0.01, ***p < 0.001 and ****p < 0.0001. Label "n.d." denotes not detected.

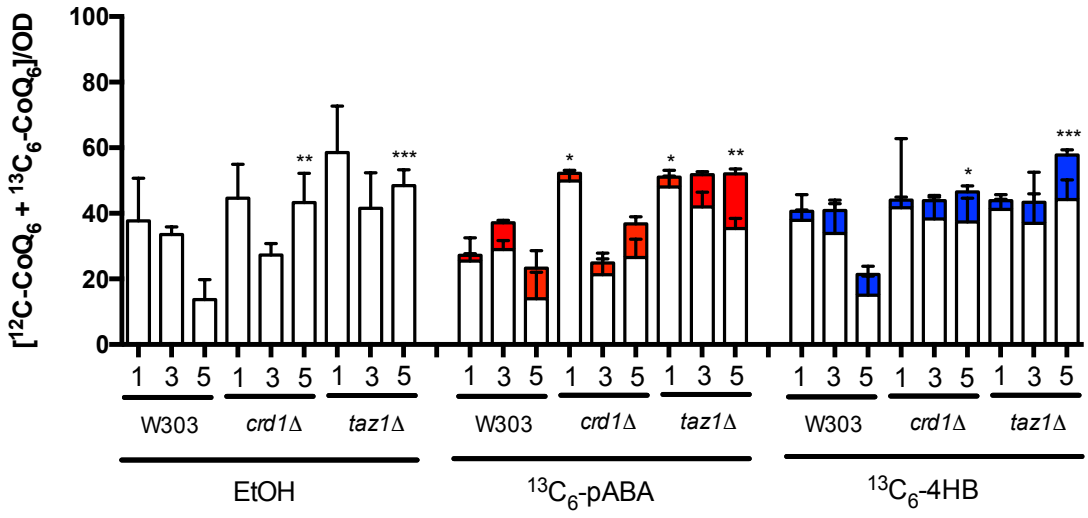

Figure 9. Great changes in the total CoQ_6 content are observed at late time point, particularly in the *taz1Δ* mutant under respiration condition. Total amount of CoQ_6 was plotted as the sum of de novo $^{13}C_6$-CoQ_6 and steady state CoQ_6 levels measured in whole cell lipid extracts from wild-type, *crd1Δ*, or *taz1Δ* mutants supplemented with $^{13}C_6$-4HB, $^{13}C_6$-pABA, or ethanol in YPG medium. The statistical analyses were performed using two-way ANOVA Dunnett's multiple comparison test from three biological replicates, comparing *crd1Δ* or *taz1Δ* mutants to their corresponding wild-type control. The error bar indicates mean ± SD, and the statistical significance is represented by *p < 0.05, **p < 0.01, ***p < 0.001 and ****p < 0.0001.

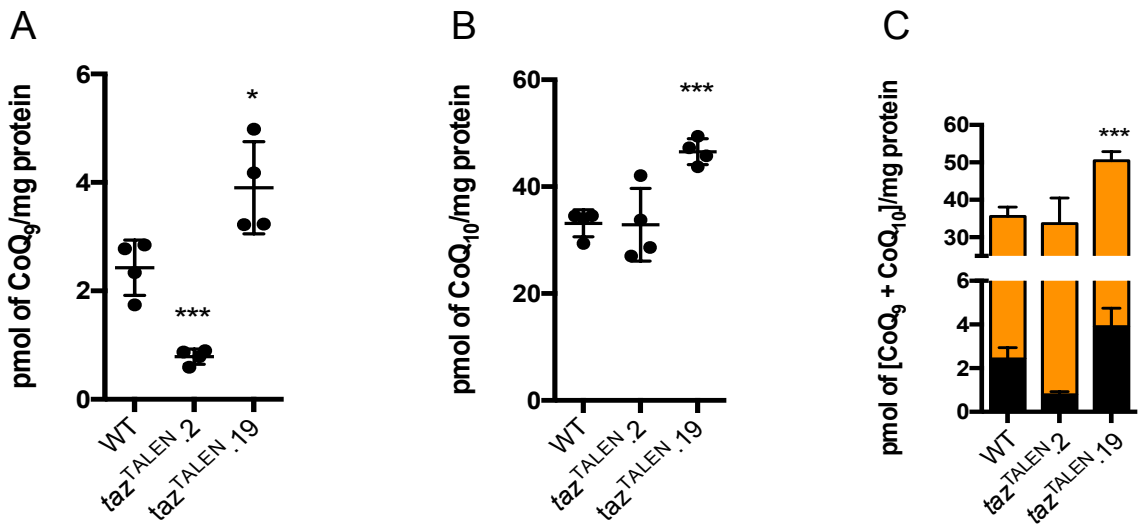

Figure 10. The HEK 293 *taz*^{TALEN}.19 cells contain increased amount of CoQ. Levels of **A)** CoQ_9, **B)** CoQ_{10}, and **C)** total CoQ were measured in whole cell lipid extracts from the *taz*^{TALEN}.2 and *taz*^{TALEN}.19 HEK 293 cell lines. The statistical analyses were performed using two-tailed nonparametric t-test from four biological replicates, comparing each mutant to the wild-type control. The error bar indicates mean ± SD, and the statistical significance is represented by *p < 0.05, **p < 0.01, ***p < 0.001 and ****p < 0.0001.

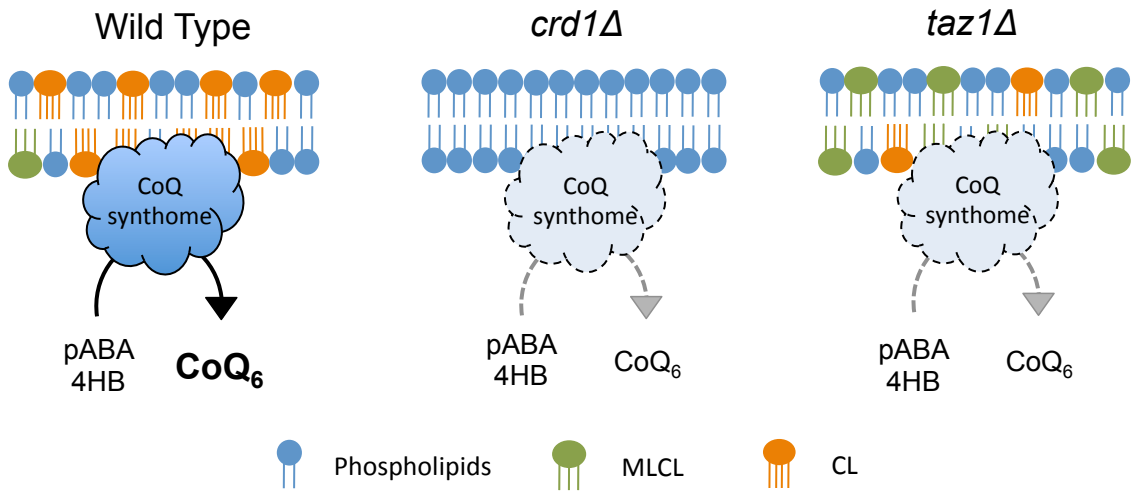

Figure 11. The presence of CL and CL remodeling is necessary to maintain CoQ synthome assembly and stability for efficient CoQ biosynthesis. Our results suggested a model of CL stabilizing the CoQ synthome for its optimal function. CL achieves this by interacting directly with individual Coq polypeptides of the CoQ synthome, and/or facilitating the overall assembly of the CoQ synthome at the mitochondrial inner membrane. The CoQ synthome became destabilized (represented by the dotted outlines) in the absence of CL (*crd1Δ*) and CL remodeling (*taz1Δ*), and resulted in inefficient CoQ biosynthesis from its precursors, pABA and 4HB (represented by the dotted lines).

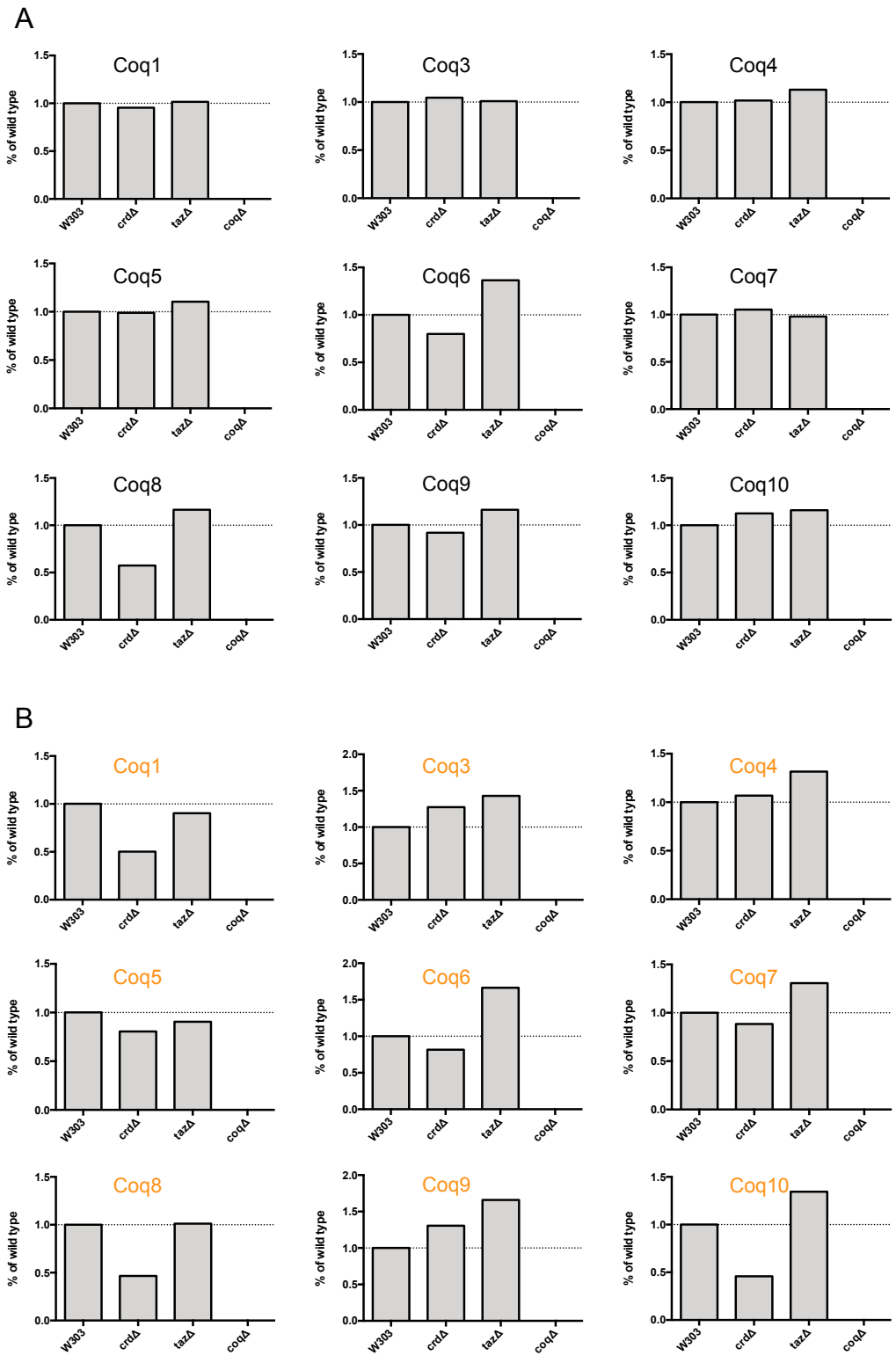
A
Coq1
Coq3
Coq4
Coq5
Coq6
Coq7
Coq8
Coq9
Coq10
% of wild type
W303
crdΔ
tazΔ
coqΔ
B
Coq1
Coq3
Coq4
Coq5
Coq6
Coq7
Coq8
Coq9
Coq10
% of wild type
W303
crdΔ
tazΔ
coqΔ

Supplemental Figure S1. Steady state levels of Coq polypeptides are more disturbed in the *crd1Δ* and *taz1Δ* mutants under respiration-requiring conditions. Relative Coq polypeptide levels shown in Figure 1 were quantified by band densitometry using Image J software (https://imagej.nih.gov/ij/). Yeast were cultured in galactose-containing medium (Panel A) or glycerol containing medium (Panel B). The densitometry reading of each *coqΔ* sample was subtracted from the reading of each sample blotted against the corresponding Coq polypeptide, then divided by the reading of the loading control Mdh1. The percentage of signal intensity from each sample relative to the wild-type control was plotted in the y-axis.

REFERENCES

1. Horvath, S. E., and G. Daum. 2013. Lipids of mitochondria. *Prog Lipid Res* **52**: 590-614.

2. Sperka-Gottlieb, C. D., A. Hermetter, F. Paltauf, and G. Daum. 1988. Lipid topology and physical properties of the outer mitochondrial membrane of the yeast, *Saccharomyces cerevisiae*. *Biochim Biophys Acta* **946**: 227-234.

3. Gaigg, B., R. Simbeni, C. Hrastnik, F. Paltauf, and G. Daum. 1995. Characterization of a microsomal subfraction associated with mitochondria of the yeast, *Saccharomyces cerevisiae*. Involvement in synthesis and import of phospholipids into mitochondria. *Biochim Biophys Acta* **1234**: 214-220.

4. Paradies, G., V. Paradies, V. De Benedictis, F. M. Ruggiero, and G. Petrosillo. 2014. Functional role of cardiolipin in mitochondrial bioenergetics. *Biochim Biophys Acta* **1837**: 408-417.

5. Jiang, F., H. S. Rizavi, and M. L. Greenberg. 1997. Cardiolipin is not essential for the growth of *Saccharomyces cerevisiae* on fermentable or non-fermentable carbon sources. *Mol Microbiol* **26**: 481-491.

6. Tuller, G., C. Hrastnik, G. Achleitner, U. Schiefthaler, F. Klein, and G. Daum. 1998. YDL142c encodes cardiolipin synthase (Cls1p) and is non-essential for aerobic growth of *Saccharomyces cerevisiae*. *FEBS Lett* **421**: 15-18.

7. Schlame, M., and M. L. Greenberg. 2017. Biosynthesis, remodeling and turnover of mitochondrial cardiolipin. *Biochim Biophys Acta Mol Cell Biol Lipids* **1862**: 3-7.

8. Beranek, A., G. Rechberger, H. Knauer, H. Wolinski, S. D. Kohlwein, and R. Leber. 2009. Identification of a cardiolipin-specific phospholipase encoded by the gene *CLD1* (YGR110W) in yeast. *J Biol Chem* **284**: 11572-11578.

9. Abe, M., Y. Hasegawa, M. Oku, Y. Sawada, E. Tanaka, Y. Sakai, and H. Miyoshi. 2016. Mechanism for remodeling of the acyl chain composition of cardiolipin catalyzed by *Saccharomyces cerevisiae* tafazzin. *J Biol Chem* **291**: 15491-15502.

10. Xu, Y., A. Malhotra, M. Ren, and M. Schlame. 2006. The enzymatic function of tafazzin. *J Biol Chem* **281**: 39217-39224.

11. Schlame, M. 2008. Cardiolipin synthesis for the assembly of bacterial and mitochondrial membranes. *J Lipid Res* **49**: 1607-1620.

12. Schlame, M., M. Ren, Y. Xu, M. L. Greenberg, and I. Haller. 2005. Molecular symmetry in mitochondrial cardiolipins. *Chem Phys Lipids* **138**: 38-49.

13. Malhotra, A., Y. Xu, M. Ren, and M. Schlame. 2009. Formation of molecular species of mitochondrial cardiolipin. 1. A novel transacylation mechanism to shuttle fatty acids between sn-1 and sn-2 positions of multiple phospholipid species. *Biochim Biophys Acta* **1791**: 314-320.

14. Schlame, M., D. Acehan, B. Berno, Y. Xu, S. Valvo, M. Ren, D. L. Stokes, and R. M. Epand. 2012. The physical state of lipid substrates provides transacylation specificity for tafazzin. *Nat Chem Biol* **8**: 862-869.

15. Schlame, M., Y. Xu, and M. Ren. 2017. The basis for acyl specificity in the tafazzin reaction. *J Biol Chem* **292**: 5499-5506.

16. Ren, M., C. K. Phoon, and M. Schlame. 2014. Metabolism and function of mitochondrial cardiolipin. *Prog Lipid Res* **55**: 1-16.

17. Claypool, S. M., Y. Oktay, P. Boontheung, J. A. Loo, and C. M. Koehler. 2008. Cardiolipin defines the interactome of the major ADP/ATP carrier protein of the mitochondrial inner membrane. *J Cell Biol* **182**: 937-950.

18. Saric, A., K. Andreau, A. S. Armand, I. M. Moller, and P. X. Petit. 2015. Barth syndrome: from mitochondrial dysfunctions associated with aberrant production of reactive oxygen species to pluripotent stem cell studies. *Front Genet* **6**: 359.

19. Ikon, N., and R. O. Ryan. 2017. Cardiolipin and mitochondrial cristae organization. *Biochim Biophys Acta Biomembr* **1859**: 1156-1163.

20. Lou, W., H. C. Ting, C. A. Reynolds, Y. Y. Tyurina, V. A. Tyurin, Y. Li, J. Ji, W. Yu, Z. Liang, D. A. Stoyanovsky, T. S. Anthonymuthu, M. A. Frasso, P. Wipf, J. S. Greenberger, H.

Bayir, V. E. Kagan, and M. L. Greenberg. 2018. Genetic re-engineering of polyunsaturated phospholipid profile of *Saccharomyces cerevisiae* identifies a novel role for Cld1 in mitigating the effects of cardiolipin peroxidation. *Biochim Biophys Acta Mol Cell Biol Lipids* **1863**: 1354-1368.

21. Planas-Iglesias, J., H. Dwarakanath, D. Mohammadyani, N. Yanamala, V. E. Kagan, and J. Klein-Seetharaman. 2015. Cardiolipin interactions with proteins. *Biophys J* **109**: 1282-1294.

22. Lange, C., J. H. Nett, B. L. Trumpower, and C. Hunte. 2001. Specific roles of protein-phospholipid interactions in the yeast cytochrome bc1 complex structure. *EMBO J* **20**: 6591-6600.

23. Shinzawa-Itoh, K., H. Aoyama, K. Muramoto, H. Terada, T. Kurauchi, Y. Tadehara, A. Yamasaki, T. Sugimura, S. Kurono, K. Tsujimoto, T. Mizushima, E. Yamashita, T. Tsukihara, and S. Yoshikawa. 2007. Structures and physiological roles of 13 integral lipids of bovine heart cytochrome *c* oxidase. *EMBO J* **26**: 1713-1725.

24. Eble, K. S., W. B. Coleman, R. R. Hantgan, and C. C. Cunningham. 1990. Tightly associated cardiolipin in the bovine heart mitochondrial ATP synthase as analyzed by ^{31}P nuclear magnetic resonance spectroscopy. *J Biol Chem* **265**: 19434-19440.

25. Acehan, D., A. Malhotra, Y. Xu, M. Ren, D. L. Stokes, and M. Schlame. 2011. Cardiolipin affects the supramolecular organization of ATP synthase in mitochondria. *Biophys J* **100**: 2184-2192.

26. Zhang, M., E. Mileykovskaya, and W. Dowhan. 2002. Gluing the respiratory chain together. Cardiolipin is required for supercomplex formation in the inner mitochondrial membrane. *J Biol Chem* **277**: 43553-43556.

27. Pfeiffer, K., V. Gohil, R. A. Stuart, C. Hunte, U. Brandt, M. L. Greenberg, and H. Schagger. 2003. Cardiolipin stabilizes respiratory chain supercomplexes. *J Biol Chem* **278**: 52873-52880.

28. Jiang, F., M. T. Ryan, M. Schlame, M. Zhao, Z. Gu, M. Klingenberg, N. Pfanner, and M. L. Greenberg. 2000. Absence of cardiolipin in the *crd1* null mutant results in decreased mitochondrial membrane potential and reduced mitochondrial function. *J Biol Chem* **275**: 22387-22394.

29. Xu, Y., C. K. Phoon, B. Berno, K. D'Souza, E. Hoedt, G. Zhang, T. A. Neubert, R. M. Epand, M. Ren, and M. Schlame. 2016. Loss of protein association causes cardiolipin degradation in Barth syndrome. *Nat Chem Biol* **12**: 641-647.

30. Awad, A. M., M. C. Bradley, L. Fernández-del-Río, A. Nag, H. S. Tsui, and C. F. Clarke. 2018. Coenzyme Q_{10} deficiencies: pathways in yeast and humans. *Essays Biochem* **62**: 361-376.

31. Stefely, J. A., and D. J. Pagliarini. 2017. Biochemistry of mitochondrial coenzyme Q biosynthesis. *Trends Biochem Sci* **42**: 824-843.

32. Kar, A., H. Beam, M. B. Borror, M. Luckow, X. Gao, and S. L. Rea. 2016. *CLD1* reverses the ubiquinone insufficiency of mutant *cat5/coq7* in a *Saccharomyces cerevisiae* model system. *PLoS One* **11**: e0162165.

33. Xie, L. X., E. J. Hsieh, S. Watanabe, C. M. Allan, J. Y. Chen, U. C. Tran, and C. F. Clarke. 2011. Expression of the human atypical kinase ADCK3 rescues coenzyme Q biosynthesis and phosphorylation of Coq polypeptides in yeast *coq8* mutants. *Biochim Biophys Acta* **1811**: 348-360.

34. Stefely, J. A., A. G. Reidenbach, A. Ulbrich, K. Oruganty, B. J. Floyd, A. Jochem, J. M. Saunders, I. E. Johnson, C. E. Minogue, R. L. Wrobel, G. E. Barber, D. Lee, S. Li, N. Kannan, J. J. Coon, C. A. Bingman, and D. J. Pagliarini. 2015. Mitochondrial ADCK3 employs an atypical protein kinase-like fold to enable coenzyme Q biosynthesis. *Mol Cell* **57**: 83-94.

35. Reidenbach, A. G., Z. A. Kemmerer, D. Aydin, A. Jochem, M. T. McDevitt, P. D. Hutchins, J. L. Stark, J. A. Stefely, T. Reddy, A. S. Hebert, E. M. Wilkerson, I. E. Johnson, C. A. Bingman, J. L. Markley, J. J. Coon, M. Dal Peraro, and D. J. Pagliarini. 2018. Conserved lipid

and small-molecule modulation of COQ8 reveals regulation of the ancient kinase-like UbiB family. *Cell Chem Biol* **25**: 154-165 e111.

36. Lohman, D. C., D. Aydin, H. C. Von Bank, R. W. Smith, V. Linke, E. Weisenhorn, M. T. McDevitt, P. Hutchins, E. M. Wilkerson, B. Wancewicz, J. Russell, M. S. Stefely, E. T. Beebe, A. Jochem, J. J. Coon, C. A. Bingman, M. Dal Peraro, and D. J. Pagliarini. 2019. An isoprene lipid-binding protein promotes eukaryotic coenzyme Q biosynthesis. *Mol Cell* **73**: 763-774 e710.

37. Burke, D., Dawson, D., and Stearns, T. . 2000. Methods in yeast genetics. *Cold spring Harbor Laboratory Press*.

38. Barkovich, R. J., A. Shtanko, J. A. Shepherd, P. T. Lee, D. C. Myles, A. Tzagoloff, and C. F. Clarke. 1997. Characterization of the *COQ5* gene from *Saccharomyces cerevisiae*. Evidence for a C-methyltransferase in ubiquinone biosynthesis. *J Biol Chem* **272**: 9182-9188.

39. Allan, C. M., A. M. Awad, J. S. Johnson, D. I. Shirasaki, C. Wang, C. E. Blaby-Haas, S. S. Merchant, J. A. Loo, and C. F. Clarke. 2015. Identification of Coq11, a new coenzyme Q biosynthetic protein in the CoQ-Synthome in *Saccharomyces cerevisiae*. *J Biol Chem* **290**: 7517-7534.

40. Lu, Y. W., L. Galbraith, J. D. Herndon, Y. L. Lu, M. Pras-Raves, M. Vervaart, A. Van Kampen, A. Luyf, C. M. Koehler, J. M. McCaffery, E. Gottlieb, F. M. Vaz, and S. M. Claypool. 2016. Defining functional classes of Barth syndrome mutation in humans. *Hum Mol Genet* **25**: 1754-1770.

41. Glick, B. S., and L. A. Pon. 1995. Isolation of highly purified mitochondria from *Saccharomyces cerevisiae*. *Methods Enzymol* **260**: 213-223.

42. Schagger, H., W. A. Cramer, and G. von Jagow. 1994. Analysis of molecular masses and oligomeric states of protein complexes by blue native electrophoresis and isolation of membrane protein complexes by two-dimensional native electrophoresis. *Anal Biochem* **217**: 220-230.

43. Wittig, I., H. P. Braun, and H. Schagger. 2006. Blue native PAGE. *Nat Protoc* **1**: 418-428.

44. Marbois, B., L. X. Xie, S. Choi, K. Hirano, K. Hyman, and C. F. Clarke. 2010. para-Aminobenzoic acid is a precursor in coenzyme Q_6 biosynthesis in *Saccharomyces cerevisiae*. *J Biol Chem* **285**: 27827-27838.

45. Fernández-del-Río, L., A. Nag, E. Gutiérrez Casado, J. Ariza, A. M. Awad, A. I. Joseph, O. Kwon, E. Verdin, R. de Cabo, C. Schneider, J. Z. Torres, M. I. Burón, C. F. Clarke, and J. M. Villalba. 2017. Kaempferol increases levels of coenzyme Q in kidney cells and serves as a biosynthetic ring precursor. *Free Radic Biol Med* **110**: 176-187.

46. He, C. H., L. X. Xie, C. M. Allan, U. C. Tran, and C. F. Clarke. 2014. Coenzyme Q supplementation or over-expression of the yeast Coq8 putative kinase stabilizes multi-subunit Coq polypeptide complexes in yeast *coq* null mutants. *Biochim Biophys Acta* **1841**: 630-644.

47. Hsieh, E. J., P. Gin, M. Gulmezian, U. C. Tran, R. Saiki, B. N. Marbois, and C. F. Clarke. 2007. *Saccharomyces cerevisiae* Coq9 polypeptide is a subunit of the mitochondrial coenzyme Q biosynthetic complex. *Arch Biochem Biophys* **463**: 19-26.

48. Tran, U. C., and C. F. Clarke. 2007. Endogenous synthesis of coenzyme Q in eukaryotes. *Mitochondrion* **7 Suppl**: S62-71.

49. Zardeneta, G., and P. M. Horowitz. 1993. Physical characterization of a reactivatable liposome-bound rhodanese folding intermediate. *Biochemistry* **32**: 13941-13948.

50. Sedlak, E., and N. C. Robinson. 1999. Phospholipase A_2 digestion of cardiolipin bound to bovine cytochrome c oxidase alters both activity and quaternary structure. *Biochemistry* **38**: 14966-14972.

51. Hoffmann, B., A. Stockl, M. Schlame, K. Beyer, and M. Klingenberg. 1994. The reconstituted ADP/ATP carrier activity has an absolute requirement for cardiolipin as shown in cysteine mutants. *J Biol Chem* **269**: 1940-1944.

52. Khadria, A. S., B. K. Mueller, J. A. Stefely, C. H. Tan, D. J. Pagliarini, and A. Senes. 2014. A Gly-zipper motif mediates homodimerization of the transmembrane domain of the mitochondrial kinase ADCK3. *J Am Chem Soc* **136**: 14068-14077.

53. Claypool, S. M., P. Boontheung, J. M. McCaffery, J. A. Loo, and C. M. Koehler. 2008. The cardiolipin transacylase, tafazzin, associates with two distinct respiratory components providing insight into Barth syndrome. *Mol Biol Cell* **19**: 5143-5155.

54. He, C. H., D. S. Black, T. P. Nguyen, C. Wang, C. Srinivasan, and C. F. Clarke. 2015. Yeast Coq9 controls deamination of coenzyme Q intermediates that derive from para-aminobenzoic acid. *Biochim Biophys Acta* **1851**: 1227-1239.

55. Gu, Z., F. Valianpour, S. Chen, F. M. Vaz, G. A. Hakkaart, R. J. Wanders, and M. L. Greenberg. 2004. Aberrant cardiolipin metabolism in the yeast *taz1* mutant: a model for Barth syndrome. *Mol Microbiol* **51**: 149-158.

56. Baile, M. G., M. Sathappa, Y. W. Lu, E. Pryce, K. Whited, J. M. McCaffery, X. Han, N. N. Alder, and S. M. Claypool. 2014. Unremodeled and remodeled cardiolipin are functionally indistinguishable in yeast. *J Biol Chem* **289**: 1768-1778.

57. Baile, M. G., K. Whited, and S. M. Claypool. 2013. Deacylation on the matrix side of the mitochondrial inner membrane regulates cardiolipin remodeling. *Mol Biol Cell* **24**: 2008-2020.

58. Ye, C., W. Lou, Y. Li, I. A. Chatzispyrou, M. Huttemann, I. Lee, R. H. Houtkooper, F. M. Vaz, S. Chen, and M. L. Greenberg. 2014. Deletion of the cardiolipin-specific phospholipase Cld1 rescues growth and life span defects in the tafazzin mutant: implications for Barth syndrome. *J Biol Chem* **289**: 3114-3125.

59. Moon, Y., K. H. Lee, J. H. Park, D. Geum, and K. Kim. 2005. Mitochondrial membrane depolarization and the selective death of dopaminergic neurons by rotenone: protective effect of coenzyme Q_{10}. *J Neurochem* **93**: 1199-1208.

60. Papucci, L., N. Schiavone, E. Witort, M. Donnini, A. Lapucci, A. Tempestini, L. Formigli, S. Zecchi-Orlandini, G. Orlandini, G. Carella, R. Brancato, and S. Capaccioli. 2003. Coenzyme

Q_{10} prevents apoptosis by inhibiting mitochondrial depolarization independently of its free radical scavenging property. *J Biol Chem* **278**: 28220-28228.

61. Menke, T., G. Gille, F. Reber, B. Janetzky, W. Andler, R. H. Funk, and H. Reichmann. 2003. Coenzyme Q_{10} reduces the toxicity of rotenone in neuronal cultures by preserving the mitochondrial membrane potential. *Biofactors* **18**: 65-72.

62. Ting, H. C., Y. J. Chao, and Y. H. Hsu. 2015. Polyunsaturated fatty acids incorporation into cardiolipin in H9c2 cardiac myoblast. *J Nutr Biochem* **26**: 769-775.

63. Tyurina, Y. Y., W. Lou, F. Qu, V. A. Tyurin, D. Mohammadyani, J. Liu, M. Huttemann, M. A. Frasso, P. Wipf, H. Bayir, M. L. Greenberg, and V. E. Kagan. 2017. Lipidomics characterization of biosynthetic and remodeling pathways of cardiolipins in genetically and nutritionally manipulated yeast cells. *ACS Chem Biol* **12**: 265-281.

64. Hill, S., C. R. Lamberson, L. Xu, R. To, H. S. Tsui, V. V. Shmanai, A. V. Bekish, A. M. Awad, B. N. Marbois, C. R. Cantor, N. A. Porter, C. F. Clarke, and M. S. Shchepinov. 2012. Small amounts of isotope-reinforced polyunsaturated fatty acids suppress lipid autoxidation. *Free Radic Biol Med* **53**: 893-906.

65. Andreyev, A. Y., H. S. Tsui, G. L. Milne, V. V. Shmanai, A. V. Bekish, M. A. Fomich, M. N. Pham, Y. Nong, A. N. Murphy, C. F. Clarke, and M. S. Shchepinov. 2015. Isotope-reinforced polyunsaturated fatty acids protect mitochondria from oxidative stress. *Free Radic Biol Med* **82**: 63-72.

66. Chen, S., Q. He, and M. L. Greenberg. 2008. Loss of tafazzin in yeast leads to increased oxidative stress during respiratory growth. *Mol Microbiol* **68**: 1061-1072.

67. Hsu, P., and Y. Shi. 2017. Regulation of autophagy by mitochondrial phospholipids in health and diseases. *Biochim Biophys Acta Mol Cell Biol Lipids* **1862**: 114-129.

68. Shi, Y. 2010. Emerging roles of cardiolipin remodeling in mitochondrial dysfunction associated with diabetes, obesity, and cardiovascular diseases. *J Biomed Res* **24**: 6-15.

69. Paradies, G., G. Petrosillo, V. Paradies, and F. M. Ruggiero. 2011. Mitochondrial dysfunction in brain aging: role of oxidative stress and cardiolipin. *Neurochem Int* **58**: 447-457.

70. Fouret, G., E. Tolika, J. Lecomte, B. Bonafos, M. Aoun, M. P. Murphy, C. Ferreri, C. Chatgilialoglu, E. Dubreucq, C. Coudray, and C. Feillet-Coudray. 2015. The mitochondrial-targeted antioxidant, MitoQ, increases liver mitochondrial cardiolipin content in obesogenic diet-fed rats. *Biochim Biophys Acta* **1847**: 1025-1035.

71. McManus, M. J., M. P. Murphy, and J. L. Franklin. 2011. The mitochondria-targeted antioxidant MitoQ prevents loss of spatial memory retention and early neuropathology in a transgenic mouse model of Alzheimer's disease. *J Neurosci* **31**: 15703-15715.

72. Skulachev, V. P., Y. N. Antonenko, D. A. Cherepanov, B. V. Chernyak, D. S. Izyumov, L. S. Khailova, S. S. Klishin, G. A. Korshunova, K. G. Lyamzaev, O. Y. Pletjushkina, V. A. Roginsky, T. I. Rokitskaya, F. F. Severin, Severina, II, R. A. Simonyan, M. V. Skulachev, N. V. Sumbatyan, E. I. Sukhanova, V. N. Tashlitsky, T. A. Trendeleva, M. Y. Vyssokikh, and R. A. Zvyagilskaya. 2010. Prevention of cardiolipin oxidation and fatty acid cycling as two antioxidant mechanisms of cationic derivatives of plastoquinone (SkQs). *Biochim Biophys Acta* **1797**: 878-889.

73. Gin, P., and C. F. Clarke. 2005. Genetic evidence for a multi-subunit complex in coenzyme Q biosynthesis in yeast and the role of the Coq1 hexaprenyl diphosphate synthase. *J Biol Chem* **280**: 2676-2681.

74. Do, T. Q., J. R. Schultz, and C. F. Clarke. 1996. Enhanced sensitivity of ubiquinone-deficient mutants of *Saccharomyces cerevisiae* to products of autoxidized polyunsaturated fatty acids. *Proc Natl Acad Sci U S A* **93**: 7534-7539.

75. Hsu, A. Y., T. Q. Do, P. T. Lee, and C. F. Clarke. 2000. Genetic evidence for a multi-subunit complex in the O-methyltransferase steps of coenzyme Q biosynthesis. *Biochim Biophys Acta* **1484**: 287-297.

76. Gin, P., A. Y. Hsu, S. C. Rothman, T. Jonassen, P. T. Lee, A. Tzagoloff, and C. F. Clarke. 2003. The *Saccharomyces cerevisiae COQ6* gene encodes a mitochondrial flavin-dependent monooxygenase required for coenzyme Q biosynthesis. *J Biol Chem* **278**: 25308-25316.

77. Marbois, B. N., and C. F. Clarke. 1996. The *COQ7* gene encodes a protein in *Saccharomyces cerevisiae* necessary for ubiquinone biosynthesis. *J Biol Chem* **271**: 2995-3004.

78. Johnson, A., P. Gin, B. N. Marbois, E. J. Hsieh, M. Wu, M. H. Barros, C. F. Clarke, and A. Tzagoloff. 2005. *COQ9*, a new gene required for the biosynthesis of coenzyme Q in *Saccharomyces cerevisiae*. *J Biol Chem* **280**: 31397-31404.

79. Barros, M. H., A. Johnson, P. Gin, B. N. Marbois, C. F. Clarke, and A. Tzagoloff. 2005. The *Saccharomyces cerevisiae COQ10* gene encodes a START domain protein required for function of coenzyme Q in respiration. *J Biol Chem* **280**: 42627-42635.

80. Poon, W. W., R. J. Barkovich, A. Y. Hsu, A. Frankel, P. T. Lee, J. N. Shepherd, D. C. Myles, and C. F. Clarke. 1999. Yeast and rat Coq3 and *Escherichia coli* UbiG polypeptides catalyze both O-methyltransferase steps in coenzyme Q biosynthesis. *J Biol Chem* **274**: 21665-21672.

81. Belogrudov, G. I., P. T. Lee, T. Jonassen, A. Y. Hsu, P. Gin, and C. F. Clarke. 2001. Yeast *COQ4* encodes a mitochondrial protein required for coenzyme Q synthesis. *Arch Biochem Biophys* **392**: 48-58.

82. Baba, S. W., G. I. Belogrudov, J. C. Lee, P. T. Lee, J. Strahan, J. N. Shepherd, and C. F. Clarke. 2004. Yeast Coq5 C-methyltransferase is required for stability of other polypeptides involved in coenzyme Q biosynthesis. *J Biol Chem* **279**: 10052-10059.

83. Tran, U. C., B. Marbois, P. Gin, M. Gulmezian, T. Jonassen, and C. F. Clarke. 2006. Complementation of *Saccharomyces cerevisiae coq7* mutants by mitochondrial targeting of the

Escherichia coli UbiF polypeptide: two functions of yeast Coq7 polypeptide in coenzyme Q biosynthesis. *J Biol Chem* **281**: 16401-16409.

84. Hsieh, E. J., J. B. Dinoso, and C. F. Clarke. 2004. A $tRNA^{TRP}$ gene mediates the suppression of cbs2-223 previously attributed to *ABC1/COQ8*. *Biochem Biophys Res Commun* **317**: 648-653.

85. Eisenberg-Bord, M., H. S. Tsui, D. Antunes, L. Fernández-del-Río, M. C. Bradley, C. D. Dunn, T. P. T. Nguyen, D. Rapaport, C. F. Clarke, and M. Schuldiner. 2019. The ER-Mitochondria Encounter Structure (ERMES) complex coordinates coenzyme Q biosynthesis. *Contact* **2**: 1-14.

CHAPTER 6

Protein partners and lipid ligands: clues to the function of the Coq10 polypeptide in respiration and CoQ biosynthesis

INTRODUCTION

S. cerevisiae Coq10 is a unique Coq protein because its absence causes respiratory deficiency, but not CoQ deficiency (1). In contrast, deletion of any of the *COQ1-COQ9* genes renders yeast CoQ-less as well as respiratory deficient (2). The respiratory deficiency in the *coq10Δ* mutant is thought to result from a defect in delivering CoQ to its proper site in complex III, and the failure to transfer electrons through cytochrome *c* (3). Additionally, the yeast *coq10Δ* mutant is exquisitely sensitive to polyunsaturated fatty acid (PUFA) treatment, suggesting that the antioxidant function of CoQ also relies on Coq10 to transfer CoQ to sites where it functions (4). Coq10 co-purifies with CoQ (1, 5), and in vitro Coq10-CoQ binding assays identify the quinone ring as the feature important for binding (4). Interestingly, the steroidogenic acute regulatory (StAR) related lipid transfer (START) domain of Coq10 mediates its binding to CoQ, and also allows binding to late-stage CoQ-intermediates (4), implying possible role(s) in biosynthesis or sequestering CoQ-intermediates.

Recent studies indicate that several Coq polypeptide members of the CoQ synthome (including Coq3, Coq4, Coq5, Coq6, Coq7 and Coq9) are organized in distinct domains within mitochondria that coincide with the endoplasmic reticulum (ER) and mitochondria junctions, and reside in close proximity to the ER-mitochondria encounter structure (ERMES) complex and the Ltc1/Tom70 complex, which consists of the ER-localized membrane sterol transporter Ltc1 and the mitochondrial import receptor Tom70 at the mitochondrial outer membrane (6, 7). In contrast, Coq10 does not assemble into specific domains, and is uniformly distributed within the mitochondria (7). However, the number of CoQ domains within mitochondria is significantly reduced in cells lacking Coq10 (6, 7).

One approach to decipher Coq10's function is to look at the proteins that it interacts with. The monomeric form of unprocessed Coq10 has a molecular weight of 24 kDa, but the

digitonin-solubilized Coq10 from mitochondrial extract migrates in a fraction corresponding to a high molecular mass complex >140 kDa on a sucrose gradient (1). Thus, characterization of the high molecular weight Coq10-containing complex has the potential to provide important clues about the molecular interactions required for Coq10 function. A second approach is to purify Coq10 and investigate the ability of Coq10 to mediate lipid transfer by liposome binding assays. Members of the START domain family bind to lipids such as cholesterol and polyketides at their hydrophobic cavities, and they function as lipid transporters and/or sensors for regulating lipid metabolism, homeostasis, as well as cell signaling (8). Liposome binding assays would enable tests of Coq10's function as a lipid transfer protein in addition to its lipid binding ability. This chapter includes some of the preliminary results and describes methods used to conduct these experiments.

MATERIALS AND METHODS

Yeast strains and growth media

S. cerevisiae strains used in this study are described in Table 1. Yeast growth media included YPD (1% Bacto yeast extract, 2% Bacto peptone, 2% dextrose), YPG (1% Bacto yeast extract, 2% Bacto peptone, 3% glycerol), YPGal (1% Bacto yeast extract, 2% Bacto peptone, 2% galactose, 0.1% dextrose), synthetic dextrose minimal-Complete (SD−Complete) and synthetic dextrose minimal without histidine (SD−His) (0.18% Difco yeast nitrogen base without amino acids and ammonium sulfate, 0.5% $(NH_4)_2SO_4$, 0.14% NaH_2PO_4, 2% dextrose, complete amino acid supplement or amino acid supplement lacking histidine) (9, 10), drop out dextrose (DOD) medium (0.68% yeast nitrogen base with ammonium sulfate without folic acid without pABA, 0.14% NaH_2PO_4, 2% dextrose, complete amino acid supplement). Solid media contained additional 2% Bacto agar.

Construction of Protein C-cMyc$_9$-tagged yeast strains

The coding sequence for the Protein C (PC) epitope (EDQVDPRLIDGK), in tandem with nine repeats of cMyc epitope (EQKLISEEDL), and a *HIS5* auxotrophic marker was amplified from pGA2254 (11) using primers containing 5' flanking regions homologous to ~50 base pair upstream and ~50 base pair downstream of the stop codon of the *COQ4*, *COQ5*, and *COQ10* ORF for chromosomal integration (Table 2). Following PCR cleanup (Thermo Fisher Scientific), the PCR products were transformed into the yeast W303 wild-type cells using the lithium acetate/PEG method (12), and transformed cells were selected on SD−His plate medium. Colony PCR and DNA sequencing (Laragen) verified the integration of the PCcMyc$_9$ tag at the correct gene locus.

Yeast mitochondria isolation

Yeast strains grown in YPD were sub-inoculated into 600 mL YPGal medium for overnight growth at 30°C 250 rpm until the cell density had reached <4.0 OD_{600}/mL. The yeast cells were harvested, spheroplasted, and the mitochondria were isolated as described previously (13), in the presence of Complete EDTA-free protease inhibitor mixture (Roche), phosphatase inhibitor cocktail set II (EMD Millipore) and phosphatase inhibitor cocktail set 3 (Sigma-Aldrich) over Nycodenz (Sigma-Aldrich). Gradient purified mitochondria were flash frozen in liquid nitrogen and stored at −80°C until use. The isolated mitochondrial protein concentration was measured by the bicinchoninic acid (BCA) assay (Thermo Fisher Scientific) using bovine serum albumin as the standard (Thermo Fisher Scientific).

Immunoblot analysis of PCcMyc$_9$ tagged proteins

Purified mitochondria were resuspended in SDS sample buffer (50 mM Tris, pH 6.8, 10% glycerol, 2% SDS, 0.1% bromophenol blue, and 1.33% β-mercaptoethanol), and separated on 12% Tris-glycine polyacrylamide gels. Proteins were subsequently transferred to 0.45 µm nitrocellulose membrane (Bio-Rad), and blocked with blocking buffer (0.5% BSA, 0.1% Tween 20, 0.02% SDS in phosphate-buffered saline). The presence of PCcMyc$_9$-tagged proteins was confirmed with rabbit polyclonal antibodies against Coq4 (1:2,000), Coq5 (1:5,000), and Coq10 (1:400), as well as with 0.25 µg/mL mouse anti-cMyc polyclonal antibody all prepared in blocking buffer, followed by 1:10,000 dilution of the secondary IRDye 680LT goat anti-rabbit IgG antibody, or IRDye 800CW goat anti-mouse IgG antibody (LiCOR) in the same blocking buffer. Immunoblot images were visualized with LiCOR Odyssey Infrared Scanner (LiCOR).

Two-dimensional blue native/SDS-PAGE analysis of the high molecular weight complexes

Two-dimensional blue native/SDS-PAGE was performed as described previously (14-16). Aliquots of isolated mitochondria were solubilized at 4 mg/mL with solubilization buffer (11

mM HEPES, pH 7.4, 0.33 M sorbitol, 1x NativePAGE sample buffer (Thermo Fisher Scientific), 16 mg/mL digitonin (Biosynth), Complete EDTA-free protease inhibitor mixture, phosphatase inhibitor cocktail set II, and phosphatase inhibitor cocktail set 3) for 1 hour on ice with mixing every 10 min. After centrifugation at 100,000 *g* for 10 min, the soluble protein concentration in the supernatant was measured by BCA assay. Aliquots of 80 µg of soluble protein were mixed with the NativePAGE 5% G-250 sample additive (Thermo Fisher Scientific) to a final concentration of 0.25%, and were subjected to gel electrophoresis on NativePAGE 4-16% Bis-Tris gel (Thermo Fisher Scientific) in the first dimension, followed by 12% Tris-glycine polyacrylamide gel in the second dimension. Immunoblot analyses of the CoQ synthome and Coq10-containing complex were performed as described above using antibodies against Coq4 and Coq9 (1:1,000), and Coq10.

Analyses of de novo and steady state levels of CoQ_6

Yeast whole cell lipid extraction, and quantification of de novo and steady state levels of CoQ_6 by reversed phase (RP)-HPLC tandem mass spectrometry were described previously (4, 17). Overnight cultures of yeast wild type, *coq4Δ*, *coq5Δ*, *coq10Δ*, Coq4PCcMyc$_9$, Coq5PCcMyc$_9$, and Coq10PCcMyc$_9$ grown in SD-Complete medium were back diluted with DOD medium to 0.1 OD_{600}/mL and grown to 0.5 OD_{600}/mL at 30°C 250 rpm. To trace de novo CoQ_6 biosynthesis, $^{13}C_6$-labeled ring precursors pABA or 4HB were dissolved in ethanol and added to yeast cultures at a final concentration of 5 µg/mL. Vehicle control samples contained a final concentration of 0.1% ethanol. The cells were incubated for three hours at 30°C 250 rpm before triplicates of 5 mL culture were harvested. Yeast whole cell lipids were extracted twice with 2 mL petroleum ether in the presence of internal standard CoQ_4 from methanol dissolved cell pellets, and dried under a stream N_2 gas. A series of CoQ_6 standards containing CoQ_4 were prepared and lipid extracted concurrently with yeast samples to construct a CoQ_6 standard curve. The dried lipid extracts were reconstituted in 200 µL of 0.5 mg/mL benzoquinone in

ethanol and were subjected to mass spectrometry analysis with a 4000 QTRAP linear MS/MS spectrometer (Applied Biosystems). Lipid extracts were separated on a Luna phenyl-hexyl column (100 x 4.6 mm, 5 µm; Phenomenex) with mobile phase of solvent A (95:5 methanol/isopropanol, 2.5 mM ammonium formate) and solvent B (isopropanol, 2.5 mM ammonium formate). Unlabeled and $^{13}C_6$-labeled CoQ_6 eluted from the column with a linearly increased gradient of solvent B from 0 to 10%. Elution of CoQ_4, CoQ_6 and $^{13}C_6$-CoQ_6 at distinct retention times were monitored under multiple reaction monitoring mode (MRM) scanning precursor to product ion transitions: CoQ_4 *m/z* 455.4/197.0, CoQ_6 *m/z* 591.4/197.0, $^{13}C_6$-CoQ_6 *m/z* 597.4/203.0, and *m/z* 472.0/197.0, *m/z* 608.0/197.0, *m/z* 614.0/203.0 for their ammoniated adducts. Analyst 1.4.2 software (Applied Biosystems) was used for data acquisition and processing.

Tandem affinity purification of PCcMyc$_9$-tagged proteins

Aliquots of 12 mg of purified mitochondria were solubilized at 4 mg/mL with solubilization buffer (20 mM HEPES-KOH, pH 7.4, 100 mM NaCl, 10% glycerol, 1 mM $CaCl_2$, 8 mg/mL n-dodecyl β-D-maltoside (DDM), Complete EDTA-free protease inhibitor mixture, phosphatase inhibitor cocktail set II, and phosphatase inhibitor cocktail set 3) for 1 hour on ice with mixing every 10 min. The insoluble fraction was removed by centrifugation at 100,000 *g* at 4°C for 15 min. The remaining supernatant was mixed with 8 mL of PC resin equilibration buffer (20 mM HEPES-KOH, pH 7.4, 100 mM NaCl, 1 mM $CaCl_2$), and incubated with 1 mL anti-PC resin (Roche) at 4°C for 2 hours. After the first affinity binding, the anti-PC resin mitochondrial lysate mixture was applied to a gravity column, washed four times each with 10 mL anti-PC wash buffer (20 mM HEPES-KOH, pH 7.4, 100 mM NaCl, 1 mM $CaCl_2$, 1 mg/mL DDM), followed by elution of bound proteins with 10 mL of anti-PC elution buffer (25 mM Tris-HCl, pH 7.2, 150 mM NaCl, 5 mM EDTA, pH 8.0, 10% glycerol, 1 mg/mL DDM). The collected eluate was incubated with 1 mL anti-cMyc resin (Thermo Fisher Scientific) pre-equilibrated with anti-cMyc equilibration

buffer (25 mM Tris-HCl, pH 7.2, 150 mM NaCl) for second affinity binding at 4°C for additional 2 hours. The anti-cMyc resin slurry was applied to a gravity column, washed four times each with 10 mL anti-cMyc wash buffer (25 mM Tris-HCl, pH 7.2, 150 mM NaCl, 1 mg/mL DDM). The bound protein was eluted twice each with 1 mL anti-cMyc elution buffer (25 mM Tris-HCl, pH 7.2, 150 mM NaCl, 1 mg/mL DDM, 1 mg/mL cMyc peptide (APExBio)) at room temperature. The final eluates were kept at −80°C until use.

In-gel trypsin digestion and proteomic analysis

A mixture containing 500 µL of eluate 1 and 500 µL of eluate 2 from the tandem affinity purification were concentrated to a final volume of ~10 µL using a SpeedVac at 60°C, and resuspended in 42 µL of SDS sample buffer. The proteins were separated on an 8-16% Criterion TGX stain-free gel (Bio-Rad), and stained with a 1:1 mixture of fresh and used SYPRO Ruby (Thermo Fisher Scientific) for visualization as described previously (18). Sample lanes from the SYPRO Ruby stained gel were sliced into small pieces and subjected to in-gel trypsin digestion, followed by LC-MS/MS analysis of the digested peptides as described (18). Confirmation of potential Coq10-interacting proteins in the tandem affinity purification eluates was performed by immunoblot analyses as described above using rabbit polyclonal antibodies against Ssc1 (1:15,000), Cor1 (1:4,000), Qcr2 (1:4,000), Atp1 (1:4,000), and Atp2 (1:4,000), or mouse polyclonal antibody against Rip1 (1:4,000), followed by 1:10,000 dilution of either goat anti-rabbit or goat anti-mouse secondary antibody conjugated to horseradish peroxidase (Calbiochem). Blots were visualized using Supersignal West Pico chemiluminescent substrate (Thermo Fisher Scientific).

Cloning of Coq10$^{N\Delta30}$

DNA encoding *S. cerevisiae* Coq10$^{N\Delta30}$ (residues 31-207) was cloned into the pHis$_6$SUMO vector (LifeSensors), resulting a fusion protein consists of an N-terminal six-residue

His-tag followed by a SUMO-tag, and the mature form of Coq10 without its mitochondrial targeting pre-sequence. Residues 31-207 of Coq10 was amplified from *S. cerevisiae* wild-type W303 strain genomic DNA with Phusion High-Fidelity PCR Master Mix (New England BioLabs) using primers 5'- GGCCGGATCCTTTTTTGGTTTGAGCGGTAC-3' and 5'-GGCCCTCGAGTCACGGAGAGCCTTCTTTA-3' obtained from Eurofins Genomics. Following amplification, the PCR product was double-digested with restriction enzymes *Bam*HI and *Xho*I (New England BioLabs) at 37°C for 3 hours, and the pHis$_6$SUMO vector was double-digested with *Bam*HI and *Xho*I at 37°C for 2 hours and additional 1 hour at 37°C with addition of calf intestinal alkaline phosphatase (CIP) (New England BioLabs). Both the digested PCR product and pHis$_6$SUMO vector were subsequently purified using QIAquick Gel Extraction Kit (Qiagen). Ligation was carried out overnight at 16°C using T4 DNA ligase (New England BioLabs). After overnight incubation, the ligation mixture was transformed into DH5α competent *Escherichia coli* cells (Thermo Fisher Scientific) and single colonies were selected on LB plates containing 50 μg/mL kanamycin incubated overnight at 37°C. Cloning was confirmed by DNA sequencing (Laragen).

Expression and purification of Coq10$^{N\Delta30}$

The His$_6$SUMO-tagged Coq10$^{N\Delta30}$ was expressed in transformed *E. coli* BL21 (DE3) cells (Invitrogen). The *E. coli* culture was grown in LB with 50 μg/mL kanamycin at 37°C to an OD_{600} of 0.6-0.8 before the expression was induced with 1 mM β-D thiogalactopyranoside (IPTG) at 16°C for 18 hours. The cells were harvested by centrifugation at 4,500 *g* for 10 min at 4°C and lysed with M-110P microfluidizer (Microfluidics) in lysis buffer (50 mM NaH_2PO_4, pH 8.0, 500 mM NaCl, 10 mM imidazole, 10% glycerol, 1 mM DTT, 0.1% Triton X-100, 1 mM phenylmethylsulfonyl fluoride, Complete EDTA-free protease inhibitor). The crude lysate was centrifuged at 10,000 *g* for 45 min at 4°C and the collected soluble fraction was incubated with pre-equilibrated Ni-NTA resins (Qiagen) for 2 hours at 4°C. To remove impurities, Ni-NTA resins

were step washed three times each with 2 column volume (CV) of wash buffer (20 mM or 35 mM imidazole in 50 mM NaH_2PO_4, pH 8.0, 300 mM NaCl, 10% glycerol, 1 mM DTT, and 0.1% Triton X-100), and the protein was eluted five times each with 1.5 CV of wash buffer containing 200 mM imidazole. The protein eluates were pooled and concentrated by Amicon (Millipore), and recombinant His-tagged SUMO protease, also known as Ulp1 was added to the concentrated eluate (approximately 400 µg of His-tagged Ulp1 was added to every 10 mL of concentrated eluate) to cleave the His_6SUMO moiety during overnight dialysis against 50 mM NaH_2PO_4, pH 8.0, 300 mM NaCl, 10% glycerol, 1 mM DTT, and 0.1% Triton X-100 at 4°C using 10K MWCO Slide-A-Lyzer dialysis cassette (Thermo Fisher Scientific). After overnight dialysis, the protein inside the dialysis cassette was removed and allowed to incubate with pre-equilibrated Ni-NTA resins for 2 hours at 4°C to remove His-tagged Ulp1 protease, His_6SUMO moiety released from Ulp1 cleavage, and any uncleaved His_6SUMO-tagged $Coq10^{N\Delta30}$ fusion protein, leaving cleaved $Coq10^{N\Delta30}$ in the flow through. The Ni-NTA resins were washed four times each with 2 CV of wash buffer without imidazole. The combined flow through and washes were concentrated with Amicon and further purified by gel filtration chromatography on a Superdex 75 Increase column (GE Healthcare) to remove any residual contaminants and buffer exchange to 10 mM Tris, pH 7.0, 10 mM NaCl, 0.5 mM Tris (2-carboxyethyl)-phosphine hydrochloride (TCEP), 3% 2-methyl-2, 4-pentanediol (MPD), and 0.1% DDM.

Proteomic analysis of His_6SUMO-$Coq10^{N\Delta30}$ for identity confirmation

Before SUMO protease cleavage during overnight dialysis, a small fraction of the His_6SUMO-$Coq10^{N\Delta30}$ fusion protein was buffer exchanged and concentrated into 50 mM NaH_2PO_4, pH 8.0, 300 mM NaCl, 1 mM DTT, and 0.1% Triton X-100 to about 10 mg/mL. The total volume of the protein sample was brought up to 400 µL, and an equal volume of methanol, and 100 µL of chloroform were added. After vigorous vortexing and centrifugation at 12,000 *g* at 4°C for 10 min, the precipitated protein was collected at the interface. A 400 µL of methanol was

added to wash the protein precipitate. After centrifugation at 12,000 *g* at 4°C for 10 min, the protein precipitate was collected at the bottom of the tube and dried inside a SpeedVac. The dried protein was reconstituted with 0.1% TFA to 500 µL and concentrated to a final volume of 30 µL using Amicon 10K MWCO ultracentrifugal filter (Thermo Fisher Scientific). The protein solution was then diluted 5x in 50/50 [v/v] H_2O/acetonitrile, 1% formic acid to an estimated final concentration of 18 µM using a NanoDrop spectrophotometer (Thermo Fisher Scientific) against a standard curve prepared with bovine serum albumin. Subsequently, 4 µL of this solution was transferred to a metal-coated borosilicate capillary (Au/Pd coated, 1 µm i.d., Thermo Fisher Scientific) and mounted in the nanospray ion source. Mass spectrometry experiments were performed using a 15T SolariX FTICR instrument equipped with an infinity cell (Bruker Daltonics). The following instrument settings were used: ESI voltage 1.2 – 1.3 kV, dry gas temperature 180°C, flow rate 2.0 L/min, rf amplitude of ion funnels 200 Vpp, Funnel 1 voltage 200 V, Funnel 2 voltage 6 V, Skimmer 1 voltage 40 V (60 V for ECD), Skimmer 2 voltage 5 V, multipole 1 rf frequency 2 MHz, quadrupole rf frequency 1.4 MHz, transfer hexapole rf frequency 2 MHz, time-of-flight 1.000 ms, sweep excitation power 15.0%. Ions were accumulated for 500 ms in the collision cell before entering the infinity ICR cell. Source, quadrupole, and UHF pressures were 2.54e0, 3.72e-6, and 1.77e-9 mbar, respectively. For ECD, a pulse length of 30 ms, a bias of 0.9 V, and a lens voltage of 15.0 V were used. The hollow-cathode current was held at 1.6 A. For accurate mass determination of the intact His_6SUMO-Coq10$^{N\Delta30}$, 130 scans were combined, whereas this was increased to 350 for top-down ECD in order to obtain a sufficient signal-to-noise ratio for fragments. Spectra were processed with DataAnalysis (Bruker Daltonics), using the SNAP algorithm (quality factor threshold 0.5, S/N threshold 2, maximum charge state 45^+) for peak detection and monoisotopic mass estimation. Peak assignment was performed manually using an *in silico* generated list of possible *c* and *z* fragments.

Generation of *coqΔcoq10Δ* double deletion mutants

The *coqΔcoq10Δ* double deletion mutants were generated by replacing the *COQ10* ORF in each single *coqΔ* deletion mutant with a *URA3* auxotrophic marker amplified from pRS306 vector using primers 5'-AATAATAGGATAAGGAGCCAAACAATAAACGGCTAAAGATACCGTGGAGATCAATTCAATTCATCATTTTTTTTT-3' and 5'-GCTTATCCTGGATGGCATGATCTTTGTTATCTGAAATTATACGGAAGATATTAGTTTTGCTGGCCGCAT-3' (sequences homologous to the upstream of *COQ10* start codon and downstream of the *COQ10* stop codon were underlined). A separate *coq2Δcoq9Δ* double deletion mutant was generated by replacing the *COQ9* ORF in a yeast *coq2Δ* mutant with *KANMX4*, which was amplified from BY4741 *coq9Δ* genomic DNA using primers 5'-TTTGGGCCTACATAAGGTACTTCCGTACGCTGCAGGTCGAC-3' and 5'-CGCACAGTACCAATAAATCTGCCTAGCTACTTAAGCTCGAGC-3' (sequences homologous to the upstream of *COQ9* start codon and downstream of the *COQ9* stop codon were underlined). Transformation of the PCR product into corresponding yeast *coqΔ* cells followed the lithium acetate/PEG method (12) described above, and successful knock out of the gene of interest was confirmed by colony PCR.

RESULTS

Integration of PCcMyc$_9$ tag retains Coq4, Coq5, and Coq10 protein function

One approach to characterize Coq10-containing high molecular weight complex involves co-precipitation of its interacting protein partners with functional PCcMyc$_9$-tagged Coq10. Generation of C-terminal PCcMyc$_9$ fusion of Coq10 was accomplished by homologous integration of the tag into the genomic DNA in order to maintain endogenous expression of Coq10 within the cell.

Expression of PCcMyc$_9$-tagged Coq4, Coq5, and Coq10 was confirmed by antibodies against individual Coq polypeptide, as well as with antibody against the cMyc epitope (Figure 1). To ensure that integration of the tag does not interfere with Coq4, Coq5, or Coq10 activities, we assessed their respiration-dependent growth on non-fermentable glycerol-containing medium, assembly into high molecular weight CoQ synthome or Coq10-containing complex, and their ability to perform CoQ biosynthesis. Our results showed that C-terminal PCcMyc$_9$ fusions of Coq4, Coq5 and Coq10 did not affect the respiratory function of the corresponding cells, as indicated by their robust growth on YPG medium comparable to the wild type control cells (Figure 2). Incorporation of a C-terminal tag did not affect the assembly of corresponding Coq polypeptide into their respective high molecular weight complexes. On the two-dimensional BN/SDS-PAGE, the CoQ synthome is distributed across the entire range of high molecular weight standards, as represented by both Coq4 and Coq9 signals in the wild-type cells (Figure 3A,B). The cells expressing Coq4PCcMyc$_9$ and Coq5PCcMyc$_9$ retained the high molecular weight CoQ synthome similar to that of the wild type, as represented by Coq9 signals (Figure 3B). When Coq4 was used as the proxy for the CoQ synthome, while the distribution of the CoQ synthome appeared to be similar in both the wild-type cells and in cells expressing Coq5PCcMyc$_9$, the Coq4 signal in cells expressing Coq4PCcMyc$_9$ was detected at a molecular weight greater than 440 kDa, which matches the added weight from the tag (Figure 3A).

Likewise, PCcMyc$_9$-tagged Coq10 also remained at high molecular weight, which appeared to be at slightly higher molecular weight when compared to the Coq10-containing complex from untagged wild type cells (Figure 3C).

Next, to check if integration of the tag would affect CoQ biosynthesis, the wild-type cells, cells expressing PCcMyc$_9$-tagged Coq4, Coq5, or Coq10, as well as their respective deletion mutants were supplemented with $^{13}C_6$-labeled pABA or 4HB, and harvested at logarithmic growth phase. Levels of de novo CoQ$_6$, unlabeled CoQ$_6$, and the total CoQ$_6$ in their whole cell lipid extract were quantified. Consistent with previous findings, the absence of Coq4 or Coq5 completely abolishes CoQ$_6$ biosynthesis (Figure 4), and the de novo $^{13}C_6$-CoQ$_6$ production is less efficient in the *coq10Δ* mutants relative to the wild-type control (Figure 4A). The cells expressing Coq4PCcMyc$_9$, Coq5PCcMyc$_9$, or Coq10PCcMyc$_9$ make similar or more $^{13}C_6$-CoQ$_6$ compared to the wild-type cells originating from both $^{13}C_6$-pABA and $^{13}C_6$-4HB (Figure 4A). The cells expressing Coq4PCcMyc$_9$, or Coq10PCcMyc$_9$ accrued slightly more unlabeled CoQ$_6$ in the samples treated with the vehicle control ethanol (Figure 4B), whereas the cells expressing Coq5PCcMyc$_9$ seemed to contain less unlabeled CoQ$_6$ in samples supplemented with $^{13}C_6$-pABA or $^{13}C_6$-4HB (Figure 4B). However, the total amounts of CoQ$_6$ in cells expressing PCcMyc$_9$ fusion proteins are similar to the wild-type control cells (Figure 4C). Collectively, these results show that integration of the PCcMyc$_9$ does not affect the normal functions of Coq4, Coq5, or Coq10 in the cell.

Affinity purification of Coq10-interacting protein partners

Detergent solubilized mitochondria from wild-type cells and cells expressing Coq10PCcMyc$_9$ were subjected to tandem affinity purification against the protein C and cMyc epitopes. Eluates from the affinity purification were used to look for potential Coq10-interacting proteins by mass spectrometry using the bottom-up approach based on recovered tryptic

peptides. Interestingly, data from two independent experiments showed that Coq10 co-precipitated with Sdh1 from Complex II (Table 3, Exp.1) and Rip1 from Complex III (Table 3, Exp.2). Even through subunits Qcr2 and Cor1 from Complex III were also detected in both experiments in the Coq10PCcMyc$_9$ pull down eluates, both proteins were also present in the eluate from the wild-type control in the second experiment, which implies a possible non-specific binding (Table 3). The second trial of affinity purification of Coq10PCcMyc$_9$ also identified several ribosomal proteins with low sequence coverage (Table 3, Exp.2). To confirm the presence of some Coq10-interacting proteins in the tandem affinity purification eluate, we performed immunoblot analysis against Cor1, Qcr2, and Rip1 using eluates collected from experiment 2. Unfortunately none of these proteins were detected in the Coq10PCcMyc$_9$ pull down eluates (Figure 5).

Purification of His$_6$SUMO-Coq10$^{N\Delta30}$

In an effort to perform a liposome binding assay, an expression vector was constructed for overexpressing an N-terminal His$_6$SUMO fusion of Coq10$^{N\Delta30}$, which lacks the mitochondrial targeting sequence from the primary transcript. Inclusion of a His$_6$SUMO tag also improves the solubility of the fusion protein. Upon overexpression in *E. coli*, Coq10$^{N\Delta30}$ can be easily purified after two rounds of Ni-NTA affinity chromatography. After the first Ni-NTA affinity chromatography, the His$_6$SUMO-Coq10$^{N\Delta30}$ fusion protein was purified from the rest of the cell lysate, and the eluate containing His$_6$SUMO-Coq10$^{N\Delta30}$ fusion protein was subjected to overnight cleavage by His-Ulp1, which recognizes the secondary structure of the SUMO moiety and cleaves off the His$_6$SUMO tag. Thus, a second Ni-NTA affinity chromatography served to remove any uncleaved His$_6$SUMO-Coq10$^{N\Delta30}$ fusion, cleaved His$_6$SUMO tag, and His-Ulp1, leaving purified Coq10$^{N\Delta30}$ in the column flow through. An example of purification scheme can be found in Figure 6.

Verification of the purification of His_6SUMO-Coq10$^{N\Delta30}$

The His_6SUMO-Coq10$^{N\Delta30}$ fusion protein was detected at 33846.41299 Da (Figure 7B), which was within 4.06 ppm deviation from its theoretical value (33846.27562 Da). This detected molecular weight of His_6SUMO-Coq10$^{N\Delta30}$ corresponds to the removal of N-terminal translation initiator Met from the fusion protein by *E. coli* methionine aminopeptidases (MetAPs) (19). The molecular species result from the +178 mass shift is likely due to the post-translational phosphogluconoylation of His_6SUMO-Coq10$^{N\Delta30}$ (Figure 7A). This type of modification in *E. coli* expressing His-tagged fusion proteins has been previously documented (20). Overall, the top-down electron capture dissociation (ECD) experiment confirmed the sequence of the purified His_6SUMO-Coq10$^{N\Delta30}$ (data not shown). ECD fragment assignment shows good sequence coverage in terminal regions, and no ECD fragment is detected in the region between Leu85 and Glu216. ECD fragments at the N- and C-termini account for over 50% sequence coverage for the fusion protein. Three fragments in the N-terminal region are observed carrying +178 Da modification. Combination of accurate mass supported by ECD fragmentation data is convincing for the protein identity.

Rescue of *coqΔcoq10Δ* double deletion mutants with exogenous CoQ_6

The hallmark phenotype of CoQ-less yeast *coqΔ* deletion mutants is that their respiration deficiency can be rescued by addition of CoQ_6 to yeast whole cells, or by addition of CoQ_2 to isolated mitochondria. However, the CoQ_6-dependent rescue of respiration was found to be defective in *coq2Δcoq10Δ* double deletion mutants (21). This result is intriguing because it identifies a role for the Coq10 and Coq2 polypeptides in the assimilation of exogenous CoQ_6 from the extracellular environment into the cell and into mitochondria to support respiration. Thus, a *coqΔcoq10Δ* double knockout library was constructed, and tested for the competency of rescue by exogenous CoQ_6 in these double null mutants by following their growth in YPG medium supplemented with exogenous CoQ_6. Inconsistent with the published result, our data

demonstrate competence of rescue by exogenous CoQ_6 in the *coq2Δcoq10Δ* double deletion mutant, as well as in the control *coq2Δcoq9Δ* double deletion mutant, as indicated by its growth comparable to the wild-type cells (Figure 8).

Growth phenotype of *coqΔcoq10Δ* double deletion mutants

Although Coq10 exists in high molecular weight complexes, it has not been demonstrated to interact with any of the Coq polypeptides of the CoQ synthome. Previously, Coq10 was found to co-migrate with Coq2 and Coq8 by two-dimensional BN/SDS-PAGE (11). It is possible Coq2, Coq8 and Coq10 may represent an independent complex. Moreover, since Coq8 has been detected in the Coq6-CNAP pull down eluate (18), it is also plausible that Coq10 may interact with members of the CoQ synthome transiently. Thus, if Coq10's function requires its interaction with members of the CoQ synthome, then a double deletion mutant devoid of both Coq10 and CoqX would result in a defective growth phenotype. We tested this hypothesis by comparing the growth phenotypes of *coqΔcoq10Δ* double deletion mutants to *coq10Δ* mutants on YPD at non-permissive temperature. As expected, the yeast *coq10Δ* mutant formed petite colonies on YPD at both permissive and non-permissive temperatures (Figure 9) as has been reported previously (1). Interestingly, the petite growth phenotype of yeast *coq10Δ* mutant appears to be reversed in the absence of any one of the Coq1-Coq9 polypeptides (Figure 9).

DISCUSSION AND FUTURE DIRECTIONS

Although the integration of the PCcMyc$_9$-tag retained the function of Coq10, our attempts to look for Coq10-interacting proteins using the tandem affinity purification approach against the PCcMyc$_9$-tag were unsuccessful. We were unable to confirm the presence of potential Coq10-interacting proteins that were identified through the proteomic approach on immunoblots. Stoichiometric analysis suggests that Coq10 is approximately two orders of magnitude less abundant than other respiratory chain components (1). Thus, it seems likely that the detection of the constituent members of Complex II and III may represent non-specific interactions. For proteins detected with low sequence coverage, it is likely that these proteins are in low abundance, and requires significant enrichment in order to be detected on immunoblots. It is also possible that proteins interact with Coq10 with low affinities do not withstand the buffer conditions, and thus are not captured in the final eluate. To address this concern, one possibility is to strengthen the protein interaction with Coq10 with a small molecule crosslinker, such as dithiobis-succinimidyl propionate (DSP). DSP is membrane permeable, and contains an amine-reactive NHS-ester group at each end of the molecule. DSP reacts with primary amines on proteins forming stable amide bonds, and it crosslinks Coq10 with proteins within 12 Å range. Moreover, instead of using wild-type yeast mitochondria, PCcMyc$_9$-tagged Coq4 and Coq5 will serve as better controls to exclude proteins that interact non-specifically with the anti-PC and/or anti-cMyc resin in future studies. The PCcMyc$_9$-tagged Coq4 and Coq5 themselves will provide an opportunity to look for new members that are part of the CoQ synthome.

A general function of START domain containing proteins is to facilitate lipid transfer at membrane contact sites. Ltc1 is an ER localized, START domain containing protein (22). Ltc1 forms complexes with Tom70 or vacuolar membrane protein Vac8 at the ER-mitochondria, or ER-vacuole contact sites for sterol transport (22). Coq10 is also a START domain protein, and its ortholog CC1736 in *Caulobacter crescentus* binds CoQ_6 and late-stage CoQ_6-intermediates

(4, 23). Thus, we can take advantage of purified His_6SUMO-Coq10$^{N\Delta30}$ or Coq10$^{N\Delta30}$ to perform in vitro lipid transfer assay to see if Coq10 may be involved in facilitating movement of CoQ_6 and CoQ_6-intermedaites between membranes. While short chain CoQ_n isoforms (n denotes the number of isoprene units) with n<4 distribute between membranes via free diffusion, more hydrophobic CoQ_6 requires lipid chaperones to facilitate its traffic between membranes. Thus, we can set up an in vitro lipid transfer assay (24), in which donor liposomes containing pyrene and CoQ_6 are added to acceptor liposomes containing pyrene alone, in the presence and absence of Coq10. The efficiency of CoQ_6 transfer between liposomes will be measured as a function of varying Coq10 concentration and a function of time. The fluorescence readout from the acceptor liposomes with pyrene will be quenched if Coq10 was able to extract the CoQ_6 from the donor liposomes and deliver it to the acceptor liposomes. The result will consolidate Coq10 function as a CoQ transfer protein.

So far, the lipid binding function of Coq10 is well established, and newly emerged studies point towards a regulatory role of Coq10. The mitochondrial CoQ domain formation requires CoQ_6 and late-stage CoQ_6-intermediates. The yeast *coq10Δ* mutant makes CoQ_6 and accumulates CoQ_6-intermediates, but contains fewer mitochondrial CoQ domains compared to the wild-type cells (6, 7). It seems plausible that Coq10 may dictate the formation of mitochondrial CoQ domain, and/or guide the positioning of CoQ synthome at the ER-mitochondria junction. Thus, it will be interesting to take a closer look at the position of mitochondrial CoQ domains relative to the ERMES complex and Ltc1/Tom70 complex in the *coq10Δ* mutant. Does absence of Coq10 disrupt CoQ domain formation specifically at the ER-mitochondria tether formed by ERMES complex, or Ltc1/Tom70 complex, or both? In the *S. cerevisiae* genome, *COQ10* shares a bi-directional promoter with *MDM12*, which encodes a member of the ERMES complex. This particular arrangement suggests a possible functional link between Coq10, ERMES complex, and/or the positioning of the CoQ domain at the ER-

mitochondria contact sites. We have shown in Chapter 3 that absence of ERMES complex subunits did not affect the steady state levels of Coq10. It will be very interesting to check if the steady state levels of ERMES complex subunits are affected in the mutant cells lacking Coq10. Furthermore, there exists a network of membrane contact sites between mitochondria, ER, vacuoles, peroxisomes and lipid droplets in yeast, and it is also worth investigating the position of CoQ domains relative to other organelles aside from the ER.

So far, one major challenge for studying CoQ biosynthetic pathway is that the yeast mutant cells lacking CoQ biosynthetic enzymes in the pathway (*coq3Δ-coq9Δ*) accumulate prenylated early CoQ-intermediates, namely hexaprenyl-4-aminobenzoic acid (HAB) and hexaprenyl-4-hydroxybenzoic acid (HHB) (15), and do not produce diagnostic CoQ-intermediates, making it impossible for diagnosis of the impaired enzymatic step in the pathway. In Chapter 3, we have shown that the ERMES deletion mutants are inefficient for CoQ_6 production, and as a result *ERMESΔ* mutants accumulate CoQ_6-intermediates in their whole cell lipid extract (6). Thus, the *ERMESΔ* mutants provide a platform to look for uncharacterized CoQ_6-intermediates. Tropylium-like [*m/z* = 150] and chromenylium-like [*m/z* = 190] ions are known transition ions generated from prenylated aromatic and benzoquinone rings under electronspray ionization conditions (17). Using these two signature fragmentation ions, we can perform a precursor ion scan in the *ERMESΔ* mutants to look for new CoQ-intermediates in the pathway.

In Chapter 2, protein sequence similarity network analysis revealed RatA from *E. coli* belongs to the Coq10-like protein family. RatA modulates cell cycle on the translation level by inhibiting 70S ribosome association, in response to stresses such as nutrient starvation (25). Based on the identification of several ribosomal proteins in the $Coq10PCcMyc_9$ pull down eluate (Table 3, Exp.2), we think that Coq10 may have a similar regulatory role. In Chapter 3, we

discussed that Mdm12 may enter the nucleus upon overexpression (26). If nucleus localized Mdm12 were to function as a feedback control of its own expression, how is it going to affect the expression of Coq10 given that they share a same promoter sequence? Meanwhile, we should also look into how RatA maybe related to the recently identified Ubi complex and its component subunits the are responsible for CoQ_8 biosynthesis in *E. coli* (27).

Last but not least, we speculated that Coq10 may function to sequester/remove potentially toxic CoQ or CoQ-intermediates. This hypothesis is supported by the observation that deletion of *COQ1-COQ9* in *coq10Δ* single mutants improves the growth phenotype of *coq10Δ* under heat stress at non-permissive temperature (Figure 9). CoQ may undergo one electron reduction, forming semiquinone radical. CoQ-intermediates themselves or their metabolites can also act as electrophiles. A combination of both oxidative and electrophilic stress may render *coq10Δ* mutant cells sensitive to heat stress at elevated temperature. We think that deletion of Coq1-Coq9 in the yeast *coq10Δ* mutant abolishes the production of potentially toxic CoQ-intermediates, demethoxy-CoQ_6 (DMQ_6), imino-demethoxy-CoQ_6 ($IDMQ_6$), demethyl-demethoxy-CoQ_6 ($DDMQ_6$), as well as HAB and HHB present in the *coq10Δ* mutant, thus improves the growth of *coqΔcoq10Δ* mutants as observed. However, this hypothesis begs for further validation, which can be achieved either by comparing the expression profile of antioxidant enzymes, such as glutathione peroxidase, catalase, and superoxide dismutase in the *coq10Δ* mutant and in the *coqΔcoq10Δ* mutants, or we can obtain a direct readout of oxidative damage to the cells using ROS-sensitive dye upon exogenous addition of suspect CoQ-intermediates. Hopefully, all fore mentioned experiments will provide insights to help determine the molecular function of Coq10.

Table 1. Genotype and source of yeast strains

Strain	Genotype	Source
W303 1B	MAT α *ade2-1 can1-100 his3-11,15 leu2-3,112 trp1-1 ura3-1*	R. Rothstein[a]
W303 Coq4PCcMyc$_9$	MAT α *ade2-1 can1-100 his3-11,15 leu2-3,112 trp1-1 ura3-1 COQ4::COQ4-PC-cMyc-HIS5*	This study
W303 Coq5PCcMyc$_9$	MAT α *ade2-1 can1-100 his3-11,15 leu2-3,112 trp1-1 ura3-1 COQ5::COQ5-PC-cMyc-HIS5*	This study
W303 Coq10PCcMyc$_9$	MAT α *ade2-1 can1-100 his3-11,15 leu2-3,112 trp1-1 ura3-1 COQ10::COQ10-PC-cMyc-HIS5*	This study
W303 *cor1Δ*	MAT α*, ade2-1 can1-100 his3-11,15 leu2-3,112 trp1-1 ura3-1 cor1::HIS3*	(28)
W303 *coq1Δ*	MAT α*, ade2-1 can1-100 his3-11,15 leu2-3,112 trp1-1 ura3-1 coq1::LEU2*	(29)
W303 *coq2Δ*	MAT **a**, *ade2-1 can1-100 his3-11,15 leu2-3,112 trp1-1 ura3-1 coq2::HIS3*	(30)
CC303	MAT α*, ade2-1 can1-100 his3-11,15 leu2-3,112 trp1-1 ura3-1 coq3::LEU2*	(31)
W303 *coq4Δ*	MAT **a**, *ade2-1 can1-100 his3-11,15 leu2-3,112 trp1-1 ura3-1 coq4::TRP1*	(32)
W303 *coq5Δ*	MAT α*, ade2-1 can1-100 his3-11,15 leu2-3,112 trp1-1 ura3-1 coq5::HIS3*	(9)
W303 *coq6Δ*	MAT **a**, *ade2-1 can1-100 his3-11,15 leu2-3,112 trp1-1 ura3-1 coq6::LEU2*	(33)

Table 1. Genotype and source of yeast strains (Cont.)

Strain	Genotype	Source
W303 *coq7Δ*	MAT α*, ade2-1 can1-100 his3-11,15 leu2-3,112 trp1-1 ura3-1 coq7::LEU2*	(34)
W303 *coq8Δ*	MAT **a***, ade2-1 can1-100 his3-11,15 leu2-3,112 trp1-1 ura3-1 coq8::HIS3*	(32)
W303 *coq9Δ*	MAT α*, ade2-1 can1-100 his3-11,15 leu2-3,112 trp1-1 ura3-1 coq9::URA3*	(35)
W303 *coq10Δ*	MAT **a***, ade2-1 can1-100 his3-11,15 leu2-3,112 trp1-1 ura3-1 coq10::HIS3*	(1)
W303 *coq1Δcoq10Δ*	MAT α*, ade2-1 can1-100 his3-11,15 leu2-3,112 trp1-1 ura3-1 coq1::LEU2 coq10::URA3*	This study
W303 *coq2Δcoq10Δ*	MAT **a***, ade2-1 can1-100 his3-11,15 leu2-3,112 trp1-1 ura3-1 coq2::HIS3 coq10::URA3*	This study
W303 *coq3Δcoq10Δ*	MAT α*, ade2-1 can1-100 his3-11,15 leu2-3,112 trp1-1 ura3-1 coq3::LEU2 coq10::URA3*	This study
W303 *coq4Δcoq10Δ*	MAT **a***, ade2-1 can1-100 his3-11,15 leu2-3,112 trp1-1 ura3-1 coq4::TRP1 coq10::URA3*	This study
W303 *coq5Δcoq10Δ*	MAT α*, ade2-1 can1-100 his3-11,15 leu2-3,112 trp1-1 ura3-1 coq5::HIS3 coq10::URA3*	This study
W303 *coq6Δcoq10Δ*	MAT **a***, ade2-1 can1-100 his3-11,15 leu2-3,112 trp1-1 ura3-1 coq6::LEU2 coq10::URA3*	This study

Table 1. Genotype and source of yeast strains (Cont.)

Strain	Genotype	Source
W303 *coq7Δcoq10Δ*	MAT α*, ade2-1 can1-100 his3-11,15 leu2-3,112 trp1-1 ura3-1 coq7::LEU2 coq10::URA3*	This study
W303 *coq8Δcoq10Δ*	MAT **a***, ade2-1 can1-100 his3-11,15 leu2-3,112 trp1-1 ura3-1 coq8::HIS3 coq10::URA3*	This study
W303 *coq9Δcoq10Δ*	MAT α*, ade2-1 can1-100 his3-11,15 leu2-3,112 trp1-1 ura3-1 coq9::URA3 coq10::HIS3*	This study
W303 *coq2Δcoq9Δ*	MAT **a***, ade2-1 can1-100 his3-11,15 leu2-3,112 trp1-1 ura3-1 coq2::HIS3 coq9::kanMX4*	This study

[a] Dr. Rodney Rothstein, Department of Human Genetics, Columbia University, New York, NY.

Mating type a (MAT **a**) is in bold to distinguish it from mating type alpha (MAT α).

Table 2. Primers used in this study

Primer	Primer sequence
Coq4PCcMyc$_9$ forward primer	5'GGAGATTGACGCAAAATACAACTCACAGAAACGAGCCACGACTCCAGCAAGTGGTGGTGCTGGTGGT**GAAGACCAAGTCGATCCCAGACTTATAGACGGTAAA**TCCGGTTCTGCTGCTAG3'
Coq4PCcMyc$_9$ reverse primer	5'ATCGCAAGATCGCCTTGGACGACCATCCTATATAGTATATTATAGCTGACCCTCGAGGCCAGAAGAC 3'
Coq5PCcMyc$_9$ forward primer	5'ACGAAAGTTTAACTTTTGGTATATGTGCCATCCATTGGGGCATTAAAGTTAGTGGTGGTGCTGGTGGT**GAAGACCAAGTCGATCCCAGACTTATAGACGGTAAA**TCCGGTTCTGCTGCTAG3'
Coq5PCcMyc$_9$ reverse primer	5'CTGCACATCACAGCAAAATATATGGCTATCACATGGCACAGGTATTACTACCTCGAGGCCAGAAGAC3'
Coq10PCcMyc$_9$ forward primer	5'CATTTAGTAAGATTAGCAATGCTAAAACCTTCTTCTAAAGAAGGCTCTCCGAGTGGTGGTGCTGGTGGT**GAAGACCAAGTCGATCCCAGACTTATAGACGGTAAA**TCCGGTTCTGCTGCTAG3'
Coq10PCcMyc$_9$ reverse primer	5'ATTTAACCATGCATACGCTTATCCTGGATGGCATGATCTTTGTTATCTGCCTCGAGGCCAGAAGAC3'

The underlined sequences represent flanking regions that are homologous to the approximately 50 base pair upstream and downstream of the stop codon of the gene of interest. The coding sequence for the protein C (PC) epitope is bolded.

Table 3. Proteins identified in the eluates from anti-Protein C and anti-cMyc tandem affinity purification

WT (Exp.1)			Coq10PCcMyc$_9$ (Exp.1)		
Protein Name	Description	% Coverage	Protein Name	Description	% Coverage
Ubi4	Ubiquitin	27.48	Coq10	Coenzyme Q (ubiquinone) binding protein	55.07
Hhf1	Histone H4	18.45	Ssc1	Hsp70 family ATPase	29.23
Por1	Mitochondrial outer membrane porin	13.38	Ubi4	Ubiquitin	28.87
Hta1/Hta2?	Histone H2A	12.4	Atp1	ATP synthase subunit alpha	21.1
Hht1	Histone H3	10.29	Hhf1	Histone H4	18.45
Act1	Actin	7.78	Por1	Mitochondrial outer membrane porin	17.47
Tef1	Translation elongation factor 1-alpha	6.57	Act1	Actin	15.56
Ssa4	Hsp70 family heat shock protein	5.61	Hta1/Hta2?	Histone H2A	12.4
Did4	Class E Vps protein of the ESCRT-III complex	3.97	Hsp60	Heat shock protein	10.69
Ssc1	Hsp70 family ATPase	3.78	Hht1	Histone H3	10.29
Atp1	ATP synthase subunit alpha	3.67	Kar2	ATPase involved in protein import into the ER	9.83
Hsp60	Heat shock protein	2.8	Qcr2	Subunit 2 of ubiquinol cytochrome-c reductase (Complex III)	8.42
			Cor1	Core subunit of ubiquinol cytochrome c reductase (Complex III)	6.78
			Ald4	Mitochondrial aldehyde dehydrogenase	6.52
			Ssa4	Hsp70 family heat shock protein	5.61
			Atp2	ATP synthase subunit beta	5.28
			Nde1	Mitochondrial external NADH dehydrogenase; type II NAD(P)H:quinone oxidoreductase that catalyzes the oxidation of cytosolic NADH	4.69
			Tef1	Translation elongation factor 1-alpha	4.59
			Gpd1/Gpd2	Glycerol-3-phosphate dehydrogenase	4.24
			Ssa3	Hsp70 family ATPase	4.2
			Ilv2/Ilv6	Acetolactate synthase	4.11
			Did4	Class E Vps protein of the ESCRT-III complex	3.97
			Sdh1	Flavoprotein subunit of succinate dehydrogenase in complex II	2.9
			Afg3	Mitochondrial inner membrane m-AAA protease component	2.71
			Eft1	Translation elongation factor 2	1.92

Table 3. Proteins identified in the eluates from anti-Protein C and anti-cMyc tandem affinity purification (cont.)

WT (Exp.2)			Coq10PCcMyc$_9$ (Exp.2)		
Protein Name	Description	% Coverage	Protein Name	Description	% Coverage
Qcr2	Subunit 2 of ubiquinol cytochrome-c reductase (Complex III)	6.47	Ssc1	Hsp70 family ATPase	28.08
Rpl26A	60S ribosomal protein L26-A	4.72	Coq10	Coenzyme Q (ubiquinone) binding protein	15.94
Atp2	ATP synthase subunit beta	4.7	Rpl36	60S ribosomal protein L36	12.35
Atp1	ATP synthase subunit alpha	4.22	Rpl25	60S ribosomal protein L25	9.15
Tef1	Translation elongation factor 1-alpha	3.81	Rip1	Rieske iron-sulfur protein of ubiquinol cytochrome-c reductase (Complex III)	7.96
Did4	Class E Vps protein of the ESCRT-III complex	3.45	Rps18B	40S ribosomal protein S18-B	7.53
Cor1	Core subunit of ubiquinol cytochrome c reductase (Complex III)	2.41	Rps14A	40S ribosomal protein S14-A	7.3
Ssc1	Hsp70 family ATPase	1.97	Rps13	40S ribosomal protein S13	7.28
Hfa1-like protein	Hfa1 is the mitochondrial acetyl-coenzyme A carboxylase	0.3	Cor1	Core subunit of ubiquinol cytochrome c reductase (Complex III)	6.35
			Adh2	Cytoplasmic NAD-dependent alcohol dehydrogenase	5.17
			Qcr2	Subunit 2 of ubiquinol cytochrome-c reductase (Complex III)	4.98
			Rpl26A	60S ribosomal protein L26-A	4.72
			Tef1	Translation elongation factor 1-alpha	4.15
			Rpl32	60S ribosomal protein L32	3.85
			Aac3	Mitochondrial inner membrane ADP/ATP translocator	3.02
			Atp2	ATP synthase subunit beta	2.74
			Atp1	ATP synthase subunit alpha	1.83
			Cdc19	Pyruvate kinase	1.8

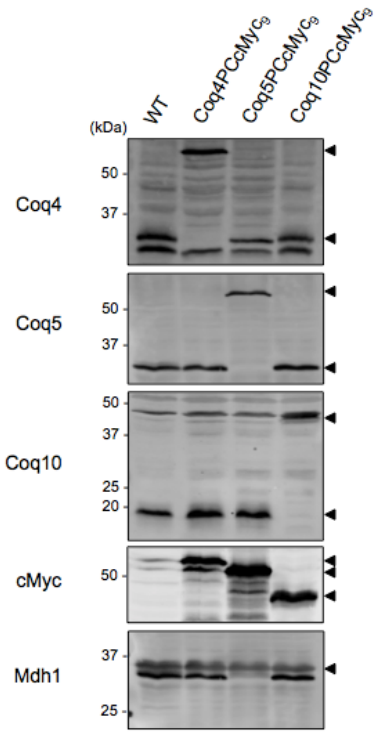

Figure 1. Expression of PCcMyc$_9$-tagged Coq4, Coq5, and Coq10 are detected in isolated mitochondria. An aliquot of 25 µg of purified mitochondrial protein from wild type, Coq4PCcMyc$_9$, Coq5PCcMyc$_9$, and Coq10PCcMyc$_9$ were loaded in each lane and separated on 12% SDS-PAGE gels. Expression of Coq4PCcMyc$_9$, Coq5PCcMyc$_9$, and Coq10PCcMyc$_9$ was confirmed by immunoblot analyses against Coq4, Coq5, Coq10, as well as the cMyc tag. Yeast mitochondrial malate dehydrogenase (Mdh1) was included as loading control.

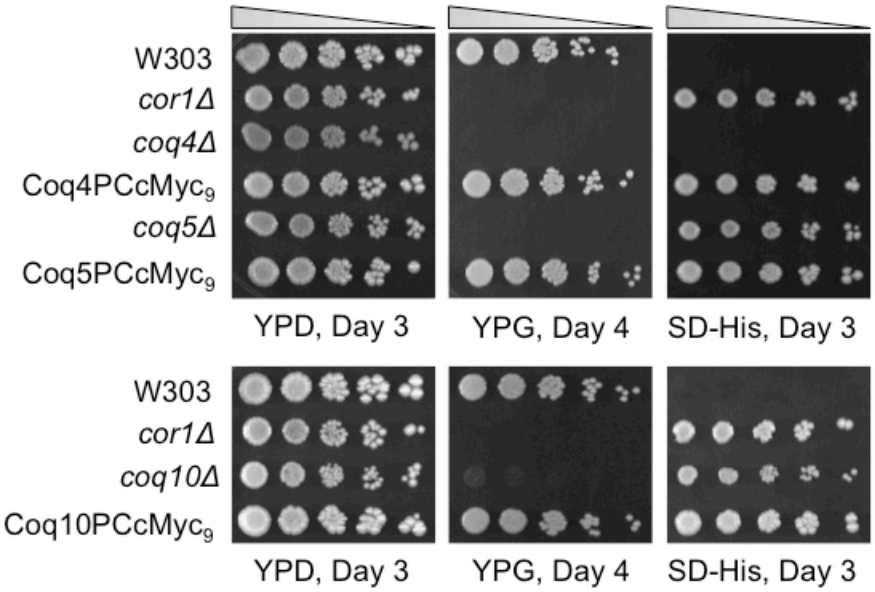

Figure 2. Integration of $PCcMyc_9$ tag retains the function of Coq proteins. Overnight cultures of wild-type W303, respiratory deficiency *cor1Δ* mutant, CoQ-less *coq4Δ* and *coq5Δ* mutants, *coq10Δ*, and cells expression $Coq4PCcMyc_9$, $Coq5PCcMyc_9$, and $Coq10PCcMyc_9$ grown in YPD were diluted to 0.2 OD_{600}/mL, from which a series of five-fold diluted samples were prepared. Beginning with the sample at 0.2 OD_{600}/mL, an aliquot of 2 µL of series of five-fold diluted sample was plated in each spot on YPD, YPG and SD-His plate medium. Pictures were taken three to four days after incubation at 30°C.

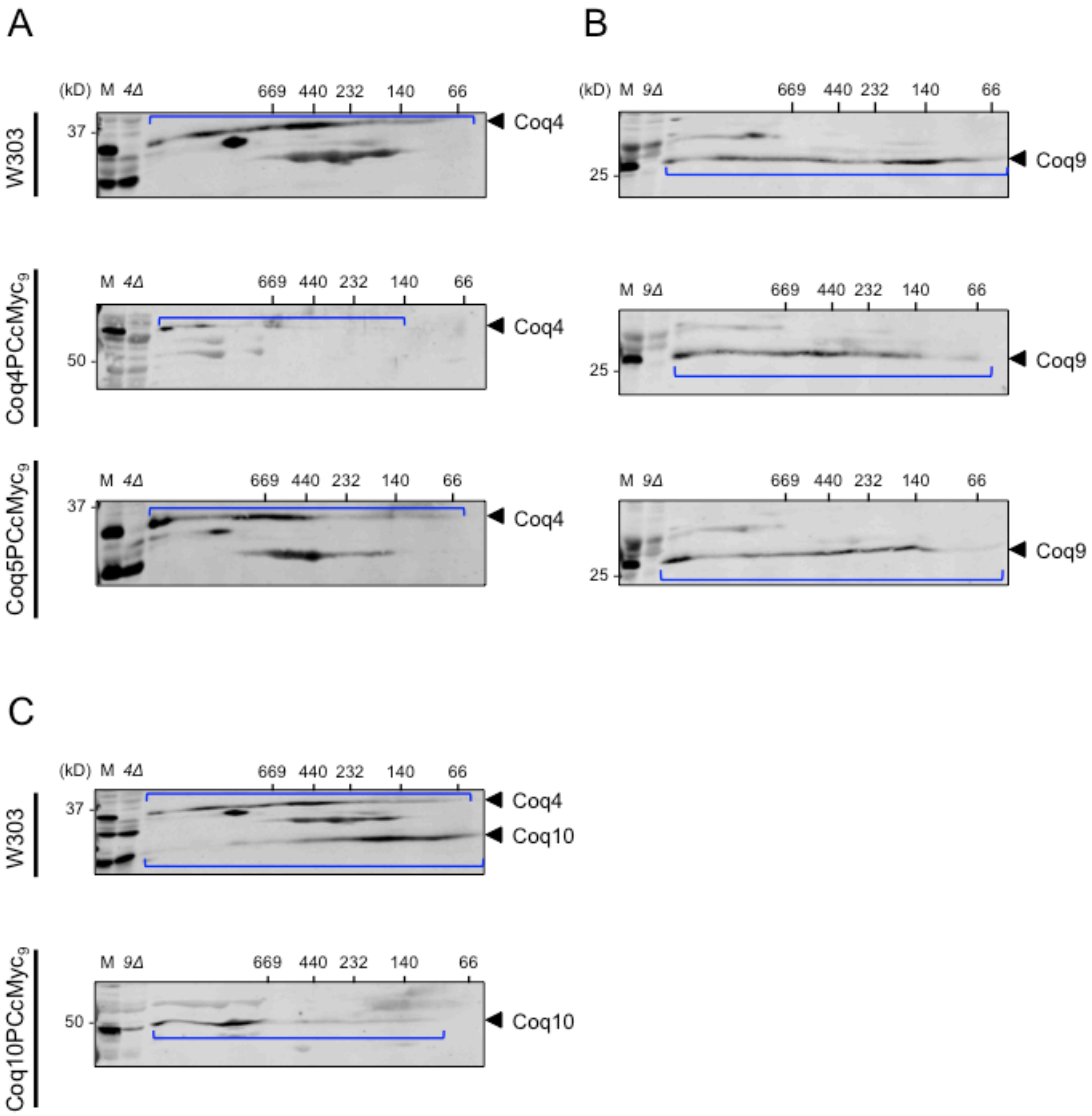

Figure 3. Integration of the PCcMyc$_9$ tag does not affect Coq protein assembly into high molecular weight complexes. An aliquot of 80 µg of purified mitochondrial protein from wild type, and strains expression Coq4PCcMyc$_9$, Coq5PCcMyc$_9$, and Coq10PCcMyc$_9$ was resolved on a two-dimensional BN/SDS-PAGE, and blotted against **A)** Coq4, **B)** Coq9, and **C)** Coq4 and Coq10. An aliquot of 25 µg of the intact mitochondria from each sample was loaded in the lane labeled "M", and a same amount of *coq4Δ* or *coq9Δ* mitochondria was loaded in the lanes labeled "4*Δ*", or "9*Δ*" as negative controls.

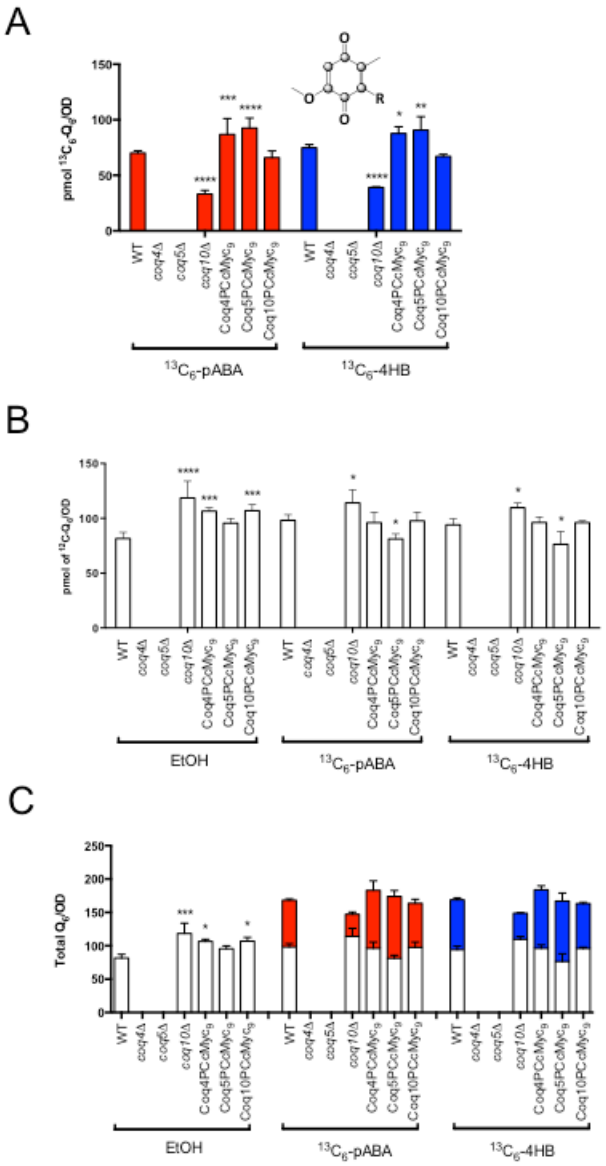

Figure 4. Integration of the PCcMyc$_9$ tag has no negative effect on CoQ$_6$ biosynthesis.

The **A)** de novo, **B)** unlabeled, and **C)** total amount of CoQ_6 were measured from yeast whole cell lipid extracts from wild type, *coq4Δ, coq5Δ, coq10Δ*, and strains expressing Coq4PCcMyc$_9$, Coq5PCcMyc$_9$, and Coq10PCcMyc$_9$, labeled with $^{13}C_6$-pABA (red), OR $^{13}C_6$-4HB (blue) in DOD medium for 3 hours. The statistical analyses were performed using two-way ANOVA multiple comparison from three biological replicates, comparing each sample to the wild-type control. The error bar indicates mean ±SD, and the statistical significance is represented by *p < 0.05, **p < 0.01, ***p <0.001 and ****p < 0.0001.

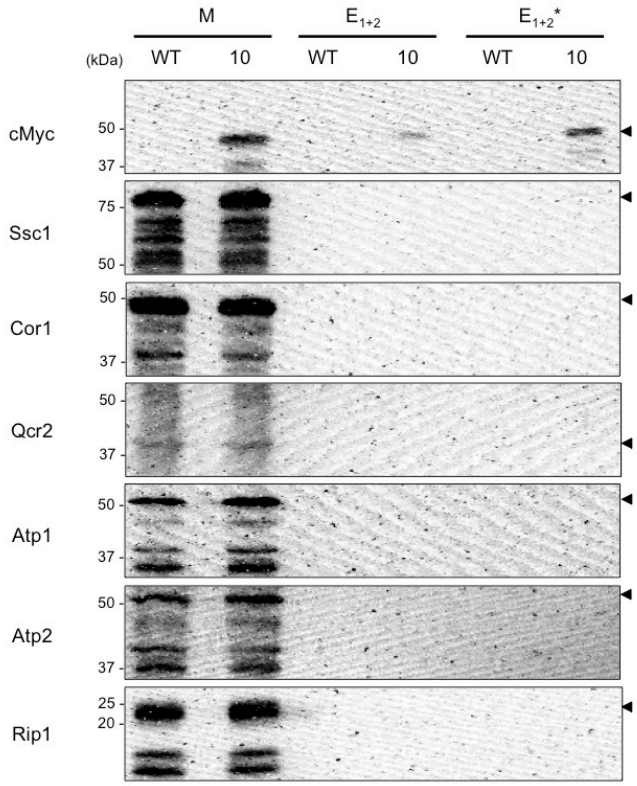

Figure 5. Immunoblot analyses of Coq10PCcMyc$_9$ pull down eluates (Exp.2) for potential Coq10-interacting protein partners. An aliquot of 25 µg of purified intact mitochondrial protein from wild type and Coq10PCcMyc$_9$ was loaded in the lanes labeled "M". An aliquot of 5 µL sample from a mixture containing 200 µL of eluate 1 and 200 µL of eluate 2 was loaded in the lanes labeled "E_{1+2}", and an aliquot of 5 µL from a four-fold more concentrated E_{1+2} was loaded in the lanes labeled "E_{1+2}*". The presence of Coq10PCcMyc$_9$ in the intact mitochondria before solubilization and in elutes was confirmed by immunoblot analyses against the cMyc tag. Rabbit polyclonal antibodies against Ssc1 (1:15,000), Cor1 (1:4,000), Qcr2 (1:4,000), Atp1 (1:4,000), and Atp2 (1:4,000), and mouse polyclonal antibody against Rip1 (1:4,000) were used to detect potential Coq10-interacting proteins in the eluates.

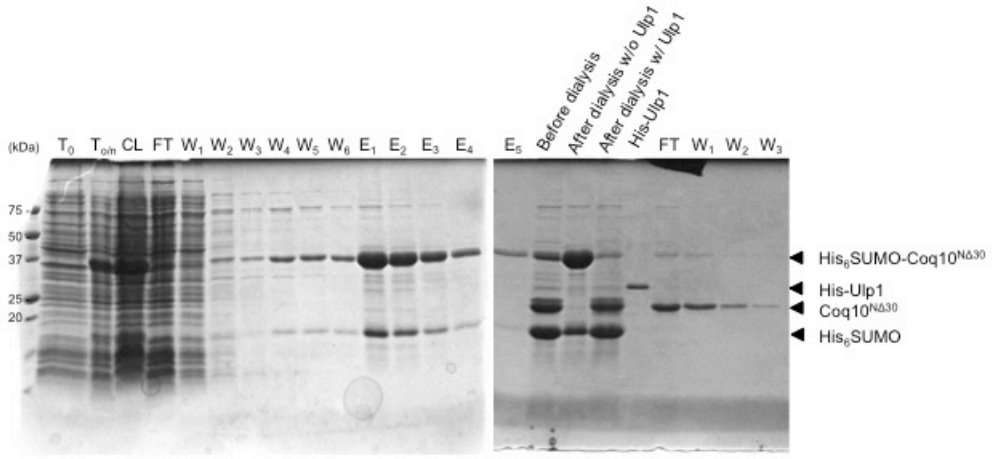

Figure 6. A representative purification scheme of Coq10$^{N\Delta30}$. Each lane contains 5 µL of each fraction, labeled as T_0, uninduced; $T_{o/n}$, overnight induction; CL, crude lysate; FT, flow through; W, wash; E, eluate, separated on 12% SDS-PAGE. The gel was subsequently stained with Coomassie and destained for visualization.

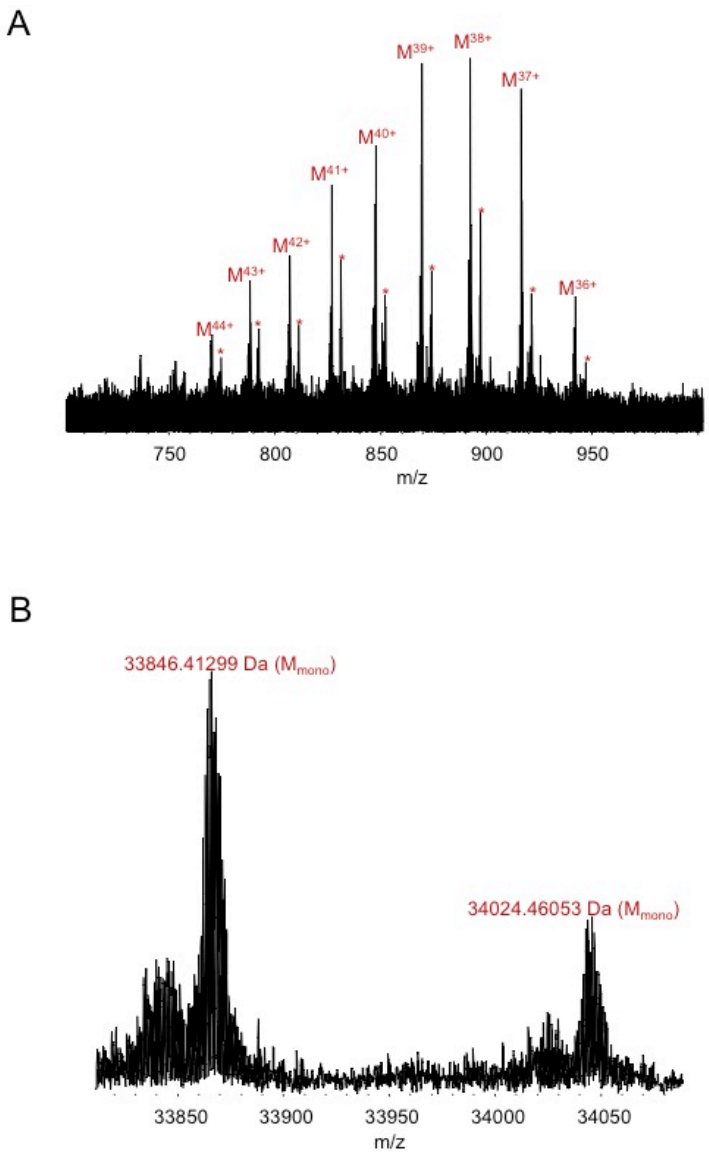

Figure 7. ESI FTICR MS spectrum of intact His_6SUMO-$Coq10^{N\Delta30}$ suggests possible post-translational modification of the fusion protein. A) ESI FTICR MS spectrum of His_6SUMO-$Coq10^{N\Delta30}$ indicates the presence of two molecular species. The asterisk denotes a molecular ion with +178 Da mass shift. **B)** The deconvoluted ESI spectrum shows a predominant peak with monoisotopic mass of 33846.41299 Da, and a second peak of 34024.46053 Da.

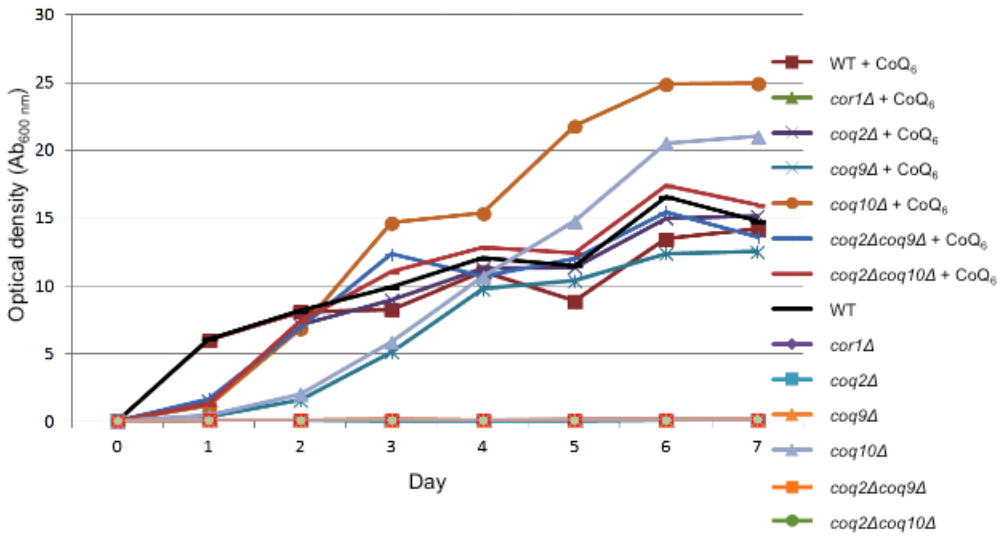

Figure 8. The yeast *coq2Δcoq9Δ and coq2Δcoq10Δ* double deletion mutants are rescued by exogenous supplementation of CoQ_6. The growth as indicated by OD_{600} of wild type, *cor1Δ*, *coq2Δ*, *coq9Δ*, *coq10Δ*, *coq2Δcoq9Δ,* and *coq2Δcoq10Δ* in YPG, with or without 12.5 μM CoQ_6, was followed for seven days at 30°C 250 rpm. Respiration-dependent growth of *coq2Δ*, *coq9Δ*, *coq10Δ* single mutants, and *coq2Δcoq9Δ* and *coq2Δcoq10Δ* double mutants was rescued by supplementation of CoQ_6. The *cor1Δ* mutant was included as a negative control and was respiratory deficient even with the supplementation of CoQ_6.

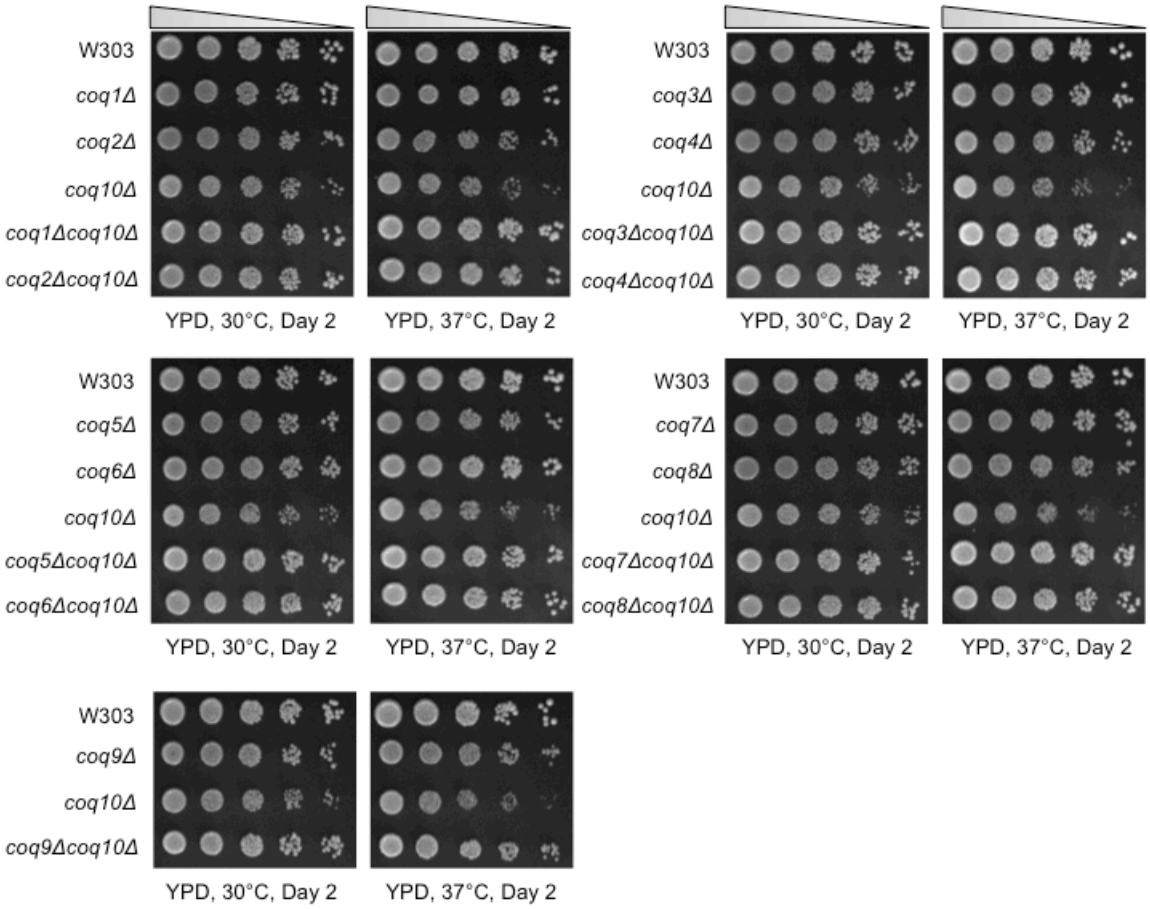

Figure 9. The *coqΔcoq10Δ* double deletion mutants appear to rescue *coq10Δ* single mutant growth phenotype at non-permissive temperature. Overnight cultures of wild-type W303, *coq1Δ-coq10Δ* single deletion mutants, and ***coqΔcoq10Δ* double deletion mutants** grown in YPD were diluted to 0.2 OD_{600}/mL, from which a series of five-fold diluted samples were prepared. Beginning with the sample at 0.2 OD_{600}/mL, an aliquot of 2 µL of series of five-fold diluted samples was plated in each spot on YPD. Pictures were taken two days after incubation at permissive 30°C, or at non-permissive 37°C.

REFERENCES

1. Barros, M. H., A. Johnson, P. Gin, B. N. Marbois, C. F. Clarke, and A. Tzagoloff. 2005. The *Saccharomyces cerevisiae COQ10* gene encodes a START domain protein required for function of coenzyme Q in respiration. *The Journal of biological chemistry* **280**: 42627-42635.

2. Awad, A. M., M. C. Bradley, L. Fernandez-Del-Rio, A. Nag, H. S. Tsui, and C. F. Clarke. 2018. Coenzyme Q_{10} deficiencies: pathways in yeast and humans. *Essays Biochem* **62**: 361-376.

3. Busso, C., E. B. Tahara, R. Ogusucu, O. Augusto, J. R. Ferreira-Junior, A. Tzagoloff, A. J. Kowaltowski, and M. H. Barros. 2010. *Saccharomyces cerevisiae coq10* null mutants are responsive to antimycin A. *The FEBS journal* **277**: 4530-4538.

4. Allan, C. M., S. Hill, S. Morvaridi, R. Saiki, J. S. Johnson, W. S. Liau, K. Hirano, T. Kawashima, Z. Ji, J. A. Loo, J. N. Shepherd, and C. F. Clarke. 2013. A conserved START domain coenzyme Q-binding polypeptide is required for efficient Q biosynthesis, respiratory electron transport, and antioxidant function in *Saccharomyces cerevisiae*. *Biochimica et biophysica acta* **1831**: 776-791.

5. Cui, T. Z., and M. Kawamukai. 2009. Coq10, a mitochondrial coenzyme Q binding protein, is required for proper respiration in *Schizosaccharomyces pombe*. *The FEBS journal* **276**: 748-759.

6. Eisenberg-Bord, M., H. S. Tsui, D. Antunes, L. Fernandez-Del-Rio, M. C. Bradley, C. D. Dunn, T. P. T. Nguyen, D. Rapaport, C. F. Clarke, and M. Schuldiner. 2019. The ER-Mitochondria Encounter Structure (ERMES) complex coordinates coenzyme Q biosynthesis. *Contact* **2**: 1-14.

7. Subramanian, K., A. Jochem, M. Le Vasseur, S. Lewis, B. R. Paulson, T. R. Reddy, J. D. Russell, J. J. Coon, D. J. Pagliarini, and J. Nunnari. 2019. Coenzyme Q biosynthetic proteins assemble in a substrate-dependent manner into domains at ER-mitochondria contacts. *J Cell Biol*.

8. Alpy, F., and C. Tomasetto. 2005. Give lipids a START: the StAR-related lipid transfer (START) domain in mammals. *J Cell Sci* **118**: 2791-2801.

9. Barkovich, R. J., A. Shtanko, J. A. Shepherd, P. T. Lee, D. C. Myles, A. Tzagoloff, and C. F. Clarke. 1997. Characterization of the *COQ5* gene from *Saccharomyces cerevisiae*. Evidence for a C-methyltransferase in ubiquinone biosynthesis. *The Journal of biological chemistry* **272**: 9182-9188.

10. Burke, D., Dawson, D., and Stearns, T. . 2000. Methods in yeast genetics. *Cold spring Harbor Laboratory Press*.

11. Tauche, A., U. Krause-Buchholz, and G. Rodel. 2008. Ubiquinone biosynthesis in *Saccharomyces cerevisiae*: the molecular organization of *O*-methylase Coq3p depends on Abc1p/Coq8p. *FEMS Yeast Res* **8**: 1263-1275.

12. Gietz, R. D., and R. A. Woods. 2006. Yeast transformation by the LiAc/SS Carrier DNA/PEG method. *Methods Mol Biol* **313**: 107-120.

13. Glick, B. S., and L. A. Pon. 1995. Isolation of highly purified mitochondria from *Saccharomyces cerevisiae*. *Methods in enzymology* **260**: 213-223.

14. Schagger, H., W. A. Cramer, and G. von Jagow. 1994. Analysis of molecular masses and oligomeric states of protein complexes by blue native electrophoresis and isolation of membrane protein complexes by two-dimensional native electrophoresis. *Analytical biochemistry* **217**: 220-230.

15. He, C. H., L. X. Xie, C. M. Allan, U. C. Tran, and C. F. Clarke. 2014. Coenzyme Q supplementation or over-expression of the yeast Coq8 putative kinase stabilizes multi-subunit Coq polypeptide complexes in yeast *coq* null mutants. *Biochimica et Biophysica Acta (BBA) - Molecular and Cell Biology of Lipids* **1841**: 630-644.

16. Wittig, I., H. P. Braun, and H. Schagger. 2006. Blue native PAGE. *Nature protocols* **1**: 418-428.

17. Marbois, B., L. X. Xie, S. Choi, K. Hirano, K. Hyman, and C. F. Clarke. 2010. para-Aminobenzoic acid is a precursor in coenzyme Q_6 biosynthesis in *Saccharomyces cerevisiae*. *The Journal of biological chemistry* **285**: 27827-27838.

18. Allan, C. M., A. M. Awad, J. S. Johnson, D. I. Shirasaki, C. Wang, C. E. Blaby-Haas, S. S. Merchant, J. A. Loo, and C. F. Clarke. 2015. Identification of Coq11, a new coenzyme Q biosynthetic protein in the CoQ-Synthome in *Saccharomyces cerevisiae*. *The Journal of biological chemistry* **290**: 7517-7534.

19. Liao, Y. D., J. C. Jeng, C. F. Wang, S. C. Wang, and S. T. Chang. 2004. Removal of N-terminal methionine from recombinant proteins by engineered *E. coli* methionine aminopeptidase. *Protein Sci* **13**: 1802-1810.

20. Geoghegan, K. F., H. B. Dixon, P. J. Rosner, L. R. Hoth, A. J. Lanzetti, K. A. Borzilleri, E. S. Marr, L. H. Pezzullo, L. B. Martin, P. K. LeMotte, A. S. McColl, A. V. Kamath, and J. G. Stroh. 1999. Spontaneous alpha-N-6-phosphogluconoylation of a "His tag" in *Escherichia coli*: the cause of extra mass of 258 or 178 Da in fusion proteins. *Analytical biochemistry* **267**: 169-184.

21. Zampol, M. A., C. Busso, F. Gomes, J. R. Ferreira-Junior, A. Tzagoloff, and M. H. Barros. 2010. Over-expression of *COQ10* in *Saccharomyces cerevisiae* inhibits mitochondrial respiration. *Biochem Biophys Res Commun* **402**: 82-87.

22. Murley, A., R. D. Sarsam, A. Toulmay, J. Yamada, W. A. Prinz, and J. Nunnari. 2015. Ltc1 is an ER-localized sterol transporter and a component of ER-mitochondria and ER-vacuole contacts. *J Cell Biol* **209**: 539-548.

23. Shen, Y., S. Goldsmith-Fischman, H. S. Atreya, T. Acton, L. Ma, R. Xiao, B. Honig, G. T. Montelione, and T. Szyperski. 2005. NMR structure of the 18 kDa protein CC1736 from *Caulobacter crescentus* identifies a member of the START domain superfamily and suggests residues mediating substrate specificity. *Proteins* **58**: 747-750.

24. James, A. M., H. M. Cocheme, M. Murai, H. Miyoshi, and M. P. Murphy. 2010. Complementation of coenzyme Q-deficient yeast by coenzyme Q analogues requires the isoprenoid side chain. *The FEBS journal* **277**: 2067-2082.

25. Zhang, Y., and M. Inouye. 2011. RatA (YfjG), an *Escherichia coli* toxin, inhibits 70S ribosome association to block translation initiation. *Mol Microbiol* **79**: 1418-1429.

26. Weill, U., I. Yofe, E. Sass, B. Stynen, D. Davidi, J. Natarajan, R. Ben-Menachem, Z. Avihou, O. Goldman, N. Harpaz, S. Chuartzman, K. Kniazev, B. Knoblach, J. Laborenz, F. Boos, J. Kowarzyk, S. Ben-Dor, E. Zalckvar, J. M. Herrmann, R. A. Rachubinski, O. Pines, D. Rapaport, S. W. Michnick, E. D. Levy, and M. Schuldiner. 2018. Genome-wide SWAp-Tag yeast libraries for proteome exploration. *Nat Methods* **15**: 617-622.

27. Chehade, M. H., L. Pelosi, C. D. Fyfe, L. Loiseau, B. Rascalou, S. Brugière, K. Kazemzadeh, C.-D.-T. Vo, L. Ciccone, L. Aussel, Y. Couté, M. Fontecave, F. Barras, M. Lombard, and F. Pierrel. 2019. A soluble metabolon synthesizes the isoprenoid lipid ubiquinone. *Cell Chemical Biology* **In press.**

28. Tzagoloff, A., M. Wu, and M. Crivellone. 1986. Assembly of the mitochondrial membrane system. Characterization of *COR1*, the structural gene for the 44-kilodalton core protein of yeast coenzyme QH_2-cytochrome c reductase. *Journal of Biological Chemistry* **261**: 17163-17169.

29. Gin, P., and C. F. Clarke. 2005. Genetic evidence for a multi-subunit complex in coenzyme Q biosynthesis in yeast and the role of the Coq1 hexaprenyl diphosphate synthase. *The Journal of biological chemistry* **280**: 2676-2681.

30. Ashby, M. N., S. Y. Kutsunai, S. Ackerman, A. Tzagoloff, and P. A. Edwards. 1992. *COQ2* is a candidate for the structural gene encoding para-hydroxybenzoate:polyprenyltransferase. *J. Biol. Chem.* **267**: 4128-4136.

31. Do, T. Q., J. R. Schultz, and C. F. Clarke. 1996. Enhanced sensitivity of ubiquinone-deficient mutants of *Saccharomyces cerevisiae* to products of autoxidized polyunsaturated fatty acids. *Proc Natl Acad Sci U S A* **93**: 7534-7539.

32. Hsu, A. Y., T. Q. Do, P. T. Lee, and C. F. Clarke. 2000. Genetic evidence for a multi-subunit complex in the O-methyltransferase steps of coenzyme Q biosynthesis. *Biochimica et biophysica acta* **1484**: 287-297.

33. Gin, P., A. Y. Hsu, S. C. Rothman, T. Jonassen, P. T. Lee, A. Tzagoloff, and C. F. Clarke. 2003. The *Saccharomyces cerevisiae COQ6* gene encodes a mitochondrial flavin-dependent monooxygenase required for coenzyme Q biosynthesis. *The Journal of biological chemistry* **278**: 25308-25316.

34. Marbois, B. N., and C. F. Clarke. 1996. The *COQ7* gene encodes a protein in *Saccharomyces cerevisiae* necessary for ubiquinone biosynthesis. *The Journal of biological chemistry* **271**: 2995-3004.

35. Johnson, A., P. Gin, B. N. Marbois, E. J. Hsieh, M. Wu, M. H. Barros, C. F. Clarke, and A. Tzagoloff. 2005. *COQ9*, a new gene required for the biosynthesis of coenzyme Q in *Saccharomyces cerevisiae*. *The Journal of biological chemistry* **280**: 31397-31404.